UNIVERSITY OF Southampton

University of Southampton Research Repository
ePrints Soton

Copyright © and Moral Rights for this thesis are retained by the author and/or other copyright owners. A copy can be downloaded for personal non-commercial research or study, without prior permission or charge. This thesis cannot be reproduced or quoted extensively from without first obtaining permission in writing from the copyright holder/s. The content must not be changed in any way or sold commercially in any format or medium without the formal permission of the copyright holders.

When referring to this work, full bibliographic details including the author, title, awarding institution and date of the thesis must be given e.g.

AUTHOR (year of submission) "Full thesis title", University of Southampton, name of the University School or Department, PhD Thesis, pagination

http://eprints.soton.ac.uk

UNIVERSITY OF SOUTHAMPTON

FACULTY OF ENGINEERING AND THE ENVIRONMENT

Engineering Materials

Electrodeposition of Nickel Coatings on Aluminium Alloy 7075 through a Modified Single Zincating Process

by

Intan Sharhida Othman

Thesis for the degree of Doctor of Philosophy

April 2016

UNIVERSITY OF SOUTHAMPTON

ABSTRACT

FACULTY OF ENGINEERING AND THE ENVIRONMENT

Engineering Materials

Thesis for the degree of Doctor of Philosophy

ELECTRODEPOSITION OF NICKEL COATINGS ON ALUMINIUM ALLOY 7075 THROUGH A MODIFIED SINGLE ZINCATING PROCESS

Intan Sharhida Othman

Electrodeposition on aluminium alloy substrates often is often difficult in producing a coating with good adhesion when compared to other metals. This is due to the rapid formation of oxide layers on the substrate's surface when exposed to air and water, preventing metallic bonds from forming between the nickel coating and the aluminium alloy substrate which in turn resulting in poor adhesion. Adhesion of the coating on the substrate influences the quality of the coating. To overcome this problem, a series of critical surface pre-treatment procedures are required for a successful electrodeposition process with a strong coating adhesion. The pre-treatment process consists of mechanical grinding and polishing, alkaline and acidic cleaning, zincating and activation process. This study focuses on the zincating process to obtain a strong adherence coating on the substrate.

An aim of this study was to replace the complex double zincating process. To this end, modification has been made to a conventional single zincating process, as the process results in a non-homogenous deposition of zinc particles on the substrate which leads to a poor adhesion of the coating. The modified process, for which the duration of the single zincating process was extended from 1 to 20 minutes, was based on the electrochemistry measurements of aluminium alloy 7075 substrate in the zincating

solution. For comparison, nickel coatings prepared using a double zincating process at 60/10, 60/20, 60/30, 60/40 and 60/50 seconds were also produced in this study.. By replacing the double zincating with a modified single zincating process, two pre-treatment steps of double zincating process will be eliminated. Thus, the waste disposal problem in terms of the chemical used in the zincating solution is reduced. In addition, copper activation was applied before the single zincating process in order to overcome the high dissolution of the substrate in the zincating solution.

The surface pre-treated samples were characterized after alkaline cleaning, acid cleaning, zincating process and copper activation at various immersion durations by scanning electron microscopy (SEM), energy dispersive X-ray (EDX) and atomic force microscopy (AFM). The modified single zincated samples were found to contain larger zinc particles, as compared to the conventional single and double zincated samples. The modified single zincating process also showed an increasing trend in the nucleation density and size of zinc particles with time. A gradual decrease in the surface roughness values with the extension of the modified single zincating duration was also observed.

Then, the influence of multiple zincating processes (conventional and modified single zincating with and without copper activation, and double zincating) at various durations on the coating adhesion was investigated using scratch adhesion test. Scratch failure modes were analysed using acoustic emission signals, frictional force, and microscopy observation. The conventional single zincating and double zincating processes resulted in poor adhesion of the nickel coatings to the substrate, as both the cohesive and adhesion failures occurred during the scratch test. The adhesion of the coating to the substrate was improved by extending the single zincating duration from 1 to 5, 10, 15 and 20 minutes, with only cohesive failure found for the samples. This result was supported by the number of acoustic emission activity (N_{AE}) events recorded during the test, which showed the highest N_{AE} at about 130 for the sample produced from the conventional single zincating process. An increase in the zincating duration to 5 minutes resulted in a drastic reduction of the N_{AE} to 30. The similar adhesion behaviour was also observed on modified single zincated samples with copper activation.

The corrosion tests were carried out by immersing the coatings in a 3.5 wt. % NaCl solution at room temperature. It was found that a modified single zincating process at a longer duration provided a significant enhancement of corrosion resistance as compared to the conventional single zincating process, due to the increase in corrosion potential and decrease in corrosion current density of the conventional single zincated sample.

These much improved performance of coating adhesion and corrosion resistance may be explained by homogenous distribution of zinc particles and good coverage of the zinc particles on the aluminium alloy substrate.

Table of Contents

ABSTRACT ..... **ii**

List of tables ..... **xvii**

DECLARATION OF AUTHORSHIP ..... **xxiii**

Acknowledgements ..... **xxv**

Dedication ..... **xxvii**

Nomenclature ..... **xxviii**

1 INTRODUCTION **1**

1.1 Background of Project **1**
1.2 Problem Statement **4**
1.3 Objectives **8**
1.4 Thesis Outline **9**

2 LITERATURE REVIEW **10**

2.1 Electrodeposition Process for Surface Protection **10**
2.1.1 Introduction 10
2.1.2 Surface Pre- treatment Process for the Electrodeposition 13
2.1.3 Principles of Electrodeposition Process 14
2.1.4 Properties of Electrodeposited Materials 18
2.1.5 Factors Influencing the Properties of Electrodeposited Materials 22
2.2 Electrodeposition of Nickel Coating **25**
2.2.1 Introduction 25
2.2.2 Fundamentals of Electrodeposition of Nickel 25
2.2.3 Faraday's Law for Nickel Coating 26
2.2.4 Functions of Constituents in the Watts Bath and Deposit Properties 27
2.3 Electrodeposition on the Substrate of Aluminium and its Alloys **28**
2.3.1 Introduction 28
2.3.2 Properties of Aluminium and Its Alloys 29
2.3.3 Problems Associated with Electrodeposition on Aluminium and Its Alloys Substrates 30

2.3.4 Classification of Methods for Electrodeposition on Aluminium and Its Alloys ……32
2.3.5 Preparation of Aluminium and Its Alloys Surfaces before Electrodeposition Process 34
2.4 Zincating Process 41
2.4.1 Introduction 41
2.4.2 Fundamentals 42
2.4.3 Nucleation and Growth of Zinc Particles 43
2.4.4 Factors That Influence the Properties of Zincated Samples 44
2.4.5 Environmental Issue of the Zincating Solution 59
2.5 Adhesion of Coatings 60
2.5.1 Introduction 60
2.5.2 Method of Adhesion Testing 63
2.5.3 Variables Affecting Scratch Test Results 64
2.5.4 Scratch Test Failure Modes 67
2.5.5 Evaluation of Coating Failure from Scratch Test 70
2.6 Summary of the Literature Review 74

3 METHODOLOGY 75

3.1 Introduction 75
3.2 Surface Pre-treatment Procedures 76
3.2.1 Substrate Material 76
3.2.2 Mechanical Surface Pre-treatment 76
3.2.3 Chemical Surface Pre-treatment 78
3.2.4 Multiple Zincating Processes 79
3.3 Electrodeposition Process 81
3.4 Characterization Techniques and Testing 82
3.4.1 Open-Circuit Potential Measurement 85
3.4.2 Scanning Electron Microscopy and Energy Dispersive X-ray 85
3.4.3 Atomic Force Microscopy 86
3.4.4 Scratch Adhesion Test 87
3.4.5 Corrosion Test 92

4 RESULTS 93

4.1 Introduction 93

4.2 Electrochemical Behaviour of AA7075 Substrate during Various Surface Pre-treatment Processes 93

4.2.1 Electrochemical Behaviour of AA7075 during Alkaline Cleaning and Acid Pickling Processes 93

4.2.2 Electrochemical Behaviour of AA7075 during Single Zincating Process 95

4.2.3 Electrochemical Behaviour of AA7075 during Various Double Zincating Durations 96

4.2.4 Electrochemical Behaviour of AA7075 during the Single Zincating Process with Copper Activation 104

4.3 Surface Morphology and Element Composition of AA7075 Substrate after Various Surface Pre- treatment Processes 106

4.3.1 Surface Morphology and Element Composition of AA7075 Substrate surface after Alkaline Cleaning and Acid Cleaning Processes 106

4.3.2 Surface Morphology and Element Composition of AA7075 Substrate after Copper Activation Process 108

4.3.3 Surface Morphology and Element Composition of AA7075 Substrate after Conventional and Modified Single Zincating Process at Various Durations 113

4.3.4 Surface Morphology and Element Composition of AA7075 Substrate after Double Zincating Process at Various Durations 118

4.3.5 Surface Morphology and Element Composition of AA7075 Substrate after Conventional and Modified Single Zincating Process at Various Durations with Copper Activation 124

4.4 Surface Topography and Roughness of AA7075 Substrate after Various Surface Pre-treatment Processes 128

4.4.1 Surface Topography and Roughness of AA7075 Substrate after Polishing, Alkaline Cleaning and Acid Cleaning 128

4.4.2 Surface Topography and Roughness of AA7075 Substrate after Copper Activation Process 131

4.4.3 Surface Topography and Roughness of AA7075 Substrate after Conventional and Modified Single Zincating Process at Various Durations 134

4.4.4 Surface Topography and Roughness of AA7075 Substrate after Double Zincating Process at Various Durations 137

4.4.5 Surface Topography and Roughness of AA7075 Substrate after Conventional and Modified Single Zincating Process at Various Durations with Copper Activation 140

4.5 Surface Morphology and Composition of Interface of Nickel Coating Electrodeposited on AA7075 Substrate through a Conventional and Modified Single Zincating Process at Various Durations 143

4.6 Adhesion of Nickel Coatings on AA7075 Substrate Produced from Multiple Zincating Processes 146

4.6.1 Effect of Conventional and Modified Single Zincating Process at various Durations on the Adhesion of the Nickel Coatings Electrodeposited on AA7075 Substrate 146

4.6.2 Effect of Various Double Zincating Durations on Adhesion of the Nickel Coatings Electrodeposited on AA7075 Substrate 156

4.6.3 Effect of Conventional and Modified Single Zincating Process at various Durations with Copper Activation on the Adhesion of the Nickel Coatings Electrodeposited on AA7075 Substrate 166

4.7 Electrochemical Corrosion Behaviour of Nickel Coatings on AA7075 Substrate Produced from Multiple Zincating Processes 176

4.7.1 Introduction 176

Electrochemical Corrosion Behaviour of Nickel Coatings on AA7075 Substrate Produced from Conventional and Modified Single Zincating Process at Various Durations 176

4.7.2 176

Electrochemical Corrosion Behaviour of Nickel Coatings on AA7075 Substrate Produced from Double Zincating Process at Various Durations..... 177

4.7.3 177

4.7.4 Corrosion Behaviour of Nickel Coatings on AA7075 Substrate Produced from Conventional and Modified Single Zincating Process at Various Durations with Copper Activation 179

5 DISCUSSIONS..... 181

5.1 Introduction 181

5.2 Electrochemical Behaviour of AA7075 Substrate during Various Surface Pre- treatment Processes ……..181

5.3 Surface Morphology and Elemental Composition of AA7075 Substrate after Various Surface Pre-treatment Processes 187

5.4 Surface Topography and Roughness of AA7075 after Various Surface Pre- treatment Processes 190

Surface Morphology and Elemental Composition of Coating's Interface between Nickel Coatings and AA7075 Substrate through a Conventional and Modified Single Zincating Process at Various Durations..... 192

5.5 Adhesion of the Nickel Coatings Electrodeposited on AA7075 Substrate Produced from Multiple Zincating Processes 194

5.6 Electrochemical Corrosion Behaviour of the Nickel Coatings Electrodeposited on AA7075 Substrate Produced from Multiple Zincating Processes 201

5.7 Overall Discussion of the Results 203

6 CONCLUSION 206

7 FUTURE WORKS 214

REFERENCES

List of Figures

Figure 1-1 Comparison between conventional single and double zincating with modified single zincating process ……7

Figure 2-1 Types of deposits produced from electrodeposition process (a) homogenous, (b) dispersed phase, (c) multilayer, (d) patterned and (e) gradient (from Ref. [67])..... 13

Figure 2-2 An electrolytic cell for electrodeposition of metal from an aqueous solution 16

Figure 2-3 Illustration of several stages in electrodeposition process, (1) migration of hydrated metal ions to a cathode, (2) surrender of the hydration sheath, (3) formation of adsorbed atoms and (4) formation of crystal nuclei at the cathode surface [66] 17

Figure 2-4 Scanning electron micrographs of electroless Ni-P layers on aluminium alloys at respective electroless duration (a) 1, (b) 2, (c) 3 and (d) 4 minutes (from Ref. [19])..... 20

Figure 2-5 Cross-section of nickel coating electrodeposited on an Al 2014 alloy (from Ref.[18])21

Figure 2-6 Potentiodynamic polarization curves obtained from the corrosion test of the aluminium coatings deposited on AZ91D magnesium alloy produced using BCP and GP methods with and without zincating process in 3.5 wt.% NaCl solution (from the ref. [95]) 22

Figure 2-7 SEM micrographs showing the topography of 100 µm thick nickel layers deposited at 323 K and at various current densities, (a) 0.5 A/dm^2 and (b) 20 A/dm^2 (from Ref.[72]) 23

Figure 2-8 Methods of producing coatings on aluminium alloys 34

Figure 2-9 Surface pre- treatment procedures for wrought aluminium alloys that contain high amount of silicon or do not contain interfering microconstituents (1100 and 3003) and for aluminium casting alloys 413,319,356 and 380 (from the Ref. [108])..... 36

Figure 2-10 Surface pre-treatment procedures for all wrought aluminium alloys, for 37

Figure 2-11 Surface pre-treatment procedures for most aluminium casting alloys, for wrought aluminium alloys that contain less than approximately 3% Mg (1100, 3003, 3004, 2011, 2017, 2024, 5052, 6061) and for aluminium alloys whose identities are not known (from Ref. [108])37

Figure 2-12 Zincating pre- treatment process (a) as-received ion beam sputter-deposited aluminium film, (b) first zincating process, (c) acid immersion process and (d) second zincating process (from Ref. [43]) 43

Figure 2-13 Proposed model of the nucleation and growth of zinc particles (from Ref. [42]) .. 44

Figure 2-14 Effect of concentration of the zincating solution on the weight of the zinc immersion coating formed on 2S alloy sheet at a temperature of 21º C (from Ref. [46])..... 46

Figure 2-15 (a) Effect of the concentration of the zincating solution on the weight of the zinc immersion coating formed during a given time, (b) details of the components concentration in the different zincating solution (from Ref. [107]) 47

Figure 2-16 Mixed potentials as a function of time at various zincate concentrations. (a) 0.5, (b) 0.1, (c) 0.05, (d) 0.01 and (e) 0 M. Sodium hydroxide concentration is at 3.0 M, temperature at 25º C and rotation speed at 230 rpm (from Ref. [50])..... 48

Figure 2-17 The potential difference between commercial purity aluminium after various pre-treatment conditions in a concentrated simple zincating solution (100 g/l ZnO + 500 g/l NaOH) (from the Ref. [5]).....49

Figure 2-18 Effect of different conditioning treatments on the weight of zinc immersion coating on 2S alloy. Treatment A, carbonate-phosphate cleaner; treatment B, same cleaner + 25% sulphuric acid etch + zinc dip; treatment C, same cleaner + double zinc dip; treatment D, Alcoa R5 Bright Dip + zinc dip (from Ref. [46]).....50

Figure 2-19 Effect of different wrought aluminium alloys on the weight of zinc immersion coating using same conditioning treatment, concentrated simple zincating solution of 100 g/l ZnO + 525 g/l NaOH (from Ref. [46]).....51

Figure 2-20 Effect of temperature of the zincating pre-treatment on the weight of the zinc immersion coating deposited on 2S aluminium alloys sheet (from Ref. [46]) 52

Figure 2-21 FE-SEM images of zincated specimen for 10 s (a) zincating temperature of 20 C, (c) zincating temperature at 50 C, while (b) and (d) are the further grown deposit of (a) and (c), respectively (from Ref. [42]). 53

Figure 2-22 Effect of solution concentration on adhesion of zinc deposit obtained after 30 seconds immersion in zincating solution (from Ref. [5]) 55

Figure 2-23 Effect of solution concentration on adhesion of zinc deposit obtained after 3 minutes immersion in zincating solution (from Ref. [5]) 55

Figure 2-24 Effect of solution concentration on adhesion of zinc deposit obtained after 5 minutes immersion in zincating solution (from Ref. [5]) 55

Figure 2-25 Adhesion strength of Ni-P electrodeposition on various type of zincating treatment (from Ref. [1]) ……..58

Figure 2-26 Secondary electron of the surface after zincating pre- treatment (a) without zincating, (b) single, (c) double, (d) triple (from Ref. [1]).....59

Figure 2-27 Illustration of the local stress state during scratching procedure [from ref. [146]) ..64

Figure 2-28 Schematic diagram showing the map of the main scratch test failure modes in terms of substrate and coating hardness (from ref.[139]) 67

Figure 2-29 Failure modes classification of scratch test results 68

Figure 2-30 Illustration of the main stages in buckling failure modes in the scratch test. (i) pile-up ahead of the moving indenter, (ii) interfacial failure leading to buckling. Through- thickness cracking results in removal of coating material, (iii) SEM micrograph of buckle failure in TiN coated stainless steel (from ref. [139]).....69

Figure 2-31 Illustration of the main stages in wedge spallation failure modes in the scratch test. (i) wedge crack forms some way ahead of the moving indenter, (ii) further motion drives the coating up the wedge opening up an interfacial crack, (iii) through- thickness cracking close to the indenter leads to spallation, (iv) SEM micrograph of a wedge spallation failure in an alumina scale (from ref. [139]) 70

Figure 2-32 Illustration of critical load damage features in progressive load test (from ref. [167]72

Figure 2-33 Optical micrographs of critical load failure events for the CrN coating with scratch direction from left to right. (a) L_{C1}, (b) L_{C2} and (c) L_{C3}. 72

Figure 2-34 Correlation between the amplitude of frictional force and failure mode for DLC coating……..74

Figure 3-1 Dimension of the substrate 76

Figure 3-2 Entire process of electrodeposition nickel on AA7075 substrate 77

Figure 3-3 Electrodeposition process arrangement of nickel coating on AA7075 substrate..... 83

Figure 3-4 Electrochemical experiment arrangement used for zincating process and corrosion test……...……..86

Figure 3-5 Schematic diagram of Atomic Force Microscope [148, 180] 87

Figure 3-6 Schematic diagram of scratch adhesion test system [167]..... 88

Figure 3-7 Typical results of scratch test which shows the AE signal and friction force versus scratch distance (f), optical micrograph of the scratch track (e) and SEM images of the failure events ((c) and (d)). An EDX analysis using the 'point and ID' mode was used and drawn on the fracture surfaces, in order to check whether the substrate is revealed or not ((a) and (b)). 91

Figure 3-8 Through-thickness cracking (cohesive) failure modes in the scratch test (a) brittle tensile cracking, (b) ductile tensile cracking, (c) hertz cracking and (d) conformal cracking [123]91

Figure 3-9 Interfacial (adhesive) failure modes in the scratch test (a) buckling, (b) buckle spallation, (c) wedging/ spallation and (d) recovery spallation [123] 92

Figure 4-1 Changes in immersion potential of AA7075 substrate in alkaline solution (10 wt. % NaOH) at room temperature. The labels 1, 2 and 3 indicate the first, second and third stage, respectively……...94

Figure 4-2 Changes in immersion potential of AA7075 substrates in acid solution (50 vol. % HNO_3) at room temperature. The labels 1, 2 and 3 indicate the first, second and third stage, respectively……..95

Figure 4-3 Changes in immersion open circuit potential (E_{OC}) of the AA7075 substrate during the single zincating process. The labels 1, 2 and 3 indicate the first, second and third stage, respectively……..96

Figure 4-4 Changes in immersion open circuit potential (E_{OC}) of the AA7075 substrate during the double zincating process. (a) The changes of E_{OC} during the zincating process up to 3600 seconds. (b) A time- expansion plot for the initial stage of the zincating process (a). (c) A time-expansion plot for the second stage of the zincating process (a). (d) A time- expansion plot for the third stage of the zincating process (a). 99

Figure 4-5 Changes in immersion open circuit potential (E_{OC}) of the AA7075 substrate during the single and double zincating process. (a) The changes of E_{OC} during the zincating process up to 3600 s. (b) A time-expansion plot for the initial stage of the zincating process (a). 102

Figure 4-6 Comparison in immersion open circuit potential (EOC) of various substrates during the single and double zincating process 103

Figure 4-7 Changes in immersion open circuit potential (E_{OC}) of the AA7075 substrate with copper activation during single zincating process for 1000 seconds 105

Figure 4-8 Changes in immersion open circuit potential (E_{OC}) of the AA7075 substrate with and without copper activation during the single zincating process and double zincating process for 1000 seconds……..106

Figure 4-9 SEM morphology of AA7075 substrate after various surface pre- treatment processes (a) as- received substrate, (b) alkaline cleaning (10 wt. % NaOH, 10 s, room temperature (RT)) and (c) acid cleaning (50 vol. % HNO_3, 20 s, RT).....108

Figure 4-10 SEM micrographs (SEI and BEI modes) of AA7075 substrates after copper activation process in 0.5 M H_2SO_4 + 3.13 x 10^{-4} M $CuSO_4$ at RT for (a) 5, (b) 10 and (c) 15 minutes……...110

Figure 4-11 EDX analysis of particles after copper activation, confirming they are copper particles……..110

Figure 4-12 EDX analyses of AA7075 substrates after copper activation process at various durations (a) 5, (b) 10 and (c) 15 minutes.....111

Figure 4-13 EDX analysis of average copper composition (wt. %) present on AA7075 substrates after various copper activation duration.....112

Figure 4-14 EDX analysis of other elements composition (wt. %) present on AA7075 substrates after various copper activation duration.....113

Figure 4-15 SEM micrographs of AA7075 substrates after (a) conventional single zincating process at 1 minute and modified single zincating process at various durations: (b) 5, (c) 10, (d) 15 and (e) 20 minutes.....115

Figure 4-16 Analysis of zinc particles size deposited on AA7075 substrate at 1, 10 and 20 minutes of zincating process.....116

Figure 4-17 EDX analysis of particles after modified single zincating process for 10 minutes, confirming they are zinc particles.....117

Figure 4-18 EDX analysis of sample surfaces for the conventional and modified single zincating processes at various durations.....118

Figure 4-19 SEM micrographs of AA7075 substrate after double zincating process at various durations (a) 60/10, (b) 60/20, (c) 60/30, (d) 60/40, (e) 60/50 seconds and (f) zinc stripping process……121

Figure 4-20 Analysis of zinc particles size deposited on AA7075 substrate at 60/10, 60/40 and 60/50 seconds of zincating process.....122

Figure 4-21 EDX analysis of zinc composition (wt. %) present on AA7075 substrates after various double zincating durations. FZ: first zincating process, ZS: zinc stripping process 123

Figure 4-22 EDX analysis of sample surfaces after various double zincating durations.....123

Figure 4-23 SEM micrographs of AA7075 substrates after (a) conventional single zincating process at 1 minute and modified single zincating process at various durations, such as (b) 5, (c) 10, (d) 15 and (e) 20 minutes with copper activation 126

Figure 4-24 Analysis of zinc particles size deposited on AA7075 substrate at 1, 10 and 20 minutes of zincating process with copper activation 127

Figure 4-25 EDX analysis of sample surfaces for the conventional and modified single zincating processes at various durations with copper activation 128

Figure 4-26 AFM images of AA7075 substrate after various surface pre-treatment processes. (a) after polishing using 1µm diamond paste, (b) after alkaline cleaning in 10 wt.% NaOH at room temperature for 10 seconds, (c) after acid pickling in 50 vol.% HNO_3 solution at room temperature for 20 seconds. 130

Figure 4-27 Surface roughness of after various surface pre- treatment processes prior to zincating process 131

Figure 4-28 AFM images of AA7075 substrates after (a) immersion in 0.5 M H_2SO_4 solution without copper particles for 20 seconds at room temperature and copper activation process in 0.5 M H_2SO_4 + 3.13 x 10^{-4} $CuSO_4$ solution at (b) 5, (c) 10 and (d) 15 minutes at room temperature 133

Figure 4-29 Surface roughness (Ra) of AA7075 substrate at various durations of copper activation process. 134

Figure 4-30 AFM images (three dimensional view) of AA7075 substrate after (a) conventional single zincating process at 1 minute and modified single zincating process at various durations, such as (b) 5, (c) 10 , (d) 15 and (e) 20 minutes 136

Figure 4-31 Surface roughness of substrates after conventional and modified single zincating process at various durations. CZ: conventional single zincating process, MZ: modified single zincating process. 137

Figure 4-32 AFM images of AA7075 after double zincating process (a) first zincating at 60 seconds, (b) zinc stripping in 50 vol. % HNO_3 at room temperature for 30 minutes, (c)- (d) double zincating at 60/10, 60/30 and 60/50 seconds, respectively. 139

Figure 4-33 Surface roughness of double zincating process. FZ: first zincating at 60 seconds, SZ1: second zincating at 60/10 s and SZ5: second zincating at 60/50 s. 140

Figure 4-34 AFM images (three dimensional view) of AA7075 substrate after (a) conventional single zincating process at 1 minute and modified single zincating process at various durations, such as (b) 5, (c) 10, (d) 15 and (e) 20 minutes with copper activation 141

Figure 4-35 Surface roughness of modified single zincating processes with copper activation. CZ: conventional single zincating process, MZ: modified single zincating process. 142

Figure 4-36 SEM morphology and EDX analysis on the cross-section of the nickel coatings electrodeposited on AA7075 substrate through (a) conventional single zincating process at 1 minute and modified single zincating process at various durations, such as (b) 5, (c) 10, (d) 15 and (e) 20 minutes 145

Figure 4-37 Frictional force and acoustic emission signal intensity as a function of the scratch distance for nickel coatings produced at (a) conventional single zincating process at 1 minute and modified single zincating process at various durations, (b) 5, (c) 10, (d) 15 and (e) 20 minutes 147

Figure 4-38 Coefficient of friction and acoustic emission signal intensity as a function of the scratch distance for nickel coatings produced using (a) conventional single zincating process at 1 minute and modified single zincating process at various durations, (b) 5, (c) 10, (d) 15 and (e) 20 minutes……..149

Figure 4-39 Average critical loads of nickel electrodeposited on AA7075 produced at various single zincating durations as measured by scratch testing 150

Figure 4-40 Correlation between number of acoustic emission activity (N_{AE}) and various single zincating durations 151

Figure 4-41 Optical micrographs of the scratch tracks of nickel electrodeposited on AA7075 substrate produced with the conventional single zincating process for 1 minute and modified single zincating process for 5, 10, 15, and 20 minutes 154

Figure 4-42 SEM images and EDX analysis showing the middle and end of the scratch tracks of nickel electrodeposited on AA7075 produced at (a) conventional single zincating process for 1 and (b) modified single zincating process for 20 minutes 155

Figure 4-43 Frictional force and acoustic emission signal intensity versus scratch distance curves of nickel coatings produced at various double zincating durations (a) 60/10, (b) 60/20, (c) 60/30, (d) 60/40 and (e) 60/50 seconds.....157

Figure 4-44 Coefficient of friction and acoustic emission signal intensity versus scratch distance curves of nickel coatings produced using various double zincating durations (a) 60/10, (b) 60/20, (c) 60/30, (d) 60/40 and (e) 60/50 seconds. 159

Figure 4-45 Average critical loads of nickel electrodeposited on AA7075 produced at various double zincating durations measured by scratch testing 160

Figure 4-46 Correlation between number of acoustic emission activity (N_{AE}) and double zincating durations 161

Figure 4-47 Optical micrographs of the scratch tracks of nickel electrodeposited on AA7075 produced at various double zincating durations.....164

Figure 4-48 SEM images showing the middle and end of the scratch tracks of nickel electrodeposited on AA7075 produced at 60/10 and 60/50 seconds of double zincating durations……165

Figure 4-49 Variation of the frictional force and acoustic emission signal intensity curves as a function of the scratch distance for nickel coatings produced at (a) conventional single zincating process at 1 minute and modified single zincating process at various durations, such as (b) 5, (c) 10, (d) 15 and (e) 20 minutes with copper activation 167

Figure 4-50 Variation of the coefficient of friction and acoustic emission signal intensity curves as a function of the scratch distance for nickel coatings produced at (a) conventional single zincating process at 1 minute and modified single zincating process at various durations, such as (b) 5, (c) 10, (d) 15 and (e) 20 minutes with copper activation 169

Figure 4-51 Average critical loads of nickel electrodeposited on AA7075 substrate produced from conventional and modified single zincating process at various durations with copper activation……170

Figure 4-52 Correlation between number of acoustic emission activity (N_{AE}) and conventional and modified single zincating process at various durations with copper activation..... 171

Figure 4-53 EDX analysis on a void which is formed from electrodeposition process. 172

Figure 4-54 Optical micrographs of the scratch tracks of nickel electrodeposited on AA7075 produced at conventional single zincating process for 1 minute and various modified single zincating durations for 5, 10, 15 and 20 minutes with copper activation 174

Figure 4-55 SEM images showing the middle and end of the scratch tracks of nickel electrodeposited on AA7075 produced at (a) conventional single zincating for 1 minute and (b) modified single zincating process for 20 minutes, with copper activation..... 175

Figure 4-56 Tafel polarization curves of the as received AA7075 substrate and electrodeposited nickel coatings on AA7075 substrate produced at conventional and modified single zincating process at various durations..... 177

Figure 4-57 Tafel polarization curves of as- received AA7075 substrate and electrodeposited nickel coatings on AA7075 substrate produced at various double zincating durations. 178

Figure 4-58 Tafel polarization curves of the as- received AA7075 substrate and electrodeposited nickel coatings on AA7075 substrate produced at conventional and various modified single zincating durations with copper activation process. 180

Figure 5-1 Comparison of immersion open circuit potential (E_{OC}) of AA7075 substrate during single and double zincating process with pure zinc plate during the single zincating process . 185

Figure 5-2 Schematic representations of the various zincating processes on AA7075. (a) conventional and modified single zincating process and (b) double zincating process. 188

Figure 5-3 EDX analysis on copper detection of copper activated AA7075 substrates at 10 minutes……...190

Figure 5-4 Direction of the bubbles moving upwards of the sample 194

Figure 5-5 Average critical loads of nickel electrodeposited on AA7075 produced from conventional and modified single zincating process with and without copper activation..... 197

Figure 6-1Correlation between the surface morphology and the EOC curve for single zincating process with and without copper activation 209

List of tables

Table 2-1 Coating processes used to protect functional surface (from the Ref. [66]) 11

Table 2-2 Comparison of electrochemical methods for metal deposition (from Ref. [67, 68] 11

Table 2-3 Selection of processes which may be involved in electrodeposition process (from Ref. [67, 86]……14

Table 2-4 Types of nickel electroplating solution and some deposits properties (from the Ref. [99])……..28

Table 2-5 Properties of selected aluminium and its alloys at room temperature (from ref. [101])29

Table 2-6 The standard electromotive force (EMF) table (from the Ref. [5]) 31

Table 2-7 Mean coefficient of linear expansion of the common metals (from the Ref. [5]) 31

Table 2-8 Metals for possible direct deposition on aluminium (from the Ref. [5]) 32

Table 2-9 Various types of finishes (from the Ref. [100]).....33

Table 2-10 Control of alkaline cleaner (from Ref. [5]).....39

Table 2-11 Various type of modified zincating solutions for use with aluminium alloys (from Ref.[108])……45

Table 2-12 Effect of various pre-treatment conditions on the zinc deposits of commercial purity aluminium (from the Ref. [5]).....49

Table 2-13 Potentials of some metals and aluminium alloys in 53 g/l NaCl + 3 g/l H_2O_2 with reference to the 0.1 KCl calomel electrode (from Ref. [5]) 51

Table 2-14 A summary of previous research on zincating process of aluminium and its alloys .56

Table 2-15 Hazard identification of chemicals used in zincating solution 60

Table 2-16 Various methods of adhesion test (from Ref. [67]) 63

Table 2-17 Intrinsic and extrinsic parameters influencing the scratch test results.....64

Table 2-18 Summary of the list of references on each technique 71

Table 3-1 Composition of alkaline cleaning solution 78

Table 3-2 Composition of acid cleaning solution 78

Table 3-3 Composition of the zincating solutions used to produce nickel deposits on AA7075 substrate……80

Table 3-4 Matrix table of samples produced at various immersion durations of zincating processes……...80

Table 3-5 Concentration of chemical reagents in modified Watt's bath solution.....82

Table 3-6 Summary of characterisation techniques and testing 83

Table 4-1 Slope value for steady state potential of specimens produced from double zincating process using various first zincating durations 100

Table 4-2 Element composition (wt. %) of the substrate surface as determined by EDX after various surface pre- treatment processes 108

Table 4-3 Tafel polarization parameters for the electrodeposited nickel on AA7075 substrate produced at conventional and modified single zincating process at various durations 177

Table 4-4 Tafel polarization parameters for the electrodeposited nickel coatings on AA7075 substrate produced at various double zincating durations. 179

Table 4-5 Tafel polarization parameters for the electrodeposited nickel coatings on AA7075 substrate produced at conventional and various modified single zincating durations with copper activation……180

Table 5-1 Comparison table of Tafel polarization parameters for the electrodeposited nickel coatings on AA7075 substrate produced at conventional and modified single zincating process without and with copper activation. 203

Table 5-2 Summary of the zincating process used by other researchers 204

Table 6-1A summary of previous research on zincating process of aluminium and its alloys . 206

Table 6-2 Duration for multiple zincating process used in this research..... 210

DECLARATION OF AUTHORSHIP

I, **Intan Sharhida Othman**

declare that the thesis entitled

Electrodeposition of Nickel Coatings on Aluminium Alloy 7075 through a Modified Single Zincating Process

and the work presented in the thesis are both my own, and have been generated by me as the result of my own original research. I confirm that:

- this work was done wholly or mainly while in candidature for a research degree at this University;
- where any part of this thesis has previously been submitted for a degree or any other qualification at this University or any other institution, this has been clearly stated;
- where I have consulted the published work of others, this is always clearly attributed;
- where I have quoted from the work of others, the source is always given. With the exception of such quotations, this thesis is entirely my own work;
- I have acknowledged all main sources of help;
- where the thesis is based on work done by myself jointly with others, I have made clear exactly what was done by others and what I have contributed myself;
- none of this work has been published before submission, or [delete as appropriate] parts of this work have been published as: [please list references]

Signed: ……..

Date: 29 April 2016

Acknowledgements

First and foremost, all praises to Allah S.W.T. for his everlasting blessing and guidance to me in completing this study. I would like to take this opportunity to express my sincere gratitude to my supervisors, Professor Marco Starink and Dr. Shuncai Wang, for their helps and supports throughout my PhD. study. It was a great experience working under their supervision and I am deeply indebted to them for their continuous guidance and encouragement.

I am also thankful Dr. John Nunn at National Physics Laboratory, Teddington, United Kingdom for helping me with the scratch test and Dr. Jurgita Zekonyte at national Centre for Advanced Tribology at Southampton University (nCats) for the surface topography observation and surface roughness measurement using the atomic force microscopy (AFM). I also would like to acknowledge and appreciate Professor Steve Bull from the Newcastle University, who willing to share his knowledge on adhesion of the coating.

I am very much thank the assistance of all the staffs in the School of Engineering and Environment, in particular Mrs. Sue Berger for the administration support and Mr. David Beckett, Mr. Eric and all the technical staffs for the technical support throughout my PhD. study. My sincere appreciation also goes to Dr. Richard Wills for his helps and guidance during my working period in the electrochemistry laboratory. I also would like to thank all my research colleagues for sharing these wonderful moments of PhD. journey together; Dr. Chao Ma, Dr. Chuanting Wang, Dr. Danial Bull, Dr. Yang He, Feifei Zhang, Dr. Pawee Kuchita and many more.

Finally, words cannot truly express my deepest gratitude and appreciation to my beloved husband, parents, parents in law, sons and family members, who always gave me their love and emotional support throughout my PhD. journey, without their supports, this PhD. would not be easily went through.

Dedication

This thesis is fully dedicated to my beloved husband, ***Syahrul Azwan Suandi****, my dear mother,* ***Juhuriah Ramli****, farther,* ***Othman Dari****, parents in law,* ***Siti Mariam Ahmad*** *and* ***Sundi @ Suandi Alang Ahmad*** *and my four lovely sons,* ***Muhammad Muizzuddin Qayyum****,* ***Muhammad Hafiyuddin Hasif****,* ***Muhammad Waqiyuddin Wafiy*** *and* ***Muhammad Izzuddin Mishary*** *for their love, patience, encouragement, prayers and understanding throughout this journey.*

Nomenclature

Symbols

M	metal
M^{z+}	metal ions
e	electron
z	number of electron
I	current
t	time
a	current efficiency ratio
J	current density
s	seconds
W_A	work of adhesion
γ_s	surface free energies of metal
γ_{s1s2}	interfacial free energy
R	radius
d	depth
τ	shear strength
F_C	critical normal load
F_N	normal load
H_S	substrate hardness

H_C	coating hardness
L_C	critical load
N_{AE}	number of acoustic emission events
E_{OC}	open circuit potential
Ra	surface roughness
F_f	friction force
E_{corr}	corrosion potential
I_{corr}	corrosion current density
D	coefficient of diffusion

Acronyms

OM	Optical Microscope
SEM	Scanning Electron Microscopy
AFM	Atomic Force Microscopy
BEI	Backscattered Electrons Images
EPA	Environment Protection Agency
CVD	Chemical Vapour Deposition
PVD	Physical Vapour Deposition
EMF	Standard Electromotive Force
AE	Acoustic Emission
WE	Working Electrode
SCE	Saturated Calomel Electrode
CE	Counter Electrode
EMF	Electromotive Force

1 INTRODUCTION

1.1 Background of Project

Aluminium and its alloys are materials of choice for a wide spread spectrum of technological applications due to their light weight, excellent workability, corrosion resistance, good appearance, and recyclability [1-4]. They are divided into two main groups, namely cast alloys and wrought alloys. Cast alloys are produced by pouring molten metals into the desired mould, while wrought alloys are cast in ingots or billets and go through hot and cold working of metal processing to make such products as extrusions, forgings, sheet, foil, tube, and wire [5, 6]. Wrought alloys are categorized into several major classes according to their principal alloying element. The classes include 2000 series (Al-Cu alloys), which are high-strength materials used mainly in the aircraft industry, 3000 series (Al-Mn alloys) used in the canning industry, 5000 series (Al-Mg alloys) used in structural and architectural applications, 6000 series (Al-Mg-Si alloys) used in the building industry, and the 7000 series (Al-Zn-Mg alloys), which are high-strength alloys for aircraft and military transport applications [5, 7].

Among these alloys, aluminium alloy 7075 (AA7075), a heat treatable wrought alloy, is an important engineering material in manufacturing aircraft and aerospace structures, such as top wing skin panels and landing gear components [8]. AA7075 is also used in the automotive industries for bumper applications [5, 7]. This is due to its superior strength to weight ratio compared to other aluminium alloys series [8-10]. Although this alloy possesses attractive tensile properties and good fabrication properties, its alloying elements such as copper contribute to the reduction of the corrosion resistance [7, 11]. Other alloying elements in this alloy are zinc and magnesium.

In relation to this weakness, pitting corrosion is known to be the main damage mechanism which affects the integrity of this alloy when used without any surface protection [12, 13]. This type of corrosion can affect the strength of structural parts, and is thus the main constraint for engineers designing structural parts for aircraft [12]. In

addition, the low hardness, low wear resistance and low corrosion resistance of aluminium and its alloys all require surfaces to be covered with a hard, wear and corrosion-resistant protective layer.

Electroplating of cadmium and hard chromium has been used for protective coatings to overcome the drawbacks of the surface properties in most metals [14]. Although cadmium and hard chromium coatings offer superior properties such as excellent corrosion resistance with low cost, the electrodeposition process of these coatings is heavily regulated, due to the presence of serious human health and environmental hazards [14-16]. Electrodeposition of cadmium normally involves plating solutions containing cyanide, which is highly toxic to human and animal life [16]. Chromic acid (H_2CrO_4), which is mainly used in hard chromium electrodeposition, is also a highly toxic and carcinogenic chemical [17].

Many studies have been conducted in order to find alternative process, substitute materials and new designs that do not involve these hazardous materials. According to technical reports prepared by the National Defence Centre for Environmental Excellence, Pennsylvania [15], Institute for Aerospace Research, National Research Council, Canada [14] and United States Environmental Protection Agency (EPA), Washington [16], electrodepositing of zinc and zinc- alloys may be used to replace cadmium coating in automotive and aerospace applications, due to the good corrosion resistance of zinc. According to EPA report, the zinc-nickel alloy has better wear resistance than cadmium and the zinc-cobalt alloy acts as a good surface protector when used in atmospheres containing SO_2 [16]. Other attempts to replace the conventional hard chromium deposit include pure nickel [18-23], nickel-cobalt (Ni-Co) [24, 25], nickel-tungsten (Ni-W) [26], cobalt-tungsten (Co-W) [27], nickel-phosphorus (Ni-P) [1, 3, 19, 28, 29], nickel-boron (Ni-B) [30-32] and ternary or quaternary alloys [17]. Among all these options, pure nickel coatings are widely used in surface finishing processes of aluminium and its alloys, ranging from simple application for decorative purposes, to engineering applications for corrosion resistance and wear resistance, when use in hostile environments [18, 33-35].

A nickel coating can be deposited on an aluminium alloys substrate through electrodeposition and electroless techniques, depending on the properties required and applications for the end product. A considerable amount of work has been published on surface modification of aluminium alloy using electroless techniques [1-3, 10, 19, 28-31, 36-39]. However, the electroless technique is more expensive, laborious, time consuming and causes more waste disposal problems than the electrodeposition technique [18, 20]. The electrodeposition technique is a relatively economical and convenient technique which can deposit various types of pure metals, alloys and composites at a high rate of production [34].

Many published studies have explored the reliability of alternative coating materials for replacing cadmium and hard chromium coating on aluminium alloys. However, the most important factor for a successful electrodeposition process is the surface pre- treatment process of the substrate, as this can affect the final properties of the coating.

Extensive research has been carried out in academia and in industry to find the most suitable and effective method of surface pre-treatment on aluminium alloys. The research included direct plating on aluminium alloys [38], a pre-electrodeposition process [5, 28], zincating processes [3, 18-22, 29, 40-46], zincating process with copper pre-treatment [47, 48], and nickel striking [29]. Among these, the most satisfactory and practical method of surface pre-treatment process for plating on aluminium alloys is the zincate immersion treatment, which is known as zincating. Studies have shown that the zincating treatment produces a zinc layer on the surface of the aluminium alloys, thus preventing the formation of aluminium oxide and providing adequate contact with any metal electroplated onto these alloys [1, 49-52].

1.2 Problem Statement

Aluminium is a strong electropositive metal based on its high position in the electromotive force series, thus resulting in a rapid formation of a natural oxide layer when exposed to the air or water [5, 36, 53]. The oxide layer is very persistent and when it is removed, it can immediately re-form [21]. The electrical insulation properties of the oxide layer hinder the metallic bonding from forming in between the metal coating and metal substrate, which leads to a poor adhesion of coating to the substrate. Therefore, aluminium and its alloys require a special surface pre-treatment for a successful electrodeposition process. This is supported by a study by Monteiro et al. [21], which states that surface pre- treatment process is the most important factor for a successful electrodeposition process, as this can affect the final properties of the coating in terms of adhesion. Therefore, an appropriate surface pre-treatment process is essential to obtain high adhesive strength between substrate and coating materials in order to improve the hardness, wear resistance, corrosion resistance, and aesthetic properties of the coating [2, 3, 19].

Zincating is a traditional method of surface pre- treatment in preparing aluminium alloy substrates for electrodeposition process and is mostly used by industry and research institutes to improve the coating adhesion on an aluminium substrate. Zincating is an electrochemical exchange process between zinc complexes in zincating solution and aluminium, depositing zinc crystallites at the expense of aluminium dissolution [54]. The zincated surfaces may then be electroplated with metal materials, such as nickel, copper, or chromium. According to the American Society for Metals (ASM) [53], both the quality and adhesion of a coating depend on the formation of a thin, continuous layer of zinc particles deposited during the zincating process.

Numerous studies of zincating treatment have concluded that the behaviour of the zinc deposits are controlled by the zincating process parameters, such as bath components [2, 55], bath concentration [46, 49-51, 56-59], duration [22, 40-44, 46, 49, 58], temperature [42, 44, 46, 50], number of processes [1-3, 21, 40, 41, 44-46, 58, 60], rotation [50], ultrasonication [22, 54], types of substrate [3, 46, 49] and effect of different conditioning treatments [46]. Most of these studies have only focused on the surface characterization of the zincated aluminium alloys under various zincating

conditions. However, few researchers were able to explain the relationship of the zincating treatment to the final properties of the coating, such as adhesion [1-3, 21, 22, 54].

According to a series of studies done by Hino et al., the adhesion of the Ni-P coatings and aluminium substrates varies depending on the alloying element [1, 3]. Palaniappa et al. [22, 54] and Jin et al. [22] have shown that significant coating adhesion can be attained by applying ultrasonic agitation during the zincating treatment. Their studies showed that a uniform and dense layer of zinc deposit produced by ultrasonic agitation contributed to the improvement of coating adhesion.

Research to date on the zincating process has tended to focus on double zincating treatment rather than a single zincating process. A single zincating process which is involves only one time dipping in the zincating solution for less than 1 minute, resulted in a granular zinc deposition and this surface is not suitable for a subsequent electrodeposition process [1, 3, 40, 41 and 57]. A double zincating process in which the first zincating is followed by zinc stripping in a concentrated HNO_3 solution and then by a second zincating, produces a smooth and uniform zinc deposition layer, leading to strong adhesion between substrate and deposit. One of the most significant discussions in this research is the surface morphology evolution of the zincated samples and the roughening effect due to the dissolution of the substrate in zincating solution at multiple zincating treatment. A number of studies have shown that a dense, thin, uniform and fine grain zinc deposit can be obtained after multiple zincating treatments [1-3, 22, 40, 41, 43, 45, 54, 58, 60]. Murakami et al. ’s [2] and Hino et al. ’s [3] comparative studies on the effect of multiple zincating treatments on coating adhesion found that the surface morphology of the zincated samples played a role in adhesion. They concluded that coating adhesion was improved through double zincating treatments, in which a uniform and dense layer of zinc deposits were obtained, whereas the single zincating treatment resulted in formation of coarse zinc particles with a non-uniform layer which not suitable for subsequent plating process.

However, a number of studies show that the multiple zincating process has several problems such as resulting in a complex process and producing an excess dissolution of aluminium substrate in a concentrated nitric acid solution during the zinc stripping

process [22, 41, 61]. Studies by Arshad et al. [60] and Lin et al. [40] find that the surface of the substrate becomes smoother if the substrate is etched during the zinc stripping process. According to Hutt et al. [41], based on the observation of the aluminium bondpad surface after the zinc stripping process, the zinc particles from the first zincating process are completely removed and revealing the underlying pitting on the aluminium surface. This is supported by a study by Azumi et al. [43] which shows dissolution traces and holes on the substrate surface after the zinc stripping process.

Simultaneously, a multiple zincating process which comprises several dipping processes in the zincating solution requires a larger amount of chemicals because more zincating tanks are needed. Environmental pollution issues may arise due to an increasing amount of chemicals utilized in this process. Based on the material safety data sheet of the chemicals used for making zincating solution, the hazard identification for three out of four chemicals involved are classified according to the Regulation (EC) No. 1272/ 2008 [EU- GHS/ CLP] or EU Directives 67/ 548/ EEC or 1999/ 45/ EC. Under this regulation, three chemicals are classified as very toxic, corrosive and harmful to aquatic organisms which may cause long- term adverse effects in the aquatic environment, they are zinc oxide (ZnO), sodium hydroxide (NaOH) and ferric chloride ($FeCl_3$).

Therefore, this research aimed to improve the conventional single zincating process by producing a homogenous distribution of zinc deposits which cover the whole substrate surface, by extending the immersion duration of the aluminium alloy substrate in zincating solution. According to Yang et al. [45], the zincating duration for single, double or even triple zincating is an important factor in obtaining a thin and uniform zinc deposition on the substrate. A homogenous deposition of zinc particles on the substrate is believed to produce a uniform layer of nickel coating on the substrate, thus, enhancing the adhesion and corrosion resistance of the coating.

Modification of the conventional single zincating process has been made in terms of the immersion duration in order to improve the deposition of the zinc particles on the substrate (Figure 1.1). Selection of immersion duration for the modified single zincating process was based on the electrochemical measurement of the AA7075 substrate in the zincating solution. A double zincating process was also applied to the substrate as a

comparison to the modified single zincating process. In addition, copper activation was applied before the conventional and modified single zincating process, in order to prevent high dissolution of AA7075 in zincating solution. Azumi et al. [61] find that the electrochemical measurement of aluminium alloys in zincating solution shows a continuous dissolution of the substrate during the first and second zincating. The high dissolution reaction of the aluminium substrate in a concentrated alkaline zincating solution may lead to a serious damage of the substrate [62]. The dissolution of substrates and uniform distribution of zinc deposits can be improved by applying a copper pre-treatment before the zincating process [47, 61, 63]. A substitution reaction between aluminium dissolution and copper deposition occurs on the substrate during immersion in an etching solution of sulphuric acid containing low concentration of Cu^{2+} ions [63]. The layer of copper particles then provides nucleation sites for zinc deposition during the subsequent zincating process [47].

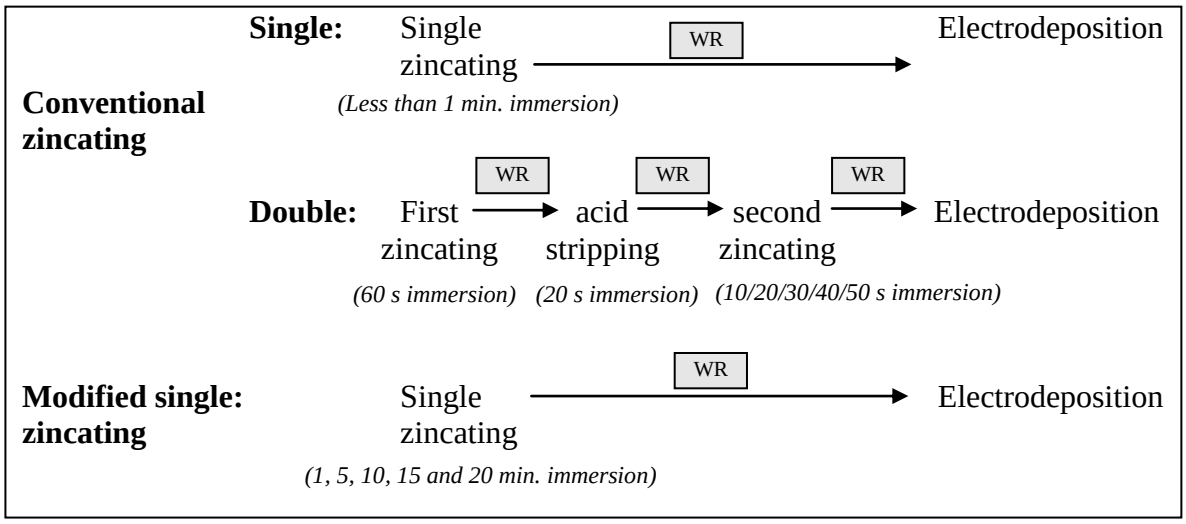

Figure 1-1 Comparison between conventional single and double zincating with modified single zincating process

By doing this modification, the complexity of the double zincating process has been simplified to only single dipping in the zincating solution and the zinc stripping process has been eliminated, thus reducing the amount and quantity of chemicals needed for the zincating process. This will overcome the issues on the waste disposal problem of the chemicals used in the zincating solution and the excess dissolution of the substrate during zinc stripping process.

This research has been divided into three parts; (i) characterization of the surface pre-treated substrates through electrochemistry study; scanning electron microscopy (SEM), energy-dispersive analysis of X-rays (EDX), optical microscopy (OM), and atomic force microscopy (AFM), (ii) electrodeposition of the coatings based on the optimum zincating duration found in stage (i), and (iii) analysis of the nickel coatings electrodeposited during a multiple zincating process with various durations using an adhesion scratch test and corrosion test. The relationship between coating adhesion and corrosion resistance of electrodeposited nickel on AA7075 substrate, and the properties of zincating deposits on AA7075 substrate, are the main focuses in this research.

1.3 Objectives

The present study aims to develop an environmentally friendly and simpler zincating process for aluminium alloys substrate with outstanding adhesion between coating and the substrate, in order to replace the poor adhesion of conventional single zincating process and the complicated double zincating process. In order to obtain the desired coating adhesion and corrosion resistance, the influence of the modified single zincating process on the nickel coatings electrodeposited on AA7075 substrate was investigated.

The objectives of this research are as follows:

i. Investigate the electrochemistry behaviour of the AA7075 substrate in the zincating solution during single zincating, double zincating and single zincating processes with and without copper activation
ii. Find the optimum zincating duration from the electrochemistry measurement of the AA7075 substrate in the zincating solution
iii. Study the microstructural evolution and zinc composition changes of the zincated samples during conventional single zincating with and without copper activation, double zincating and modified single zincating processes with and without copper activation using SEM and EDX

iv. Investigate the surface roughness of the zincated samples after conventional single zincating with and without copper activation, double zincating and modified single zincating process with and without copper activation using AFM

v. Electrodeposit nickel coatings on AA7075 substrate, based on the optimum zincating duration obtained for modified single zincating and double zincating from electrochemistry measurements

vi. Investigate the influence of conventional single zincating with and without copper activation, double zincating and modified single zincating process with and without copper activation on the adhesion and corrosion resistance of the coating, using an adhesion scratch test and corrosion test

vii. Analyze the scratch failure modes using acoustic emission signals, frictional forces and microscopy observations

1.4 Thesis Outline

Chapter 1 introduces the background, problem statement and objectives of the present research. Chapter 2 will provide a literature review of topics related to this research, such as electrodeposition process for surface protection, electrodeposition of nickel coating, electrodeposition on aluminum and its alloys, zincating process and adhesion of coatings. In Chapter 3, the surface pre-treatment procedure, electrodeposition process and characterization techniques and testing will be explained. Chapter 4 will present the results obtained and analysis of the results. Chapter 5 will discuss the results obtained from this research. Finally, Chapter 6 will present the conclusions of the study, while Chapter 7 will describe potential future works and novelties of this research.

2 LITERATURE REVIEW

2.1 Electrodeposition Process for Surface Protection

2.1.1 Introduction

Surface technology may be defined as the application of a metallic or organic coating onto a metallic or non-metallic substrate; or the treatment of a metallic substrate using physical, chemical or mechanical process to enhance the appearance and functional properties of a material.

Surface technology is vital to metallic and non-metallic materials, since they have a limited lifetime which depends on the action of the external factors and operating environment. There will be chemical or electrochemical reactions with the environment which, by attacking the surface, will sooner or later damage functionality and may lead to a catastrophic breakdown. Thus, suitable surface protection is always needed to improve the surface properties of the materials. The main functions of the technical surfaces of a material are minimising corrosion, wear, frictional energy losses, acting as a diffusion barrier, providing thermal and electrical insulation, and improving the aesthetic appearance of the surface [64, 65].

One of the examples of surface protection on material is coating technology, which can has several classifications, such as evaporation, hot metal processes, painting, thermal spraying, and electrochemical techniques (Table 2-1). The following table depicts the diversity of coating processes that can be applied to enhance surface functionality and extend the life of a component or piece of equipment [66]. These different techniques produce distinct coating properties in terms of thickness, hardness, ductility and residual stress [67]. Among these techniques, electrochemical methods are good at controlling the coating thickness and morphology of the deposit [67].

Table 2-1 Coating processes used to protect functional surface (from the Ref. [66])

Process	Process Variants
Evaporation	Chemical vapour deposition (CVD) Physical vapour deposition (PVD) Sputtering
Hot metal processes	Weld- surfacing Hot- dip galvanizing Roll- coating
Painting	Application of inorganic coatings Application of organic coatings Application of low friction coatings
Thermal spraying	Atmosphere-pressure plasma spraying Low-pressure plasma spraying Flame spraying
Electrochemical	Electroless metal coatings Electrodeposition metal coatings

Electrochemistry methods are categorized into three groups, namely electrodeposition, immersion deposition and electroless deposition. An overview of these various electrochemistry methods is given in Table 2-2 [68].

Table 2-2 Comparison of electrochemical methods for metal deposition (from Ref. [67, 68]

Property	Electroplating	Immersion plating	Electroless deposition
Driving force	Power supply	Chemical displacement	Autocatalytic redox reaction
Cathode reaction	$M^{n+} + ne^- \rightarrow M^o$	$M^{n+} + ne^- \rightarrow M^o$	$M^{n+} + ne^- \rightarrow M^o$
Anode reaction	$M^n - ne^- \rightarrow M^o$ or $n/2(H_2O) - ne^- \rightarrow n/4(O_2) + nH^+$	$M_1 - ne^- \rightarrow M_1^{n+}$	$R - ne^- \rightarrow O$
Overall cell reaction	$M_A \rightarrow M_C$ or $n/2(H_2O)+M^{n+} \rightarrow n/4(O_2)+ nH^++M^0$	$M^{n+} + M_1 \rightarrow M + M_1^{n+}$	$M^{n+} + R \rightarrow M^o + O$
Site of cathode reaction	Substrate	Substrate which must remain partially exposed	Substrate which must have a catalytic surface
Site of anode	Separate anode	Substrate which dissolves	Substrate

reaction			
Anode reactant	M or H_2O	M_1, dissolving metal	R, reducing agent in solution
Nature of deposit	Pure metal or alloy	Pure metal, but may be porous and poorly adherent	Usually M contaminated by O- or R- derived species
Typical thickness limit	1- 50 µm	1- 5 µm	1- 100 µm
Applications	Wear surfaces & restore dimensions	Wear surfaces & break-in wear	Wear surfaces

Electrodeposition is a process in which electrons are supplied from an external applied voltage to deposit a thin layer coating of metals or alloys on top of other materials. This improves appearance, corrosion resistance, wear resistance and hardness (or a combination of these factors) by the action of electric current. Electrodeposition of metals and alloys onto substrates in an electrolyte may involve the reduction of metal ions from aqueous, organic, and fused salt electrolytes [69, 70].

Electrodeposition is one of the most complex unit operations due to the involvement of a large number of process steps which control the overall electrodeposition process. For example, metal distribution during the electrodeposition process is related to electrodeposition variables such as dimension and shape of tank and electrodes, bath composition, process conditions, and applied current [68]. There have been many studies investigating electrodeposition process parameters, such as electrolyte type [71-73], deposition technique (direct or pulse plating) [33, 74, 75], pulse parameters [33, 75-81], applied current density in direct current electroplating [82], pH of electrolyte [71, 83], concentration and effect of additives [33, 81-84], and the rotation speed of the electrode [84].

The advantages of this technique include control of coating thickness as a function of time, control of deposition rate by current density, and the ability to stop the electrodeposition process by switching off the current. Disadvantages include the need for power supply, a conducting substrate, and non-uniform current distribution [67]. Electrodeposition processes may also use various types of deposit such as homogenous, dispersed phase, multilayer, patterned, and gradient (Figure 2-1) [67].

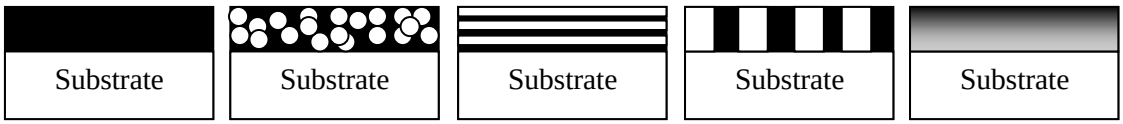

(a) (b) (c) (d) (d)

Figure 2-1 Types of deposits produced from electrodeposition process (a) homogenous, (b) dispersed phase, (c) multilayer, (d) patterned and (e) gradient (from Ref. [67])

Electroless deposition is a process in which the reducing agent in the solution is the electron source [70], while immersion deposition takes place between a solid metal and a metallic ion [67]. Both immersion deposition and electroless deposition techniques do not involve an external current to form a metal coating; however, they are distinguished in that the immersion deposition technique deposition stops when the immersed metal is covered, while electroless deposition continues even after the substrate is covered [67].

Extensive research has proven that the electroless method is highly efficient for obtaining uniform deposits and performs equally well on conducting and non-conducting materials [20, 85]. However, this method is more expensive than electrodeposition, as it is more laborious, takes a longer time to achieve desired thickness of coating deposit and causes a chemical waste disposal problem [18, 20].

2.1.2 Surface Pre- treatment Process for the Electrodeposition

The goal of coating is production of a coating with a good adhesion between the base material (substrate) and the coating material (deposit), thus protecting the substrate in any condition. This high adhesion between substrate and coating material can be achieved through a surface pre-treatment process before subsequent plating. Essentially, the electrodeposition process involves a sequence of important processes, such as pre-treatment process on the substrate surface, coating processes, followed by surface finishing process per Table 2-3.

Table 2-3 Selection of processes which may be involved in electrodeposition process (from Ref. [67, 86]

Process	Type	Description
Mechanical grinding and polishing	Pre-treatment	Eliminate mechanical distorted surface layers
Alkaline immersion	Pre-treatment	Surface wetting, degreasing and cleaning of substrate from foreign contaminants (soil, dirt, tarnish and so on)
Acid immersion	Pre-treatment	Removal of oxide films and surface roughening for keying electrodeposit to substrate
Solvent soak	Pre-treatment	Degreasing and surface cleaning, typically with an organic solvent
Metal strike	Pre-treatment	Formation of a thin metallic base layer. Used when the primary coating material does not easily deposit on to the substrate
Plating	Deposition	Electrodeposition of the coating onto the substrate
Polishing	Finishing	Smoothing or grinding the deposit for aesthetic appeal
Heating	Finishing	Heat treating the deposit to improve characteristics such as hardness
Sealing	Finishing	Application of a secondary electrolytic deposit or lacquer to protect the main deposit

These surface pre-treatment processes require good knowledge and control, since they involve many parameters such as different types of chemical solutions, component concentrations, temperatures, durations, pH, and agitation, all of which can significantly affect the properties of the metal deposit.

2.1.3 Principles of Electrodeposition Process

The electrodeposition process of metallic layers from aqueous solution involves the immersion of two metal electrodes into the electrolyte and a connection to the power supply terminals in order to pass current through the electrolyte. The anode is the

electrode connected to the positive terminal while the cathode is connected to the negative pole. Positive electric current is the flow through the electrolyte from the anode to the cathode. During the electrodeposition process, the deposition of the metallic layers is based on the discharge of metal ions present in the electrolyte at a cathodic surface (also known as substrate or component), in which the ions in the electrolyte move to the opposite charged electrodes. Cations are the positive ions moving to the cathode and anions are the negative ions moving to the anode [66, 87]. At the solid-electrolyte interface, the metal ions accept an electron from the electrically-conducting material and then are deposited as metal atoms on the surface [66, 87]. The metal ions used in this process are supplied by metal salts added to the solution by the sacrificial anodes. This process involves a dissolution of an anode made of the same metal to be deposited on the cathode [66]. A schematic diagram of the process is shown in Figure 2-2.

The process of electrodeposition of metal (*M*) is represented by [70]:

$$M^{z+}{}_{\text{(solution)}} + ze \xrightarrow{\text{electrode}} M_{\text{(lattice)}} \qquad (2\text{- }1)$$

During the electrodeposition process, *z* electrons are supplied by an external power supply.

During the electrodeposition process, the current density, as defined in Equation 2- 2, and its distribution play an important role in determining the quality of the final deposit [70]:

$$J = d_i / d_s \qquad (2\text{- }2)$$

where J is the magnitude of the current density, d_i is the current impinging on d_s, which is an element of cathode surface area.

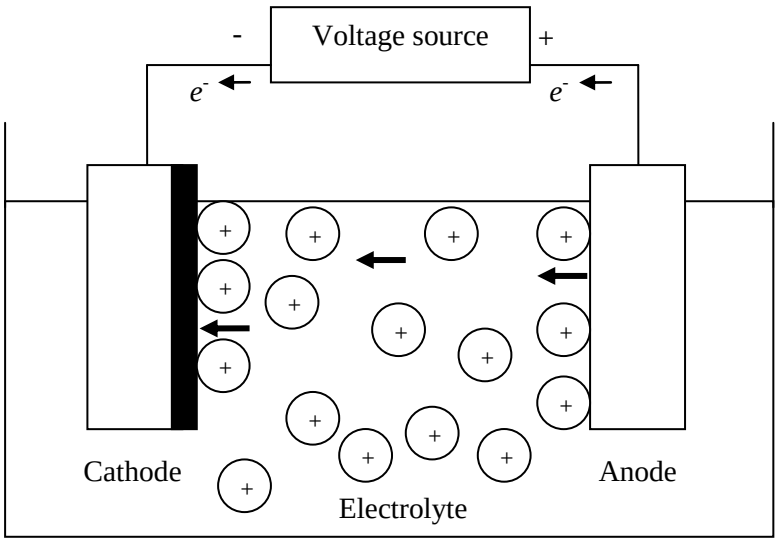

Figure 2-2 An electrolytic cell for electrodeposition of metal from an aqueous solution

Electrodeposition is a complex process involving several stages as follows. The steps are illustrated in Figure 2-3 [66]:

(1) Transport of the hydrated metal ion or complex from bulk solution to the cathode
(2) Stripping the hydration sheath from the metal ion at the metal- solution interface
(3) Charge transfer with formation of adsorbed atom at the cathode surface
(4) Formation of crystal nuclei through diffusion of adsorbed atoms at the cathode interface
(5) Fusion of thermodynamically stable crystal nuclei to form a metallic layer

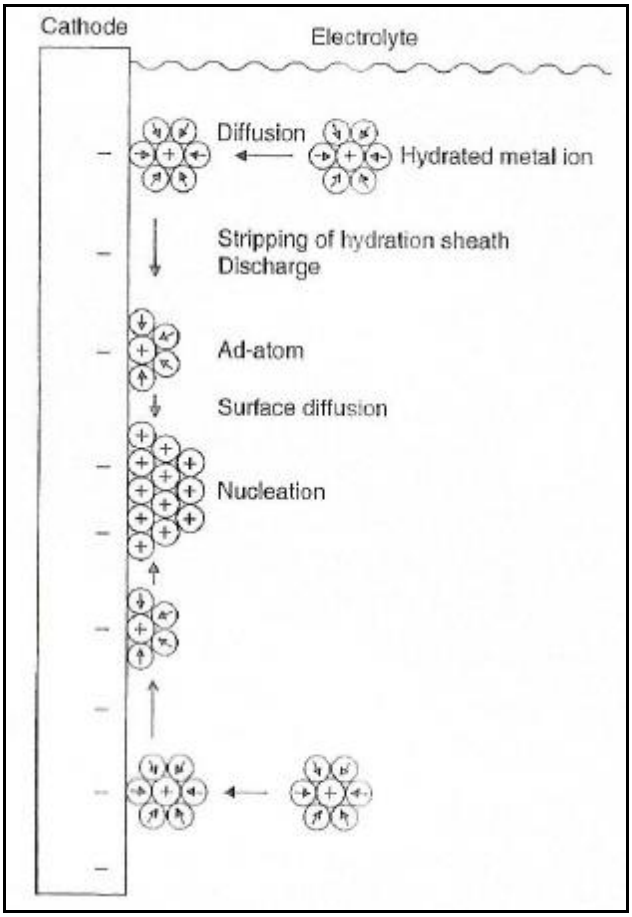

Figure 2-3 Illustration of several stages in electrodeposition process, (1) migration of hydrated metal ions to a cathode, (2) surrender of the hydration sheath, (3) formation of adsorbed atoms and (4) formation of crystal nuclei at the cathode surface [66]

During electrodeposition, the transportation of the metal ions from the bulk solution to the cathode is obtained by migration, convection and diffusion. This process begins with ionic migration, in which the hydrated ions in the electrolyte migrate toward the cathode under the influence of the applied potential as well as through diffusion and/ or convection [88]. Then, during electron transfer the hydrated metal ions enter the diffusion double layer at the cathode surface area, where the water molecules of the hydrated ion are aligned by the field present in this field. At the cathode surface, the individual ion may be neutralized and adsorbed as the metal ions enter the fixed double layer due to the higher field present and the hydrated shell is lost. Next, nucleation and growth (also known as electrocrystallization) must occur to form a coherent coating on the substrate [66]. The nucleation process occurs due to the diffusion-controlled

migration of the adsorbed atoms on the surface, while the growth process begins once the nuclei have reached critical size.

Until quite recently, the electrodeposition process has been carried out using direct current (DC), in which two electrodes are immersed in a solution and connected to the output of a DC current source. Due to the limitations of the direct current plating, pulse current (PC) plating, which has been intensively investigated in recent years, has been considered a possible alternative plating method [33, 77, 80, 89-91]. Improved properties of PC coatings were illustrated in research by Chang et al. [90] on the effects of different plating modes on microstructure and corrosion resistance of Zn-Ni alloy coatings. They found that the grain size of the coatings deposited by PC was smaller than DC; thus, coating deposited by PC had the highest corrosion resistance, as corrosion resistance is related to the grain size of the coatings.

More recently, the benefits of using interrupted current have become clear. These benefits were supported in one study which demonstrated that the application of pulse current electrodeposition drastically affects the structural characteristic and properties of the deposits. This may lead to the preparation of nanostructured materials with improved mechanical properties [74].

2.1.4 Properties of Electrodeposited Materials

A typical engineering coating should be uniform, compact and fully cover the substrate surface evenly. For decorative purposes, the coating surface must be smooth and defect-free with a mirror-like finish. Some electrodeposition processes may lead to electrodeposited coating materials with an unacceptable surface with, for example, pits, crack, voids and delamination. They are influenced by numerous process variables such as electrolyte pH, electrolyte temperature, chemicals concentration, current density, electrolyte type, electrical current mode, electrolyte additives, substrate conditions and surface pre-treatment process. Material performance depends on their properties; these properties in turn depend on their atomic structure, composition, microstructure, defects, and interfaces [92].

The following section will discuss the properties of metal coatings, including visual appearance, structure, thickness and hardness.

Visual Appearance

Visual appearance is an important property for quality control of coating materials. It relates to coating surface finish and coating defects like blisters, scratchers, unplated areas, pits, defective buffing and delamination. These properties are typically evaluated through visual examination in terms of size, shape and spacing of the irregularities of the coating surface, as well as smoothness and brightness. Nickel and nickel alloys with matte or dull finishes are deposited on substrates in order to improve corrosion and wear resistance or modify magnetic and other properties [88]. Surface smoothness is related to the surface irregularities of the coating materials and can be measured using various microscopic techniques, including direct surface observation, cross-sections, and taper sections [69]. However, brightness, smoothness and defect-free surface are imperative in decorative applications but are not inclusively for functional applications.

Structure

Structure can be defined as the arrangement of the internal components of electron structure (on a subatomic level), crystal structure (on an atomic level) and microstructure (on a microscopic level) [93]. SEM is typically used to reveal the structure of electrodeposits. There are a few advantages offered by SEM compared to optical microscope such as large depth of field, better resolution and the ability to perform elemental analysis or chemical characterization of a sample with the assistance of EDX attached to a scanning electron microscope. Khan et al. [19] studied the morphology of the electroless Ni-P coating on aluminium alloys as a function of electroless deposition duration. They found that the nickel-phosphorus grain growth continues until nickel has been deposited on almost the entire substrate surface within 4 minutes of deposition (Figure 2-4).

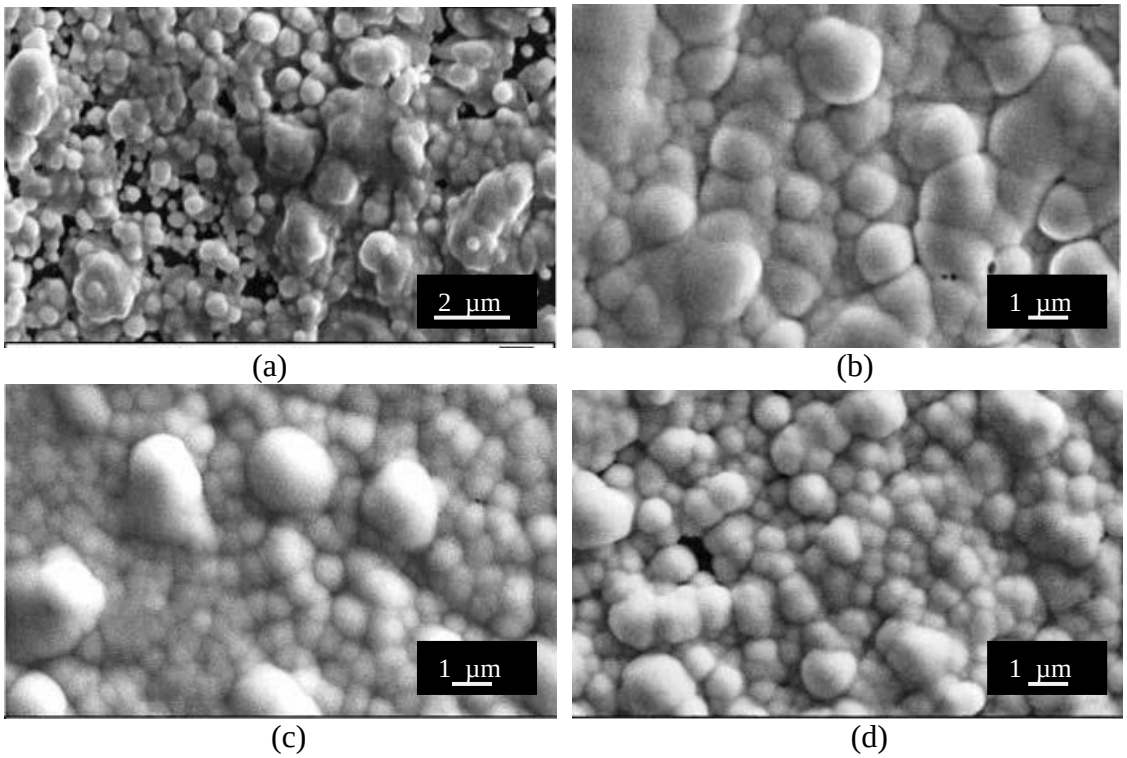

Figure 2-4 Scanning electron micrographs of electroless Ni-P layers on aluminium alloys at respective electroless duration (a) 1, (b) 2, (c) 3 and (d) 4 minutes (from Ref. [19])

Thickness

Coating thickness is one of the basic physical properties of a coating. Awareness of the thickness of coating, a suitable load and indenter for the hardness test can be determined, in order to prevent failure on the coating during indentation. The thickness of the coating can be measured from the distance between two points. The cross-section microscopy technique, which involves typical metallographic procedures such as cutting, mounting, grinding, polishing and etching of the sample is the simplest method in thickness measurement. Using this technique, the coating thickness produced is determined from a magnified image of a cross-section of the coated specimen. An example of thickness measurement from SEM micrograph is shown in Figure 2-5 [18].

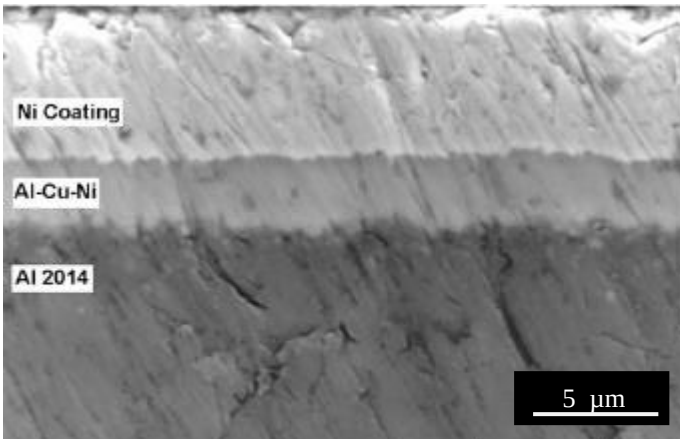

Figure 2-5 Cross-section of nickel coating electrodeposited on an Al 2014 alloy (from Ref.[18])

Hardness

Hardness measurements are quite useful since they are an indication of strength, ductility and wear resistance of electrodeposits. This can be easily measured using microhardness tests, such as Vickers and Knoop test. This test involves making an indentation on the coating material using a suitable indenter with a specified geometry under a specific load. The diagonal of the indentation is measured with a microscope to calculate the hardness value. The hardness test must be done on a smooth and shiny coating surface, so that the tiny indentation can be measured at high magnification. Besides that, the coating thickness should be about 15 times the depth of the indentation in order to avoid any effects of the substrate [69].

Corrosion resistance

Corrosion is defined as a material or metal deterioration or surface damage in an aggressive environment, which involves electrolytes as they have their own conductivity for electron transfer [94]. Corrosion is an electrochemical process in which a chemical reaction occurs due to electron transfer from one chemical species to another species [93]. In surface engineering purposes, a metallic coating is one of the techniques used to prevent corrosion on substrate. According to [68], metallic coatings protect metallic substrates in three ways, namely (i) cathodic protection, provided by a sacrificial corrosion of coating, such as cadmium on steel; (ii) barrier action, using a

more corrosion resistance deposit between the environment and the substrate to be protected; and (iii) environmental modification or control. Tang et al. [95] found in their research that the aluminium coating deposited on AZ91D magnesium substrate through a combination of bipolar current pulse (BCP) polarization technique and zincating process improves corrosion resistance. This is due to the formation of a dense and packed structure of aluminium coating, as shown in Figure 2-6.

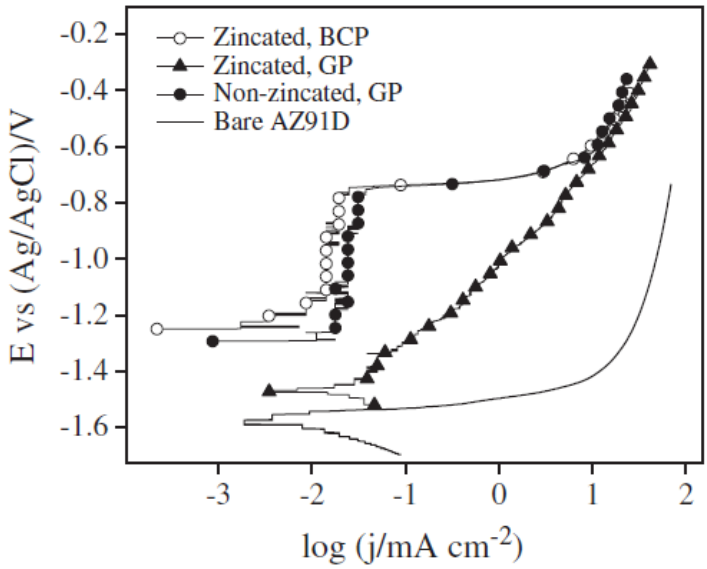

Figure 2-6 Potentiodynamic polarization curves obtained from the corrosion test of the aluminium coatings deposited on AZ91D magnesium alloy produced using BCP and GP methods with and without zincating process in 3.5 wt.% NaCl solution (from the ref. [95])

2.1.5 Factors Influencing the Properties of Electrodeposited Materials

Electrodeposition process parameters influence the properties of the deposited material. Important process parameters include current density, temperature, metal concentration, addition agent, type of bath and rotating electrode. Two basic aspects controlling the deposit are (1) the rate of formation of metal nuclei on the cathode surface and (2) the rate of growth of these nuclei [87]. Each parameter that one chooses will influence other factors [34, 78, 81, 96]. Following are factors which influence the properties of the coating materials:

Current Density

At low current density, deposits have a coarse grain due to the longer time for the metal nuclei to grow, while high current density produced deposits with fine-grain metal [87]. Rasmussen et al. [72] demonstrated that at low current density, 0.5 A/dm^2 (Figure 2-7(a)), the nickel layer has a rough surface topography, compared to a higher current density (20 A/dm^2), for which the nickel layer appeared as a small grains within the bulb- shape (Figure 2-7(b)).

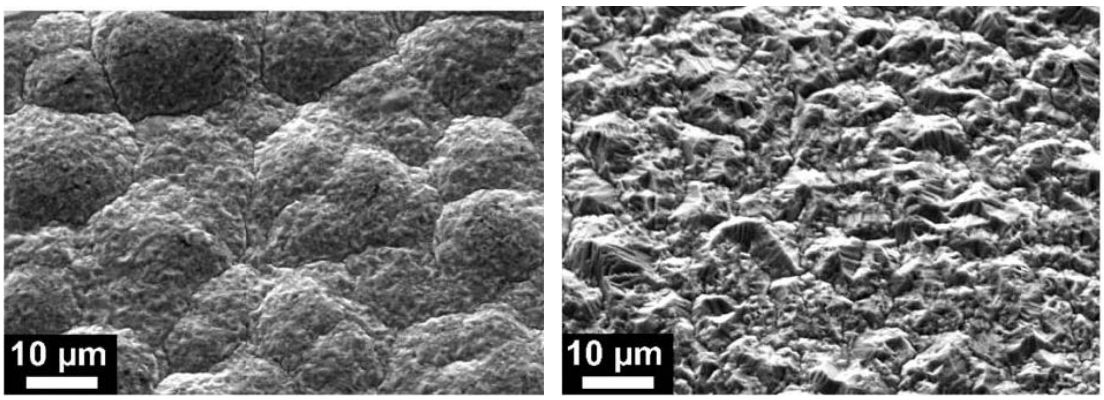

(a) (b)

Figure 2-7 SEM micrographs showing the topography of 100 µm thick nickel layers deposited at 323 K and at various current densities, (a) 0.5 A/dm^2 and (b) 20 A/dm^2 (from Ref.[72])

Temperature

Effective control of the deposition process operating temperature contributes to the consistent performance of a deposition bath. According to Paunovic et al. [70], deviations of more than 5°C from the optimum temperature of a deposition bath are sufficient to harm deposit quality and the properties. They reported that an increase in deposition rates, an improvement in anode corrosion, and ability to operate more dilute baths without loss of performance could all be obtained at high operating temperatures. Parthasaradhy [87] reported that an electrodeposition process using the combination of high current density and high temperatures (within limits) yielded good deposits.

Metal Concentration

The main component in a deposition bath is the metal salt from the desired metal to be deposited over the substrate. According to Lowenheim [69], alloy deposits are denser, harder, and more corrosion resistant in certain composition ranges, as well as being more protective of the basis metal, tougher, stronger, wear-resistant, better in terms of magnetic properties, suitable for subsequent electroplate overlays and conversion chemical treatments, and superior in antifriction compared to pure metals deposits.

Among the various types of coating alloys, Ni-B alloy coatings are promising due to their high hardness and superior wear resistance. Bekish et al. [97] reported that an increase of the boron content in the homogeneous nanocrystalline Ni-B coatings led to a significant increase in their microhardness and wear resistance, as well as decrease in coefficient of friction.

Addition agent

The use of additives in aqueous electrodeposition solutions plays an important role in influencing the kinetics of electrodeposition and the growth mechanism by changing the concentration of growth sites on a surface, the concentration of adions on the surface, the diffusion coefficient *D*, and the activation energy of surface diffusion of adions [88]. There are some important benefits of additives, such as brightening the deposits, reducing grain size, increasing the current density range, promoting levelling, changing mechanical and physical properties, reducing stress, and reducing pitting [68].

pH of the Electrolyte

The pH of electrolyte is influenced by a range of factors and bath additions, including hydrogen discharge potential, the precipitation of basic inclusions, the composition of the complex or hydrate from which the metal is deposited and the extent of adsorption of addition agents [69]. Electrolyte pH is an important factor in the

electrodeposition process, influencing the efficiency and physical properties of the deposits. Parthasaradhy [87] mentioned that electrodeposition carried out outside the recommended pH range will produce deposits with pitting, cracking or curling, and that a pH below optimum may lead to hydrogen evolution and a consequent decrease in metal deposition efficiency. This may lead to an accumulation of hydroxyl ions in the vicinity of the cathode and consequent precipitation of basic salts, altering deposit properties [87].

2.2 Electrodeposition of Nickel Coating

2.2.1 Introduction

Nickel is one of the most important metals applied by electrodeposition for both decorative and protection applications due to being bright, non-tarnishing, hard, corrosion-resistant and wear-resistant. Properties of the electrodeposited nickel are influenced by the electrodeposition process parameters, such as components concentration, electrolyte type, electrolyte pH, electrolyte temperature, electrolyte duration, addition of additives, current density and others. Besides, surface pre-treatment before subsequent plating on the substrates, especially from light metal alloys group, must be always considered. A cleaned surface is needed for the electrodeposition process in order to produce good adhesion between coating materials and the substrate. Nickel coating is extensively used on the exteriors of bumpers, rims, exhaust pipes in the automotive industry, bicycles, motorcycles, hand tools and household items including lighting, plumbing fixture, wire racks, and appliances.

2.2.2 Fundamentals of Electrodeposition of Nickel

The fundamentals of the electrodeposition process were discussed in Section 2.1.3. In this section we will consider in more detail the electrodeposition of nickel. During the nickel electrodeposition process, nickel salt is well dissolve in water and then exists as bivalent ions within the solution [64]. At the cathode, Ni^{2+} is reduced to

metallic nickel by gaining two electrons (Equation 2-4), while at the anode, metallic nickel is oxidised to Ni^{2+} by losing two electrons (Equation 2-5) [64]:

$$Ni^{2+} + 2e \longrightarrow Ni \qquad (2\text{-}4)$$

$$Ni \longrightarrow Ni^{2+} + 2e \qquad (2\text{-}5)$$

2.2.3 Faraday's Law for Nickel Coating

The amount of nickel deposited at the cathode and the amount dissolved at the anode are directly proportional to the product of the current and time, per Faraday's law [88]:

$$M = 1.095 \text{ x } a \text{ x } I \text{ x } t \qquad (2\text{-}6)$$

where:

M = amount of nickel deposited at the cathode (or dissolved at the anode) (grams)

I = current that flows through the plating tank (amperes)

t = time that the current flows (hours)

a = current efficiency ratio

In most cases, anode efficiency for nickel dissolution is almost always 100% under practical electrodeposition conditions, which gives a = 1, while cathode efficiency of different nickel plating solutions may vary from 90 to 97%. Accordingly, a will vary from 0.90 to 0.97 [88]. During the electrodeposition process, a small percentage of the current is consumed by the discharge of hydrogen ions from water, which reduces the cathode efficiency of nickel deposition from 100% to approximately 96% in an additive-free nickel electrolyte [88]. At the cathode surface, bubbles of hydrogen gas are formed from the discharged of hydrogen atoms. Mirror-like deposits with less than 12 µm thickness can be readily produced at 90% cathode efficiencies for bright nickel plating solutions [88].

2.2.4 Functions of Constituents in the Watts Bath and Deposit Properties

A nickel deposit can be produced through electrodeposition from a Watts bath containing nickel sulphate, chloride ion, boric acid and anti-pitting agent. These main components in a Watts bath affect the properties of electrodeposited nickel. Nickel sulphate is a source for the nickel ion, while chloride ions improve anode dissolution by reducing polarization, boric acid acts a buffer which controlling the pH in the cathode film, and anti-pitting agent prevents pitting from occurring on the deposit [69]. In addition, chlorides also increase the internal stress of the deposits, refine the grain size and minimize formation of nodules and trees [88]. According to Schlesinger [88], the pitting problem can be prevented by adding the anionic wetting agents or surfactants (anti-pitting agent), which may lower the surface tension of the plating solutions such that air and hydrogen bubbles do not cling to the parts being plated.

Boric acid is always used as a buffer in nickel or nickel alloys electrodeposition process due to excellent buffering, surface activity and resistance to hydrogen evolution reaction, suppress nickel hydroxide precipitation and change the compositions of deposited alloy [69, 98]. At the same time, boric acid may also affect the appearance of the deposits, as deposits may be cracked and burnt at low concentrations [88].

Besides Watts's baths, electrodeposition of nickel can be carried out using other type of solutions, such as sulfamate, basic semi-bright, fluborate, hard nickel, all chloride, all sulphate, sulphate/ chloride, high sulphate, black nickel, and nickel phosphorus. Different composition, pH, temperature and current density ranges of these various solutions will produce electrodeposited nickel with different performance in terms of mechanical properties, such as hardness, tensile strength, elongation, and internal stress. Among all these options, Watts and sulfamate solutions are the most popular solutions for functional applications purpose and the typical formulations and properties are shown in Table 2-4 [99]. The typical semi-bright solution is the modification solution from the Watts solution.

Table 2-4 Types of nickel electroplating solution and some deposits properties (from the Ref. [99])

	Watts nickel	Nickel sulfamate	Typical semi-bright bath
Electrolyte composition (g/l)			
Nickel sulphate ($NiSO_4.6H_2O$)	225 to 400		300
Nickel sulfamate ($Ni(SO_3NH_2)_2$		300 to 450	
Nickel chloride ($NiCl_2.6H_2O$)	30 to 60	0 to 30	35
Boric acid (H_3BO_3)	30 to 45	30 to 45	45
Operating conditions			
Temperature (ºC)	22 to 66	32 to 60	54
Agitation	Air or mechanical	Air to mechanical	Air to mechanical
Cathode current density (A/dm2)	3 to 11	0.5 to 30	3 to 10
Anodes	Nickel	Nickel	Nickel
pH	2 to 4.5	3.5 to 5.0	3.5 to 4.5
Mechanical properties			
Tensile strength (MPa)	345 to 485	415 to 610	
Elongation (%)	10 to 30	5 to 30	8 to 20
Vickers hardness (100 gram load)	130 to 200	170 to 230	300 to 400
Internal stress (MPa)	125 to 185 (tensile)	0 to 55 (tensile)	35 to 150 (tensile)

2.3 Electrodeposition on the Substrate of Aluminium and its Alloys

2.3.1 Introduction

Aluminium and its alloys are widely used in aerospace and automotive applications due to their superior particular properties, such as low density, good appearance and corrosion resistance. Aluminium is generally stable in air and aqueous solutions due to the formation of a thin, protective oxide surface layer, although pores and other defects may initiate localized corrosion [4].

The electrodeposition technique has been used in the surface treatment industry to produce wear resistance coatings on aluminium alloy components. However, a specific surface pre-treatment is required before any plating can be carried out on the aluminium

alloys substrate. The instantly formed aluminium oxide film (as thin as a few nm) prevents a good adhesion between coating and aluminium.

2.3.2 Properties of Aluminium and Its Alloys

Aluminium in its pure state has a relatively high corrosion resistance and low density of approximately 2.7 g/ cm^3 (compared to steel with 7.9 g/cm^3), but is a relatively soft metal with yield strength of only 34.5 MPa and a tensile strength of 90 MPa [93, 100]. Therefore, aluminium is typically alloyed with other elements and heat treated in order to obtain higher mechanical strength. Types of improvement in the aluminium properties through alloying elements and heat treatment can be seen in Table 2.5.

Table 2-5 Properties of selected aluminium and its alloys at room temperature (from ref. [101])

Alloy	Main Alloying element	Temper	Ultimate tensile strength (MPa)	Yield strength (MPa)	Elongation in 50 mm (%)	Properties
1100	Pure aluminium	O	90	35	35-45	Excellent corrosion resistance, high electrical and thermal conductivity, good workability, low strength, not heat treatable
		H14	125	120	9-20	
2024	copper	O	190	75	20-22	High strength to weight ratio, low corrosion resistance, heat treatable
		T4	470	325	19-20	
3003	manganese	O	110	40	30-40	Good workability, moderate strength, not generally heat treatable
		H14	150	145	8-16	
5052	magnesium	O	190	90	25-30	Good corrosion resistance and weldability, moderate to high strength, not heat treatable
		H34	260	215	10-14	
6061	Magnesium and silicon	O	125	55	25-30	Medium strength, good formability, machinability, weldability, corrosion resistance, heat treatable
		T6	310	275	12-17	
7075	Zinc	O	230	105	16-17	Moderate to high strength, heat treatable
		T6	570	500	11	

However, aluminium and its alloys have low hardness and poor tribological properties. According to Sun [102], a coating system with good adhesion to the substrate can significantly enhance the surface hardness and tribological properties of the aluminium and its alloys by reducing the friction coefficient and increasing wear resistance.

2.3.3 Problems Associated with Electrodeposition on Aluminium and Its Alloys Substrates

Several factors contribute to the difficulties plating on aluminium [5].

(1) The amphoteric nature of the oxide layer on aluminium substrates, which complicates possible reactions during the surface preparation or subsequent plating.

(2) The position of aluminium in the Electromotive Force (EMF) series may lead to the ready formation of immersion deposits in plating electrolyte, thus affect the adhesion of coating (Table 2-6).

(3) A difference in coefficient of expansion of aluminium and its alloys with the metal coatings may cause sufficient strain to rupture the bond between the substrate and the coatings (Table 2-7).

(4) The difference in atomic diameter and crystal lattice structure between the aluminium substrate and the metal coatings (Table 2.8).

Table 2-6 The standard electromotive force (EMF) table (from the Ref. [5])

	Electrode Reaction	Standard Electrode Potential (V)
Increasingly inert (cathodic) ↑	$Au^{3+} + 3e^- \rightarrow Au$	+ 1.420
	$O_2 + 4H^+ + 4e^- \rightarrow 2H_2O$	+ 1.229
	$Pt^{2+} + 2e^- \rightarrow Pt$	~ + 1.2
	$Ag^+ + e^- \rightarrow Ag$	+ 0.800
	$Fe^{3+} + e^- \rightarrow Fe^{2+}$	+ 0.771
	$O_2 + 2H_2O + 4e^- \rightarrow 4(OH^-)$	+ 0.401
	$Cu^{2+} + 2e^- \rightarrow Cu$	+ 0.240
	$2H^{2+} + 2e^- \rightarrow H_2$	0.000
	$Pb^{2+} + 2e^- \rightarrow Pb$	- 0.126
	$Sn^{2+} + 2e^- \rightarrow Sn$	- 0.136
	$Ni^{2+} + 2e^- \rightarrow Ni$	- 0.250
Increasingly active (anodic) ↓	$Co^{2+} + 2e^- \rightarrow Co$	- 0.277
	$Cd^{2+} + 2e^- \rightarrow Cd$	- 0.403
	$Fe^{2+} + 2e^- \rightarrow Fe$	- 0.440
	$Cr^{3+} + 3e^- \rightarrow Cr$	- 0.744
	$Zn^{2+} + 2e^- \rightarrow Zn$	- 0.763
	$Al^{3+} + 3e^- \rightarrow Al$	- 1.662
	$Mg^{2+} + 2e^- \rightarrow Mg$	- 2.363
	$Na^+ + e^- \rightarrow Na$	- 2.714
	$K^+ + e^- \rightarrow K$	- 2.924

Table 2-7 Mean coefficient of linear expansion of the common metals (from the Ref. [5])

Metal	x 10^{-6} m/ (mK)
Chromium	7
Steel	11
Nickel	13
Gold	14
Brass	18
Copper	18
Silver	19
Aluminium	24
Tin	27
Zinc	27
Cadmium	31

Table 2-8 Metals for possible direct deposition on aluminium (from the Ref. [5])

Metals for possible direct deposition on aluminium

(Based on Schwartz and Newkirk[7])

Element	*Crystal structure*	*Lattice parameter* Å	*Atomic diameter* Å	*Valence*	*Solid solubility in Al*	*Plating process*	*Adhesion of plating on Al*
Al	fcc	4.0413	2.8577	3	–	–	–
Cu	fcc	3.607	2.551	1,2	0.1%	I*	poor
Ag	fcc	4.077	2.883	1	1.0%	–	–
Au	fcc	4.070	2.878	1	nil	–	–
Zn	cph	2.660	2.660	2	2.0%	I & E	good
Cd	cph	2.973	2.973	2	nil	I	poor
Sn	diamond tetragonal	6.476 5.830	2.804	2,4	nil	I	fair
Pb	fcc	4.940	3.493	2	nil	–	–
Cr	bcc	2.879	2.493	3,6	0.07%	E	good
Fe	bcc	2.861	2.477	2,3	nil	I	poor
Ni	fcc	3.517	2.487	2	0.005%	I	poor
Alloys							
Cu-Zn 70-30	fcc	3.693			0.2%	I	good
Zn-Ni 94-6	cph					I	good
Cu-Sn 70-30	fcc & orthogonal					I	good
Cu-Pb 80-20	fcc					E	–

*I = Immersion; E = Electroplating

2.3.4 Classification of Methods for Electrodeposition on Aluminium and Its Alloys

Protective finishes are applied on aluminium and its alloys' surfaces in order to enhance their surface properties and broaden their application. There are many choices of finishes to be used on aluminium and its alloys, which depends on operational environment, appearance desired, compatibility of the finishes to the alloys, processing cost, and technical requirements (such as abrasion resistance, formability, electrical resistance, corrosion resistance, wear resistance and so on). The finishes are classified into several types as follows (Table 2-9):

Table 2-9 Various types of finishes (from the Ref. [100])

Finishes	Details	Application
Chemical conversion coating	Thin oxide, phosphate films, chromate films	Light service condition Basis for application of paint and others organic coatings
Anodic oxidation coatings	Electrochemically produced oxide coatings, with a wide range of thickness, corrosion protection, colour, hardness, optical and electrical properties	Used when maximum protection is required
Organic finishing	Paint, lacquer, resin	Great flexibility in finish, colour, corrosion resistance and functional properties
Vitreous enamel finishes	Limited range of coloured finishes	Hollow ware and building
Electroplated finishes	Various range of metals coating, such pure metal, alloy and composite	Decorative and functional properties

In order to apply these finishes onto the aluminium and its alloys, special surface pre- treatment process is needed. There are many methods which have been proposed for producing a surface finishes on aluminium and its alloys and they are classified as follows (

Figure 2-8) [5, 69]. Among these methods, the zinc immersion procedure or zincating process is considered the most practical and economical process and has a wide commercial application [29, 55, 69, 103-106].

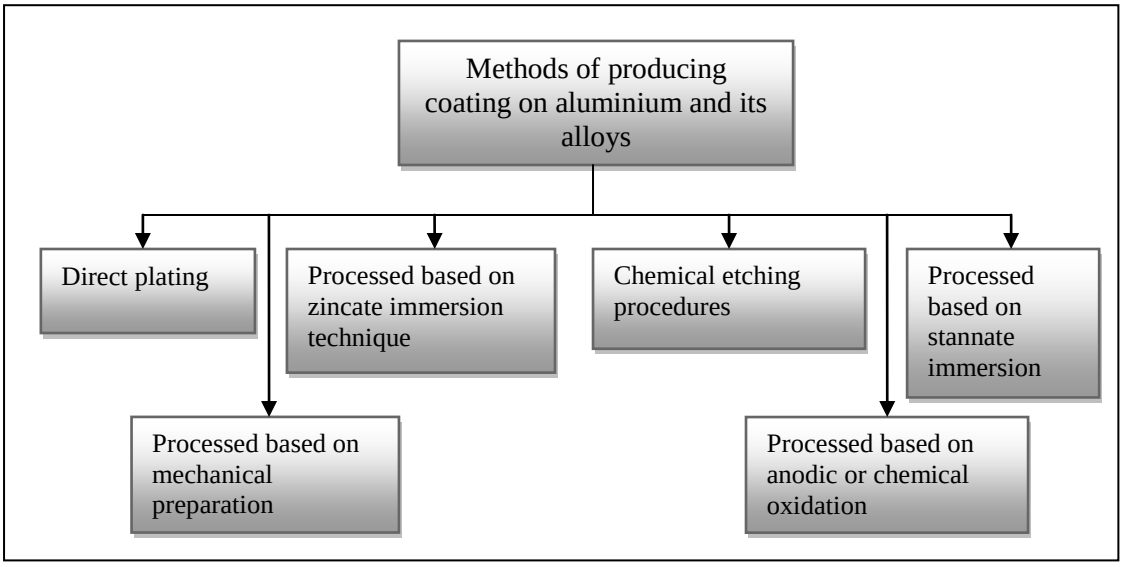

Figure 2-8 Methods of producing coatings on aluminium alloys

2.3.5 Preparation of Aluminium and Its Alloys Surfaces before Electrodeposition Process

Preparation of aluminium and its alloys prior to the electrodeposition process is very important and is typically more difficult than other metals. This is due to the oxide film which form on aluminium at room temperature at about ten times thicker than the film formed on iron under dry air, and which can be regenerated [107]. In addition, aluminium spontaneously forms a thin amorphous Al_2O_3 layer with approximately 2 to 4 nm of thickness when in contact with air or water, due to its affinity for oxygen [36]. In order to obtain a good adhesion between the coating and the aluminium substrates, the aluminium oxide layer has to be removed using suitable pre-treatment procedures. Basically, the preparation of an aluminium alloys surface involves a series of operations including mechanically grinding, cleaning and degreasing in organic solvent solutions or alkaline cleaners and acid cleaning (pickling) [21, 46, 108].

To obtain consistently good results with zinc immersion procedures, a surface preparation of uniform activity for deposition is required. Vapour degreasing or solvent cleaning followed by alkaline cleaning is used for removing oil, grease and other soils

[108]. After alkaline cleaning, the material is further treated to remove the original oxide film as well as any micro constituents which may interfere with the formation of a continuous film or which may react with subsequent plating solutions.

Though the oxide film on aluminium and its alloys can be removed by alkaline and acid cleanings, it may still be reformed during or after completion of the cleaning process [46]. However, according to Keller et al. [46], the oxide layer should be thinner and uniform and provide a more active surface for deposition of the zinc deposits.

After removing the natural oxide layer on the aluminium and its alloys, the activation process such as zincating, copper strike [47], nickel strike [28, 29], or hypophosphite adsorbed layer [29] can be carried out on the cleaned specimens. Many process parameters can vary in alkaline cleaning, acid cleaning and zincating process, such as types of solution, chemical composition, bath temperature, agitation and durations of the processes. All these parameters may influence the properties of the deposits produced.

According to ASM standard on 'Surface Engineering of Aluminium and Aluminium Alloy' [108], several methods or sequences are available for accomplishing these surface pre-treatment processes depending on the type of aluminium alloys. Figure 2-9, Figure 2.10 and Figure 2.11 show a variety of surface pre-treatment procedures, pre-treatment solutions with chemical composition, operating temperature and operating duration for wrought and cast aluminium alloys [108]. If necessary, the material goes through the copper strike process as an initial strike before any other metals are subsequently deposited. The advantage of the copper strike is to protect the thin zinc film from attack by the plating solution. Penetration of the zinc film and attack of the underlying aluminium surface by the plating solutions may result in poorly-bonded electrodeposit [108].

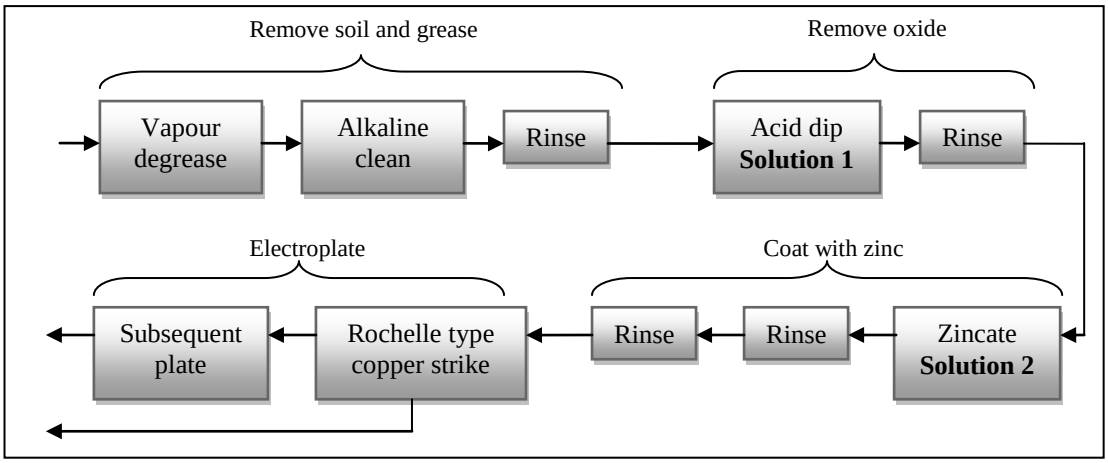

Solution No.	Type of solution	Composition	Amount	Operating temperature (ºC)	Cycle time (seconds)
Alloys 1100 and 3003					
1	Acid dip	HNO_3	50 vol%	Room	15
2	Zincating	NaOH	525 g/l	16- 27	30- 60
		ZnO	98 g/l		
Alloys 413, 319, 356 and 380					
1	Acid dip	HNO_3	75 vol%	Room	3- 5
		HF	25 vol%		
2	Zincating	NaOH	525 g/l	16- 27	30 max
		ZnO	98 g/l		

Figure 2-9 Surface pre- treatment procedures for wrought aluminium alloys that contain high amount of silicon or do not contain interfering microconstituents (1100 and 3003) and for aluminium casting alloys 413,319,356 and 380 (from the Ref. [108])

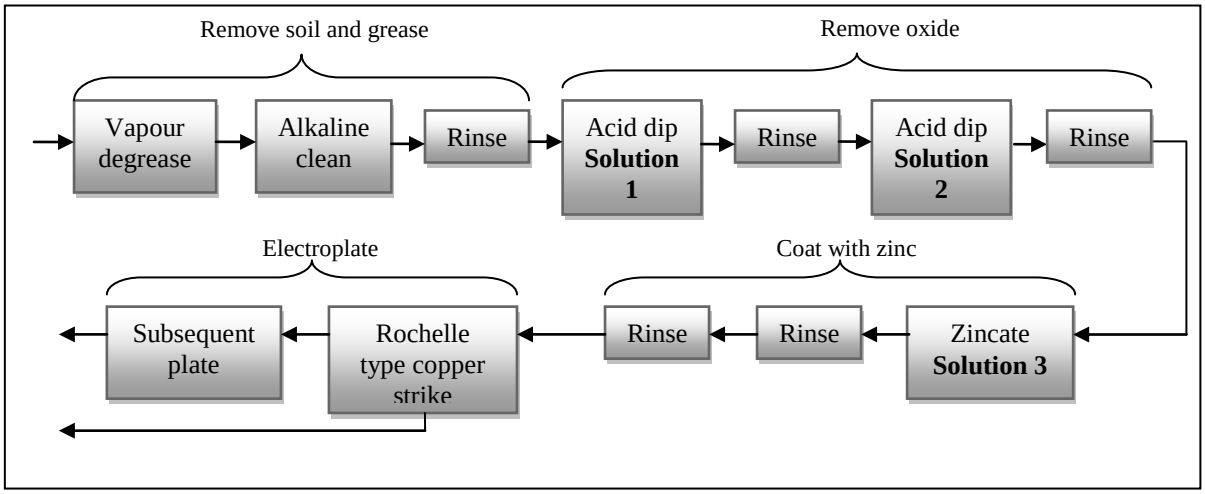

Solution No.	Type of solution	Composition	Amount	Operating temperature (ºC)	Cycle time (seconds)
1	Acid dip	H_2SO_4	15 vol%	85	120- 300
2	Acid dip	HNO_3	50 vol%	Room	15
3	Zincating	NaOH	525 g/l	16- 27	30- 60
		ZnO	100 g/l		

Figure 2-10 Surface pre-treatment procedures for all wrought aluminium alloys, for most aluminium casting alloys and for magnesium-containing aluminium alloys with interfering microconstituents (1100, 3003, 3004, 2011, 2017, 2024, 5052, 6061, 208, 295, 319 and 355) (from Ref. [108])

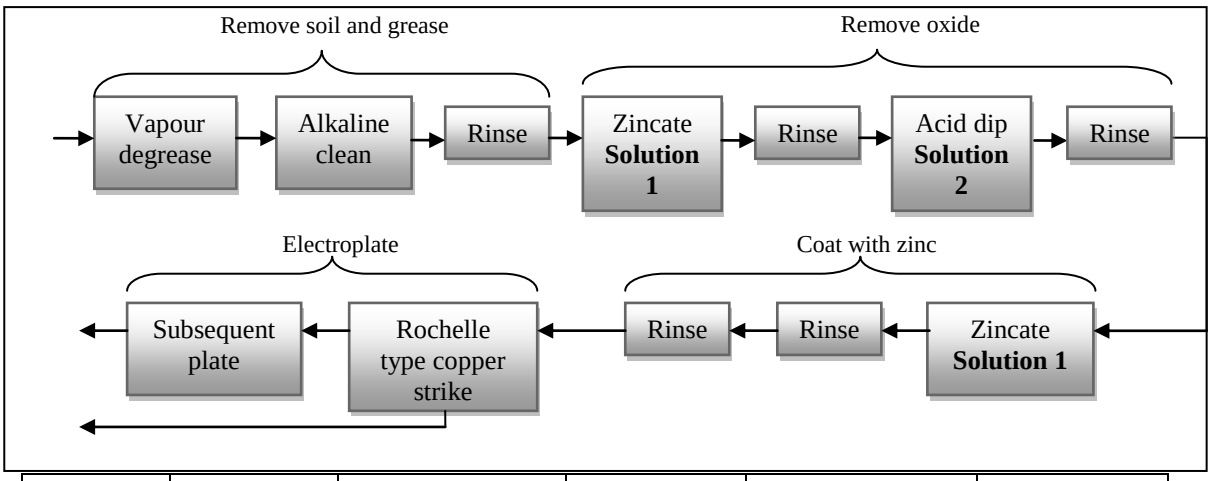

Solution No.	Type of solution	Composition	Amount	Operating temperature (ºC)	Cycle time (seconds)
1	Zincating	NaOH ZnO	525 g/l 100 g/l	16- 27	30- 60
2	Acid dip	HNO_3	50 vol%	Room	15

Figure 2-11 Surface pre-treatment procedures for most aluminium casting alloys, for wrought aluminium alloys that contain less than approximately 3% Mg (1100, 3003, 3004, 2011, 2017, 2024, 5052, 6061) and for aluminium alloys whose identities are not known (from Ref. [108])

The substrates must be carefully degreased, slightly pickled and carefully rinsed under running water after each process in order to ensure good adhesion of the electrodeposits to the substrate [107]. The rinsing process in the surface pre-treatment procedure is quite important because the cleaning process may be influenced by contaminated rinses. According to Wernick et al., the sodium hydroxide film formed on the metal surface during alkaline cleaning is difficult to remove [5]. Therefore, agitation of the rinse water is needed since it can accelerate the dilution of the sodium hydroxide film. Tang et al. also suggested the samples being washed with distilled water after each treatment and immersed immediately in the next bath in order to avoid drying [48].

Degreasing Process

Degreasing is the process of removing foreign contaminants, such as vegetable oils, animal oils, or greases using organic solvent or alkaline solutions [107, 108]. Organic solvents, such as kerosene, Stoddard solvent and mineral spirits with addition of small amounts of emulsifiers and surfactants will emulsifies the oil or grease on the surface [108]. However, these types of solutions are limited to the removal of light oil and grease only. Therefore, alkaline cleaners are widely used to remove oil and grease instead of solvents.

During the degreasing process, fatty film is broken down when a greasy metal is immersed in an alkaline solution, after which surface tension causes the grease to coagulate into drops [107]. Small gas bubbles become detached from the electrolyte near an oil drop and are retained at the interface between the oil and the solution [107]. As the gas bubbles grow due to further evolution of gas, the oil drops become extended, while their adhesion to the metal surface decreases when the contact angles become smaller. They are removed by the gas bubbles from the metal surface into the solution [107].

According to Wernick et al. [5], an ideal alkaline solution should satisfy the following conditions: the salts should be completely and easily soluble, it should be stable and possess good rinsing properties, the alkalinity of the solution should be suited to the metal, be buffered to help maintain constant activity of the solution, possess good wetting power, be able to deflocculate dirt particles and disperse them throughout the solution by colloidal action, be inhibited to minimise attack on the metal, be a non-irritant to the skin and be non-toxic, while acting acting as a water softener to prevent precipitation of hard-water salts on the metal surface. It must of course be economical. Wernick et al. [5] has listed some of the common faults of alkaline cleaning solutions and their control (Table 2-10).

Table 2-10 Control of alkaline cleaner (from Ref. [5])

Trouble	Cause	Solution
Excessive corrosion in cleaner	pH too high or loss of inhibitor.	Adjust pH, make up inhibitor.
Corrosion spots	Alkali left on surface.	Dip in $NaHSO_4$ or HNO_3 and rinse.
Does not clean properly	Weak or worn-out cleaner.	Make up or renew, adjust pH and wetting agent.
Does not clean properly	Excess foreign matter on work.	Prior degrease in vapour or solvent emulsion cleaner.
Poor paint bond	Poor rinsing or too tenacious inhibitor film; improve removal of oxide film; excessive floe pick up in cleaner.	Clean rinse tanks and increase rate of water flow. Select cleaner with easily removable inhibitors and minimum floc formation. Use solution suitable for removal of surface film.
Smut formation on work	On copper containing alloys if pH is too high.	Reduce pH, avoid free caustic cleaners, use sufficient inhibitor.
Excessive floc formulation	Breakdown of Cu, Mg and Si sequestering agents; absorption of CO_2, by cleaner or excess carbonates used in original formula; addition of acid to cleaning solution.	Select cleaner with ample reserve of sequestering agents; e.g. polyphosphates. Avoid CO_2, from gas burners, etc. by proper vents round tank area. Use cleaner with no CO_3^{2-} content. Avoid acid addition by supervision.
Insoluble film formation interfering with anodizing, wetting, etc	Too highly inhibited; excessive transfer time between cleaner and rinse.	Select proper amount of inhibitor which is soluble. Reduce transfer time and select cleaner with wetting agent which promotes good rinsing.

Therefore, a careful selection of alkaline solution is vital, as aluminium is readily attacked by alkaline solutions. According to American Standard Testing Materials on ‘Standard guide for cleaning metals prior to electroplating’ (ASTM B 322-99), good alkaline cleaning can be achieved by considering the following factors, such as concentration, temperature, immersion duration, agitation, age and degree of contamination, rinsing, and selection of suitable cleaner [109].

Normally, aluminium and its alloys are degreased in slightly alkaline solutions [107]. The selection of the suitable and effective alkaline solution in terms of the solution type and its compositions are dependent on the nature of the contaminants and type of the substrate.

There has been much plating research on aluminium alloys using sodium hydroxide (NaOH) aqueous solution [22, 40-42, 44, 45] as an alkaline cleaning solution. The most-used concentrations of sodium hydroxide (NaOH) solution are 5% NaOH [40, 41, 45] and 10% NaOH [22, 42, 44] at room temperature from 5 to 30 seconds of the immersion process. In addition to that, Keller et al. [46], one of the pioneers in the research of conditioning on aluminium alloys, suggested the preparation of mild alkaline solution for aluminium alloys using 3% of each sodium carbonate and trisodium phosphate and at a temperature of 60- 82°C for 1 to 3 minutes. Sudagar et al. [29] used 10 g/l of sodium carbonate and 50 g/l of trisodium phosphate in preparation of the alkaline cleaning solution at 65°C for 2 minutes.

Pickling Process

Pickling is the process of using an acid solution to remove the original surface oxide layer and any microconstituents which may interfere with the formation of a continuous zinc layer or which may react with the subsequent plating solution [46]. This ensures good adhesion between the deposit and substrate. According to Keller et al. [46], one of the more effective pickling processes is using a hot acid etch, which contains 25% of sulphuric acid (by weight) for about 5 minutes at 82°C. This treatment leaves the surface in excellent condition for the formation of a zinc layer during the zincating process and eliminates the undesirable effects of the magnesium containing constituents in aluminium alloys [46]. Most research uses sodium hydroxide (NaOH) as an alkaline solution for aluminium alloys, followed by an acid dipping in the range of 30% HNO_3 [22, 42, 44] to 50% HNO_3 [21, 34, 41, 45, 86].

Zincating Process

The zincating process is the most widely used method of treating aluminium and a wide range of aluminium alloys prior to electrodeposition. It is considered one of the most practical and economical processes to obtain good adherence of coating materials to the substrate [1, 3, 18-22, 29, 40-46, 49-52, 110, 111]. The details of the zincating process will be further discussed in Section 2.4.

2.4 Zincating Process

2.4.1 Introduction

In an electrochemical exchange reaction between zinc complexes in solution and the aluminium substrate, zinc crystallites are deposited at the expense of aluminium dissolution, thus removing the surface oxide film. The zincating process comprises several steps, including the pre-cleaning process in alkaline and acid dipping to thoroughly clean the substrate surface and ensuring that the oxide film is uniform on the surface, followed by the immersion of the substrate in an alkaline zincating solution.

The correct procedures of zincating process need to be followed in order to produce a uniform zinc deposit with good adherence to the substrate surface. The thinner and more uniform zinc deposits are better suited for plating preparation and service performance of the coatings. Heavy zinc deposits are usually spongy, less adherent and undesirable from the standpoint of corrosion resistance. However, zincating pre-treatment sometimes results in non-uniform zinc deposition due to non-uniform dissolution of the substrate during the zincating process. These will produce coating materials with pits as the zinc particles do not fully cover the specimen surfaces. Another drawback of the zincating process is the dissolution of the aluminium alloy in a concentrated alkaline zincate solution, which may result in serious damage to the aluminium alloy component [28].

In order to overcome the drawbacks of the zincating process, Tang et al. [47] studied the addition of a small amount of copper ions to the etching bath. They found

that the copper formed in the etching process acted as nucleation seeds for zinc deposition and can drastically improve the uniformity of zinc deposits on Al-Si alloys as well as rapidly form a zincating layer on the substrate. Besides zincating, Azumi et al.[28] have suggested an alternative technique to replace the zincating process by pre-electrodeposition of metals in the porous anodic oxide films on aluminium alloys substrate, in order to create a seed for the subsequent plating.

2.4.2 Fundamentals

The zincating process is an electrochemical exchange reaction between zinc complexes in a zincating solution and the aluminium substrate. Thus, zinc crystallites are deposited at the expense of aluminium dissolution in order to protect the aluminium surface and provide a surface for subsequent deposition [19]. During the process, some hydrogen evolution may also occur at the cathodic areas due to substrate immersion in the alkaline zincating solution. The electrochemical process of the immersion of aluminium substrate in zincating solution can be written as the following reactions [5, 36].

During the zincating process, the aluminium oxide film is first dissolved in zincating solution as follows in (1) and (2):

Anodic: $$3\,OH^- + Al \longrightarrow Al(OH)_3 + 3e^- \quad (1)$$

$$Al(OH)_3 \longrightarrow AlO_2^- + H_2O + H^+ \quad (2)$$

According to Wernick et al. [5], Einerhand et al. [112] and Peter [113], a zincate ion in alkaline zincating solution likely takes the form of $Zn(OH)_4^{2-}$. Therefore, the deposition of zinc may be expressed as follows in (3) and (4):

Cathodic: $$Zn(OH)_4^{2-} \longrightarrow Zn^{2+} + 4\,OH^- \quad (3)$$

$$Zn^{2+} + 2e^- \longrightarrow Zn \quad (4)$$

However, single zincate pre-treatment results in a granular zinc deposition and the surface is not suited for a subsequent plating process. Double zincate pre-treatment, in which the first zincate pre-treatment is followed by zinc stripping in a concentrated HNO_3 solution and then by a second zincate pre-treatment, produces a smooth and uniform zinc deposition layer, leading to strong adhesion between substrate and deposit (Figure 2-12) [43]. During the double zincating process, the first zinc layer from the first zincating process is stripped off using immersion in nitric acid. This reaction can be described as an electrochemical process by the following reaction [36]:

$$2\,HNO_3 + Zn \longrightarrow Zn(NO_3)_2 + H_2 \qquad (5)$$

The double zincating protects the aluminium substrate from reoxidation until it is ready to be electroplated with nickel. Therefore, the double zincate pre-treatment process is widely used in the plating industry.

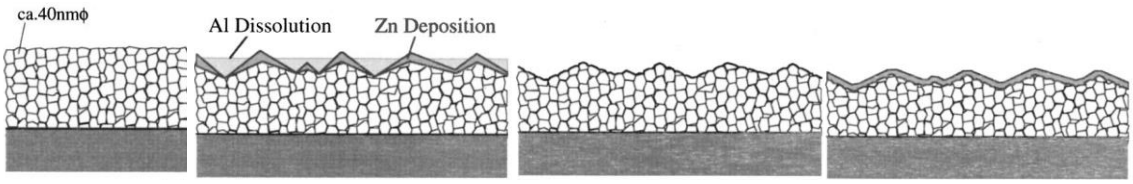

(a) (b) (c) (d)

Figure 2-12 Zincating pre- treatment process (a) as-received ion beam sputter-deposited aluminium film, (b) first zincating process, (c) acid immersion process and (d) second zincating process (from Ref. [43])

2.4.3 Nucleation and Growth of Zinc Particles

According to Lee et al. [42], during the nucleation stage, zinc particles preferentially form clusters on convex areas, such as peaks or edges of aluminium alloy surfaces. Zinc deposition does not occur on all surfaces, even though aluminium dissolution continues on all surfaces. This is because some of the zinc complex ions do not reach inside of the holes. These deep holes still cannot be covered by the zinc

particles, even using a multiple zincating process [42]. Lee et al. [42] proposed a model of the nucleation and growth of zinc particles, as shown in Figure 2-13. After the nucleation stage, zinc particles begin to grow at preferred sites and form hexagonal platelets. These zinc particles continue to stack on each other and keep the characteristic of hexagonal platelets during further deposition. Assimilation of the separate staking hexagonal platelets occur after a long deposition time and the aluminium surface cover with disperse zinc hexagonal groups.

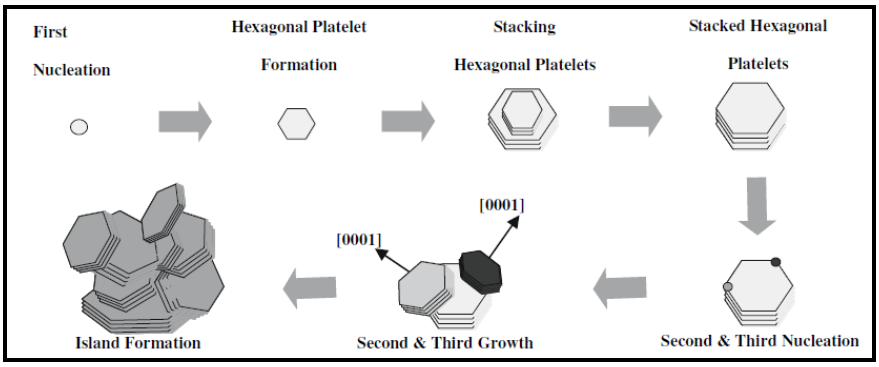

Figure 2-13 Proposed model of the nucleation and growth of zinc particles (from Ref. [42])

2.4.4 Factors That Influence the Properties of Zincated Samples

Types of the Zincating Solution

There are two types of zincating solutions, namely unmodified and modified zincating solutions. Basically, an unmodified zincating solution is a highly alkaline solution with basic components, such as sodium hydroxide (NaOH) and zinc oxide (ZnO) [43, 45, 46, 51]. However, this unmodified zincating solution does not provide strong adhesion between deposit and the substrates. Therefore, a modified zincating solution which contains additives in the form of complexing agents, such as potassium sodium tartrate (Rochelle's salt) and other metal ions such as Fe, Cu and Ni, is required [18, 20, 29, 40, 41, 47]. The basic ingredients of modified zincate solutions are zinc oxide, sodium hydroxide, potassium sodium tartrate, sodium nitrate, and ferric chloride [51]. The functions of these components are zinc oxide, providing a zinc source; ferric chloride in conjunction with the tartrate ion, improving adhesion of deposits; sodium

nitrate, limiting the amount or thickness of deposits; and sodium hydroxide, maintaining the desired pH level [51]. Table 2-11 shows details of various modified zincating solutions which may be used for the zincating process of aluminium alloys [108].

Table 2-11 Various type of modified zincating solutions for use with aluminium alloys (from Ref.[108])

Solution type	Sodium hydroxide (g/l)	Zinc oxide (g/l)	Ferric chloride (g/l)	Rochelle salt (g/l)	Sodium nitrate (g/l)	Operating temperature (ºC)	Processing time (s)
Modified (a)	525	100	1.00	9.8		15- 27	30- 60
Dilute 1(b)	50.3	5	2.03	50	0.98	21- 24	30 max
Dilute 2(b)	120	20	2.03	50	0.98	21- 24	30 max

(a) U.S. Patent 2,676,916 (1954). (b) U.S. Patents 2,676,916 (1954) and 2,650,886 (1953)

Concentration of Zincating Solution

The basic formulation for zincating solution, which contains zinc oxide (50 to 100 g/l) and sodium hydroxide (250 to 500 g/l), can produce finer-grained and compact zinc deposits [5, 86]. A diluted zincating solution (5 g/l of zinc oxide + 45 g/l sodium hydroxide) will produce thicker and large-grained zinc deposits [5]. In addition, an irregular zinc deposit is obtained from a zincating solution which contains 20 g/l of zinc oxide and 120 g/l sodium hydroxide, while a uniform zinc deposit is produced from zincating solution contains 100 g/l of zinc oxide and 500 g/l sodium hydroxide [5]. This zincating process should be carried out at 21 to 24ºC and the immersion duration should not exceed 30 seconds. This is consistent with results by Keller et al. [46], who found that concentration of sodium hydroxide can influence the formation of the zinc coating, in which a high percentage of sodium hydroxide can produce thinner and more uniform zinc deposits (Figure 2-14). According to Keller et al.[46], in their research the thinner zinc immersion coating resisted corrosive conditions better than zinc immersion coating, which produced heavier coating.

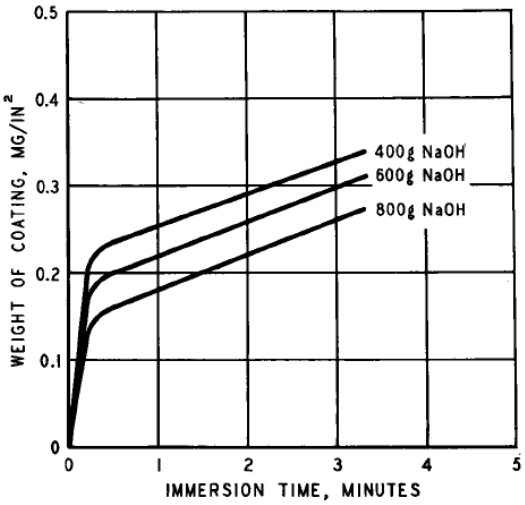

Figure 2-14 Effect of concentration of the zincating solution on the weight of the zinc immersion coating formed on 2S alloy sheet at a temperature of 21º C (from Ref. [46])

In addition, a dense zinc immersion coating can also be obtained by the addition of modifiers in a different concentration. Modifiers such as ferric chloride, Rochelle's salt, and sodium nitrate are added to the basic zincating solution, which contains zinc oxide and sodium hydroxide [107]. This can be seen in Figure 2-15, which shows that the weight of the zinc immersion coating is greatly influenced by modifiers [107]. However, the diluted modified solutions are unsuitable because of their rapidly changing composition, as indicated by Curve 2 [107]. The optimum result is shown by Curve 2.

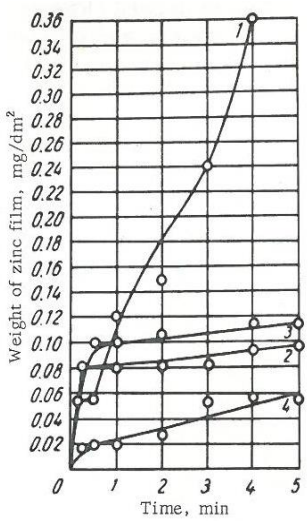

(a)

Components	Curve			
	1	2	3	4
ZnO	-	100	20	5
$ZnSO_4.7H_2O$	300	-	-	-
NaOH	400	500	120	50
$FeCl_3.6H_2O$	-	2	2	2
$KNaC_4O_6.4H_2O$	-	10	50	50
$NaNO_3$	-	1	1	1

(b)

Figure 2-15 (a) Effect of the concentration of the zincating solution on the weight of the zinc immersion coating formed during a given time, (b) details of the components concentration in the different zincating solution (from Ref. [107])

According to Morin et al. [114], the double zincating process on aluminium blanks, using a simple diluted modified zincating solution consisting of 100 g/l of NaOH, 20 g/l of ZnO and 2 g/l $FeCl_3$, exhibited poor results in the bend test. Better adhesion of metal coatings to the aluminium substrate can be achieved using an improved modified zincating solution followed by a copper strike process. In addition, according to early work by Morin et al. [114], adding 24 g/l of $NiSO_4.6H_2O$ to a modified zincating bath consisting of 273 g/l NaOH, 8.7 g/l $CuSO_4.5H_2O$, 40 g/l $ZnSO_4$, 40 g/l $ZnSO_4.7H_2O$, 1.7 g/l iron chloride, and a complexing agent to keep the ions in solution, followed by a copper strike process, showed strong adhesion between metal coating and substrate after the bend test. It was not possible to remove the coating, even using a sharp instrument. This result is similar to that of Wyszynski, who indicated that the presence of nickel in the zincating solution may improves the adhesion of nickel coating directly onto the zinc deposit [5]. Morin et al. [114] further discovered that the addition of about 10 g/l KCN to the zincating bath, as a complexing agent and a solution activator, can improve coating adhesion.

An electrochemical study of the zincating process for aluminium at various zincate concentrations shows that at a high concentration (0.5 M), the mixed potential rises rapidly until the steady state potential (Figure 2-16) [50]. This steady state potential indicates that the aluminium surface had been completely or almost covered by the zinc deposits. In comparison, at a very low zincate concentration (0.01 M), the

mixed potential starts at a very negative potential according to the dissolution of aluminium in the zincating solution.

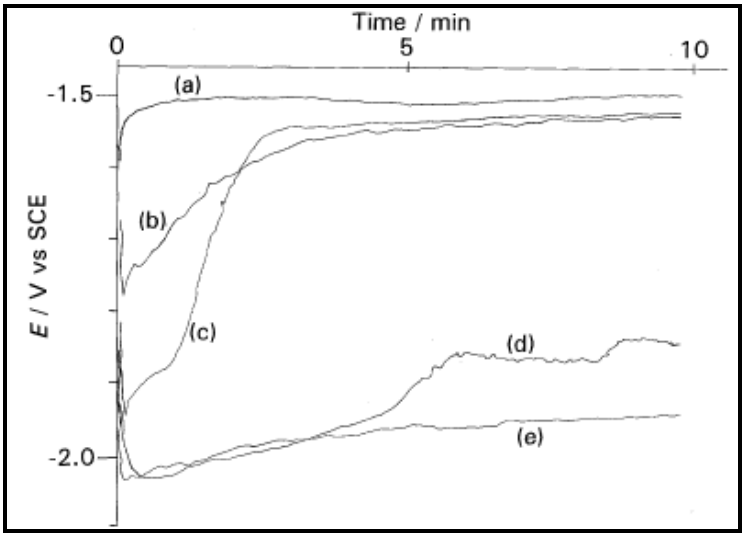

Figure 2-16 Mixed potentials as a function of time at various zincate concentrations. (a) 0.5, (b) 0.1, (c) 0.05, (d) 0.01 and (e) 0 M. Sodium hydroxide concentration is at 3.0 M, temperature at 25º C and rotation speed at 230 rpm (from Ref. [50])

Condition of Pre-treatment

Pre-treatment condition prior to zincating process may affect the zinc deposition due to the potential difference between commercial purity aluminium treated in various ways (Figure 2-17) [5]. The effects of various pre-treatment conditions on the zinc deposits are shown in Table 2-12 [5].

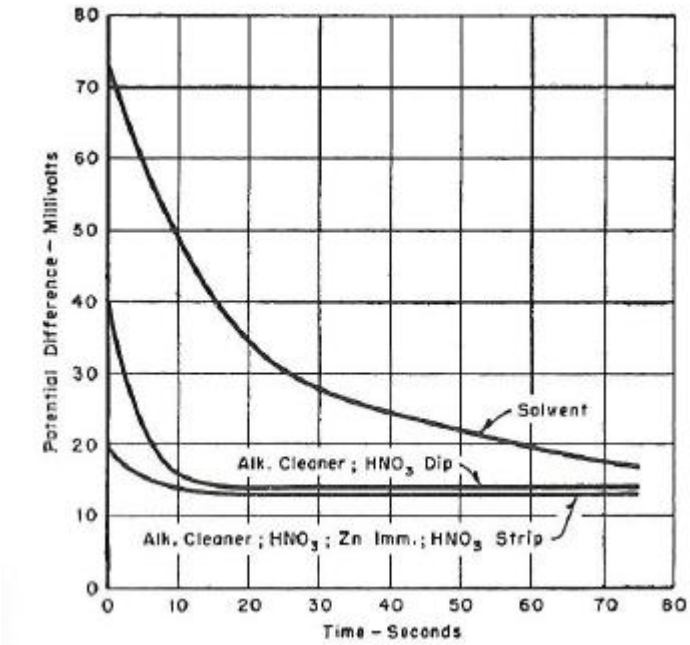

Figure 2-17 The potential difference between commercial purity aluminium after various pre-treatment conditions in a concentrated simple zincating solution (100 g/l ZnO + 500 g/l NaOH) (from the Ref. [5])

Table 2-12 Effect of various pre-treatment conditions on the zinc deposits of commercial purity aluminium (from the Ref. [5])

Treatment	Coating weight (mg/in^2)	Zinc content (%)	Resistance (μohms)
Electrodeposited zinc	-	-	5
Solvent cleaned, zincating (30 s)	1.0	1.6	10
Alkaline cleaned, HNO3 dipped, zincating (30 s)	0.33	0.53	15
Alkaline cleaned, HNO3 dipped, double zincating (30 s)	0.16	0.26	70

According to Keller et al. [46], the weight of the zinc immersion coating is significantly influenced by conditioning treatments used prior to the zincating process, as seen in Figure 2-18. The lower weight of the zinc immersion coating exhibits better resistance to corrosion after the electrodeposition process [46].

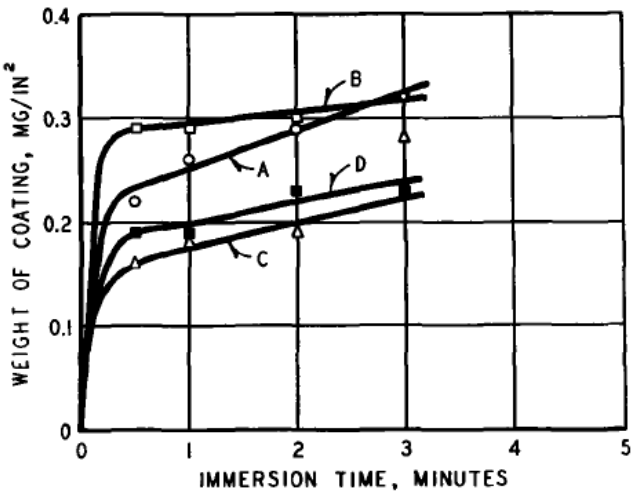

Figure 2-18 Effect of different conditioning treatments on the weight of zinc immersion coating on 2S alloy. Treatment A, carbonate-phosphate cleaner; treatment B, same cleaner + 25% sulphuric acid etch + zinc dip; treatment C, same cleaner + double zinc dip; treatment D, Alcoa R5 Bright Dip + zinc dip (from Ref. [46])

Besides a chemical pre- treatment, a mechanical pre- treatment before the zincating process also influences the surface morphology of a zincating layer. Schwankl et al. [197] find that the area coverage of zinc particles on a sandblasted substrate during the zincating process is very homogenous compared to an untreated substrate. Sandblasting process executed prior to the zincating process can be a useful tool to modify the deposition of zinc during the process, thus, influencing the coating morphology [197].

Types of Aluminium Alloys

The type and temper of aluminium alloys also influence the weight of the zinc immersion coating [46]. Even though these alloys are treated by the same procedure, the weight of the zinc immersion coating still differs depending on the type of wrought aluminium alloys (Figure 2-19). The different in chemical composition of different aluminium alloys will also affect the chemical reaction during the zincating process, due to variations in the potential differences between the alloys and zinc in the zincating solution [5]. The difference in potentials of aluminium alloys and other metals compared with zinc is shown in Table 2-13 [5].

According to Wernick et al. [5], thinner and more compact zinc deposits show better adhesion properties. On the same time, previous research by Keller et al. [46] has indicated that alloys with thinner zinc deposits before plating have better corrosion resistance than heavier zinc deposits.

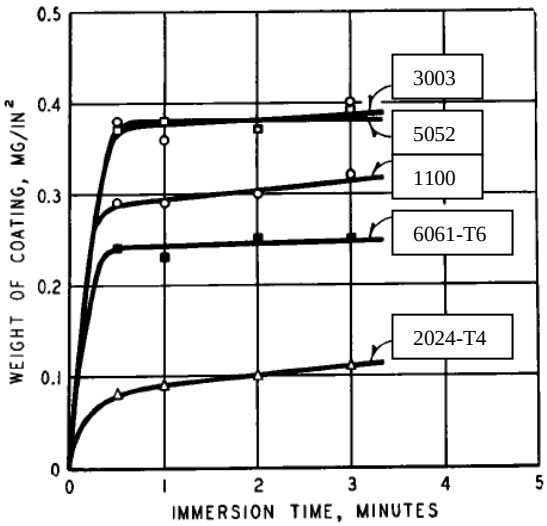

Figure 2-19 Effect of different wrought aluminium alloys on the weight of zinc immersion coating using same conditioning treatment, concentrated simple zincating solution of 100 g/l ZnO + 525 g/l NaOH (from Ref. [46])

Table 2-13 Potentials of some metals and aluminium alloys in 53 g/l NaCl + 3 g/l H_2O_2 with reference to the 0.1 KCl calomel electrode (from Ref. [5])

Metal or alloy	Potential w.r.t. 0.1 KCl calomel (volt)
Nickel	-0.07
Silver	-0.08
Brass (61% Cu- 39% Zn)	-0.28
Chromium (electrodeposited)	-0.37
Tin	-0.49
2024-T4 Al-41/2% Cu-11/2% Mg-1/2% Mn	-0.66
2024-T4 Al-41/2% Cu-1/2% Mn-3/4% Si-1/2% Mg	-0.81
Cadmium	-0.82
6061-T6 Al-1% Mg-1/2% Si-1/4% Cu-0.1% Cr	-0.83
3003, NS3, Al-11/4% Mn	-0.83
1100, S1C, commercial purity aluminium	-0.83
5052, NS4,Al-21/2% Mg	-0.85
Zinc	-1.05

Zincating Temperature

Zincating temperatures also influence the weight of zinc immersion coating, as shown in Figure 2-20 [46]. The figure shows that the weight of zinc deposits increases at high temperatures. Zincating at 16°C produces the thinnest coating compared to other higher temperatures. This thinner zinc immersion coating has better corrosion resistance compared to a heavier zinc immersion coating.

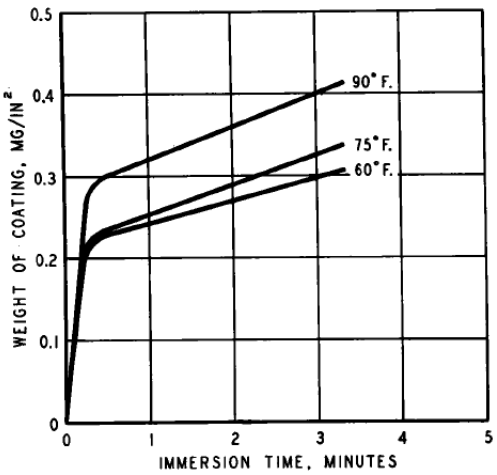

Figure 2-20 Effect of temperature of the zincating pre-treatment on the weight of the zinc immersion coating deposited on 2S aluminium alloys sheet (from Ref. [46])

On the other hand, zincating temperatures may also influence the shape and orientation of zinc particles. Lee et al. [42] reported that an increase of zincating temperature changed the zinc particles from a hexagonal shape to a starfish-like or flower-like shape with random orientation (Figure 2-21). This is because the zincating reaction is controlled by the diffusion of the zinc ion to the aluminium surface; thus, the rate of the zincating reaction may greatly change due to heat transfer. A temperature difference can affect the diffusion coefficient of the diffusing zinc ions, which can increase diffusion (mass transfer) at a high temperature [42].

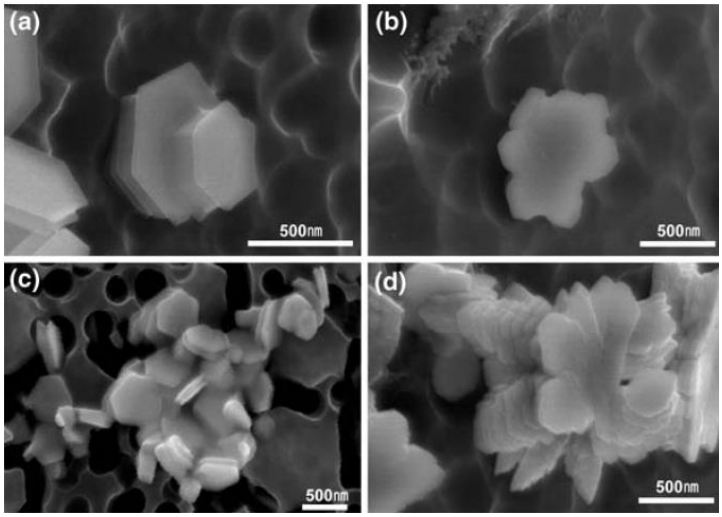

Figure 2-21 FE-SEM images of zincated specimen for 10 s (a) zincating temperature of 20 C, (c) zincating temperature at 50 C, while (b) and (d) are the further grown deposit of (a) and (c), respectively (from Ref. [42]).

Zincating Duration

Control of the zincating duration for both single and double or even triple zincating is an important factor in obtaining a thin and uniform zinc immersion coating, since coverage of the zinc particles on the substrates is closely related to the adhesion of coating materials to the substrate [45]. A sufficient and suitable duration for the zincating process provides enough time for the zinc particles to deposit on the aluminium substrate uniformly, thus produces a coating layer which covers the entire substrate surface. Yang et al. [45] concluded that if the zincating duration was too short (15 seconds), certain parts of the aluminium surface remained uncovered, while if the zincating duration was too long (45 seconds), too much zinc was deposited on the aluminium alloy surface. This is consistent with observations by Wernick et al. [5], who found that zinc crystallites nucleated preferentially around etch pits during the first five seconds, while more of the surface was covered with zinc, and the growth centres had started to coalesce after 30 seconds. However, the surface was still not completely covered with zinc deposits, even after 2 minutes of immersion [5].

These findings were also supported by research done by Lee at el. [42], as during further zincating pre-treatment, these zinc particles continued to stack, keeping

characteristic hexagonal platelets. With longer deposition times, assimilation of the separate staking hexagonal platelets occurred, and the surface was covered with dispersed zinc hexagonal groups. In addition, Lin et al. [40] concluded that a high population density of the nodules is anticipated at the end of extending a deposition reaction period such as 30 to 40 seconds; thus, this long-time operation caused a roughened surface appearance.

On the other hand, a suitable combination of zincating duration for the first and second zincating process in the double zincating process may also result in a coating free of voids, pits and delamination. Research in this aspect is very limited, but Mallory et al. [86] have recommended that the duration for the second zincating process must be shorter than the first zincating process, so that a thin and uniform zinc immersion coating layer can be produced on the substrate.

The effect of the zincating duration and the zincating concentration on adhesion of zinc deposits can be seen in Figure 2-22 to Figure 2-24 [5]. Figure 2-22 shows that 30 seconds of zincating immersion was insufficient to obtain good adhesion, while 3 to 5 minutes of zincating immersion managed to produce coating with good adhesion (Figure 2-23 & Figure 2-24). Coating adhesions are classified as follows: S = strong (no separation between the coatings and the substrate); W = weak (peeling of the nickel); MW = medium weak; and MS = medium strong (if the deposit could be separated by hammering with a chisel, MW or MS ratings were given according to the force required to pull off the coating) [5]. On the other hand, based on the coatings' adhesion ratings as shown in Figure 2-22 to Figure 2-24, a suitable zincating solution concentration should be in the range of 40- 50 g/l of zinc oxide and 400- 450 g/l of sodium hydroxide.

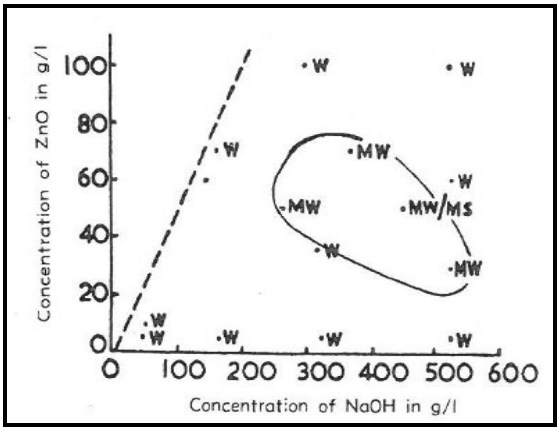

Figure 2-22 Effect of solution concentration on adhesion of zinc deposit obtained after 30 seconds immersion in zincating solution (from Ref. [5])

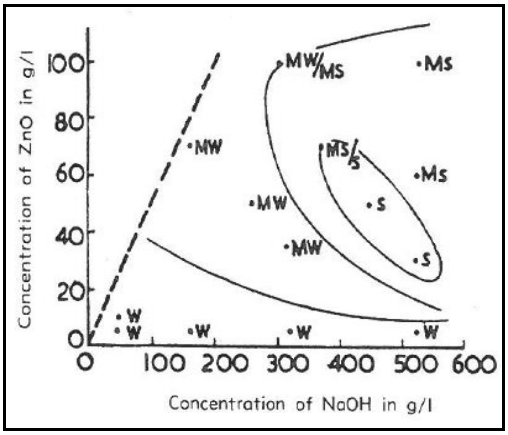

Figure 2-23 Effect of solution concentration on adhesion of zinc deposit obtained after 3 minutes immersion in zincating solution (from Ref. [5])

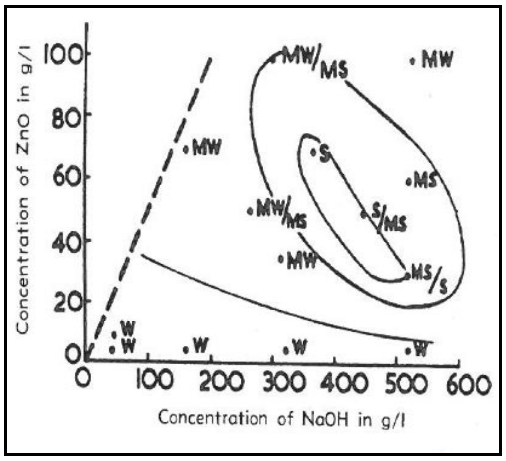

Figure 2-24 Effect of solution concentration on adhesion of zinc deposit obtained after 5 minutes immersion in zincating solution (from Ref. [5])

Ultrasonic Agitation

Ultrasonic agitation is important for increasing the mass transport of cations to the cathode surface and thus reducing concentration polarization [22]. The effects of cavitation, micro-steaming and degassing produced from ultrasonic agitation enhance the nucleation of zinc on aluminium alloys' surfaces. An increased nucleation rate will produce fine particle distribution during the first quick zincating process, while double zincating under the ultrasonic agitation will produce much smaller and denser zinc particles, which will then enhance the adhesion between nickel and aluminium alloys [22].

Degree of Zincating Process

The zincating process can be carried out in several ways such as single zincate, double zincate or triple zincate. The influence of the degree of the zincating process on the surface morphology is shown in Table 2-14. It has also been observed that the zincating duration used in the literature is less than 1 minute for both the single and double zincating process.

Table 2-14 A summary of previous research on zincating process of aluminium and its alloys

Substrate	Zincating process			Microscopy observations	Reference
	Single	Double	Triple		
Aluminium		45/ 15 s		This study focused on understanding of the role of zincating solution chemistry in achieving a good zincate morphology	[51]
AA1050 AA6061		90/ 30 s		SEM and EDX analysis indicated a uniform and dense zincated layer leading to a uniform growth of nickel deposits	[19]
Aluminium		NM		Zinc particles were observed to be nucleated on the grain boundary of the aluminium substrate	[49]
Al- Si	NM	NM		If the immersion time was too long, too much zinc was deposited on the substrate, while a short immersion time produced	[45]

				substrate which remains uncovered. Optimum double zincating was found at 45/ 15 s.	
Al- Cu- Si		1,5,10/ 10 s		The parent zinc is created on the peak or edge of aluminium substrate during the nucleation process. Then, during the growing stage, the zinc particles migrated into parent zinc and formed hexagonal platelets.	[44]
Aluminium		1/ 10 s		Further extension of the zincating duration made the zinc particles continue to stack and keep the characteristics hexagonal platelets. Assimilation of the separate staking hexagonal platelets occurred after a long deposition times.	[42]
Al-Cu	10-60 s	10-60/ 10-20 s		SEM images of single zincating process shows incomplete deposition of zinc particles with large clusters of zinc particles preferentially at the grain boundaries of aluminium substrate. Zincating process for 60 s showed a uniform distribution of large zinc clusters that were smaller in size compared to 20 s.	[41]
Aluminium	45 s	45/ 15 s		Double zincating process produced smaller crystals and more uniform coverage of zinc particles on the substrate compared to single zincating process.	[57]
Aluminium	10-40 s	10-40/ 10-40 s	10-40/10-40/10-40 s	A dense and continuous zinc layer was obtained from a multiple zincating process. Initial zincating process of the multiple zincating, produced a rough surface, which changed to a smooth surface after the latter zincating process.	[40]
Al-Cu Al-Si		30/ 30s		Most of the surface was covered by the zinc particles after the double zincating process.	[62]
Al-Si		10/ 10s		Copper activation process improves the uniformity of the zinc particles and suppressed the dissolution of the aluminium substrate during the double zincating process.	[61]
AA2017	30s	30/ 30s	30/ 30/ 30s	Single zincated sample contains spherical particles with approximately 100nm in diameter; after double zincating the surface became smooth. Triple zincating process kept the smooth surface, but with some occurrence of pits and increase in thickness.	[1]
AA1100	30s	30/ 30s		The single zincated process showed non-	[3]

AA2017 AA5052				uniform zincating layer with rough zinc deposit; double zincating process produced a uniform zincating layer with fine zinc particles.	

*Note: NM (**Not mentioned** in the journal paper by the researcher)*

Among all these methods, the double zincating process promises the highest adhesion strength, then followed by triple zincating process, as reported by Hino et al. [1] in Figure 2-25. This adhesion result can be explained by surface analysis of the zincate film, as shown in Figure 2-26 [1]. The single zincating process produced spherical zinc particles with 100 nm size (Figure 2-26(b)), while the double zincating process produce homogenous distribution of zinc particles with smoothness surface (Figure 2-26(c)). This smooth surface with homogenous distribution of zinc particles led to the uniform coverage of nickel deposits on the substrate, since the zinc particles work as nuclei for the nickel electrodeposition. After triple zincating, the surface remained smooth but had pits, through which the underlying layer or the substrate could be observed (Figure 2-26(d)).

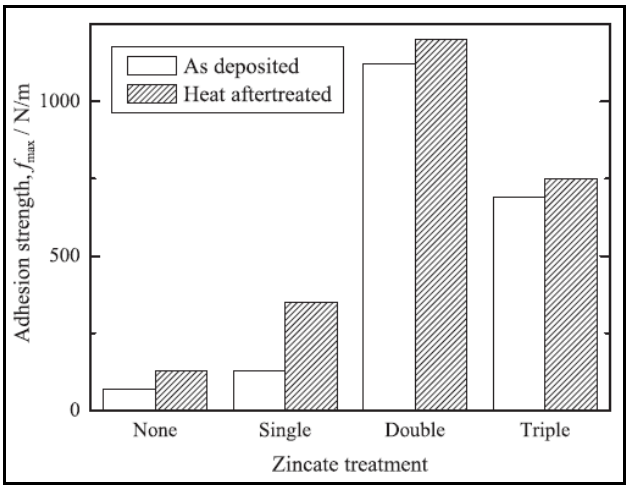

Figure 2-25 Adhesion strength of Ni-P electrodeposition on various type of zincating treatment (from Ref. [1])

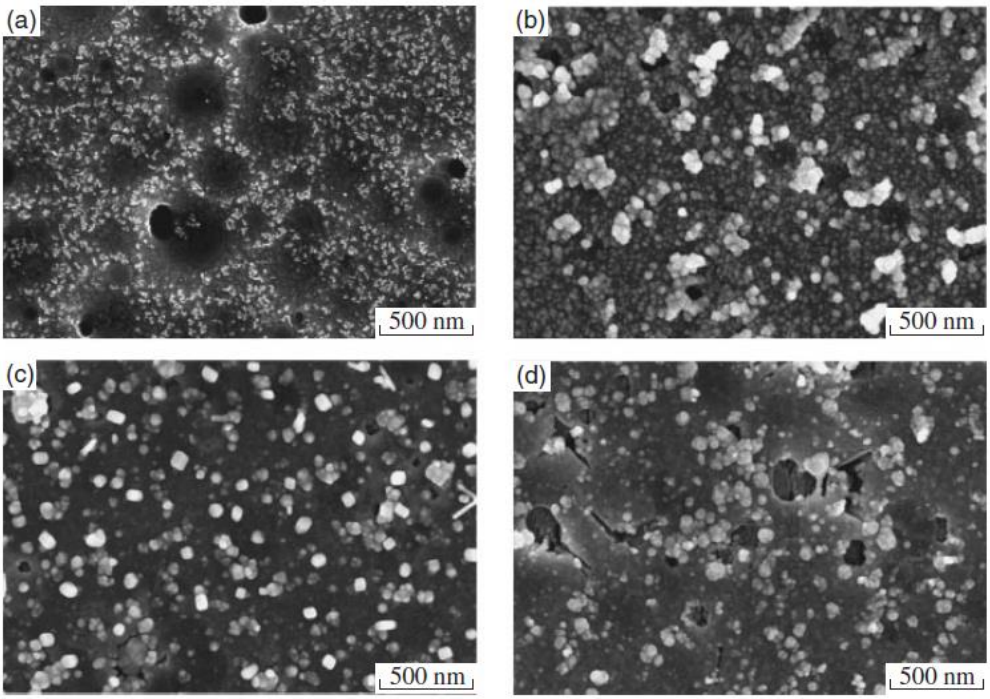

Figure 2-26 Secondary electron of the surface after zincating pre- treatment (a) without zincating, (b) single, (c) double, (d) triple (from Ref. [1])

Besides these general parameters of zincating process, a new invention has been made to the conventional zincating process. The new invention is the double zincating process, whereby the solution for second zincating is a bimetallic zincate solution which contains zinc and another metal with an affinity for electrodeposited aluminium alloy. According to Rhonda et al. [198], an addition of a minor amount of a plating solution of another metal to the zincating solution produces a bimetallic layer consisting of a continuous layer of zinc as a matrix phase and a region of dispersed metal. Then, the matrix phase is removed using an electrolytic etching process to produce a substrate surface containing dispersed seeds of a metal to be plated.

2.4.5 Environmental Issue of the Zincating Solution

A typical zincating solution used in the zincating process often contains zinc oxide (ZnO), sodium hydroxide (NaOH), ferric chloride ($FeCl_3$) and potassium sodium tartrate ($KNaC_4H_4O_6.4H_2O$). Three out of four chemicals used in this solution are

identified as hazardous and classified according to Regulation (EC) No. 1272/ 2008 [EU- GHS/ CLP] and EU Directives 67/ 548/ EEC or 1999/ 45/ EC [115]. The details of hazard identification of these chemicals are listed in Table 2-15.

Table 2-15 Hazard identification of chemicals used in zincating solution

Chemical	Safety sign	Regulation (EC) No. 1272/ 2008 [EU- GHS/ CLP]	EU Directives 67/ 548/ EEC or 1999/ 45/ EC	Pre- cautionary statement
Zinc oxide (ZnO) [116, 117]		Acute aquatic toxicity (Category 1) Chronic aquatic toxicity (Category 1)	Very toxic to aquatic organisms, may cause long- term adverse effects in the aquatic environment	Avoid release to the environment. Dispose of contents/ container to an approved waste disposal plant.
Sodium hydroxide (NaOH) [116]		Corrosive to metals (Category 1) Skin corrosion (Category 1A)	Corrosive	Wear protective gloves/ protective clothing/ eye protection/ face protection
Ferric Chloride ($FeCl_3$) [118]	 	Corrosive to metals (Category 1) Acute toxicity, oral (Category 4) Skin irritation (Category 2) Serious eye damage (Category 1)	Harmful	Wear protective gloves/ eye protection/ face protection

2.5 Adhesion of Coatings

2.5.1 Introduction

Good adhesion between coating and substrate is the main focus of coatings technology, as adhesion is the constraint for wider application of the coating. According to ASTM D907-70, adhesion is defined as the condition in which two surfaces are held together by either valence forces or mechanical anchoring or by both together [119].

Adhesion is a measure of the degree to which a bond has been developed from place to place at the coating- substrate interface [88]. Good adhesion between coating material and substrate is one of the most important requirements. Optimum adhesion can be achieved through the interdiffusion of substrate and deposited metal with interlocking grains, in order to give a continuous interfacial region [120]. This is because a porous interface or separation between deposited metal and substrate contributes to poor adhesion.

According to Mittal et al. [121], adhesion can be grouped into three different forms as follows: (i) fundamental adhesion, (ii) thermodynamic adhesion and (iii) practical adhesion. The definition of fundamental adhesion is the summation of all interfacial intermolecular interactions between the contacting materials, which represents the energy required to break chemical bonds at the weakest plane in the film-substrate adhering system under adhesion measurements. Thermodynamic adhesion is defined as the change in free energy when an interface is formed or separated and is expressed as follows [122]:

$$W_A = \gamma_{S1} + \gamma_{S2} - \gamma_{S1S2}$$

where,

W_A = work of adhesion
γ_{S1} = surface free energies of material 1 (substrate)
γ_{S2} = surface free energies of material 2 (coating)
γ_{S1S2} = interfacial free energy

Practical adhesion is the force or the work required to remove or detach a film or coating from the substrate irrespective of the locus of failure, such as at the interface, in the interphase or in the bulk coating (cohesive failure), including the energy required to deform both the coating and substrate, energy dissipated as heat or stored in the coating, and the components representative of the actual fundamental adhesion.

The correlation between the practical adhesion and the fundamental adhesion is as follows [122]:

Practical adhesion = *f* (fundamental adhesion, other factors)

where;

Other factors = stress in the coating, thickness of the coating, mechanical properties of the coating and substrate, work consumed by plastic deformation and viscous dissipation; mode of failure; mode and rate of applying the force or the energy to detach the film

In addition, according to Dini et al. [68], adhesion can be divided into several categories, such as (1) interfacial adhesion; in which adhesive forces are focused around a narrow well defined interface, with minimal atomic mixing, such as gold on silica, (2) interdiffusion adhesion; in which film and substrate are diffuse into one another, over a wider interfacial region, (3) intermediate layer; in which the film and substrate are separated by one or more layers of materials of different compositions and (4) mechanical interlocking; in which the substrate surface is not atomically flat and accounts for some degree of random fluctuation of adhesive forces.

In reviewing the literature related to the adhesion of coatings, many researchers have evaluated adhesion in coating-substrate systems in terms of practical adhesion [123-137]. However, this practical adhesion does not provide the work of adhesion, which is a measure of the chemical bonding across the interface. To overcome this restriction, some studies have been performed analysing the stress state developed by a sliding circular indenter and then evaluating interfacial adhesion strength using the energy approach [138-144].

There are many ways to determine the adhesion properties of the coatings, as indicated in Table 2-16 [67]. In all adhesion tests, a force is applied to the test specimen, which tends to pull the coating away from the substrate. Of these, the scratch test is fairly reliable, simple to use, and requires no special specimen shape or preparation. The scratch test has been chosen by many academicians and people in industry as a comprehensive tool for quantifying scratch results, such as scratch resistance, cohesion failure, and adhesion failure of a wide range of substrate-coating systems, based on the acoustic emission (AE) signals, friction force analysis, and microscopy examination.

Table 2-16 Various methods of adhesion test (from Ref. [67])

Properties to be measured	Adhesion test
Substrate deformation	Mandrel bend test Four- point bend test Tensile test
Coating deformation	Indentation in cross-section Rockwell adhesion test Nano-impact test Scratch test
Coating pull- off	Pressure-sensitive tape test Peel test Push-off test ASTM pull-off test ASTM tensile adhesion test

2.5.2 Method of Adhesion Testing

In the scratch test, a diamond stylus is drawn across a coating's surface under a constant or progressive applied load until well defined coating failure occurs, which is known as a critical load (L_C) [145]. The L_C represents the force which induces a specific type or level of damage in the coating from the scratch test. According to Benjamin et al. [144], there are two forces acting on the samples during the test, namely (i) vertical force, in which the sample is plastically deformed by the applied load; and (ii) horizontal force, in which results from the motion of the point relative to the surface.

The complexity of the interactions of the Rockwell C diamond stylus on the coated specimen under the applied load during the test was illustrated by Berg et al. [146] in Figure 2.27. The figure shows the stress states and the real geometrical relations of the diamond stylus and the coating. In the analysis of local stress during scratching process, Berg et al. [146] find that both the coating and substrate are deformed, leading to compressive stresses in front of the diamond stylus and leaving tensile stresses behind the diamond stylus. In addition, shearing strain also occurs due to a friction between the diamond stylus and the coating. Apparently, the scratch test does not depend only on the interface properties, but also substrate and coating properties as well as equipment and procedure variables.

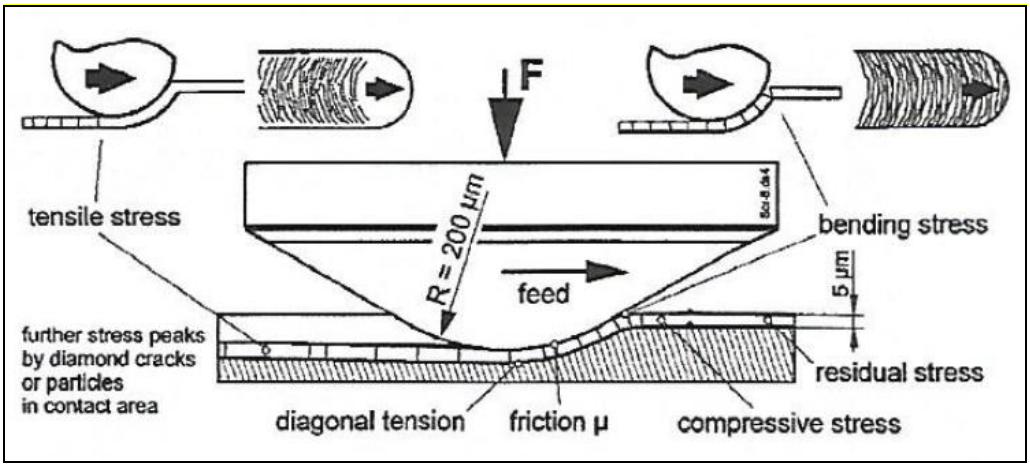

Figure 2-27 Illustration of the local stress state during scratching procedure [from ref. [146])

2.5.3 Variables Affecting Scratch Test Results

The scratch test is a complex experimental system involving numerous number of parameters which can affect the scratch testing results. The parameters are divided into the following two categories; (i) intrinsic parameters, namely the factors inherent to the experimental conditions themselves and (ii) extrinsic parameters, which are dependent on the nature and properties of the coating-substrate system [139, 147, 148]. A large and growing body of literature has investigated the effect of various parameters on the scratch test results, as shown in Table 2-17.

Table 2-17 Intrinsic and extrinsic parameters influencing the scratch test results

Parameters			
Intrinsic	[Reference]	Extrinsic	[Reference]
Loading rate	[139]	Substrate properties 1. Hardness 2. Elastic modulus	 [149-151] [152]
Scratching speed	[138]	Coating properties 1. Thickness 2. Hardness 3. Modulus 4. Residual stress	 [124, 138, 149, 150, 153-158] [124, 128, 129, 150, 151, 157, 158] [159] [155]

		5. Density	[154, 159]
Indenter tip radius	[138]	Friction coefficient	[150]
Indenter wear	[139]	Surface roughness	[134]
Machine stiffness/ design	[139]	Surface pre- treatment on the substrate 1. Plasma etching 2. Thermal sprayed coatings as interlayers 3. Gold- palladium interlayers 4. Ion implantation of carbon 5. Argon ion pre- sputtering 6. Ti and TiN intermediate layers	[138] [160] [133] [134] [161] [162]
Scratching mode	[128, 154]		

Surface pre-treatment of the substrate prior to the coating process is important for achieving the optimum adhesion of the coating and the substrate. To overcome adhesion problems, interlayers between the coating and the substrate have been applied. According to Aldrich-Smith et al. [133], an interlayer can improve adhesion through reduction of substrate surface oxide layers, chemical bonding to the coating, provision of a buffer for mechanical properties, reducing the stress gradient between the coating and substrate interface, and by providing a composition gradient when the coating is very different from the substrate. Aldrich-Smith et al. [133], find that an application of a 25 nm interlayer prior to chromium nitride (CrN) coating on stainless steel substrate provides an improvement in the critical load (L_{C1}) compared to coatings without interlayer.

A series of studies done by Shum et al. [134, 163-165] on carbon ion implantation pre-treatment on the substrate demonstrate an improvement in the adhesion of carbon coatings on steel substrates. This is due to the highly energetic ions sputter cleaning the substrate, which are implanted onto the substrate as a composition gradient layer and then work as nucleation sites for subsequent deposition [134]. On the other hand, adhesion between coating and substrate can also be enhanced by using the argon pre-sputtering technique as a pre-treatment before any deposition process. Ollendorf et al. [161] suggest a 15 minute duration for argon pre-sputtering for an optimal adhesion.

With the same objective to enhance the adhesion, Pedraza [199] conducted a pulsed laser irradiation before or after film deposition and found that this technique strongly enhances the bonding between metallic coating and ceramic substrates. The presence of oxygen during irradiation promotes strong bonding because it formed an intermediate compound in between the coating and substrate [199].

Other than surface pre- treatment on the substrate, types of coating materials also influence the scratch test result. This is because different coating material have its' own properties, such as hardness, modulus, residual stress and density. Kumar et al. [200] discovered that the highest critical load value has found for TiN (850 µN) coated on H-13 steel, while critical load has found lower for TiAlN sample (600 µN), followed by diamond like carbon (DLC) sample (400 µN). The low critical load value for DLC coating compared to nitride coating reported in [200] is also supported by Takadoum et al. [201], who found that the critical load value for DLC coating is 6 N, while TiN and TiCN are 12 and 15 N respectively. The difference in the critical load values is due to the material property effect.

A study conducted by Staia et al. [202] found that the critical load value of DLC/ NiP duplex coating on AA 2024 substrate is at 11 N, which higher than the critical value for DLC coating reported in [200] and [201]. The change in the elastic modulus with penetration depth in the duplex coating layer is believed to improve the DLC scratch resistance.

The effect of substrate type to the scratch behaviour can be seen from researches done by Kumar et al. [200] and Farokhzadeh et al. [203]. Kumar et al. [200] found that the nitrided H-13 steel sample has the lower critical value than the substrate which is at 120 µN, due to the cracked surface generated during the nitriding treatment. In contrast, Farokhzadeh et al. [203] reported that the nitrided Ti- 6Al- 4V alloy has improved the alloy resistance to surface crack initiation and propagation.

Furthermore, deposition technique also influences the critical load of the coating. Kumar et al. [200] reported that the critical load of the chemical vapour deposition (CVD) DLC coating deposited on steel has 400 µN, while Zaidi et al. [204] found that the critical load for physical vapour deposition (PVD) DLC coating on steel is at 12 N.

2.5.4 Scratch Test Failure Modes

The classification of the failure modes induced by a scratching process is depends on the hardness of both coating and substrate, as demonstrated by Bull [123] in failure mode maps (Figure 2-28). Soft coatings are defined as coating materials which have hardness value is less than 5 GPa, while hard coatings are coating materials with a hardness greater than 5 GPa [139]. As shown in Figure 2-28, soft coatings always fail through plastic deformation, whether deposited on softer or harder substrates. On the other hand, hard coatings deposited on soft substrates show that the substrate experience predominantly plastic deformation, while the coating may plastically deform or fracture as it bend into the track created by plastic deformation of the substrate [166]. According to Bull [166], for hard coatings on hard substrates, fracture dominates the scratch response with minimal plastic deformation.

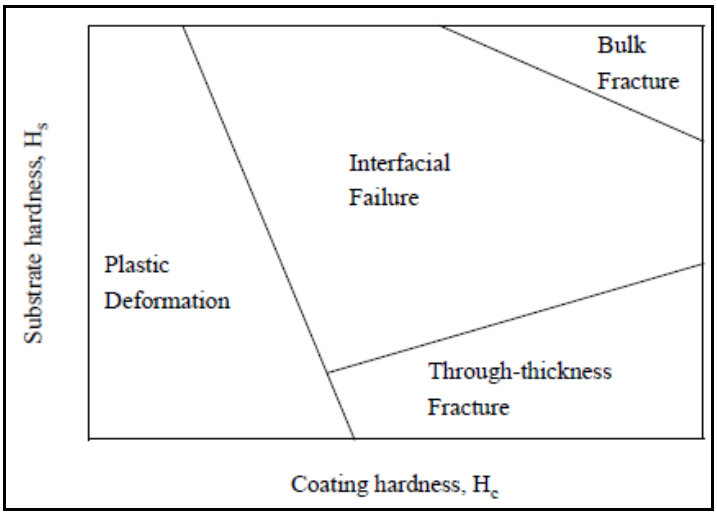

Figure 2-28 Schematic diagram showing the map of the main scratch test failure modes in terms of substrate and coating hardness (from ref.[139])

The failure modes of hard coatings can be classified into cohesive failure, adhesive failure, and chipping, as shown in Figure 2-29. Cohesive failure or through-thickness cracking failure can then be divided into several damage terms as follows [167]:

(a) Brittle tensile cracking: a series of nested micro- cracks which are semicircular with arcs open toward the direction of scratching and form behind the stylus.

(b) Hertz cracking: a series of nested nearly circular micro cracks which form within the scratch groove.

(c) Conformal cracking: cracks formed due to the coating trying to conform to the shape of the scratch groove. The cracks are less sharp than tensile or hertz cracks, with arcs open away from the direction of scratching.

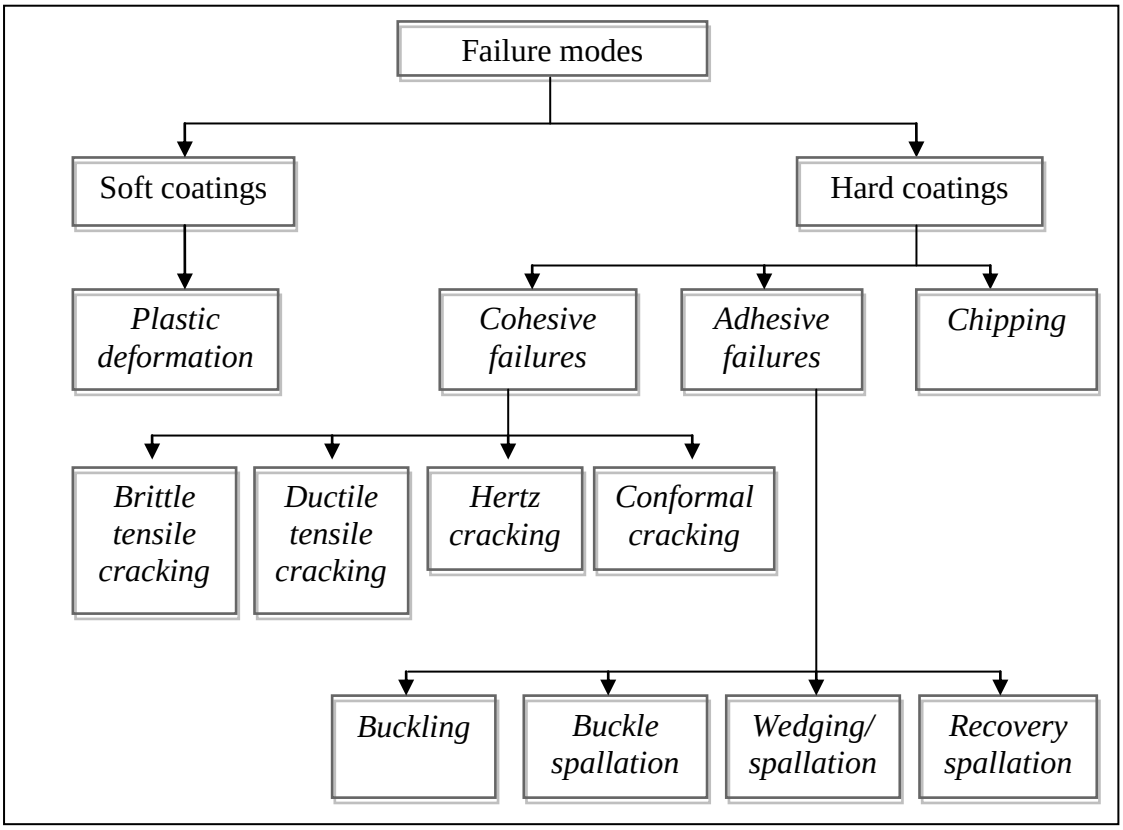

Figure 2-29 Failure modes classification of scratch test results

On the other hand, adhesive failures or interfacial failures are divided into buckling, buckle spallation, wedging spallation and recovery spallation. Detailed descriptions are as follows [123, 139]:

(a) Buckling: normally occurs on thin coatings with less than 10 µm thickness, which is able to bend under an applied stresses. This failure occurs in response to compressive stresses generated ahead of the moving indenter (Figure 2-30(i)). This is due to the interfacial defects in the localised region, which allow the coating to buckle in response to stresses (Figure 2-30(ii)). Under high tensile stress, through-thickness cracks form in the regions and lead to spallation. Further movement of the stylus over the failed region (buckle) crushes the coating into the surface of the scratch track formed in the substrate.

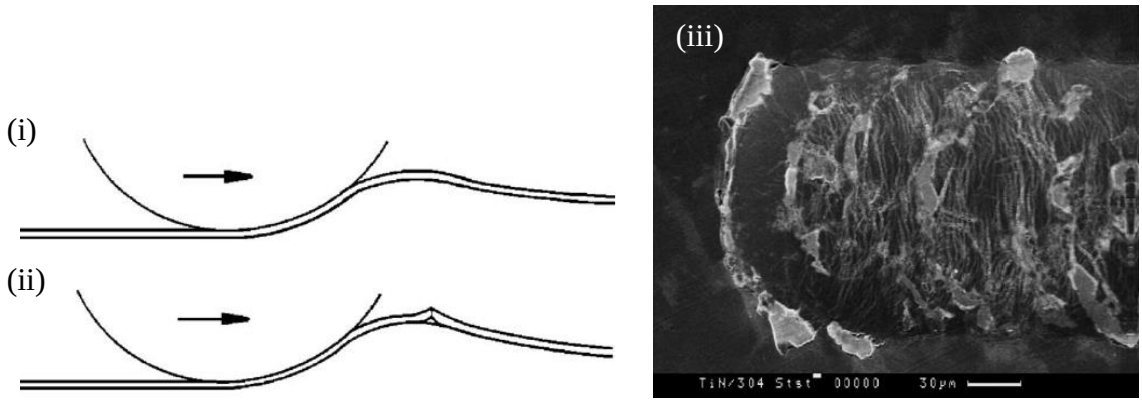

Figure 2-30 Illustration of the main stages in buckling failure modes in the scratch test. (i) pile-up ahead of the moving indenter, (ii) interfacial failure leading to buckling. Through- thickness cracking results in removal of coating material, (iii) SEM micrograph of buckle failure in TiN coated stainless steel (from ref. [139])

(b) Buckle spallation: similar to buckling failure, but with no wide, arc-shaped patches.

(c) Wedge spallation: normally occurs on thicker coatings with more than 10 µm thickness, which tends to show through-thickness fractures at stresses lower than those necessary to cause buckling. This failure begins with compressive shear cracks which form some distance ahead of the indenter through the thickness of the coating (Figure 2-31(i)). The propagation of the compressive shear cracks to the surface and interface leads to the formation of sloping sides, which act like wedges (Figure 2-31(ii)). Figure 2-31 (iii) shows the wedge lifts the coating

further away from the substrate and creating bending stresses within it, as the extent of the interfacial failure increases.

(d) Recovery spallation: failure produced by elastic recovery behind the stylus, depending on plastic deformation in the substrate and cohesive cracking in the coating. The regions of detached coating occur along one or both sides of the groove.

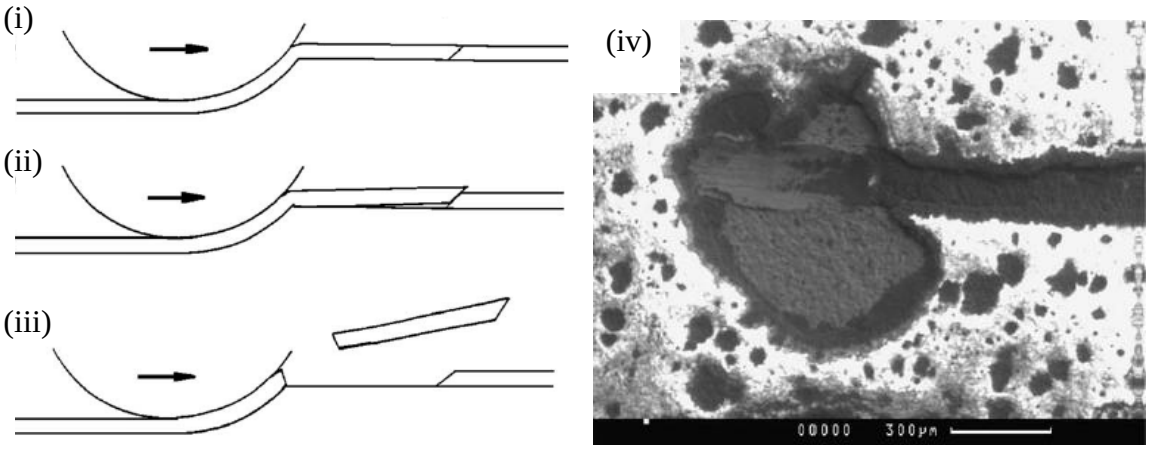

Figure 2-31 Illustration of the main stages in wedge spallation failure modes in the scratch test. (i) wedge crack forms some way ahead of the moving indenter, (ii) further motion drives the coating up the wedge opening up an interfacial crack, (iii) through-thickness cracking close to the indenter leads to spallation, (iv) SEM micrograph of a wedge spallation failure in an alumina scale (from ref. [139])

2.5.5 Evaluation of Coating Failure from Scratch Test

The most popular method to asses a quantitative value of adhesion from the scratch test is considering the critical load (L_C) value. The determination of the L_C value is normally performed by three techniques, such as microscopy observation, acoustic emission signals and frictional force. A considerable amount of literature has been published on these techniques to determine the L_C value, as shown in Table 2-18.

Table 2-18 Summary of the list of references on each technique

	Technique	Description	[Reference]
Determination of the critical load (L_C)	Microscopic observation	Optical microscopy and scanning electron microscopy observation provides the detailed view of the scratch groove and the surrounding coating surface	[135, 161, 162, 168-171]
	Acoustic emission	Acoustic emission system detects high frequency elastic waves in the coating and substrate produced from the damage events, such as cracking, delamination, chipping, spalling, buckling and so on.	[161, 168-170]
	Frictional force	Indicates how the stylus and the specimen are interacting through in-plane forces developed by the applied normal load, indenter penetration and scratch path features.	[161, 169-171]

Microscopic examination of the scratch tracks

The primary technique for determining critical load values for a progressive damage induced during the scratch test is microscopic examination on the scratch track. ASTM C1624-05 has set guidelines in identifying the critical load values as follows: L_{C1} is associated with the start of chevron cracking, indicating a cohesive failure, while L_{C2} is associated with the start of chipping failure extending from the arc tensile cracks, indicating an adhesive failure between the coating and the substrate (Figure 2-32) [167]. Beside these critical loads which are listed in the standard, Jennett et al. [172] identified an additional new failure event during the scratch test. In their repeatable scratch test on titanium nitride (TiN) and diamond-like carbon (DLC) coatings study, they found the occurrence of L_{C3} after L_{C1} and L_{C2}, identified as gross interfacial shell- shaped spallation that extends across the whole scratch track. On the other hand, Meneve et al. [173], in their study on scratch test on TiN coatings on hardened high speed steel, identified L_{C3} as a ploughing of the indenter through the coating.

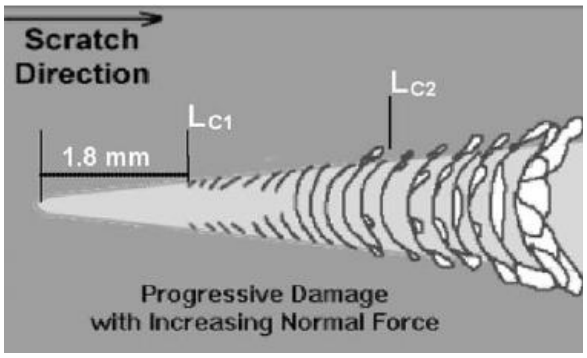

Figure 2-32 Illustration of critical load damage features in progressive load test (from ref. [167]

Research done by Aldrich- Smith et al. [133] on chromium nitride (CrN) coated stainless steel explained the detailed mechanism of damage progression on the samples. As the progressive applied load increased, forward chevron cracks occurred at the side of the scratch (cohesive failure mode), as indicated as L_{C1} and shown in Figure 2-33(a). At a high load, the crack spacing was sufficiently close and a cohesive spallation occurred along the crack borders (Figure 2-33(b)). As the cracks propagated over the scratch width, the coating was removed and a gross interfacial shell- shaped spallation occurred (Figure 2-33(c)). Further increasing the applied load showed an increasing density of conformal type buckling cracks, gross reverse chevron cracks with micro-spallation on the trailing edges, and a discontinuous ductile perforation through the coating.

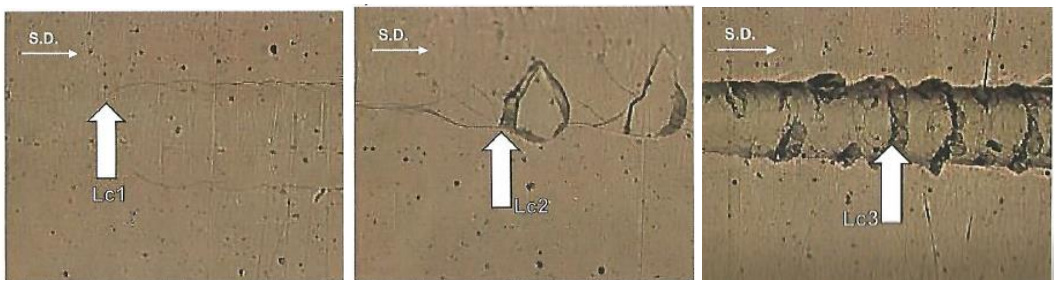

(a) (b) (c)

Figure 2-33 Optical micrographs of critical load failure events for the CrN coating with scratch direction from left to right. (a) L_{C1}, (b) L_{C2} and (c) L_{C3}.

However, the mechanism of failure modes is different from one coating to another depending on the hardness of the coating and substrate, as indicated in the map of main scratch test failure modes by Bull et al. [123]. This was shown by the study of Jacobs et al. [132], who identified four failure events for TiN coatings as follows: L_{C1} refers to longitudinal cracks at the track edges; L_{C2} refers to semi-circular coating cracks inside the scratch tracks; L_{C3} refers to cohesive chipping at the tracks edges; and L_{C4} refers to spallation at the track edges.

Acoustic emission of scratch test

AE detection is the most common way for on-line monitoring of brittle coating failure [174]. According to Piotrkowski [175], AE is constituted of elastic stress waves generated by the sudden internal stress-strain field redistribution in materials or structures under an applied load, such as crack initiation and growth, crack opening and closure, deformation, dislocation movement, void formation, and interfacial failure. A spontaneous shock wave burst occurs due to the formation and propagation of microcracks when the failure limit is reached [147]. The amplitude of the AE signals correlates to the severity of the damage between the coating and the substrate [147]. During the scratch test, further increase in the applied load results in coating damage with increasing frequency and severity; then, the resulting elastic waves are detected, measured, and recorded by the AE equipment. The AE data can then be analyzed concerning various characteristics, such as peak amplitude, frequency, event counts, rise-time, signal duration, and energy intensity. Ollendorf et al. [161] used the number of acoustic emission events (N_{AE}) as a test parameter for adhesion. They found that N_{AE} reduced with increasing the time of the argon pre-sputtering process.

Frictional force

Frictional force or tangential force is a force which opposes the relative motion between a moving stylus and the surface being scratched by the stylus, and is perpendicular to the normal force exerted by the stylus [167]. Generally, frictional force

increases with an increase in the normal force. The recorded frictional force plot exhibits a change in amplitude and shift into a stick- slip character when different types of failure modes occur during the scratch test. Bellido-Gozalez et al. [151] created a graph to demonstrate the changing amplitude of the frictional force oscillations as a function of failure mode for DLC coating (Figure 2-34).

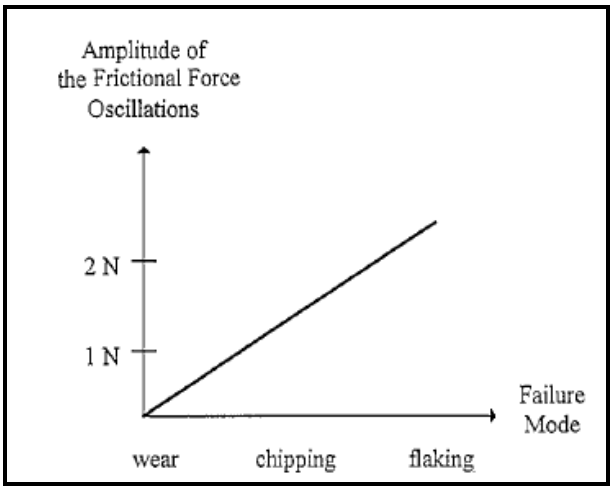

Figure 2-34 Correlation between the amplitude of frictional force and failure mode for DLC coating

2.6 Summary of the Literature Review

Success of the electrodeposition of metal on aluminium alloys substrates with a good adhesion depends on surface pre-treatment of the substrate. Surface pre-treatment on aluminium alloys involves a series of processes, including mechanical grinding, alkaline cleaning, acid cleaning, and the activation process. Zincating is the most widely used method of activating the aluminium alloys surface in order to obtain good adherence of the coating material to the substrate. There are numerous studies in the literature review which have used double zincating process, since the rough surface produced from single zincating process is not suitable for subsequent electrodeposition. However, the double zincating process is complex. Therefore, in this study a modification of the conventional single zincating duration has been made in order to improve the poor coating adhesion of the conventional single zincating process and replace the complex process of the double zincating process.

3 METHODOLOGY

3.1 Introduction

Due to the natural oxide layer formed on the substrate surface, aluminium and its alloys require a specific surface preparation for successful electrodeposition. The oxide layer prevents a metallic bonding from forming between the metallic coating and the aluminium alloy substrate. A coating produced before removing the oxide layer will result in poor adhesion. Therefore, a critical surface pre-treatment procedure is required, including a series of cleaning and activation process, such as mechanical surface pre-treatment, chemical surface pre-treatment, and zincating.

In this research, nickel coatings were prepared on the aluminium alloy 7075 (AA7075) substrate using an electrodeposition technique through a series of surface pre-treatment processes. The ultimate aim of this research is to overcome the adhesion and delamination problems in nickel coatings on aluminium alloy substrates. Therefore, this research emphasizes the zincating process in order to find the optimum process parameters of the zincating process. The zincating process is an essential step in activating the substrate for a subsequent electrodeposition process. The role of the zincating process is to provide an intermediate zinc layer on the substrate surface which can initiate the electrodeposition process.

In this research, AA7075 was chosen as a substrate. After mechanical and chemical surface pre-treatment, zincating processes were applied on the substrate. Each surface pre-treatment process is accompanied by water rinsing in order to avoid the drying of the substrate and contamination of the bath. This research is divided into several phases; (i) phase 1: investigation on the zincating process parameters, such as immersion duration and multiple processes through an electrochemical measurement, (ii) phase 2: characterization of the zincating layer on the AA7075 substrate using SEM, EDX analysis and AFM, (iii) phase 3: electrodeposition of nickel coatings on AA7075 substrates through multiple zincating processes at various durations, and (iv) phase 4: evaluation of the coating properties such as adhesion and corrosion resistance through scratch adhesion test and corrosion test.

Also, the influence of copper activation process prior to the zincating process was studied, with the goal of overcoming the high dissolution problem of AA7075 substrate in the zincating solution. The entire process of this research is depicted in Figure 3-2.

3.2 Surface Pre-treatment Procedures

3.2.1 Substrate Material

AA7075 was used as a substrate for the nickel electrodeposition. It was supplied by British Aluminium Limited (Birmingham, United Kingdom). The testing specimens were cut into rectangular pieces with a size of 70 mm x 29.5 mm x 3 mm (Figure 3-1).

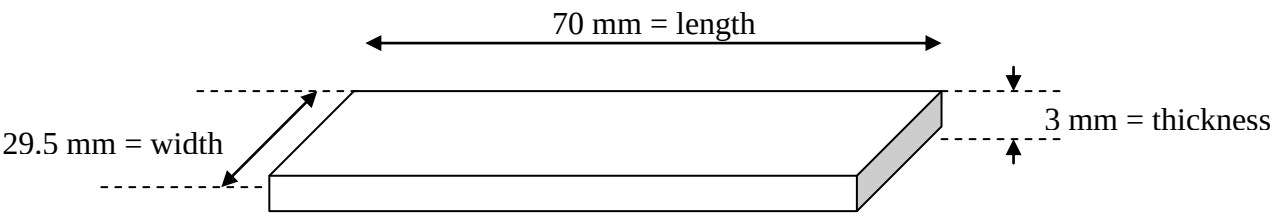

Figure 3-1 Dimension of the substrate

3.2.2 Mechanical Surface Pre-treatment

Prior to coating, AA7075 substrates were mechanically ground with silicon carbide (SiC) papers of 180, 800, 1200 and 4000 grit. They were mechanically polished with 6 and 1µm diamond, then cleaned with distilled water and dried.

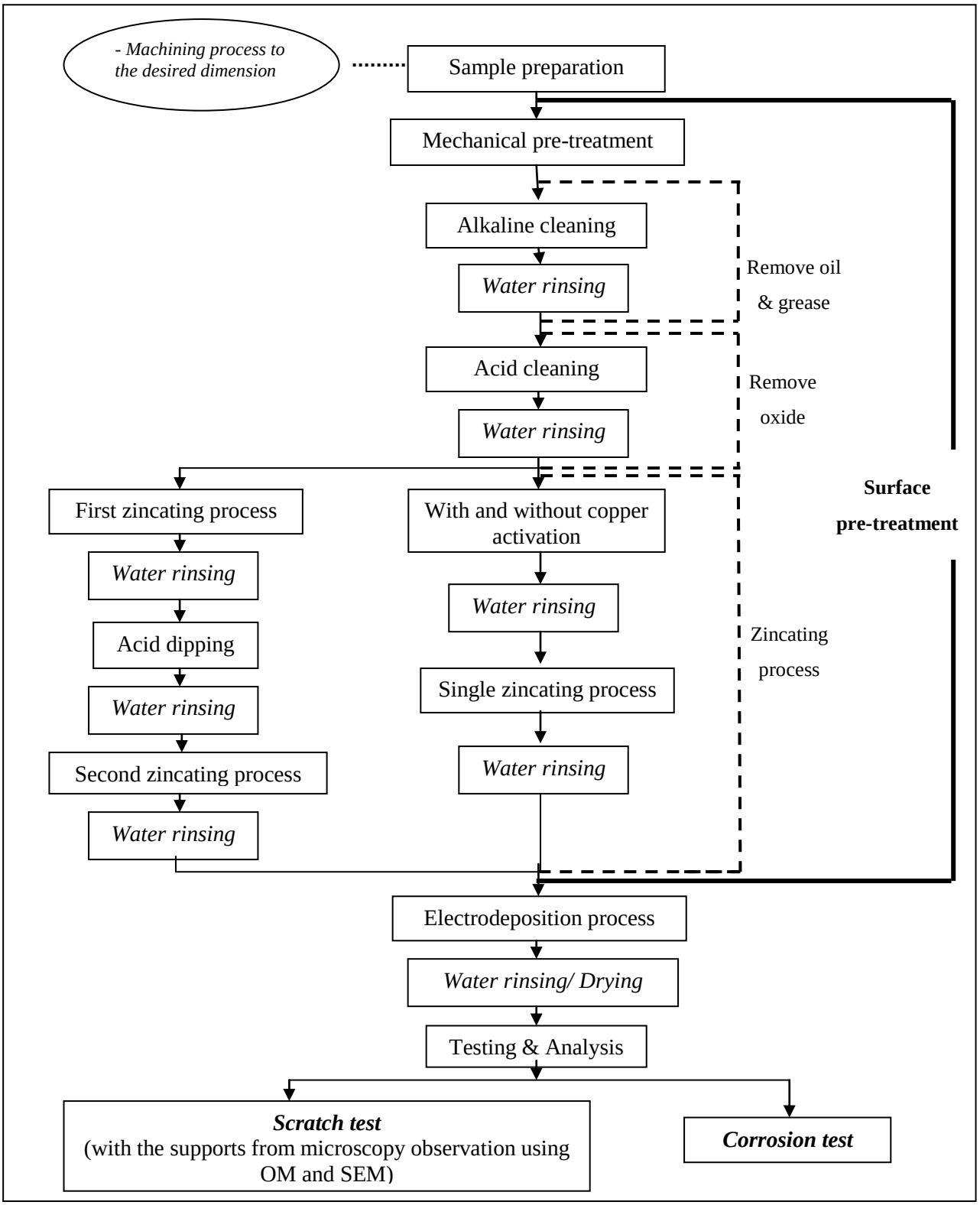

Figure 3-2 Entire process of electrodeposition nickel on AA7075 substrate

3.2.3 Chemical Surface Pre-treatment

Alkaline Cleaning

For all samples, alkaline cleaning was employed to remove organic contaminants on the substrate before the zincating process. The composition of 10 wt. % NaOH alkaline solution used in this research is shown in Table 3-1. Distilled water was used for preparation the solution. The chemical reactions occurring during immersion of the substrate in this solution were observed. The substrates were immersed in the alkaline solution for 10 seconds at room temperature. The substrates were then rinsed with water and immediately immersed in the next bath to avoid drying. The effect of this solution on the substrate surface was observed.

Table 3-1 Composition of alkaline cleaning solution

Component	Concentration (g/l)
Sodium hydroxide (NaOH) (97%)	100
Distilled water	balance

Acid Cleaning

The acid cleaning solution was prepared according to Table 3-2 in order to produce a 50 vol. % nitric acid (HNO_3) solution. The substrates were then immersed into the solution for 20 seconds at room temperature. The etch time was kept to a minimum to prevent excessive removal of aluminium from the substrate. The effect of this cleaning process on the substrate surface was observed.

Table 3-2 Composition of acid cleaning solution

Component	Concentration (g/l)
Nitric acid (HNO_3) (70%)	714
Distilled water	balance

3.2.4 Multiple Zincating Processes

The zincating solution used in this research was a mixture of sodium hydroxide (Fisher Scientific, United Kingdom), zinc oxide (Sigma Aldrich, United Kingdom), ferric chloride (Sigma Aldrich, United Kingdom), and potassium sodium tartrate (Rochelle salt) (Sigma Aldrich, United Kingdom) (Table 3-3). The composition and the procedures of preparation of the zincating solution followed ASTM Standards (B 253-87) [176]. The zincating process was carried out by dipping the pre- cleaned substrate vertically in a small glass beaker containing a zincating solution at room temperature. Two types of zincating process were studied. The conventional single zincating process involves immersion of the substrate in the zincating solution for 1 minute [29], while the double zincating requires two immersions. According to Mallory et al. [86], the second zincating process should be conducted using short immersion in order to produce a thin and uniform layer of zinc deposit. Therefore, in this research a double zincating process was conducted at 60 seconds for the first zincating and at 10, 20, 30, 40 and 50 seconds for the second zincating. Acidic etching for 20 seconds in 50 vol. % HNO_3 solution at room temperature was performed between consecutive zincating operations. Throughout this thesis, the double zincating treatments used in this study will be indicated in a shortened description, e.g. 60/20 s double zincating means a double zincating treatment applying 60 s for the first zincating and followed by 20 s for the second zincating. The immersion duration for conventional single zincating process was extended to 5, 10, 15 and 20 minutes based on the electrochemical measurement of the AA7075 substrate in the zincating solution. In order to study the effect of copper activation on the zincating process, further batches of samples treated with the conventional and modified single zincating processes were produced. The samples were first immersed in an etching solution containing 0.5 M H_2SO_4 + 3.13 x 10^{-4} M $CuSO_4$ solution at room temperature for 10 minutes. The samples were rigorously rinsed after each process to prevent contamination from bath to bath. Details of the samples produced at various durations of zincating processes are shown Table 3-4.

Table 3-3 Composition of the zincating solutions used to produce nickel deposits on AA7075 substrate

Component	Concentration (g/l)
Zinc oxide (ZnO) ($\geq$ 99.0%)	100
Sodium hydroxide (NaOH) (97%)	525
Ferric chloride (FeCl) (97%)	1
Potassium sodium tartrate ($KNaC_4H_4O_6 \cdot 4H_2O$) (ACS reagent)	9.8
Purified water	balance

Table 3-4 Matrix table of samples produced at various immersion durations of zincating processes

Multiple zincating process duration														
Conventional single zincating (60 s)		Modified single zincating (s)								Double zincating (s)				
Without copper activation	With copper activation	Without copper activation				With copper activation								
		300	600	900	1200	300	600	900	1200	60/10	60/20	60/30	60/40	60/50
P5-18	P5-38	P5-19	P5-20	P5-21	P5-22	P5-37	P5-36	P5-35	P5-34	P5-13	P5-14	P5-15	P5-16	P5-17
P5-2	P5-28	P5-3	P5-5	P5-6	P5-7	P5-29	P5-30	P5-31	P5-32	P5-8	P5-9	P5-10	P5-11	P5-12
P5-45	P5-44	P5-47	P5-48	P5-49	P5-50	P5-43	P5-42	P5-41	P5-40	P5-51	P5-52	P5-53	P5-54	P5-46
P5-55	P5-57	P5-59	P5-61	P5-63	P5-65	P5-67	P5-69	P5-71	P5-73	P5-75	P5-77	P5-79	P5-81	P5-83
P5-56	P5-58	P5-60	P5-62	P5-64	P5-66	P5-68	P5-70	P5-72	P5-74	P5-76	P5-78	P5-80	P5-82	P5-84

3.3 Electrodeposition Process

The electrolyte was prepared by dissolving chemical reagents in distilled water. The chemical reagents consisted of nickel sulphate hexahydrate (Sigma-Aldrich, South Korea) as metal sources; sodium chloride (Sigma-Aldrich, USA); boric acid (Sigma-Aldrich, Germany) as a buffer; sodium dodecyl sulphate (Fluka, Germany) as a surfactant; saccharin (Sigma-Aldrich, South Korea) as a grain refiner and stress reliever; and 2-butyne-1, 4-diol (BD) (Sigma Aldrich, USA). The detailed chemical composition of electrolyte is listed in Table 3-5. The electrolyte used for the nickel deposition was studied previously and presented in the Nine Month Report. The chemical composition in the nickel electrolyte used in this research was chosen from the optimum nickel coating on aluminium alloy 7075 with improved in microhardness and wear resistance, and produced from previous study (Appendix A). The optimum sample was obtained at 3 g/l saccharin concentration and an electrodeposition process at 45°C.

However, the electrodeposition process via pulsed current mode stated in the Nine Month Report could not be conducted because the plating instrument at the Electrochemistry Laboratory of University of Southampton, United Kingdom is unsuitable for pulsed current electrodeposition process.

Only one side of the substrate surface with an area of 20 mm in diameter was exposed to the nickel electrolyte, while the rest of the substrate was covered with a polyester tape supplied by Cole-Parmer (United Kingdom). The pre-treated substrate was then attached to a three electrode system glass cell fitted with a water jacket, through which water from a thermostated bath was circulated (Grant LTD 6G). A thermostated water bath was used to keep the electrodeposition process at the selected temperature, 45$\pm$1˚C. In the glass cell, the substrate was attached to the glass cell by using a clipper, with an insulator between of the substrate and the clipper to prevent any metal contact.

A potentio/galvanostat (AUTOLAB PGSTAT30) was employed for nickel electrodeposition using a typical three-electrode system consisting of a working electrode (WE) of AA7075, a saturated calomel electrode (SCE) as a reference electrode (RE) and a counter electrode (CE) of a nickel plate (99.99%). The nickel plate had dimensions of 30 mm x 10 mm x 1 mm and was supplied by Advent Research Materials Limited (Oxford, United Kingdom). During the electrodeposition process, the

nickel electrolyte was stirred continuously with a PTFE-coated magnetic stirrer (6 mm diameter x 30 mm length) at 300 rpm using a hot plate and magnetic stirrer equipment (Stuart, UK). The current density used for the electrodeposition process was 4 A/ dm^2 under direct current mode with the total time of electrodeposition set at one hour. The arrangement of the electrodeposition process is depicted in Figure 3-3. In addition, the electrodeposition potential- time dependence for the electrodeposition of nickel coatings was recorded during the electrodeposition process using the potentiostat/galvanostat system. Details of the coatings produced at various durations of zincating processes are shown in Table 3-4.

Table 3-5 Concentration of chemical reagents in modified Watt's bath solution

Component	Concentration (g/l)
Nickel sulphate hexahydrate, $NiSO_4.6H_20$ (>99.0%)	200
Sodium chloride, NaCl (99.5%)	20
Sodium dodecyl sulphate, $C_{12}H_{25}SO_4Na$	0.2
Saccharin, $C_7H_5NO_3S$ (>99.0%)	3
Boric acid, H_3BO_3 (99.5%)	30
2-butyne-1,4-diol, $C_4H_6O_2$ (BD)	0.5
Purified water	balance

3.4 Characterization Techniques and Testing

The characterisation techniques and testing used in this research are listed in Table 3-6. These test methods including electrochemical test, microscopy and tribological test.

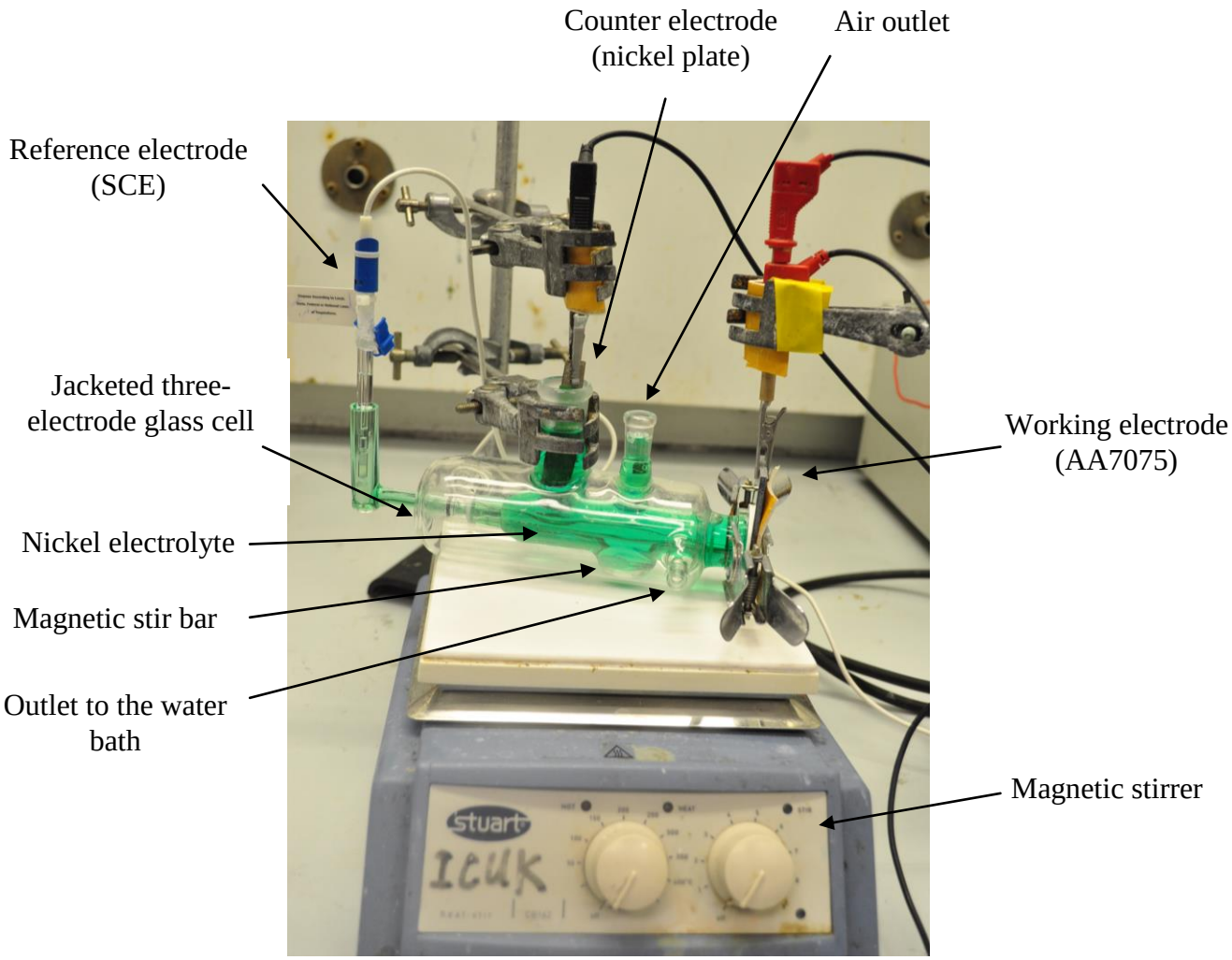

Figure 3-3 Electrodeposition process arrangement of nickel coating on AA7075 substrate.

Table 3-6 Summary of characterisation techniques and testing

Technique/ testing	Principle	Application	Information
Electrochemical method Open-circuit potential measurement (when the voltmeter is removed and leaving an open- circuit cell)	Electrochemistry deals with the chemical response of an electrode/ electrolyte system to an electrical stimulation and the electrochemical behaviour of species (ions) can be assessed, including concentration, kinetics and reaction mechanisms [94]	Zincating process	Provide the behaviour of the AA7075 substrate in zincating solution, in terms of potential changes with immersion time
Scanning electron microscopy (SEM)	The surface of the specimen is scanned with	Zincated specimens	Provide the surface morphology of the

	an electron beam and the reflected or back-scattered beam of the electrons is collected. Then, the beam will be displayed on a cathode ray tube and it represents the surface features of the specimen [93, 177]	Cross-section of the coatings Scratched coatings	AA7075 substrate after the zincating process and microstructure evolution (nucleation behaviour) of the zinc particles as a function of immersion duration Check the evidence of the zinc layer after electrodeposition process and to check the coating thickness Investigate coating failure modes
Energy dispersive X-ray (EDX)	This testing relies on the investigation of an interaction of X-ray excitation on a specimen To stimulate the emission of characteristic X-rays from a specimen, a high-energy beam of charged particles such as electrons, protons, or X-ray focused into the sample being studied [178]	Zincated specimens Cross-section of the coatings	This is used for elemental analysis of the zincated specimens at multiples zincating process and various immersion durations Check the evidence of the zinc layer after electrodeposition process and to check the coating thickness.
Atomic force microscopy (AFM)	As the stylus tip moves on the surface, it experiences both attractive and repulsive forced [Kanani]	Zincated specimens	Study the influence of multiple zincating process at various durations on the surface morphology and surface roughness
Corrosion test	Is an electrochemistry process which involves two reactions: oxidation reaction; metal atoms lose or give up electrons (corrosion site) reduction reaction; gain electrons from the oxidized metals [93]	Nickel coating	Corrosion potential, corrosion current density
Scratch adhesion test	Adhesive strength or adhesive force is the force required to part coating from substrate [Kanani].	Nickel coating	Investigate the influence of the multiple zincating processes at various durations on the adhesive properties and scratch resistance

3.4.1 Open-Circuit Potential Measurement

In the electrodeposition process, electrochemistry study on the surface pre-treatment process is very important. Therefore, the behaviour of the substrate in zincating solution was initially investigated using the open- circuit potential measurement, in order to find the suitable zincating duration. All samples were initially alkaline and acid cleaned at 10 s and 20 s, respectively. The open-circuit potential (E_{oc}) in all graphs are recorded as a function of zincating immersion duration. A potentio/galvanostat (AUTOLAB PGSTAT30) was used to monitor the open circuit potential during the zincating process of AA7075 substrate. A glass cell consisting of a typical three-electrode system of a working electrode (WE) of AA7075; a saturated calomel electrode (SCE) as a reference electrode (RE); and a counter electrode (CE) of a platinum mesh (99.99%) was used in this study (Figure 3-4).

3.4.2 Scanning Electron Microscopy and Energy Dispersive X-ray

The surface morphology of zincated sample, cross-section of the nickel coating and scratch track on the nickel coating were observed and examined using an SEM (JEOL JSM 6500 SEM). The backscattered electron image (BEI) analyses were taken of the copper pre-treated samples, in order to detect the contrast between areas with different compositions. The element composition of the zincated samples, prepared from multiple zincating process of various durations, was studied using an Oxford Instruments INCA 300 EDS installed in the SEM instrument.

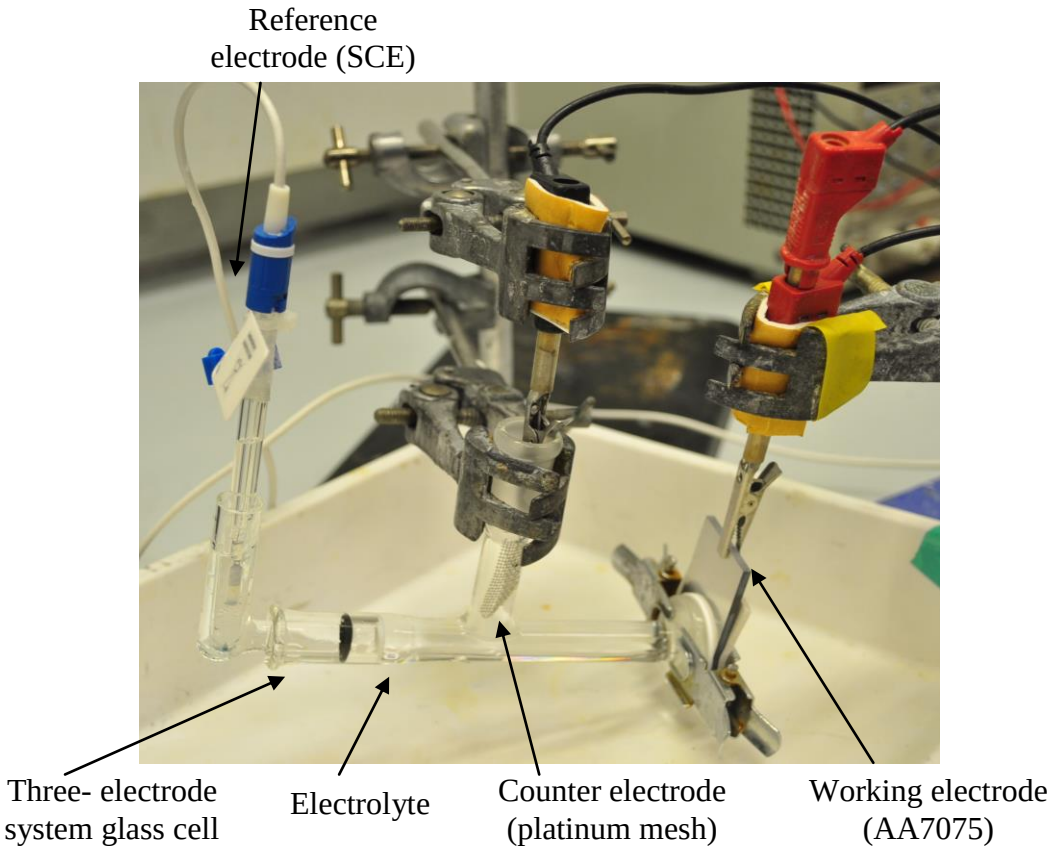

Figure 3-4 Electrochemical experiment arrangement used for zincating process and corrosion test.

3.4.3 Atomic Force Microscopy

To investigate the surface morphology and surface roughness of the zincated samples, an atomic force microscope (Agilent 5500) in contact mode was used. This equipment is sensitive to forces produced from interactions between the sample surface and a fine probe fixed to the tip of a coil spring plate or cantilever with a low spring constant [148]. As shown in the Figure 3-5, under these forces the cantilever is subject to a deflection which is recorded by measuring the variation of the laser beam position reflected by the extremity of the cantilever. Then, either the repulsive force between the tip and sample or the actual tip deflection is recorded and converted into a three-dimensional (3D) image [179]. AFM analysis was performed at two different surface areas, namely 3 x 3 µm and 10 x 10 µm. In addition, a line profile was used to determine the surface roughness of the surface. This measurement was taken 10 times from each sample.

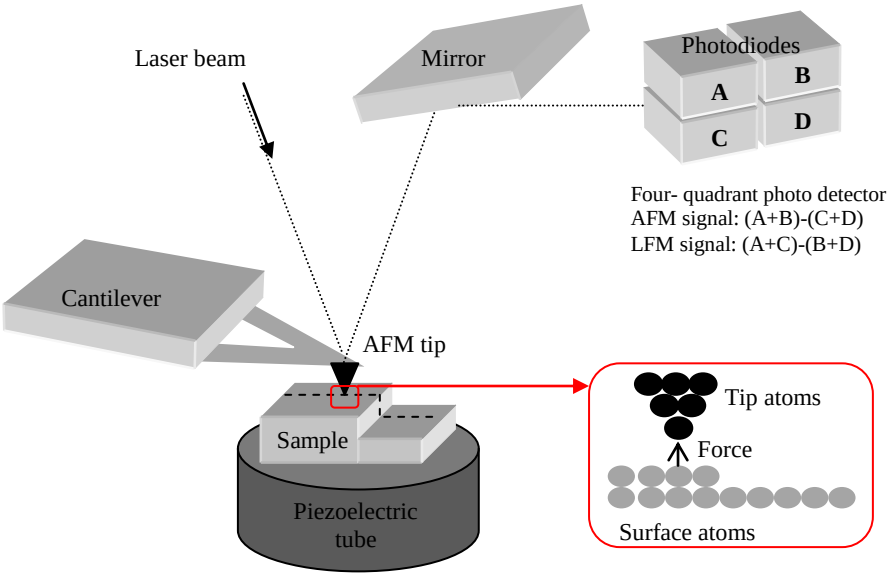

Figure 3-5 Schematic diagram of Atomic Force Microscope [148, 180]

3.4.4 Scratch Adhesion Test

A scratch test was performed on the nickel coatings electrodeposited on AA7075 substrate produced from multiple zincating process, in order to create an interfacial stresses and coating rupture in the vicinity of the scratch groove. A scratch tester (ST3001, Teer Coating, United Kingdom) equipped with an acoustic emission sensor and operated in progressive applied load mode was used in this test. The scratch tests were carried out at the National Physics Laboratory (NPL), London, United Kingdom. During this test, acoustic emission signal, normal and tangential forces and depth of penetration of the stylus were recorded. Before the scratch test, the coatings were first wiped with acetone in order to remove contaminates such as oil, grease, finger prints, debris and dust. The stylus tip also needed to be wiped with an acetone after every test in order to prevent residual debris or film (oil and grease) build-up on the stylus tip from previous tests. In this test, the scratch was developed on the coated specimens by drawing a diamond stylus (Rockwell 'C', 120º cone with a 200 µm radius) across the flat surface of the coating (Figure 3-6). An AE transducer was attached to the indenter holder and used to detect the elastic energy, consisting mainly of cracking and fracturing energy released from the specimen surface during the scratching process

[181]. The tests were done at a loading rate (100 N/min) and a horizontal displacement rate (10 mm/min), under unchanged test conditions during the testing. The test was repeated eight times on each specimen with at least 2 mm scratch spacing, in order to obtain mean and standard deviation values.

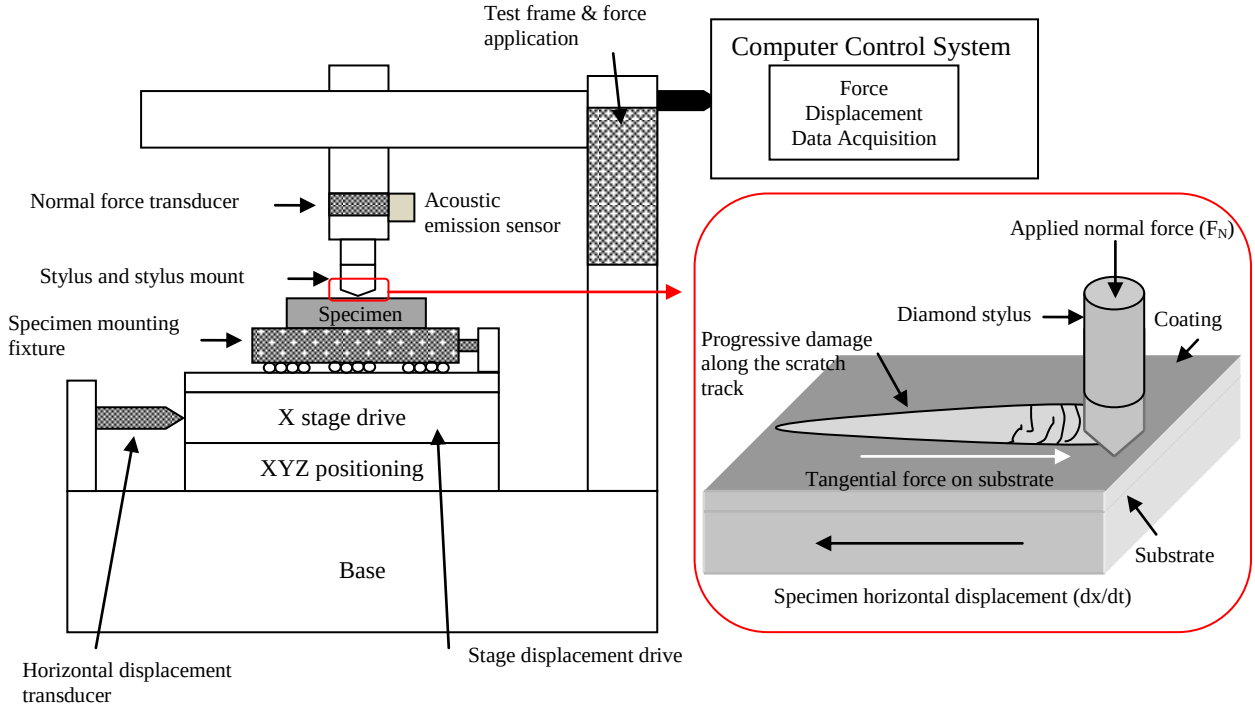

Figure 3-6 Schematic diagram of scratch adhesion test system [167]

Then, the specific levels and types of progressive damage in each scratch track were observed under an optical microscope (Olympus BH2-UMA) and scanning electron microscope (JEOL JSM 6500 FEG SEM). The scratch tracks were critically examined and captured from one point to another point using the optical microscope. Then, the images were analyzed and merged using the 'Olympus Stream Image Analysis' software.

After microscopy evaluation, the coating failure mode was identified based on the procedure used by the Heinke et al. [124], who define first critical load (L_{C1}) as the load in which first cracks occur (cohesive failure) and the second critical load (L_{C2}) as the load where the first delamination at the edge of the scratch track occurs (adhesive failure). SEM images were also taken on several samples in order to obtain a detailed

view of the scratch groove and the surrounding coating surface. In addition, the failure events of L_{C1} and L_{C2} were identified using the acoustic emission (AE) signal, due to an increasing of the AE signal intensity.

The characteristics of the scratch scars on the coating materials were also examined by the friction force (F_f) curves which were recorded during the scratch test. In this study, the scratch length was 10 mm and the normal scratch load (N) applied during the test was from 10 to 100 N. In the figure shown, the scratch was made from left to right (

Figure 3-7). The scratch test was initially conducted using 0 to 10 N of applied load. However, the results did not show any coating damage. Therefore, the progressive applied load in this study was increased from 10 to 100 N in order to scratch the coatings. These recorded frictional force (F_f) curves and acoustic emission (AE) signals were also used as a supplementary test data to identify different coating failure levels, according to the procedures of Duncan et al. [182]. Coating failures, such as cohesive failure or adhesive failure, were compared with the various failure modes as shown in Figure 3-8 and Figure 3-9, respectively.

A typical AE signal intensity and the friction force (F_f) versus the scratch distance curve and the SEM micrographs of the scratch tracks are shown in

Figure 3-7. Scratch failures which occur in a scratch test can be analysed using several different signals and observation methods. The present research utilized (1) AE signals, (2) F_f and (3) microscopy observation. The recorded AE signals during the test were analysed by looking at the significant changes in AE signals characteristics, such as (1) location of data display, (2) number of AE events (N_{AE}) and (3) location of first AE signal which value is more than the average background noise value. These characteristics were correlated with a specific scratch distance and applied load. The average background noise for the AE signals for each sample from multiple zincating process (conventional single zincating with and without copper activation, double zincating and modified single zincating with and without copper activation) was identified through an inspection of the AE versus scratch distance curve as illustrated in Figure 3.7.

Then, N_{AE} was determined by considering the number of AE signals which occurred higher than the background noise, which represented the coating failures on the track.

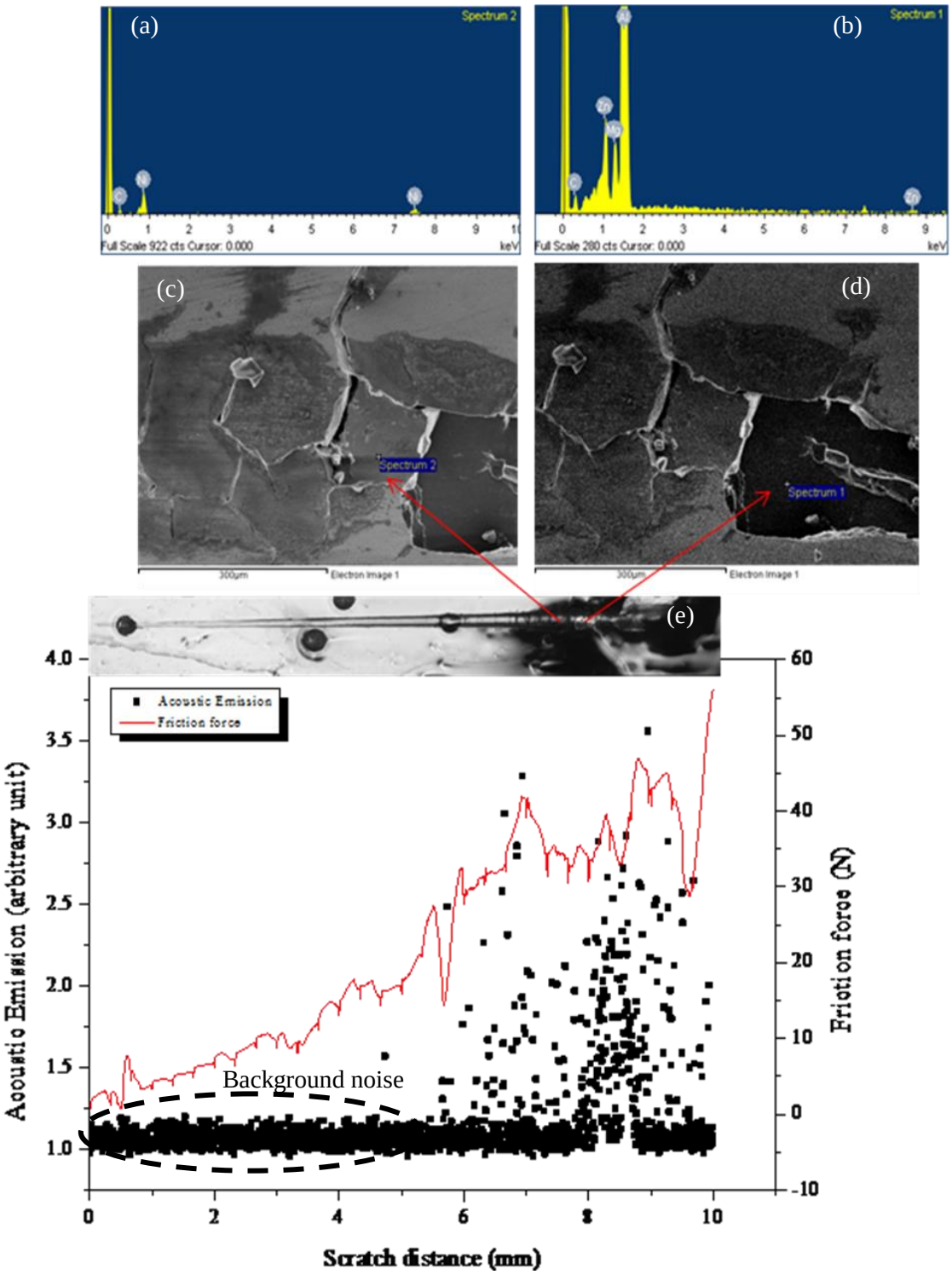

(f)

Figure 3-7 Typical results of scratch test which shows the AE signal and friction force versus scratch distance (f), optical micrograph of the scratch track (e) and SEM images of the failure events ((c) and (d)). An EDX analysis using the 'point and ID' mode was used and drawn on the fracture surfaces, in order to check whether the substrate is revealed or not ((a) and (b)).

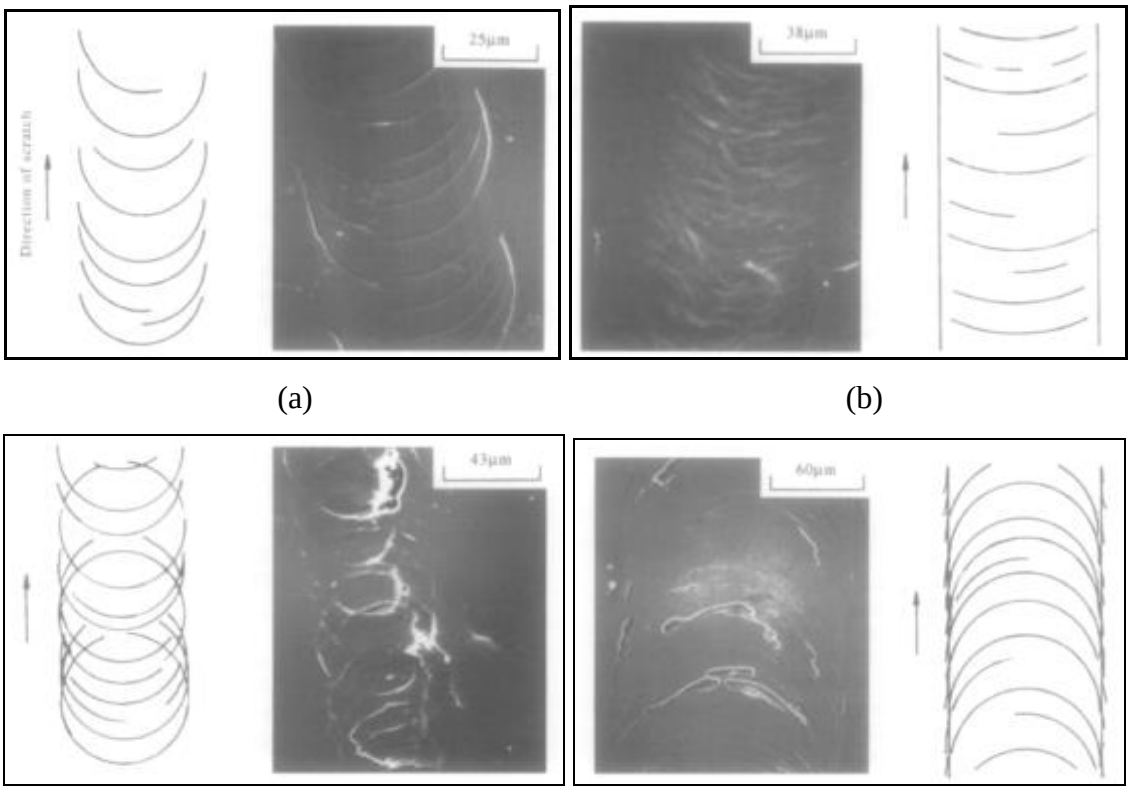

(a) (b)

(c) (d)

Figure 3-8 Through-thickness cracking (cohesive) failure modes in the scratch test (a) brittle tensile cracking, (b) ductile tensile cracking, (c) hertz cracking and (d) conformal cracking [123]

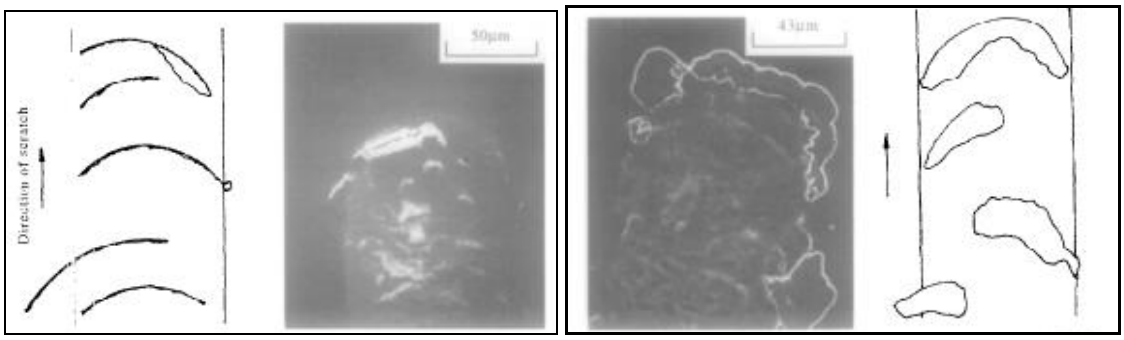

(a) (b)

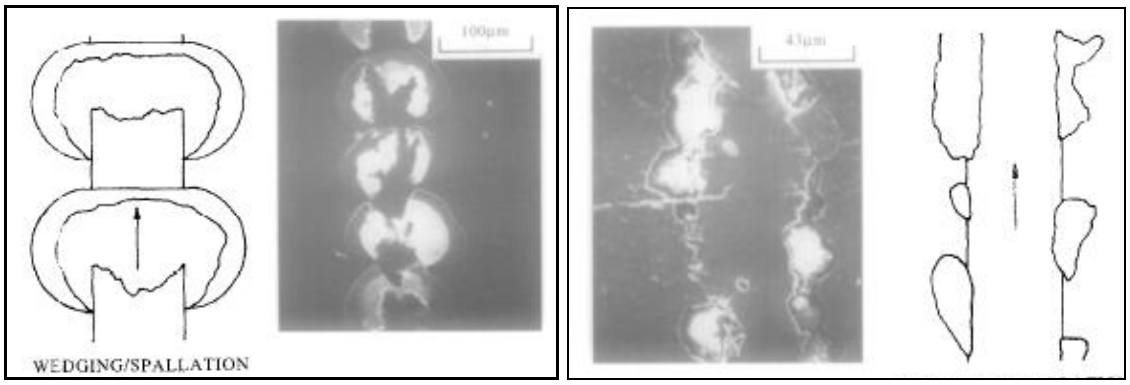

(b) (d)

Figure 3-9 Interfacial (adhesive) failure modes in the scratch test (a) buckling, (b) buckle spallation, (c) wedging/ spallation and (d) recovery spallation [123]

3.4.5 Corrosion Test

According to Perez [94], the electrochemical corrosion behavior of metals and alloys can be investigated by generating polarization curves, which provide several electrochemical regions, such as concentration polarization, activation polarization, and passivation. The corrosion behavior of the nickel coatings were evaluated by potentiodynamic polarization in 3.5 wt. % NaCl solution at room temperature using a potentiostat/galvanostat (AUTOLAB PGSTAT30) system. Work in [183] indicates that a sweep rate of 50 mV/s from cathodic to anodic currents in a range of $\pm$ 1000 mV vs. the rest potential is appropriate, and these experimental parameters have been adopted in the present work.

A glass cell consisting of a typical three- electrode system of a working electrode (WE) of nickel coating electrodeposited on AA7075 substrate (exposed area is 10 mm diameter); a saturated calomel electrode (SCE) as a reference electrode (RE); and a counter electrode (CE) of a platinum mesh (99.99%) was used in this study, as shown in Figure 3-4 in Section 3.4.1. Corrosion potential and corrosion current density were obtained using the Tafel extrapolation technique from the potentiodynamic polarisation curves recorded during the test.

4 RESULTS

4.1 Introduction

This chapter presents the results obtained from various analyses of surface pre-treatment procedures on the aluminium alloy 7075 substrate (AA7075) and mechanical and electrochemical evaluations on the nickel coatings.

The main aim of the present study is to investigate the influence of the multiple zincating processes at various durations on the nickel coatings electrodeposited on AA7075 substrate. To achieve this, the influence of conventional single zincating, modified single zincating, conventional single zincating with copper activation, modified single zincating with copper activation, and double zincating processes at various durations on the surface morphology, element composition, surface topography, surface roughness, coating interface, coating adhesion and coating corrosion resistance were investigated using electrochemical measurement, OM, SEM, EDX, AFM, scratch test, and corrosion test.

4.2 Electrochemical Behaviour of AA7075 Substrate during Various Surface Pre-treatment Processes

4.2.1 Electrochemical Behaviour of AA7075 during Alkaline Cleaning and Acid Pickling Processes

In this study, the duration for alkaline cleaning was fixed for 10 seconds, based on the literature [22, 42, 44]. The variation of the open circuit potential (E_{OC}) of the AA7075 substrate in 10 wt. % NaOH solution with time was measured in order to investigate the behaviour of the AA7075 substrate during the alkaline cleaning, as shown in Figure 4-1. The curve measured during the process can be divided into three stages. The first stage showed a decrease in E_{OC} value from approximately -1.61 V at the beginning of the immersion to approximately -1.70 V after 25 seconds of

immersion, which indicates an active dissolution of the substrate. During the second stage, E_{OC} increased rapidly in the noble direction and reached -1.60 V after 100 seconds of immersion. The shift of E_{OC} in the noble direction indicates the formation of an oxide layer on the substrate. In the third stage, E_{OC} increased gradually to reach a steady potential at approximately -1.565 V.

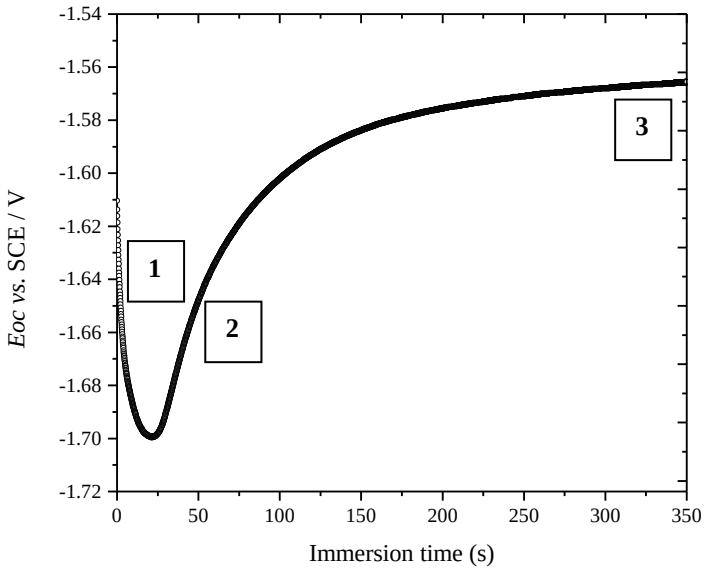

Figure 4-1 Changes in immersion potential of AA7075 substrate in alkaline solution (10 wt. % NaOH) at room temperature. The labels 1, 2 and 3 indicate the first, second and third stage, respectively.

After the alkaline cleaning, the samples were transferred to the acid cleaning bath. Duration for the acid cleaning process was fixed at 20 seconds, based on the literature [21, 34, 41, 45, 86]. Figure 4-2 shows the variation of E_{OC} with time during the acid cleaning in 50 vol. % HNO_3 solution. The curve measured can be divided into three stages. During the first stage, the E_{OC} value rapidly decreased from approximately -0.08 to -0.095 V within 10 seconds of immersion, which suggests an active dissolution of the substrate at the beginning of the process. Then, during the second stage, the E_{OC} value increased rapidly to -0.06 V at 25 seconds. Finally, the third stage showed fluctuations of the E_{OC} value between approximately -0.04 V and -0.065 V at 25 to 230 seconds of immersion.

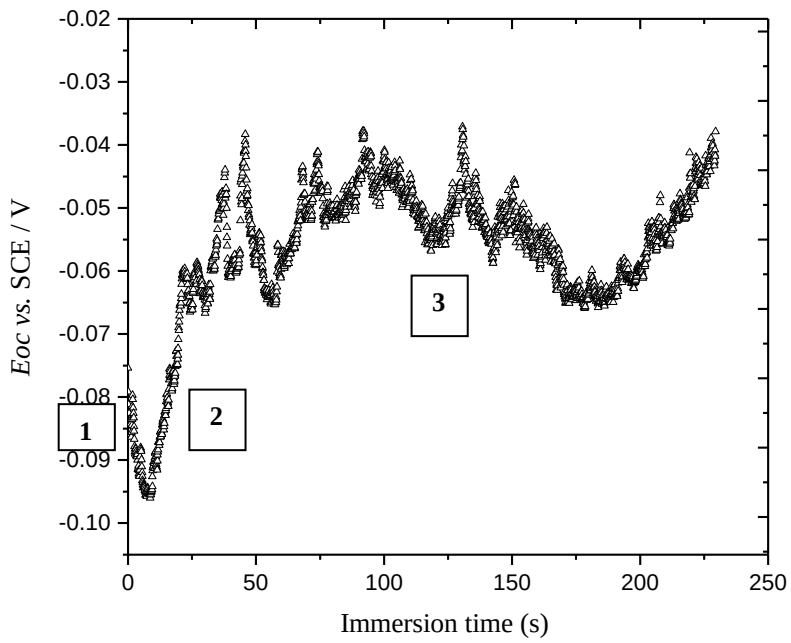

Figure 4-2 Changes in immersion potential of AA7075 substrates in acid solution (50 vol. % HNO_3) at room temperature. The labels 1, 2 and 3 indicate the first, second and third stage, respectively.

4.2.2 Electrochemical Behaviour of AA7075 during Single Zincating Process

Deposition of zinc particles on the substrate during the single zincating process was studied by measuring the variation of open circuit potential (E_{OC}), with immersion time in the zincating solution, as shown in Figure 4-3. The curve measured during this process can be divided into three stages. During the first stage, the substrate showed a rapid decrease in the E_{OC} value from approximately -1.595 V at the start of immersion to -1.614 V at 250 seconds, corresponding to the rapid dissolution of the substrate in the zincating solution. In the second stage, the E_{OC} of the substrate increased gradually in the noble direction, reaching about -1.596 V at approximately 1250 seconds. The increase in the E_{OC} value to the noble direction indicates that zinc particles were deposited rapidly on the substrate. During the third stage, the E_{OC} value slowly approached the steady potential at approximately -1.598 V, which indicates that the substrate is completely covered with the zincating layer.

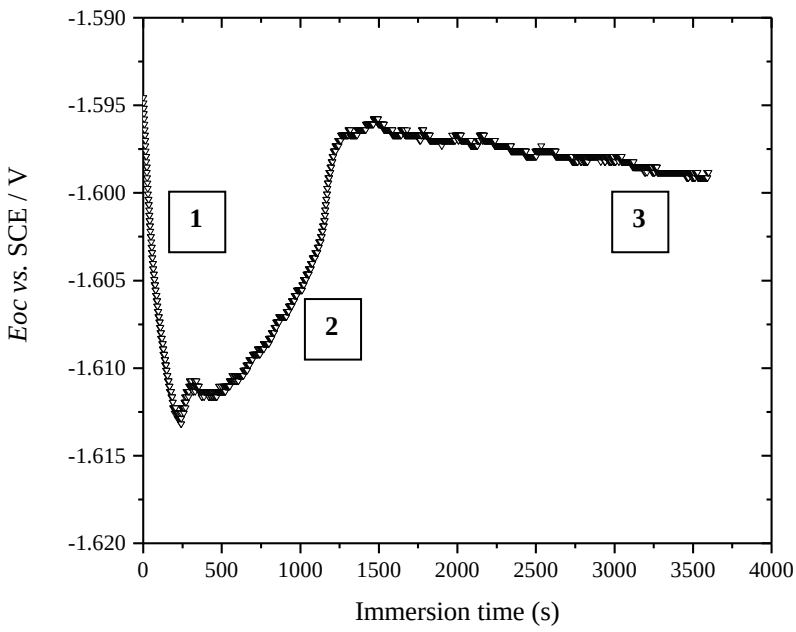

Figure 4-3 Changes in immersion open circuit potential (E_{OC}) of the AA7075 substrate during the single zincating process. The labels 1, 2 and 3 indicate the first, second and third stage, respectively.

4.2.3 Electrochemical Behaviour of AA7075 during Various Double Zincating Durations

The deposition of zinc particles on the substrate during the double zincating process was investigated by measuring the variation of E_{OC} with immersion time in the zincating solution. The specimens were first dipped in the first zincating bath for 10, 20, 30, 40, 50 or 60 seconds before entering the second zincating bath. This procedure was done in order to select the optimum duration for the first zincating process. Figure 4.4 shows the influence of the first zincating duration on the E_{OC} value of the substrate during second zincating process.

It is apparent in Figure 4.4 (b) that all six curves have similar trends. The curves measured during this process can be divided into three stages. For specimens prepared from the first zincating process at 10, 20, 40, 50 and 60 seconds, the first stage showed a steep decrease of E_{OC} within approximately 50 to 100 seconds of immersion in the

second zincating bath (Figure 4.4 (b)). However, the specimen produced at 30 seconds of first zincating process showed a gradual decreased in the E_{OC} within approximately 300 seconds of immersion.

For specimens prepared following a first zincating process of 10, 20, 40, 50 and 60 seconds, the initial part of the second stage shows a steep increase in E_{OC} values. Subsequently, the E_{OC} values gradually increased until the steady state potential. The steady state potential of the six samples in the second zincating solution is in the range of -1.596 to -1.599 V.

Among these specimens, the specimen produced from the shortest duration of first zincating process (10 seconds) showed the lowest E_{OC} value at approximately -1.6125 V at the initial time of immersion (0 second) in the second zincating bath, due to the active dissolution of the substrate (Figure 4.4 (b)). On the other hand, specimens produced from longer first zincating duration at 20, 30, 40, 50 and 60 seconds resulted in a higher E_{OC} value at the initial time of immersion compared to specimen produced from 10 seconds of immersion. This corresponds to the inactive dissolution of these substrates in the second zincating process.

Furthermore, during the second stage of zincating process, the E_{OC} values for the specimen produced from the longest first zincating process at 60 seconds is consistently more noble than the E_{OC} values for other specimens (Figure 4.4 (c)). This can be seen at the duration of 375 seconds to 1000 seconds. Then, the E_{OC} values of the 60 seconds specimen remains consistently more noble than other specimens until the steady state potential at the third stage of zincating process (Figure 4.4 (d)).

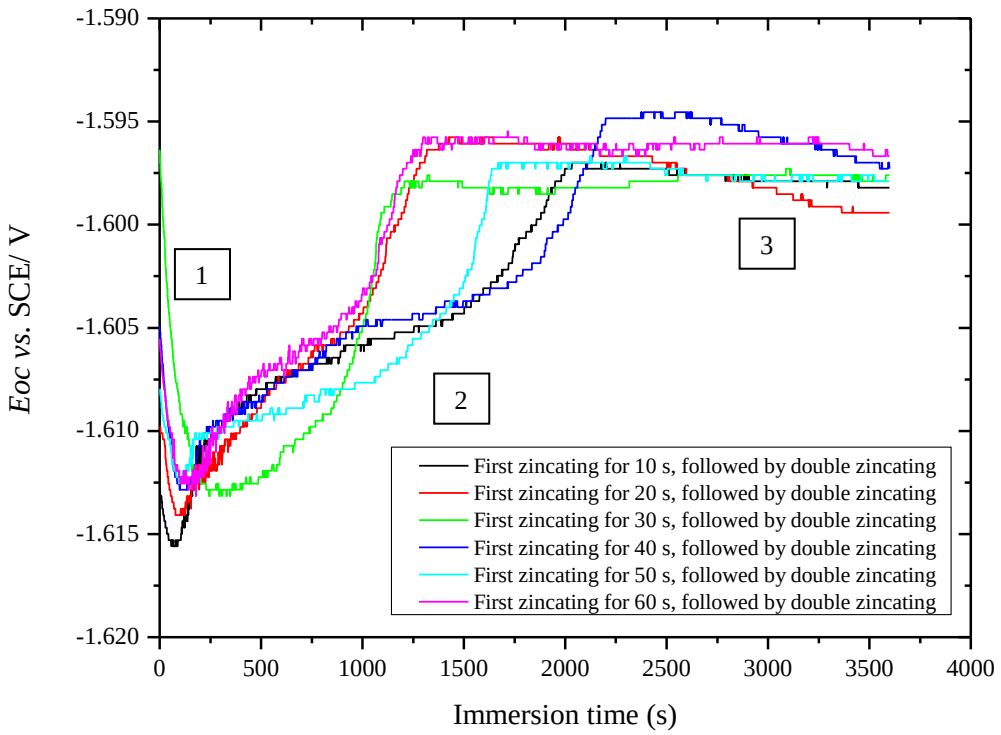
-1.590
-1.595
-1.600
-1.605
-1.610
-1.615
-1.620
Eoc vs. SCE/ V
0
500
1000
1500
2000
2500
3000
3500
4000
Immersion time (s)
1
2
3
First zincating for 10 s, followed by double zincating
First zincating for 20 s, followed by double zincating
First zincating for 30 s, followed by double zincating
First zincating for 40 s, followed by double zincating
First zincating for 50 s, followed by double zincating
First zincating for 60 s, followed by double zincating

(a)

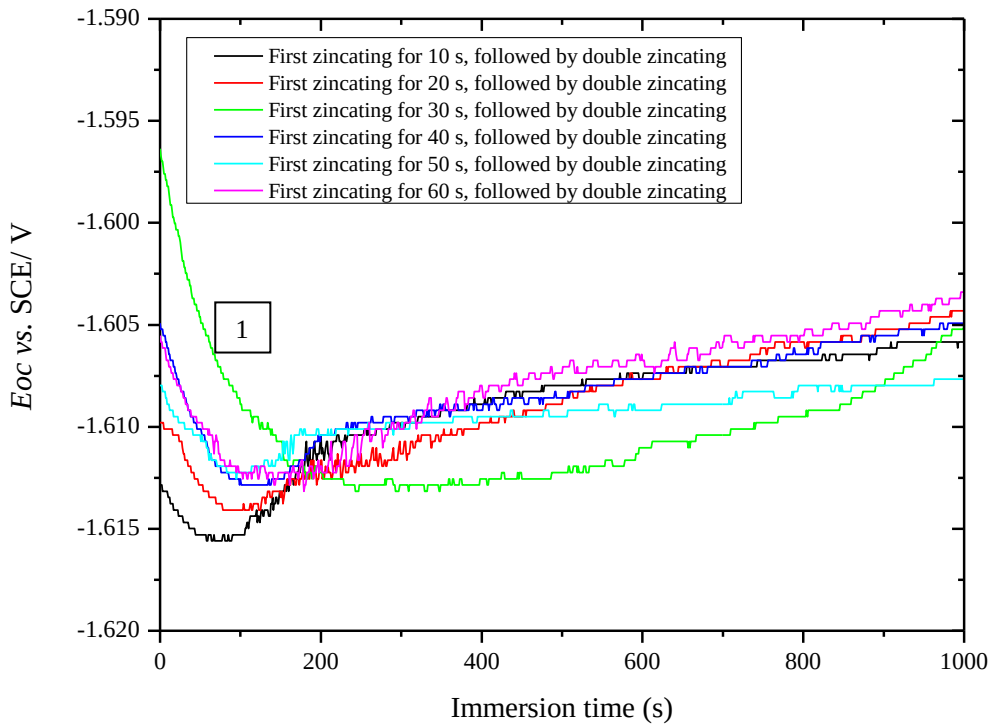
-1.590
-1.595
-1.600
-1.605
-1.610
-1.615
-1.620
Eoc vs. SCE/ V
0
200
400
600
800
1000
Immersion time (s)
1
First zincating for 10 s, followed by double zincating
First zincating for 20 s, followed by double zincating
First zincating for 30 s, followed by double zincating
First zincating for 40 s, followed by double zincating
First zincating for 50 s, followed by double zincating
First zincating for 60 s, followed by double zincating

(b)

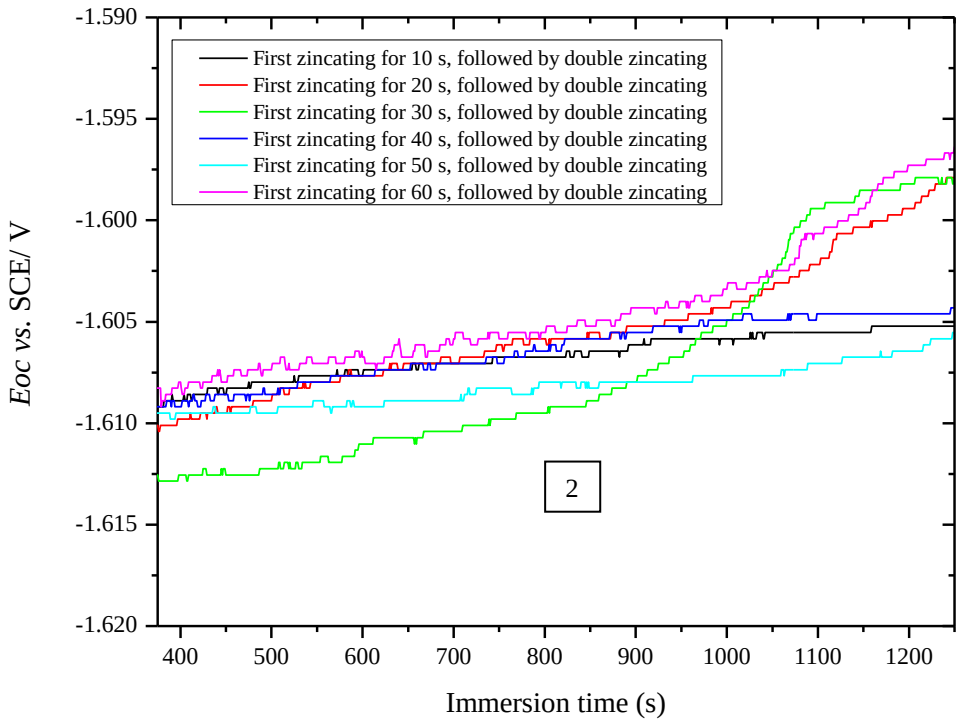

(c)

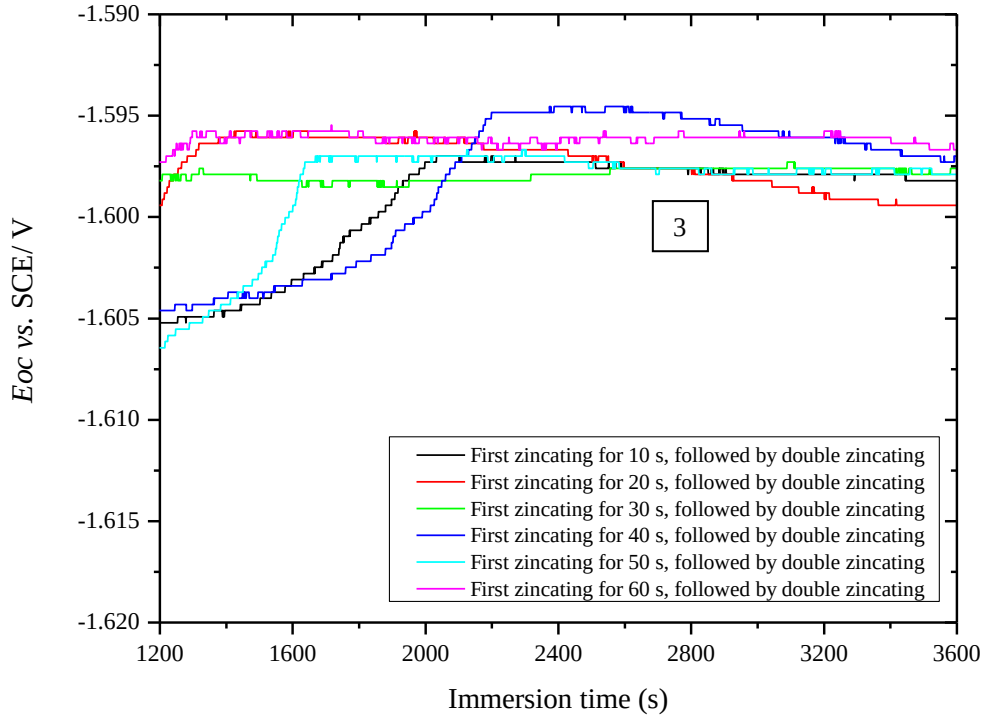

(d)

Figure 4-4 Changes in immersion open circuit potential (E_{OC}) of the AA7075 substrate during the double zincating process. (a) The changes of E_{OC} during the zincating process up to 3600 seconds. (b) A time- expansion plot for the initial stage of the zincating process (a). (c) A time- expansion plot for the second stage of the zincating process (a). (d) A time- expansion plot for the third stage of the zincating process (a).

In this study, the duration used for the first zincating process in the double zincating process was determined from Figure 4.4. In this figure, sample which was produced from first zincating process at 60 seconds shows the quickest deposition of the zinc particles, based on the consistently more noble E_{OC} values at 375 seconds until the steady state potential, compared to other specimens (Figure 4.4 (c and d)). Even though the specimen produced at 30 seconds shows more noble E_{OC} values at 1100 to 1150 seconds during the second zincating stage, the E_{OC} values is not consistently more noble than other specimens throughout the zincating process.

In addition, the duration for the first zincating process was also selected based on the minimum slope value of the steady state potential during the third stage of the double zincating process. A linear fitting analysis was carried out on steady state potential region for all curves in Figure 4.4, in order to find the minimum slope. Based on the linear fitting analysis, the minimum slope for the steady state potential region is shown by the specimen produced from the longest first zincating duration at 60 seconds (Table 4.1).

Table 4-1 Slope value for steady state potential of specimens produced from double zincating process using various first zincating durations

Duration of the first zincating process (seconds)	Slope value (V/ s)
10	7.00×10^{-7}
20	1.91×10^{-6}
30	2.90×10^{-7}
40	2.00×10^{-6}
50	5.71×10^{-7}
60	1.15×10^{-7}

Therefore, in this study the duration for the first zincating process was kept constant at 60 seconds. In the double zincating process, initially the specimen was immersed in the first zincating bath for 60 seconds and followed by a zinc stripping process in 50 vol. % HNO_3 solution for 20 seconds. Then, the specimen was immersed again in the zincating bath for the second zincating process.

The comparison of E_{OC} variation with immersion time measured for AA7075 substrates during the single and double zincating processes is shown in Figure 4.5. This figure shows the same trend of E_{OC} variation with immersion time for both specimens, and both curves measured can be divided into three stages. During the first stage, both substrates showed steep drops in E_{OC} values to approximately -1.613 V, which correspond to the rapid dissolution of the substrates. In the second stage, the E_{OC} values for both specimens increased to the noble direction. The sample produced from the double zincating process shows a rapid increased in the E_{OC} value to the noble direction at about 150 seconds. However, for a sample produced from the single zincating process, the transition to the noble direction started approximately at 250 seconds (Figure 4.5(b)). This indicates that the deposition of zinc particles on the double zincated sample is faster than single zincated sample. It was also observed in this figure that the E_{OC} values for the beginning part of the second stage increased rapidly for the double zincated sample and increased gradually for the single zincated sample. During the third stage, the E_{OC} values for both specimens changed very slowly to reach a steady potential.

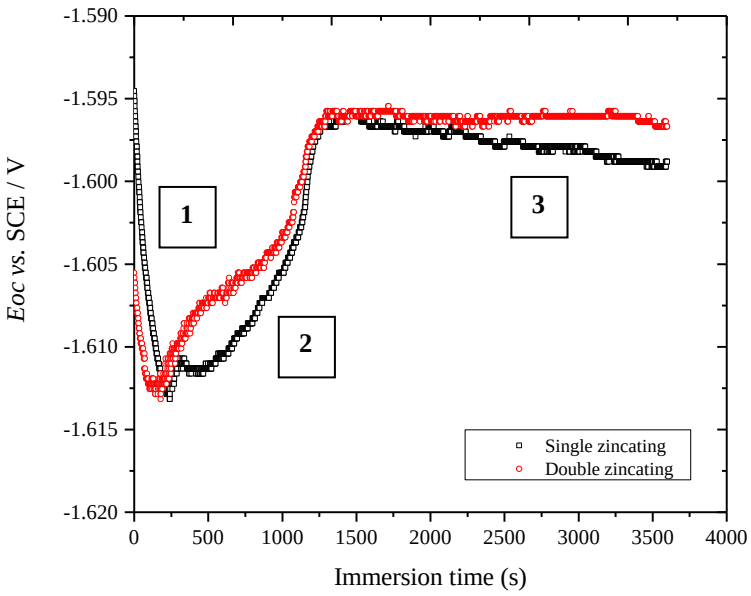

(a)

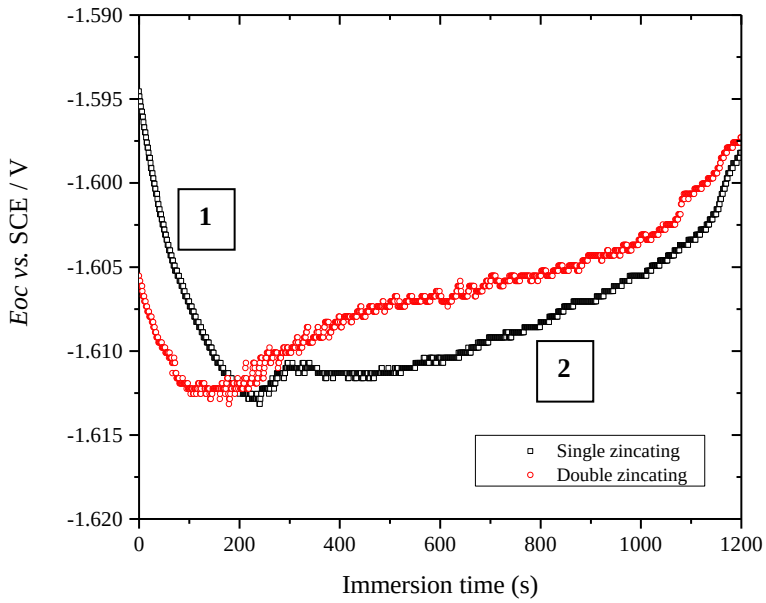

(b)

Figure 4-5 Changes in immersion open circuit potential (E_{OC}) of the AA7075 substrate during the single and double zincating process. (a) The changes of E_{OC} during the zincating process up to 3600 s. (b) A time-expansion plot for the initial stage of the zincating process (a).

The choice of optimum time for the first zincating process relies to some extend on reliability of the methods and reproducibility of the experiments described. Whilst it has not been possible to repeat all relevant tests, several procedures were carried out to provide some evidence of reproducibility. Firstly, the electrochemistry measurement of the aluminium alloy 7075 substrate during the single zincating process in Figure 4.5 was repeated. No significant difference was observed, and characteristic times the end of the characteristic stage were typically within 10%.

To test reliability of the methods, both single and double zincating processes were also carried out on both pure aluminium and aluminium alloy 2024 (AA2024) substrates, using the same equipment and procedures as applied for the AA7075 substrate. For the double zincating process, all substrates were first dipped in the first zincating bath for 60 seconds before entering the second zincating bath. Figure 4-6 shows a comparison in immersion open circuit potential (E_{OC}) of various substrates during the single and double zincating process. All substrates showed the same trends in E_{OC} vs t during single and double zincating processes. The curves showed an initial drop

in E_{OC} which represents a rapid dissolution of the substrate and followed by an increase in E_{OC} to a steady state of potential which represented the zinc deposition and completion of zinc coverage on the substrate.

On AA2024 and pure Al, the transition of E_{OC} values during the first and second stage of double zincating process were more noble than the single zincating process. This indicates less dissolution of the substrates during the double zincating compared to single zincating. However, for AA7075 substrate, the minimum E_{OC} values for both single and double zincating process were similar. The difference is that the duration for zinc deposition on AA7075 substrate during the second zincating process was quicker compared to single zincating. The steady state potential for pure Al during single and double zincating was less noble than that of the AA7075 and AA2024. This less noble potential corresponds to the incomplete coverage of zinc particles on the pure Al substrate.

The above goes some way to indicate the test setup is reliable and experiments should be reproducible. Clearly, for application of the present work in an industrial environment substantial further testing is necessary.

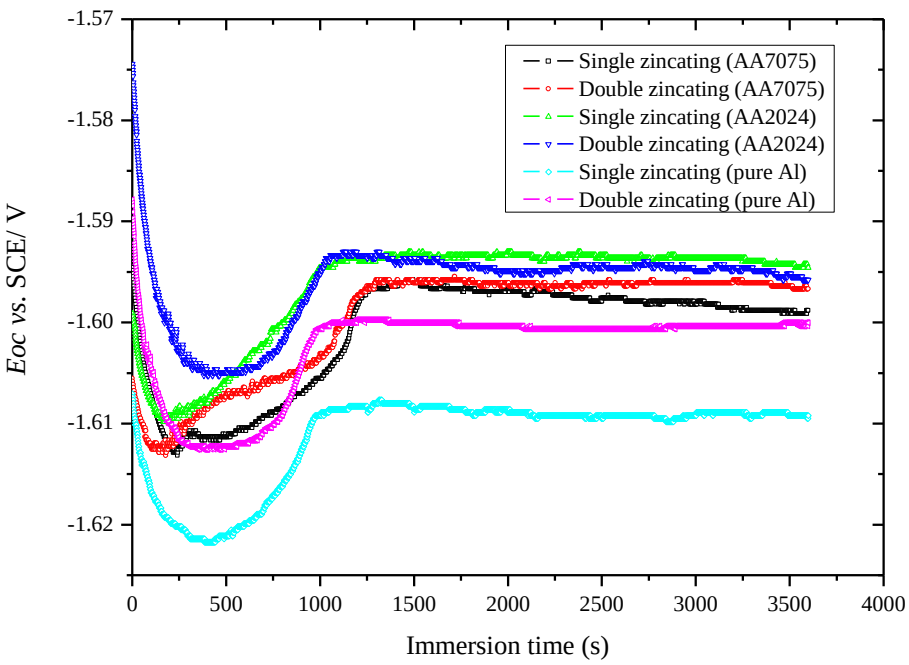

Figure 4-6 Comparison in immersion open circuit potential (EOC) of various substrates during the single and double zincating process

4.2.4 Electrochemical Behaviour of AA7075 during the Single Zincating Process with Copper Activation

In order to investigate the effect of copper activation on zinc deposition on the AA7075 substrate during the zincating process, the variation of E_{OC} with immersion time during single zincating process with various copper activation durations was measured. In Figure 4-7, the influence of the copper activation for 5, 10 and 15 minutes on the single zincating process can be observed. The curves measured can be divided into three stages, namely dissolution, deposition and steady state. Specimens produced from copper activation for 5 and 10 minutes show the same trend of E_{OC} variation. In the first stage, both specimens exhibit a gradual decrease in the E_{OC} values. Then, during the second stage, the E_{OC} values for both specimens increased gradually to the noble direction and slowly approached the steady state of potential in third stage at approximately -1.603 V after 1000 seconds.

This figure shows that the transition point of the less noble potential to the more noble potential for the specimen produced at 10 minutes of copper activation is at 150 seconds. On the other hand, a specimen produced from 5 minutes of copper activation shows the transition point from less noble to the more noble potential at 250 seconds. This indicates that a specimen produced using 10 minutes of copper activation has faster deposition of zinc particles on the substrate than the 5 minutes of copper activation. Further increasing the copper activation duration to 15 minutes results in a continuous dissolution of the substrate in the zincating solution until it reached the steady state at approximately -1.607 V.

Therefore, for this study, the copper activation duration was fixed at 10 minutes, which resulted in less dissolution of the substrate and rapid deposition of the zinc particles during the zincating process. The selection of 10 minutes of copper activation was also supported by the SEM micrographs of AA7075 substrates after copper activation at various durations in 0.5 M H_2SO_4 + 3.13 x 10_{-4} M $CuSO_4$ solution. SEM micrograph of substrate from 10 seconds of copper activation shows a quite uniform surface with no cavities, which differs from other durations. The coverage of the copper seeds was quite homogenous, with some agglomerations on the substrate. A detailed

explanation of the surface morphology after the copper activation process is provided in section 4.3.2.

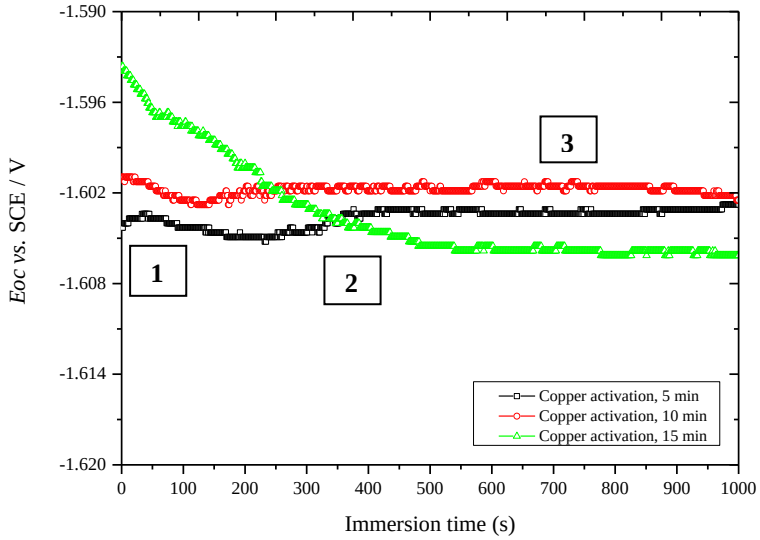

Figure 4-7 Changes in immersion open circuit potential (E_{OC}) of the AA7075 substrate with copper activation during single zincating process for 1000 seconds

A comparison of E_{OC} vs immersion time curves for specimens during single zincating, double zincating and single zincating with copper activation is shown in Figure 4-8. The curve measured for a specimen produced from single zincating with a copper activation showed a more noble potential compared to single and double zincating without a copper activation, which indicates a slow dissolution of copper pre-treated substrate in the zincating solution. This figure also shows a rapid zinc deposition on the copper pre- treated substrate.

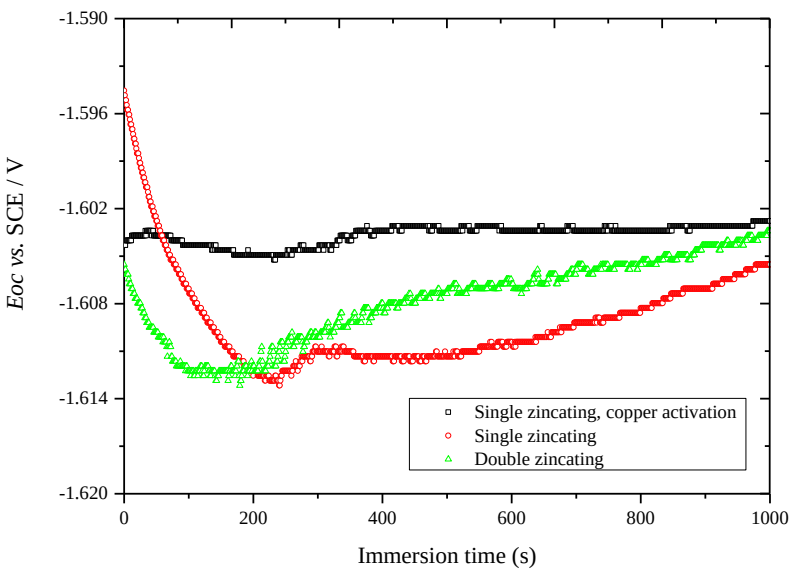

Figure 4-8 Changes in immersion open circuit potential (E_{OC}) of the AA7075 substrate with and without copper activation during the single zincating process and double zincating process for 1000 seconds

4.3 Surface Morphology and Element Composition of AA7075 Substrate after Various Surface Pre- treatment Processes

The influence of various surface pre-treatment processes, such as alkaline cleaning, acid cleaning, copper activation, conventional single zincating, modified single zincating and double zincating processes on the morphology and element composition of the AA7075 substrate surface was investigated using SEM and EDX techniques. In addition, the effect of copper activation on the morphology and element composition of the conventional and modified single zincated AA7075 substrate surface was also examined.

4.3.1 Surface Morphology and Element Composition of AA7075 Substrate surface after Alkaline Cleaning and Acid Cleaning Processes

The surface morphology of the AA7075 substrate before and after cleaning in alkaline and acid solution is shown in Figure 4-9. Figure 4-9(a) shows the morphology of the as-received AA7075 substrate (with some scratches on the surface due to the mechanical grinding and polishing processes). After an alkaline cleaning in 10 wt. %

NaOH solution for 10 seconds, the surface still displayed some scratches but smoother than before (Figure 4-9(b)). In addition, nodules were observed deposited on the surface after this cleaning process.

After the sample was cleaned in 50 vol. % HNO_3 solution for 20 seconds, the substrate surface became rough with some pits and cracks covering the surface (Figure 4-9). The grinding and polishing scars after this cleaning process appeared clearer than before. The nodules observed previously after the alkaline cleaning were removed during this process.

Table 4-2 shows the EDX analysis of the substrate surface after various surface pre- treatment processes.

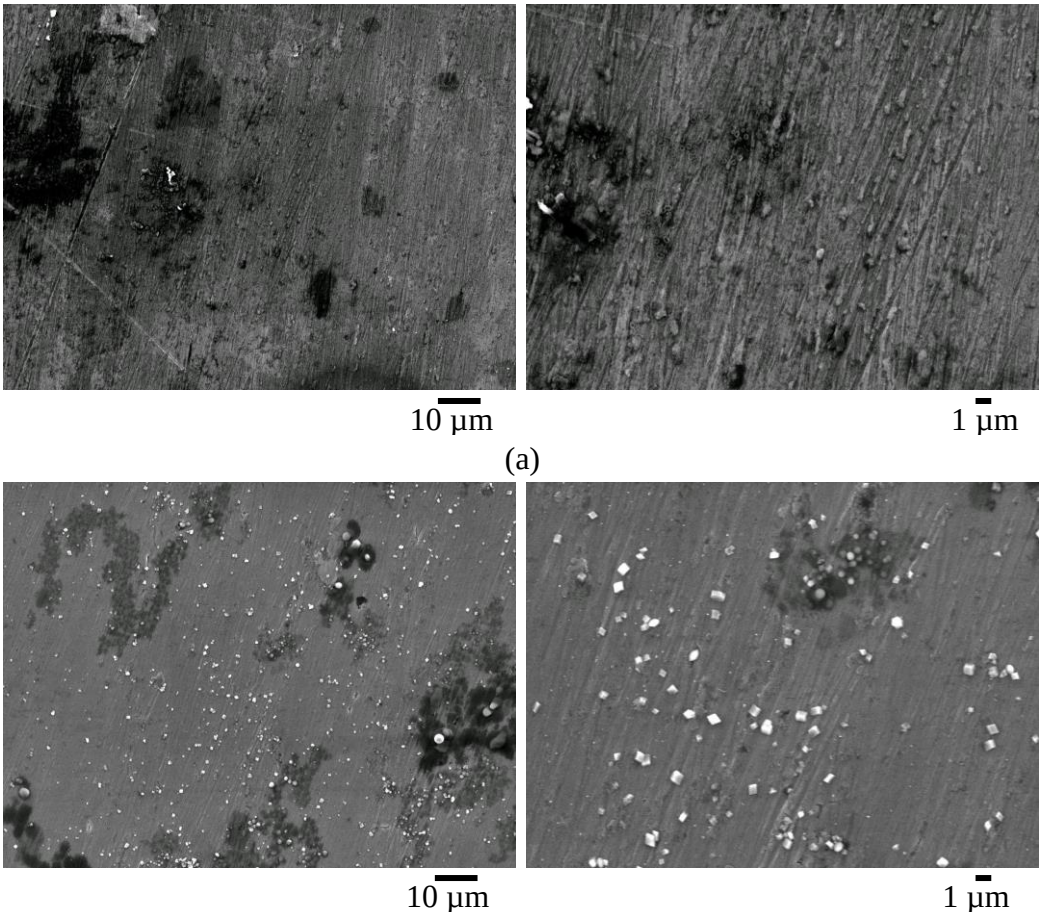

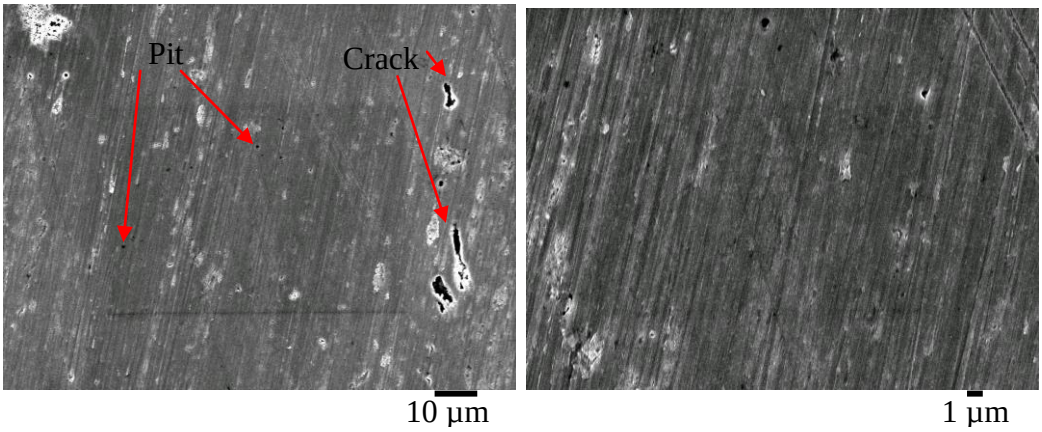

(c)

Figure 4-9 SEM morphology of AA7075 substrate after various surface pre- treatment processes (a) as- received substrate, (b) alkaline cleaning (10 wt. % NaOH, 10 s, room temperature (RT)) and (c) acid cleaning (50 vol. % HNO_3, 20 s, RT)

Table 4-2 Element composition (wt. %) of the substrate surface as determined by EDX after various surface pre- treatment processes

Element / Surface pre-treatment	Al	Zn	Mg	O
As-received AA7075	83.8	5.2	2.3	3.2
Alkaline cleaning	81.8	5.7	2.3	5.7
Acid cleaning	90.1	5.9	2.1	1.8

4.3.2 Surface Morphology and Element Composition of AA7075 Substrate after Copper Activation Process

In order to select the optimum duration for the copper activation process on the AA7075 substrate, SEM examination was carried out on samples produced at different copper activation durations, as shown in Figure 4-10. This figure shows the SEM images of AA7075 substrates after copper activation process in 0.5 M H_2SO_4 + 3.13 x 10^{-4} M $CuSO_4$ solution at room temperature for 5, 10 and 15 minutes, taken using the secondary electron (SEI) and back scattered electron modes. The BEI mode helps to detect the deposition of copper seeds more clearly, since the heavy element will appear

brighter than the light element. This was confirmed by the EDX analysis on the bright particles which were deposited on the substrate after the copper activation process, as shown in Figure 4-11.

From the analysis, it was confirmed that the bright particles are copper, due to the increasing in the copper composition compared to the as- received sample. Overall, it was observed that the size and population of the copper seeds on the substrate varied significantly with the copper activation duration.

After 5 minutes of copper activation, the BEI image shows the nucleation of the copper seeds all over the surface, as shown by the bright spots in Figure 4-10(a). The SEM image at this duration shows that the sample was uniformly corroded with some cavities formed on the surface, thus resulted in a rough surface. Per Figure 4-10(b), after the sample was immersed in 0.5 H_2SO_4 + 3.13 x 10^{-4} M $CuSO_4$ solution for 10 minutes, a quite uniform surface with no cavities was observed on the surface. The coverage of the copper seeds was quite homogenous, with some agglomerations on the substrate. However, further increasing in the duration up to 15 minutes showed an increase in the copper seeds population, with some agglomeration on the surface (Figure 4-10(c)).

Figure 4-10(c) also indicates that the surface was roughened and non- uniform with some cracks, due to the longer immersion in the copper activation solution.

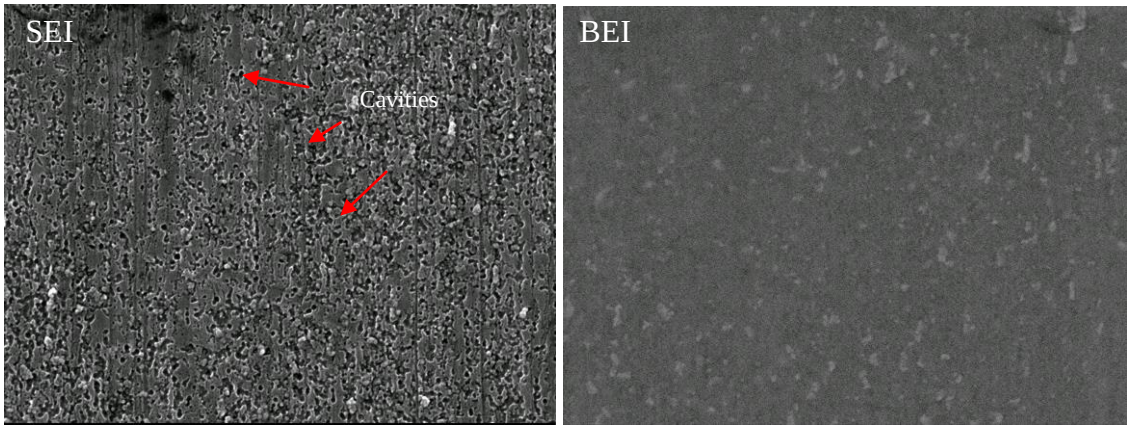

(a)

1 µm

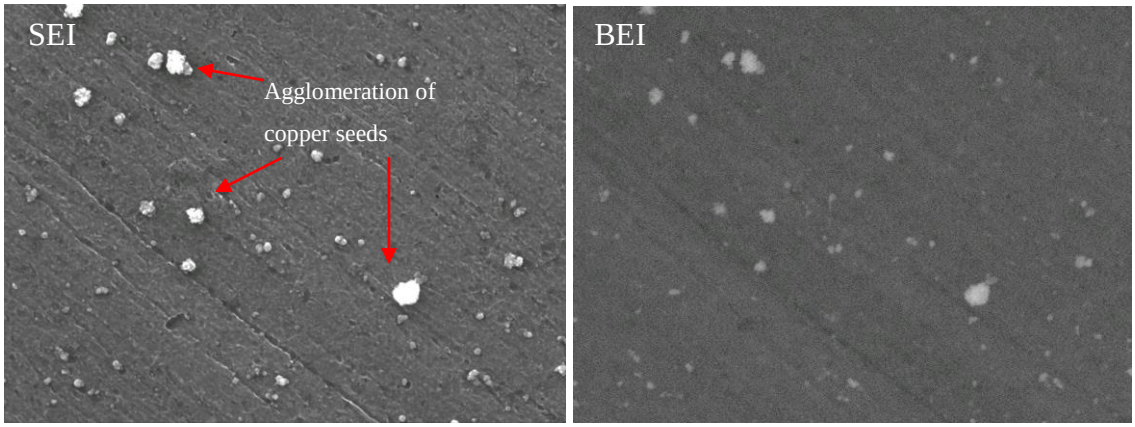

(b) 1 µm

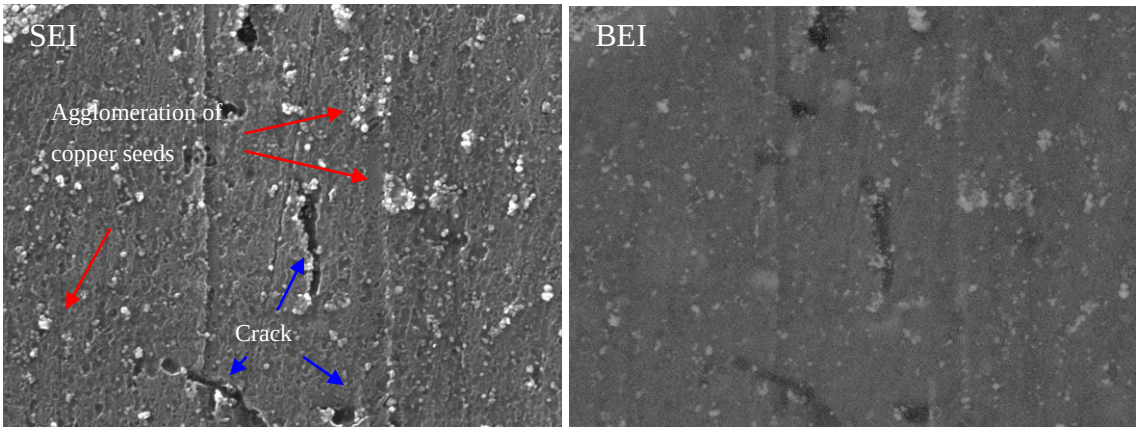

(c) 1 µm

Figure 4-10 SEM micrographs (SEI and BEI modes) of AA7075 substrates after copper activation process in 0.5 M H_2SO_4 + 3.13 x 10^{-4} M $CuSO_4$ at RT for (a) 5, (b) 10 and (c) 15 minutes.

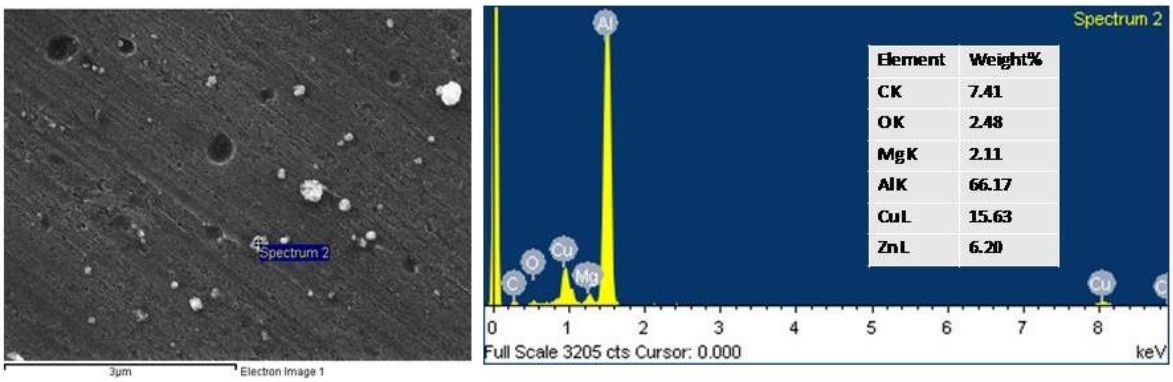

Figure 4-11 EDX analysis of particles after copper activation, confirming they are copper particles

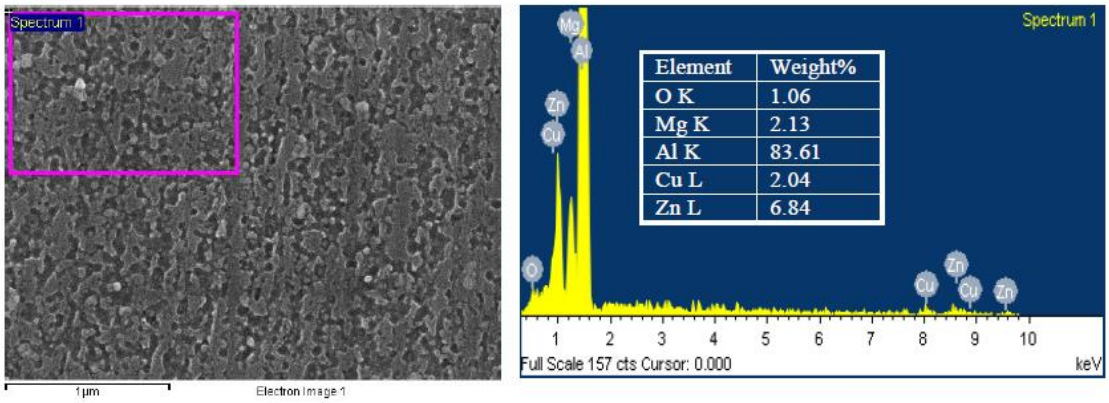

(a)

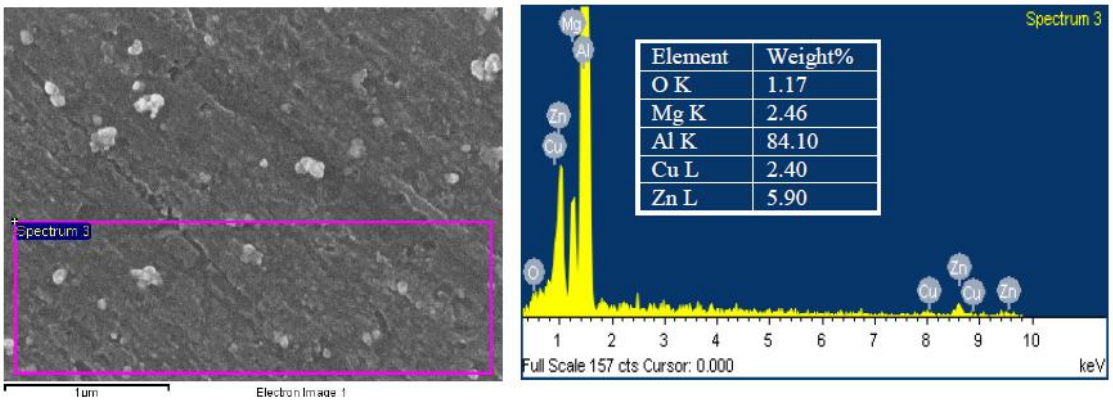

(b)

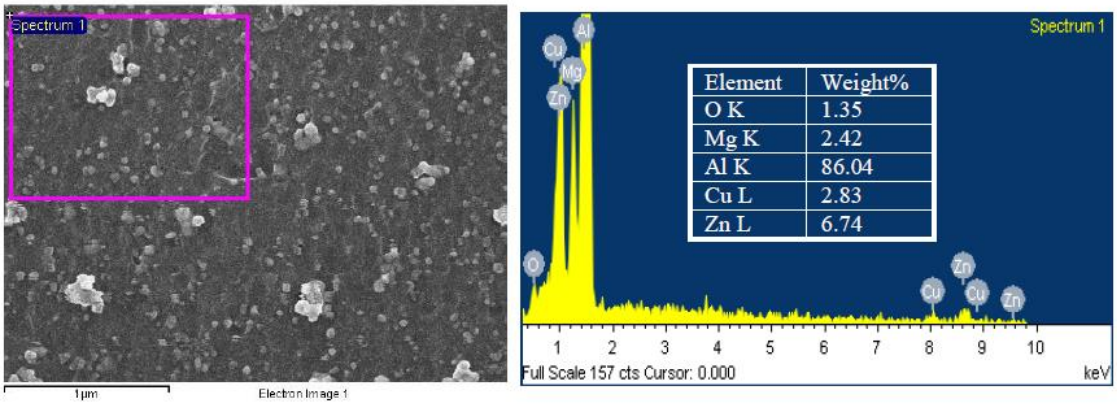

(c)

Figure 4-12 EDX analyses of AA7075 substrates after copper activation process at various durations (a) 5, (b) 10 and (c) 15 minutes

EDX analysis was performed on these samples in order to detect the evidence of copper seeds and to obtain the composition of copper seeds deposited on the substrate at various durations Figure 4-12, Figure 4-13 and Figure 4-14). Figure 4-13 shows the

average values of copper in weight percentage (wt. %) as a function of copper activation duration. This figure shows an increase in the average value of copper composition from 2 to approximately 3 wt. %, due to the increasing in the duration from 5 to 15 minutes. On the same time, other elements also were detected during the EDX analysis, such as aluminium as the substrate, zinc and magnesium as the alloying elements and oxygen as an impurity (Figure 4-14). There was no significant influence to the other elements composition as the copper activation duration increase from 5 to 15 minutes.

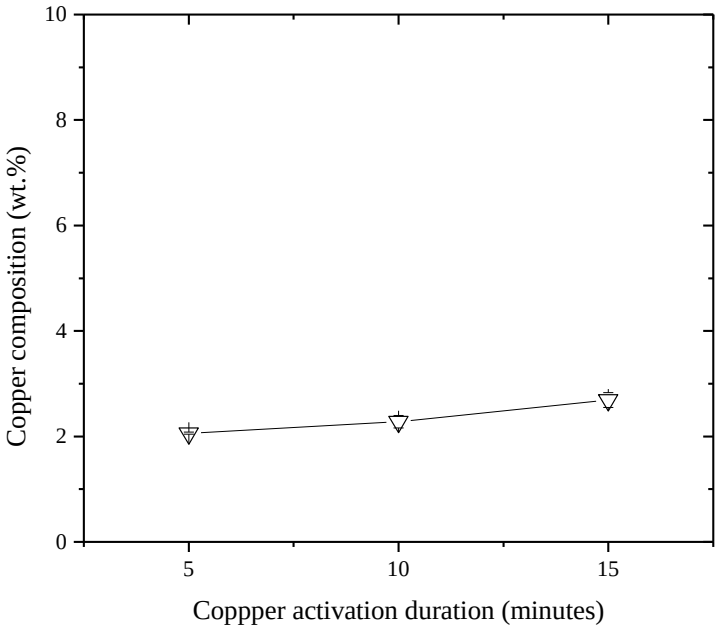

Figure 4-13 EDX analysis of average copper composition (wt. %) present on AA7075 substrates after various copper activation duration.

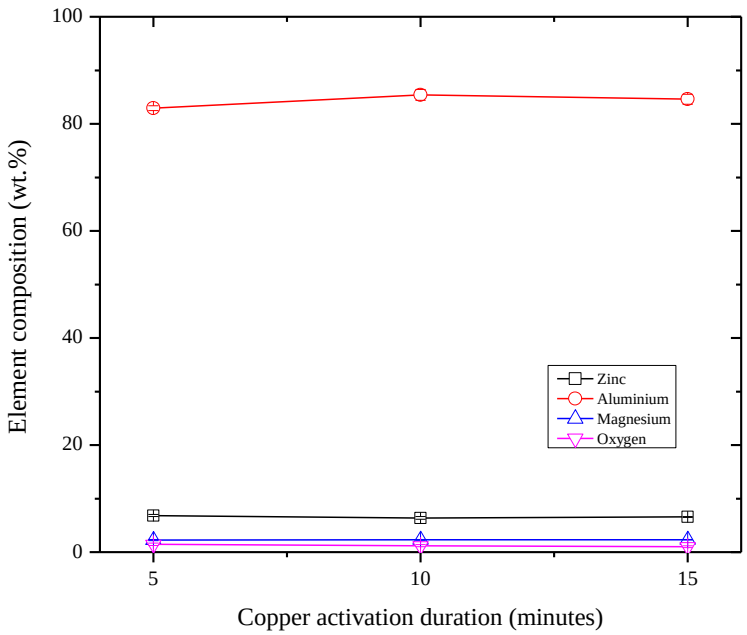

Figure 4-14 EDX analysis of other elements composition (wt. %) present on AA7075 substrates after various copper activation duration

4.3.3 Surface Morphology and Element Composition of AA7075 Substrate after Conventional and Modified Single Zincating Process at Various Durations

Figure 4-15 shows SEM images of AA7075 substrates after a conventional single zincating process at 1 minute and a modified single zincating process at 5, 10, 15 and 20 minutes. This figure shows the deposition of zinc particles on the substrate surface through zincating process, as compared to the cleaned and smooth surface of acid cleaned substrate. The evidence of the zinc deposition on the substrate was confirmed by an EDX analysis on the observed white particles which scattered randomly on the substrate, as shown in Figure 4-17.

The morphology of the conventional single zincated surface shows various sizes of zinc particles deposited non-homogenously on the AA7075 substrate. After 5 minutes, the zinc particles had grown and the density had increased (Figure 4-15 (b)). As the duration was increased from 5 to 15 minutes, the zinc density increased further and the particles covered most of the surface, with some agglomerations at certain areas

of the surface. It was observed that the zinc nucleation and growth occurred preferentially at the edges of the grinding and polishing scars, as shown by the arrows in Figure 4-15 (d). After 20 minutes, zinc particles grew continuously and became connected to each other, as seen in Figure 4-15 (e). The morphology also shows saturated layer of zinc particles which covered most of the surface. Although the zinc particles were observed preferentially deposited at the edges of the grinding and polishing scars (Figure 4-15 (d)), further increases in the zincating duration led to the deposition of zinc particles on the whole surface (Figure 4-15 (e)). It is apparent in the figure that a high density of zinc particles on the substrate is anticipated at longer zincating duration.

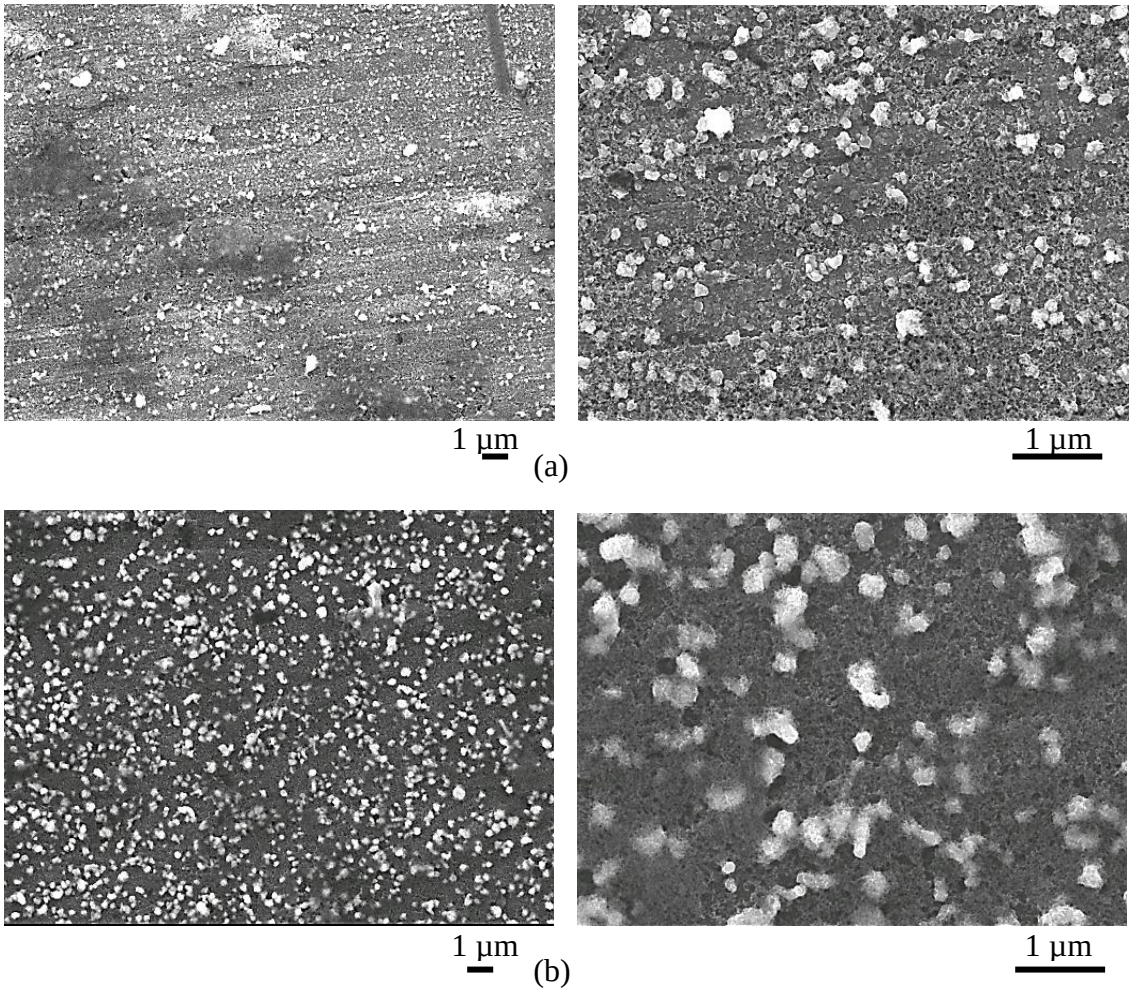

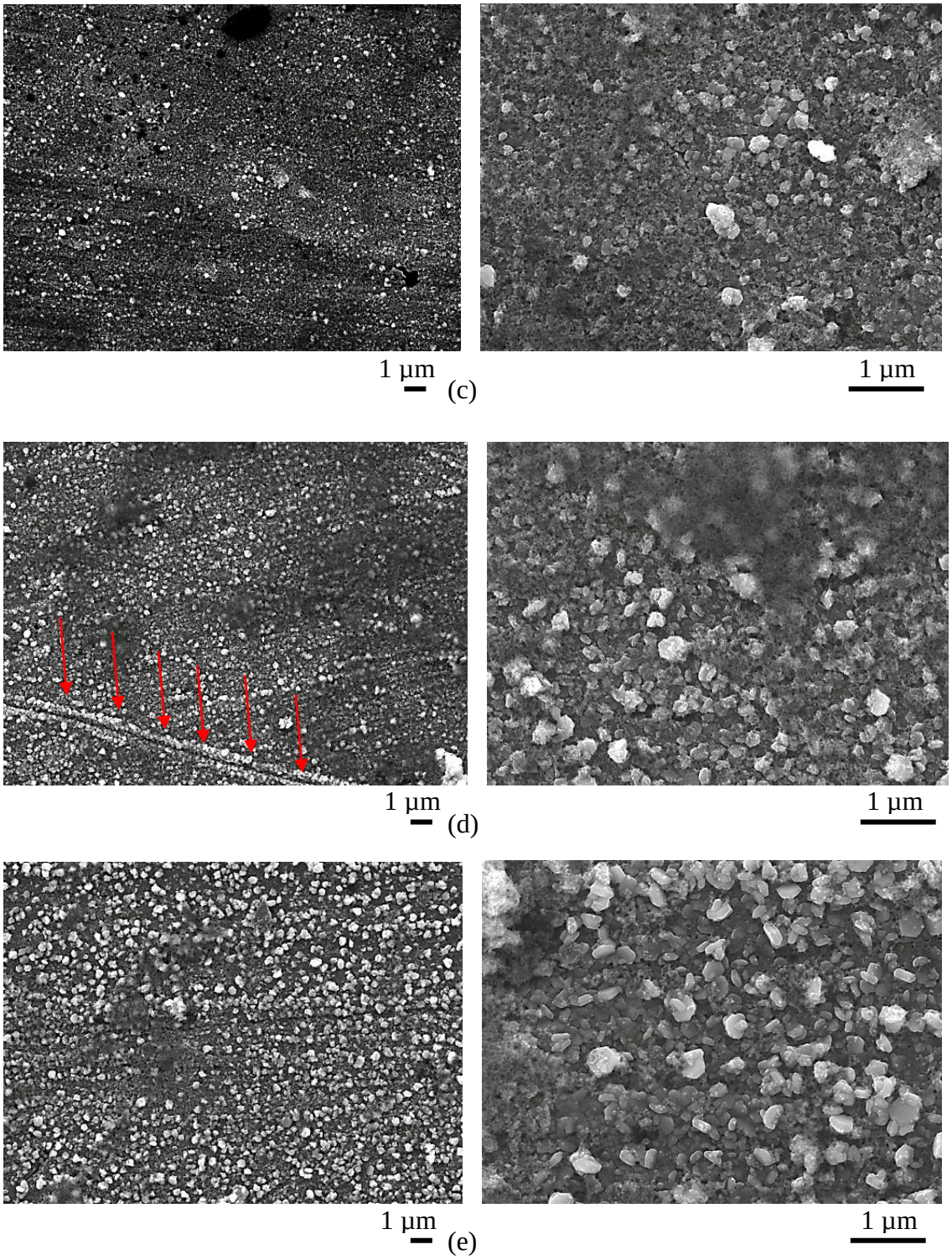

Figure 4-15 SEM micrographs of AA7075 substrates after (a) conventional single zincating process at 1 minute and modified single zincating process at various durations: (b) 5, (c) 10, (d) 15 and (e) 20 minutes.

In this study, the growth of the zinc particles was measured manually based on the SEM micrographs of the zincated samples (Figure 4-15). Figure 4-15 shows that the zinc particles deposited on the substrate after zincating process have a hexagonal shape. Therefore, in order to observe the influence of various zincating durations to the growth of the zinc particles, the length of one side of the hexagon was measured.

SEM micrographs was divided into four quadrants and in each quadrant, ten zinc particles were selected (Figure 4-15). Then, the side length of the selected zinc particles was measured. The average length to represent the sample was then calculated by taking the average of the side length of the zinc particles from each quadrate. The result showed an increase in the zinc particles' size, as the single zincating duration increased from 1 to 20 minutes (Figure 4-16).

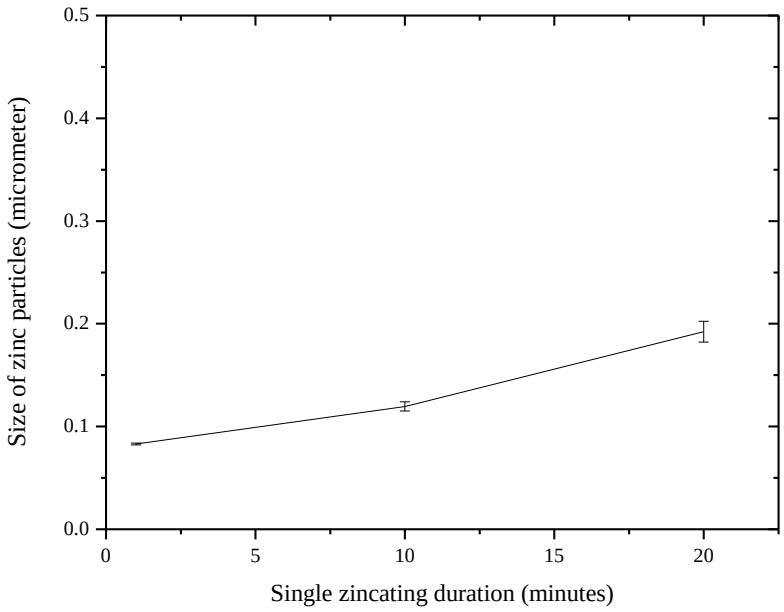

Figure 4-16 Analysis of zinc particles size deposited on AA7075 substrate at 1, 10 and 20 minutes of zincating process

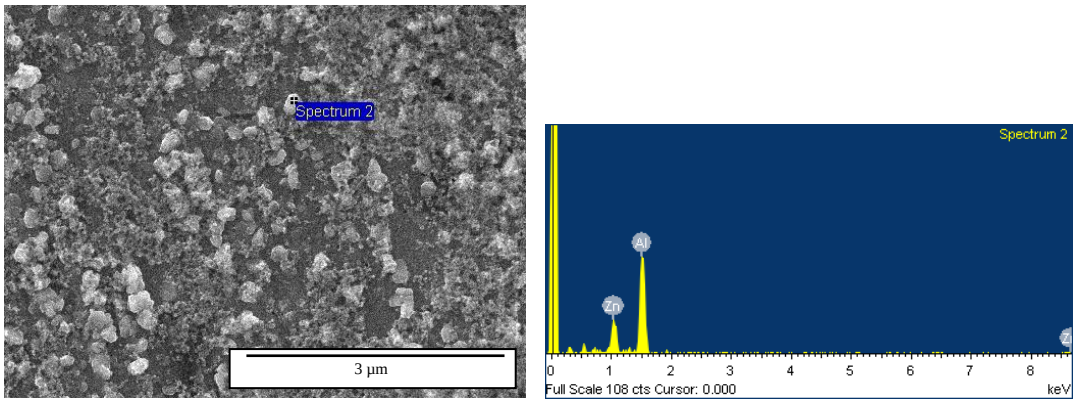

Figure 4-17 EDX analysis of particles after modified single zincating process for 10 minutes, confirming they are zinc particles.

The deposition of the zinc particles on the substrate during the conventional and modified single zincating processes at various durations was further investigated using EDX analysis. The percentage composition of zinc and aluminium during was obtained in this analysis (Figure 4-18).

Initially, the as- received AA7075 substrate contained 5.2 wt. % of zinc. After the conventional single zincating process at 1 minute, the measured composition of zinc is approximately 10 wt. %, i.e. double the AA7075 Zn content. No significant difference in the composition of zinc was found between 1 minute of conventional single zincating and 5 minutes of modified single zincating process. However, increasing the zincating duration further from 5 to 20 minutes resulted in a gradual increase in the zinc composition from approximately 10 to 25 wt.%. On the other hand, the aluminium element was gradually decreased from approximately 86 to 68 wt. %, with an increase in the single zincating duration from 1 to 20 minutes. At the same time, other element such as oxygen was also detected during the analysis. The composition of the oxygen was increased as the single zincating durations increased from 1 to 5 minutes. Increasing the single zincating durations further to 20 minutes did not result in significant difference in the oxygen composition.

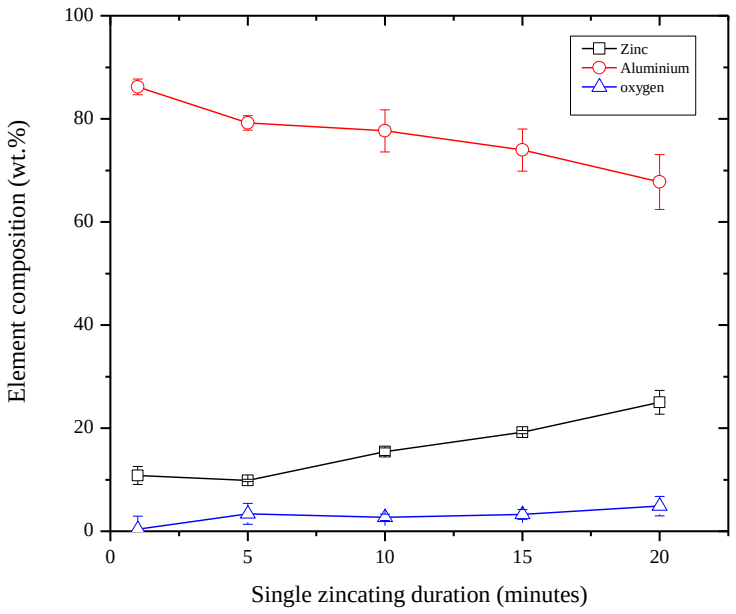

Figure 4-18 EDX analysis of sample surfaces for the conventional and modified single zincating processes at various durations

4.3.4 Surface Morphology and Element Composition of AA7075 Substrate after Double Zincating Process at Various Durations

Figure 4-19 shows the SEM micrographs of AA7075 substrates after application of the double zincating process at various durations. In this study, the first zincating duration was fixed at 60 seconds, while the second zincating duration was varied at 10, 20, 30, 40 and 50 seconds. The morphology of the first zincated sample in the double zincating process is the same as with the conventional single zincated sample as the same duration was applied for both processes. The morphology was mentioned in the Section 4.3.3.

For the double zincating process, the first zinc layer developed during the first zincating process was stripped away by the zinc stripping process in a 50 vol. % HNO_3 solution for 20 seconds. The SEM morphology of the sample after this stripping process revealed almost complete removal of the zinc particles (Figure 4-19(f)). Many pits and cracks were also observed on the sample surface. This result is consistent with the EDX analysis, which indicates a decrease in the zinc composition from 10 wt. % (first zincating process) to 5.9 wt. % (zinc stripping process) (Figure 4-21). After removal of

the first zinc layer, the zincating process was repeated for 10, 20, 30, 40 and 50 seconds in order to deposit a fresh zinc layer. As seen in Figure 4-19, morphology of the samples from double zincating process produce a more uniform and smooth zinc layer, which contained zinc particles that are refined as compared to the conventional and modified single zincating processes. Sample which was double zincated at 60/10 seconds, showed a smooth zinc layer which consisted of small-size zinc particles (Figure 4-19(a)). After this process, the surface was still not fully covered by the zinc particles, as can be seen from the cavities which occurred all over the surface.

After 60/20 seconds of double zincating process, the cavities which were previously observed on the surface were reduced in size and also number (Figure 4-19 (b)). A partial overlap of zinc layers can be seen, where small clusters of zinc particles deposited non- homogenous on the initial smooth layer of zinc particles (as shown by the square marks). The surface was improved after 60/30 seconds, as a smooth and uniform zinc layer with no voids was observed on the surface (Figure 4-19(c)). It is clearly shown in this figure that another layer of zinc particles started to develop at this duration. As the duration increased from 60/30 to 60/50 seconds, the initial layer of zinc particles became more uniform and dense (Figure 4-19(d-e)). Furthermore, an increase in density and decrease in the size of the zinc particles, which were deposited on the initial zinc layer, were also observed.

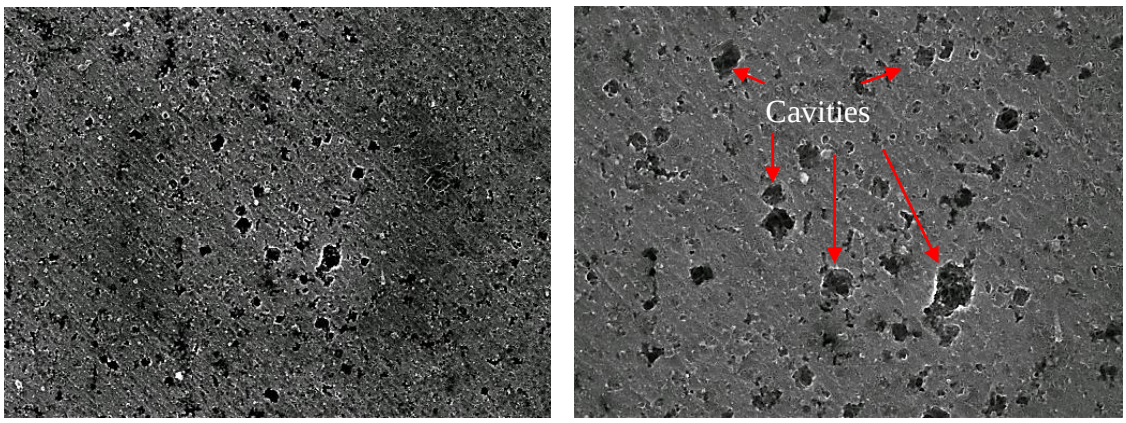

(a)

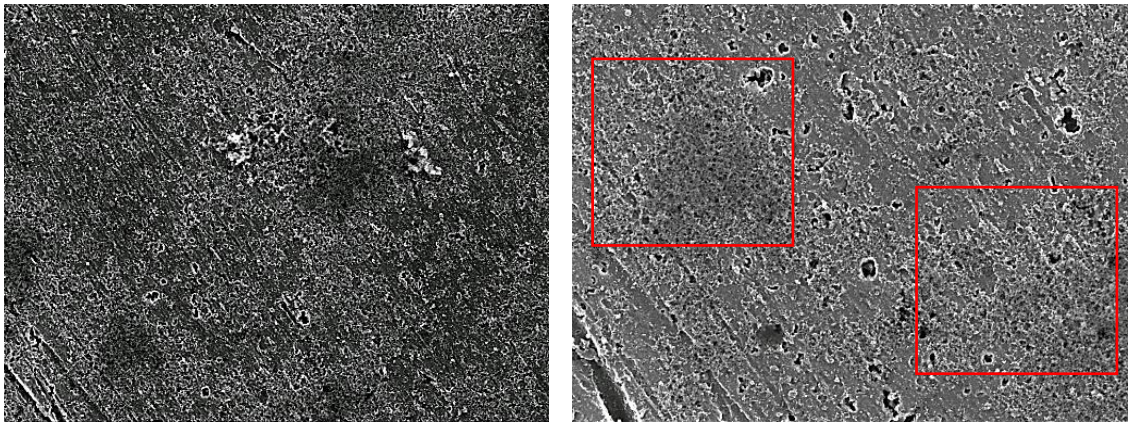

(b)

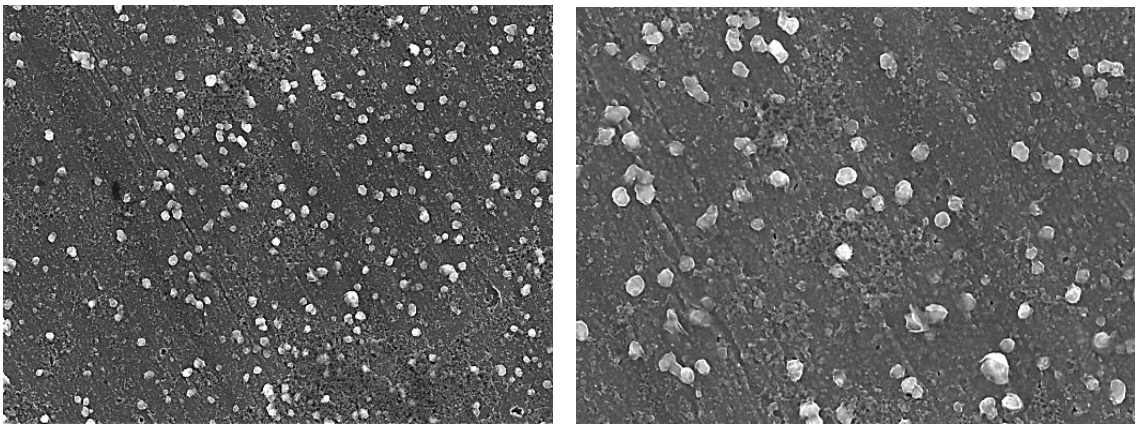

(c)

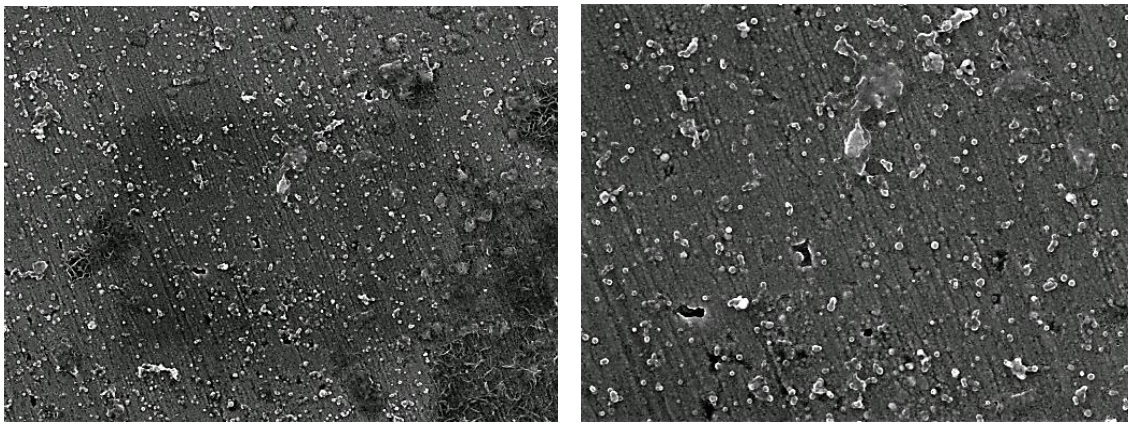

(d)

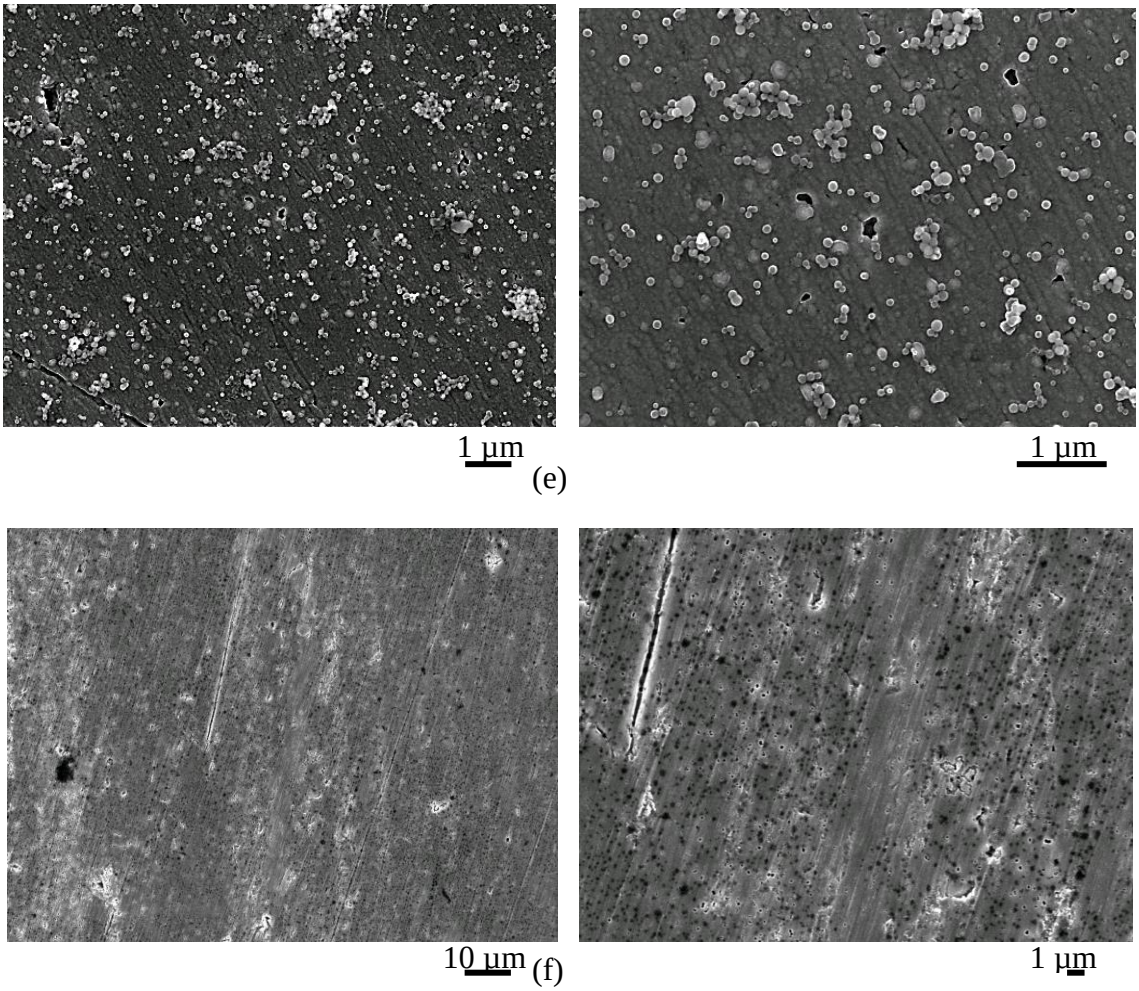

Figure 4-19 SEM micrographs of AA7075 substrate after double zincating process at various durations (a) 60/10, (b) 60/20, (c) 60/30, (d) 60/40, (e) 60/50 seconds and (f) zinc stripping process.

The technique used to determine the size of the zinc particles deposited from double zincating process is similar to the technique used for single zincating process in Section 4.3.3. Figure 4-19 shows the SEM micrographs used in this analysis. The results showed that zinc particle size increased from approximately 0.25 to 0.1 µm, when the duration of the second zincating process was increased from 10 to 50 seconds (Figure 4-20).

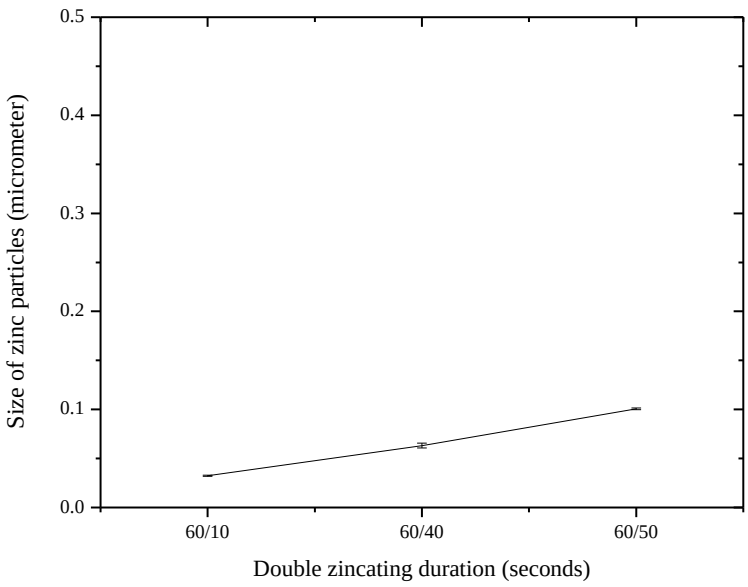

Figure 4-20 Analysis of zinc particles size deposited on AA7075 substrate at 60/10, 60/40 and 60/50 seconds of zincating process

EDX analysis was used to investigate the composition of the surface during the double zincating process at various durations. Figure 4-21 and Figure 4-22 show the composition of zinc and aluminium as a function of double zincating duration. The zinc composition increased from 7.7 to 11.17 wt. %, when the duration was increased from 60/10 to 60/50 seconds. On the other hand, the composition of the aluminium element shows a gradual decrease, as the duration increased from 60/10 to 60/30 seconds. Increasing the duration further to 60/50 seconds, shows a fluctuation pattern in the aluminium composition. At the same time, magnesium and oxygen were also detected during the analysis. For magnesium, there was no significant influence to the composition, as the double zincating duration increased from 60/10 to 60/50 seconds. However, the oxygen composition gradually increased with increasing double zincating duration from 60/30 to 60/50 seconds (Figure 4-22).

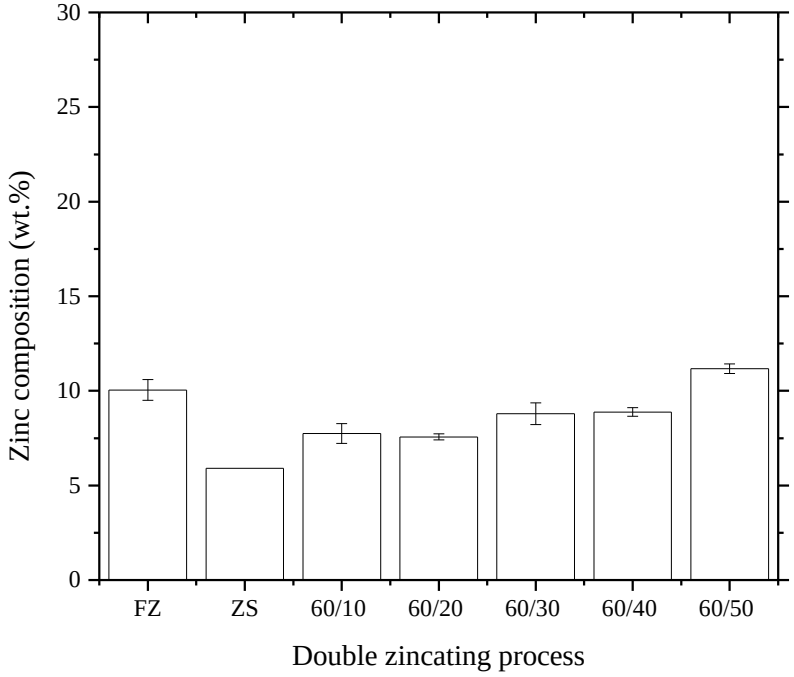

Figure 4-21 EDX analysis of zinc composition (wt. %) present on AA7075 substrates after various double zincating durations. FZ: first zincating process, ZS: zinc stripping process

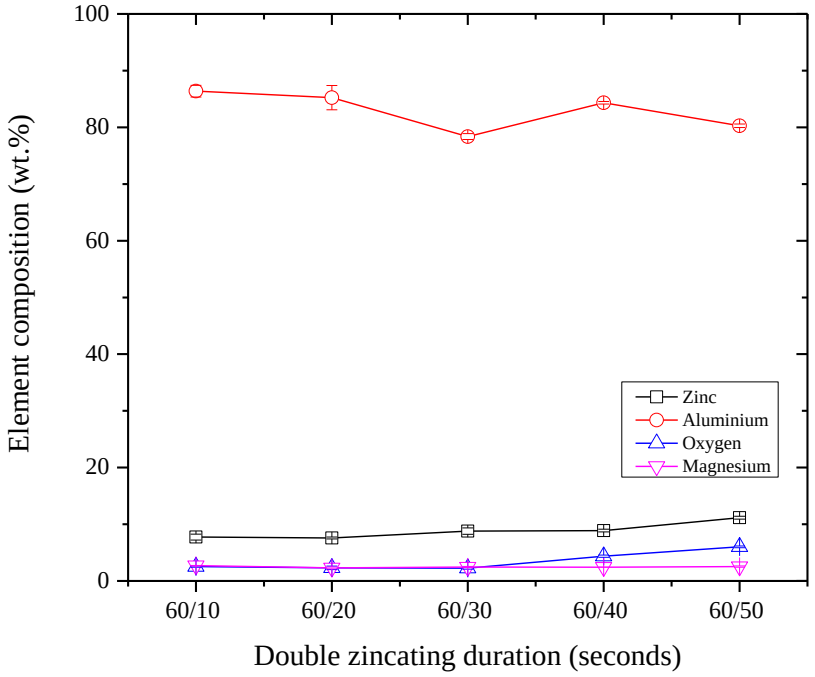

Figure 4-22 EDX analysis of sample surfaces after various double zincating durations

4.3.5 Surface Morphology and Element Composition of AA7075 Substrate after Conventional and Modified Single Zincating Process at Various Durations with Copper Activation

In order to study the effect of copper activation on the surface morphology of the substrate produced from conventional and modified single zincating processes, SEM observations were carried out. In this study, copper activation duration was fixed at 10 minutes, which has been shown to result in a homogenous distribution of the copper seeds on the substrate. SEM images of AA7075 substrate after a conventional single zincating process at 1 minute and modified single zincating process at 5, 10, 15 and 20 minutes with copper activation are shown in Figure 4-23. Overall, the figure shows that the zincating duration is important in controlling the nucleation and growth of the zinc particles during the zincating process. It is apparent from this figure that a range of sizes of zinc particles were deposited on the AA7075 substrate, due to the various durations of single zincating process applied in this process. The nucleation of the zinc particles started as early as 1 minute into the zincating process, as shown in Figure 4-23 (a). The growth of the zinc particles and increase in density were observed on the surface after 5 minutes of immersion in the zincating solution, see Figure 4-23 (b).

As the duration increased to 10 minutes, the zinc particles became bigger and some agglomerations occurred on some areas of the surface (Figure 4-23 (c)). After 15 minutes, the zinc particles were continuously growing and forming hexagonal shape particles (Figure 4-23 (d)). The surface was almost completely covered by the zinc particles, however some formation of cavities were still observed on the surface. By 20 minutes, the zinc particles were still growing and completely covered the surface (Figure 4-23 (e)). The morphology shows a compact layer containing a saturated deposition of zinc particles on the surface. It is apparent in the figure that a high density of zinc particles is certainly anticipated for longer zincating duration.

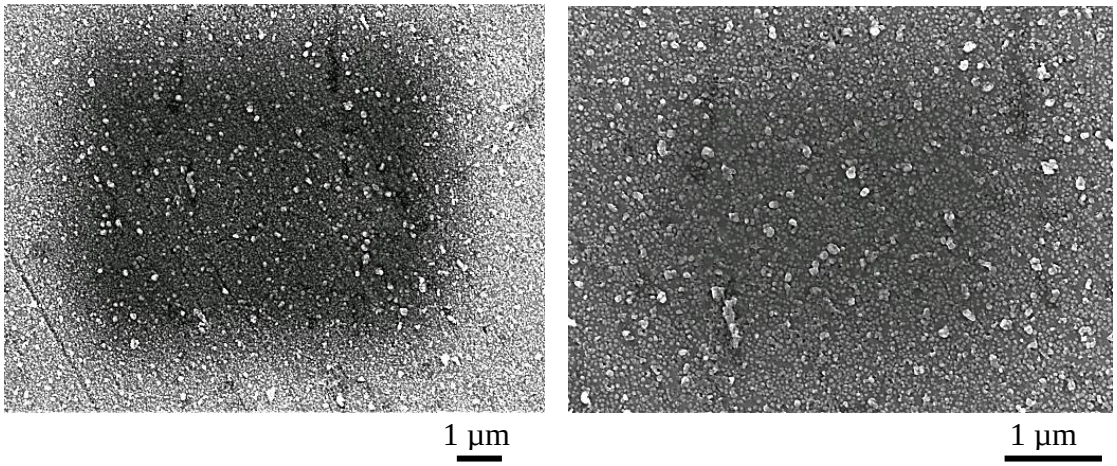

(a)

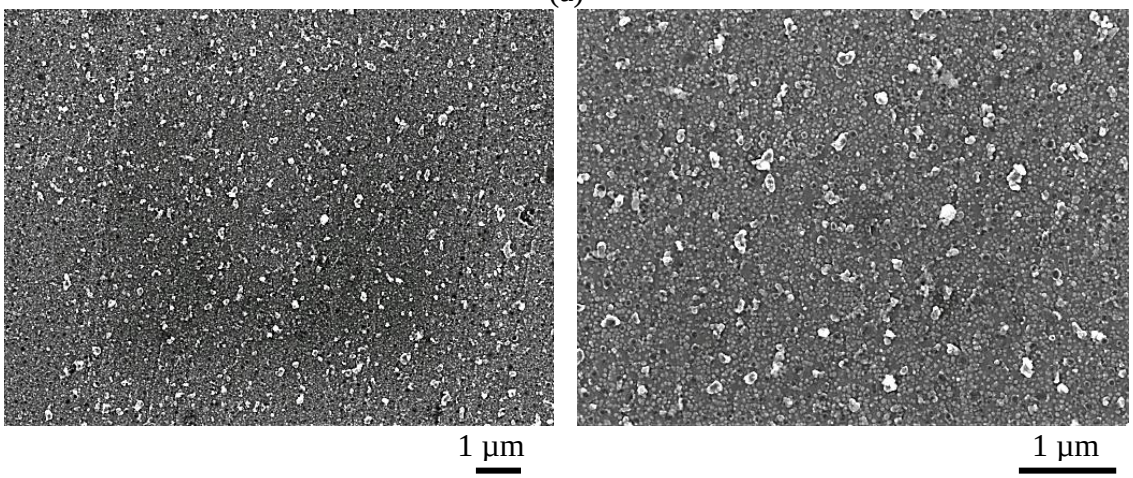

(b)

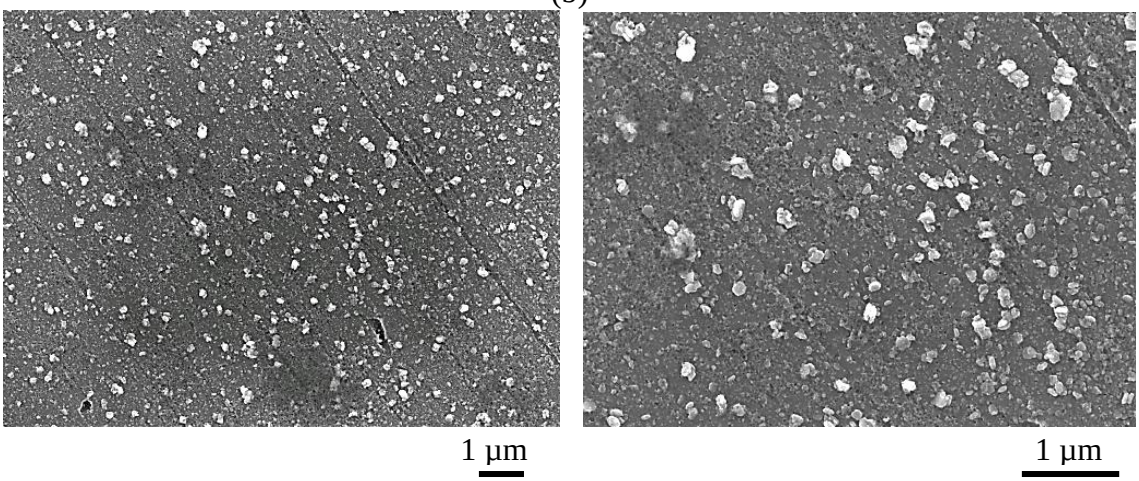

(c)

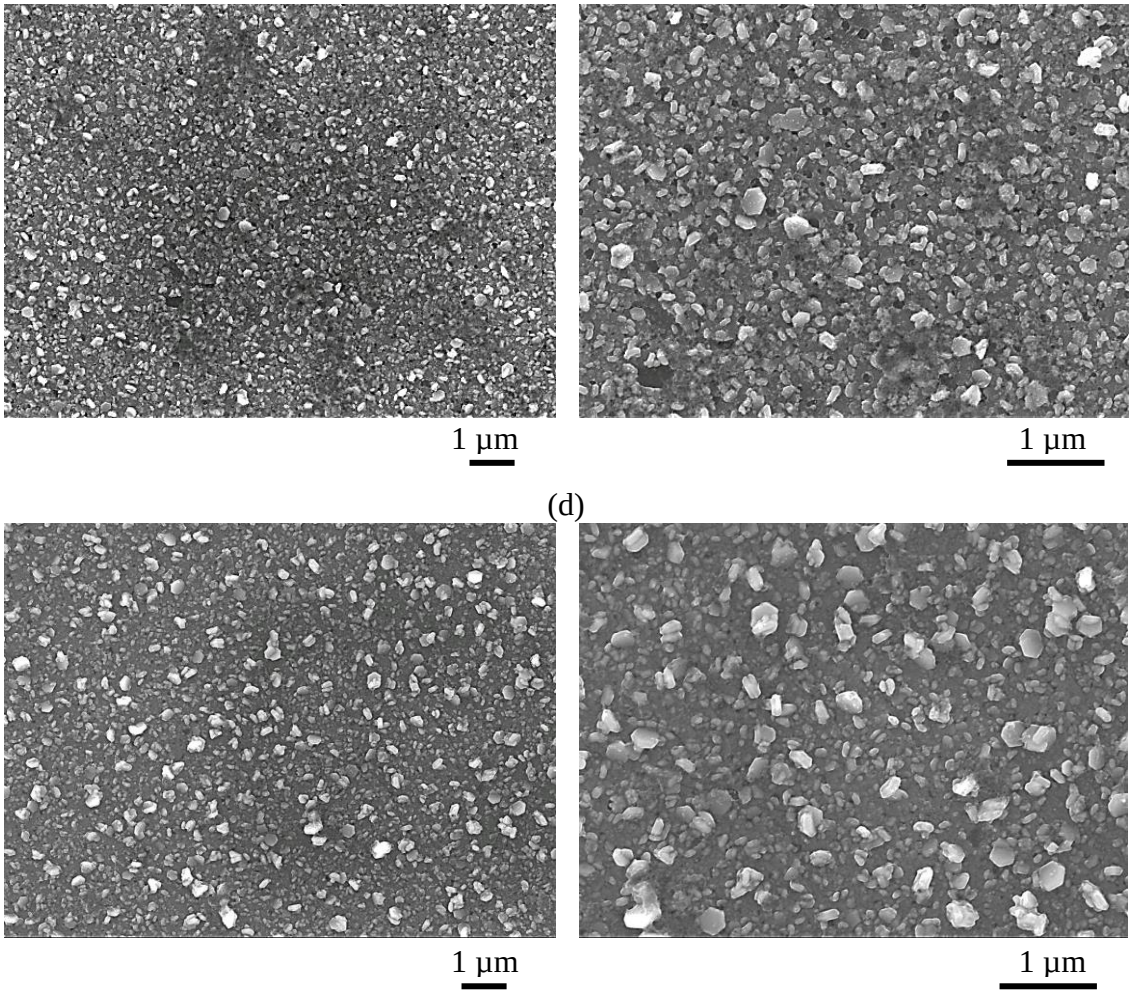

Figure 4-23 SEM micrographs of AA7075 substrates after (a) conventional single zincating process at 1 minute and modified single zincating process at various durations, such as (b) 5, (c) 10, (d) 15 and (e) 20 minutes with copper activation

Figure 4-24 shows the influence of the single zincating duration to the size of zinc particles. The zinc particle size was determined using the same technique used in single zincating process without copper activation and double zincating process. Figure 4.20 shows the SEM micrographs used in this analysis. After 10 minutes of zincating process, the zinc particles grew from approximately 0.05 to 0.1 µm. As the duration was increased from 10 to 20 minutes, the zinc particle size increased continuously to 0.15 µm.

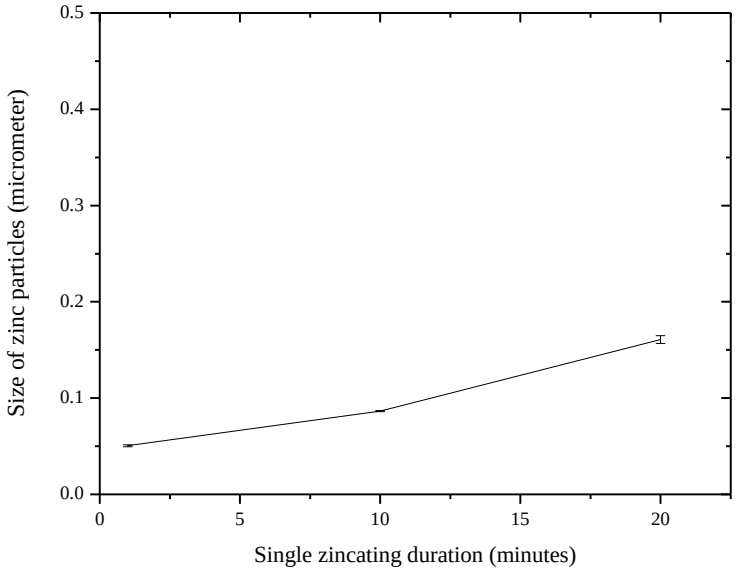

Figure 4-24 Analysis of zinc particles size deposited on AA7075 substrate at 1, 10 and 20 minutes of zincating process with copper activation

EDX analysis was used in this study to investigate the composition of the surface during the zincating process with copper activation. Figure 4-25 shows the changes in the percentage composition by weight of zinc and aluminium during the conventional and modified single zincating processes at various durations. By performing the conventional single zincating process for 1 minute, the composition of the zinc element was almost double than the as-received AA7075 composition, which was 5.21 wt. %. Increasing the zincating duration further from 1 to 20 minutes resulted in a gradual increase in the zinc content from approximately 8 wt. % to 19 wt. %. On the other hand, the aluminium content gradually decreased from approximately 79 wt. % to 68 wt. %, with an increase in duration from 1 to 20 minutes. At the same time, other elements such as, magnesium, copper and oxygen were also detected during the analysis. For these elements, there was no significant influence to the composition, as the single zincating duration increased from 1 to 20 minutes.

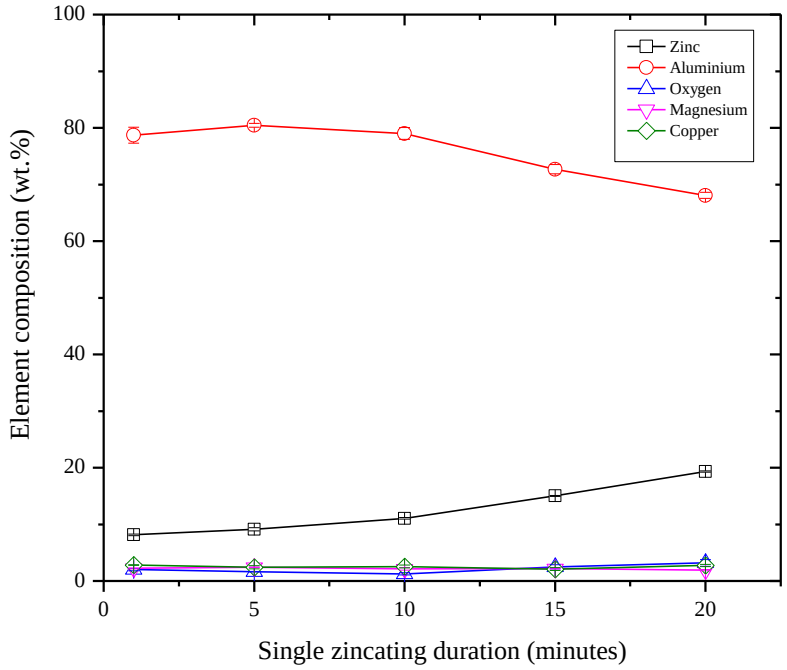

Figure 4-25 EDX analysis of sample surfaces for the conventional and modified single zincating processes at various durations with copper activation

4.4 Surface Topography and Roughness of AA7075 Substrate after Various Surface Pre-treatment Processes

4.4.1 Surface Topography and Roughness of AA7075 Substrate after Polishing, Alkaline Cleaning and Acid Cleaning

Figure 4-26 shows the surface topography images of the AA7075 substrate after polishing, alkaline cleaning and acid cleaning processes captured using AFM at two different surface areas: 3 x 3 µm and 10 x 10 µm. The three-dimensional images of the surface topography show uneven surfaces of the substrate after the polishing process, due to the polishing scars (Figure 4-26(a)). The initial rough polishing scars on the substrate was refined after the immersion process in alkaline solution for 10 seconds (Figure 4-26(b)). However, this cleaning process produced lots of cavities on the surface. Cleaning the substrate in nitric acid solution for 20 seconds highly dissolve the

substrate, as an obvious dissolution traces with larger cavities were observed on the surface (Figure 4-26(c)). The figures also show that the uneven surfaces produced by the polishing process were carried forward to the alkaline and acid cleaning process. However, the polishing scars were slowly eliminated through the surface pre- treatment processes.

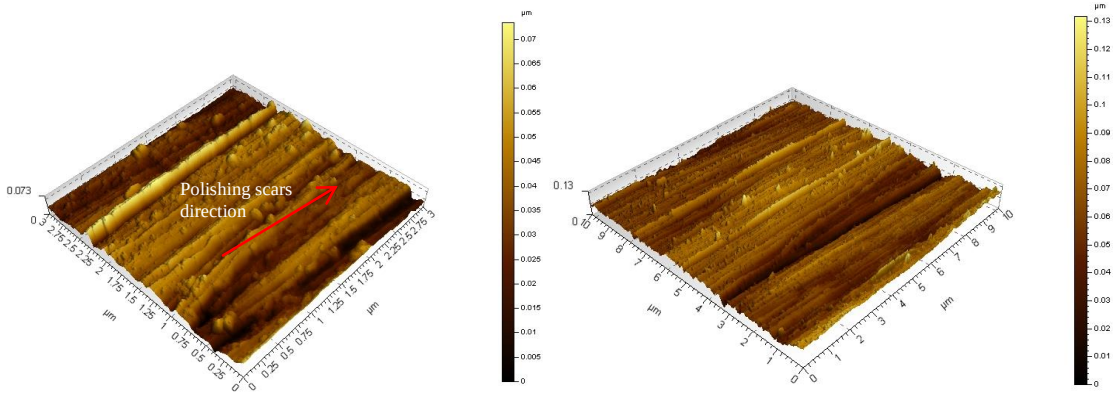

(a)

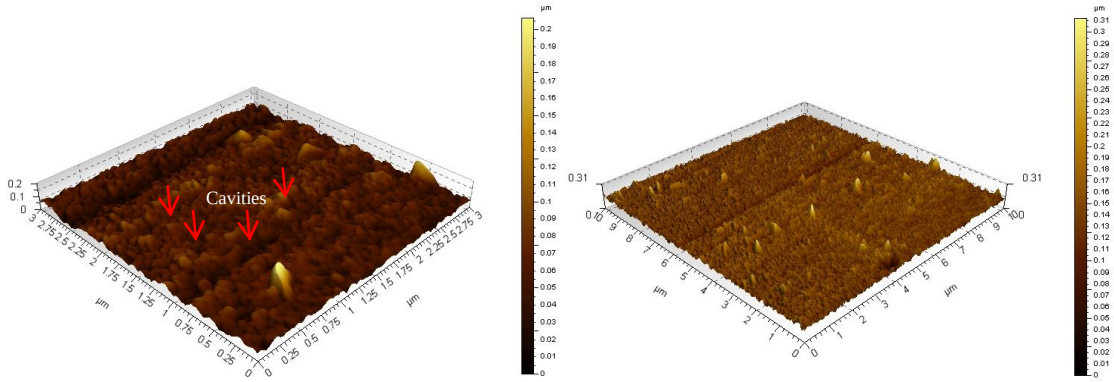

(b)

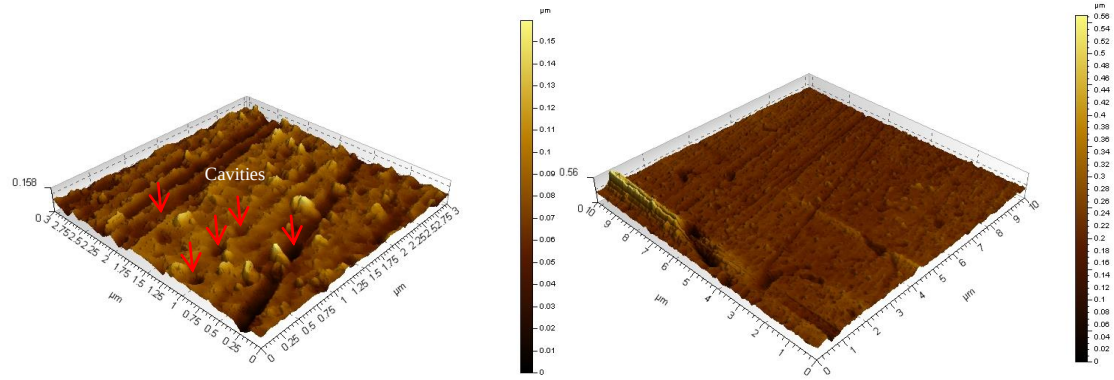

(c)

Figure 4-26 AFM images of AA7075 substrate after various surface pre-treatment processes. (a) after polishing using 1µm diamond paste, (b) after alkaline cleaning in 10 wt.% NaOH at room temperature for 10 seconds, (c) after acid pickling in 50 vol.% HNO_3 solution at room temperature for 20 seconds.

Figure 4-27 shows the surface roughness of the AA7075 substrate as a function of various surface pre- treatments processes, as measured by AFM at two different surface areas: 3 x 3 µm and 10 x 10 µm. This figure shows surface characteristics of the substrates after polishing, alkaline cleaning, and acid cleaning processes. The aim of this analysis is to understand the influence of the surface pre-treatment processes on surface roughness of the substrate.

As shown in the figure, the surface roughness of the substrate for both 3 x 3 µm and 10 x 10 µm surface areas after the alkaline cleaning process shows a higher surface roughness than the polished substrate. The AFM scans for the 3 x 3 µm area on the substrate clearly show that the polished surface was roughened after the alkaline cleaning. No significant difference was observed between the roughness before and after the acid cleaning. On the other hand, for the 10 x 10 µm surface area, the surface roughness of the polished substrate gradually increased after the alkaline cleaning and acid cleaning processes, based on the large surface area measurement. It is related to the number of cavities found on the substrates. The surface roughness of the 10 x 10 µm area was higher than 3 x 3 µm area after the acid cleaning process.

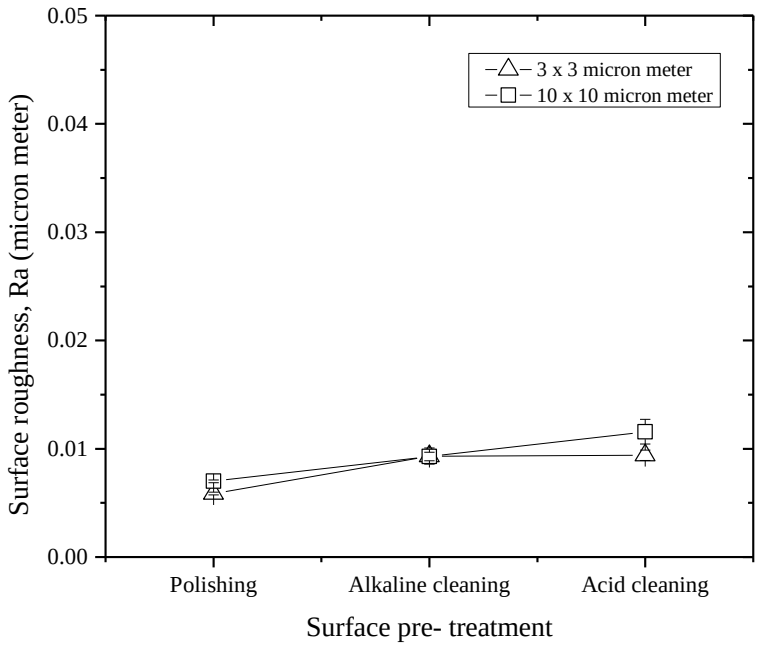

Figure 4-27 Surface roughness of after various surface pre- treatment processes prior to zincating process

4.4.2 Surface Topography and Roughness of AA7075 Substrate after Copper Activation Process

Figure 4-28 shows the AFM images of the AA7075 substrate for two different surface areas (3 x 3 µm and 10 x 10 µm) after a copper activation process at 5, 10 and 15 minutes. A substrate which was immersed in 0.5 M H_2SO_4 solution without copper particles for 20 seconds showed formation of cavities all over the surface, due to the dissolution of the substrate (Figure 4.24 (a)). After 1 minute immersion in 0.5 M H_2SO_4 + 3.13 x10^{-4} $CuSO_4$ solutions, the surface was covered by small nuclei of copper particles, as will be confirmed in Section 4.3.2. These particles were observed to deposit along the highest surface of the polishing scars. However, after 5 minutes of immersion, the polishing scars were no longer observed on the AFM images. Then, after 5 and 10 minutes, the copper particles had grown and deposited on all over the surface, with some agglomeration of copper particles observed on the surface.

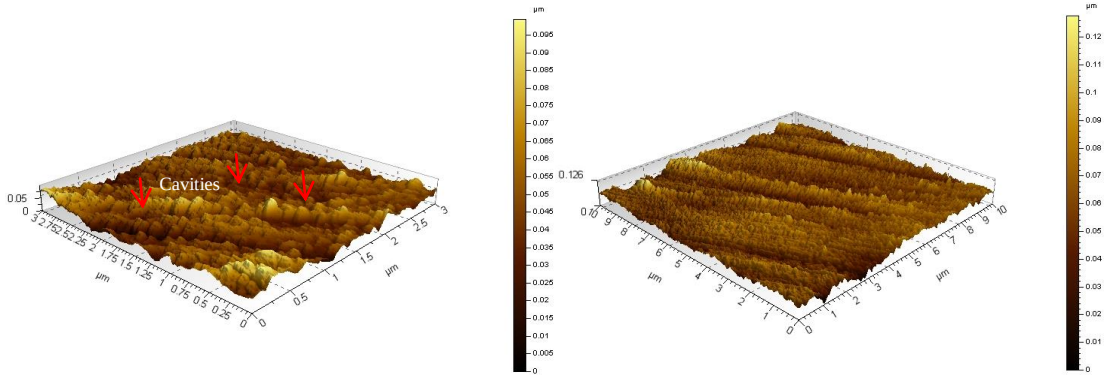
Cavities
0.05
0.126
µm

(a)

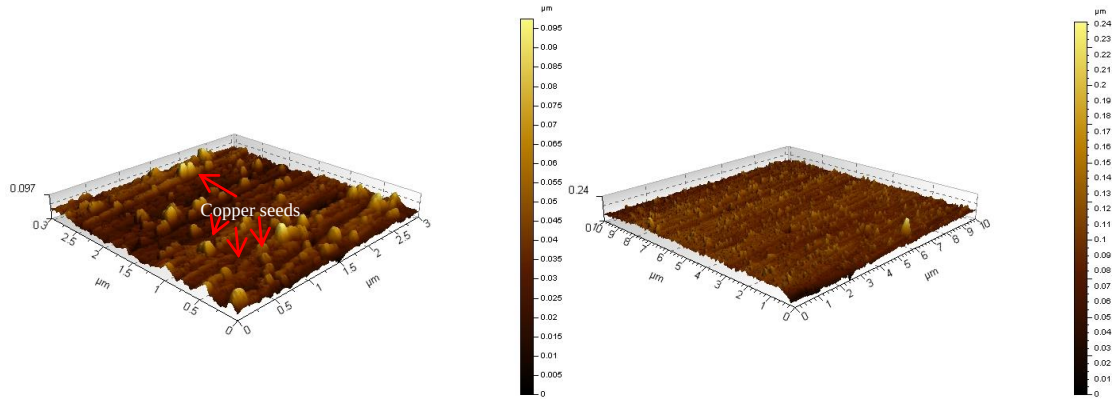
Copper seeds
0.097
0.24
µm

(b)

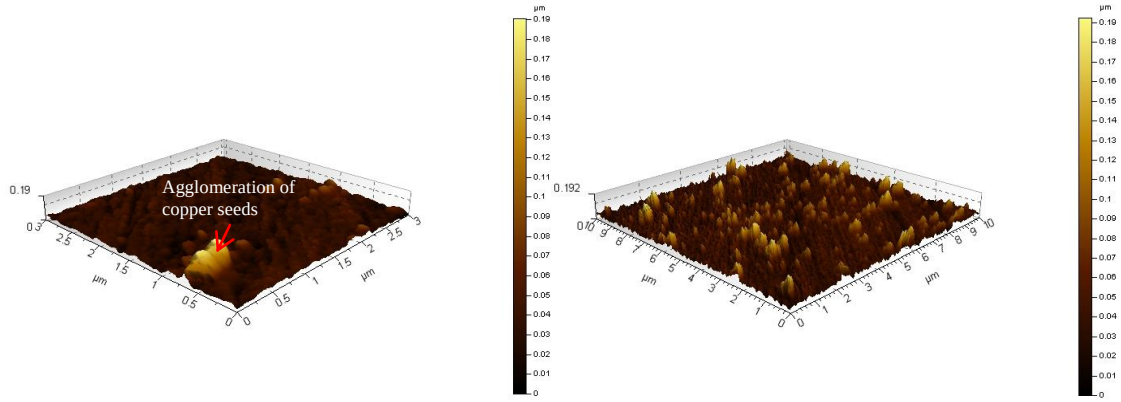
Agglomeration of
copper seeds
0.19
0.192
µm

(c)

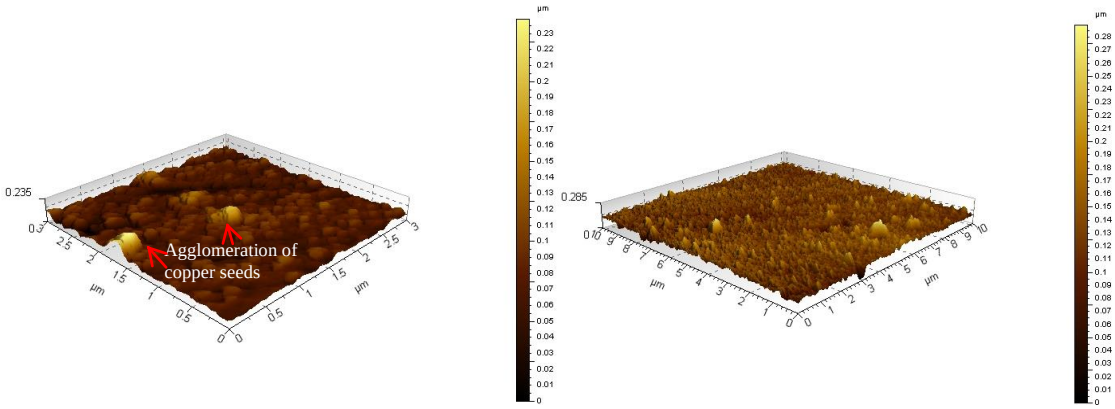

(d)

Figure 4-28 AFM images of AA7075 substrates after (a) immersion in 0.5 M H_2SO_4 solution without copper particles for 20 seconds at room temperature and copper activation process in 0.5 M H_2SO_4 + 3.13 x 10^{-4} $CuSO_4$ solution at (b) 5, (c) 10 and (d) 15 minutes at room temperature.

The surface roughness plot as a function of various copper activation duration is shown in Figure 4-29. Surface roughness was measured at two different surface areas, particularly 3 x 3 µm and 10 x 10 µm. The surface characteristics of the substrates after copper activation process at 5, 10 and 15 minutes are shown in the figure. As shown in the figure, the surface roughness for both areas gradually increased with increases in the duration of the copper activation process from 5 to 15 minutes. The surface roughness of the process at all durations for the 10 x 10 µm area was higher than the 3 x 3 µm area.

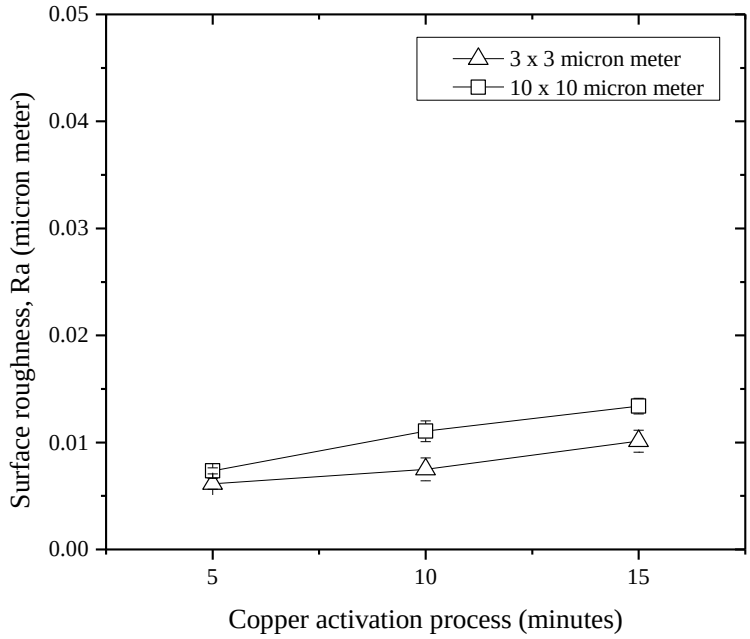

Figure 4-29 Surface roughness (Ra) of AA7075 substrate at various durations of copper activation process.

4.4.3 Surface Topography and Roughness of AA7075 Substrate after Conventional and Modified Single Zincating Process at Various Durations

Figure 4-30 shows the effect of the conventional single zincating process for 1 minute and modified single zincating process for 5, 10, 15 and 20 minutes on the surface topography for different surface areas, namely 3 x 3 µm and 10 x 10 µm. This figure shows the depth profile analysis in the horizontal direction. The nucleation and growth of the zinc particles with time can clearly be seen on the 10 x 10 µm AFM images. The AFM images show that the zincating process began with nucleation, followed by growth of the zinc deposits.

The conventional single zincating process at 1 minute shows the initiation of the zinc nuclei on the surface (Figure 4-30 (a)). Non- homogenous deposition of the small size zinc particles causes an irregular and rough surface on the substrate. At 5 minutes of modified single zincating process, the zinc particles grew and increased in population (Figure 4-30 (b)).

As the zincating duration increased from 5 to 10, 15, and 20 minutes, the zinc particles increased in number and size with some agglomeration of zinc particles at certain areas (Figure 4-30 (c- e)). After 20 minutes of modified single zincating process, the surface was extensively covered with the zinc particles which stacked on each other and formed a homogenous layer of zinc particles. The zinc particles were confirmed to have a hexagonal shape, as shown in Figure 4-30 (d).

As the single zincating duration increased from 1 to 20 minutes, zinc particles coalesced to form larger mounds, thus showing broader peaks in the profile images.

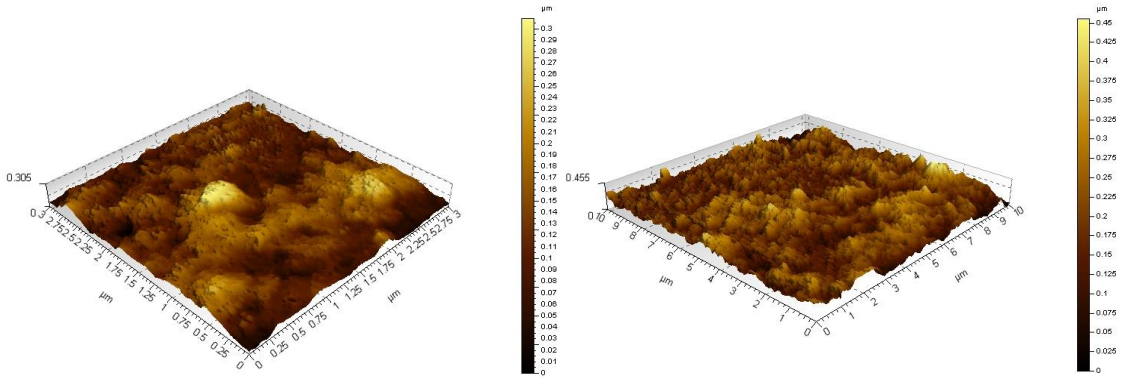

(a)

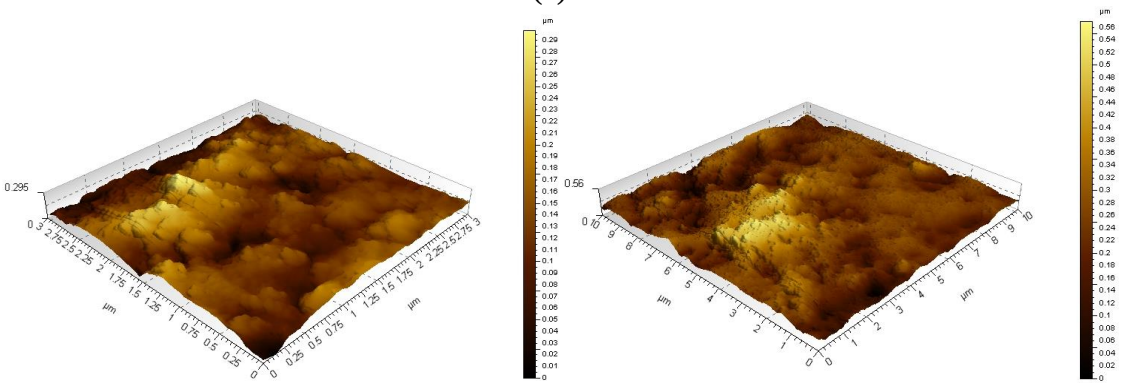

(b)

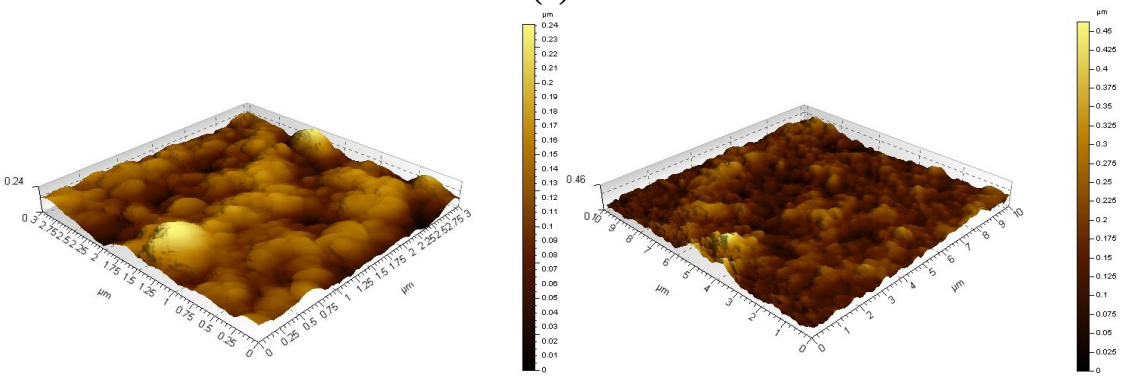

(c)

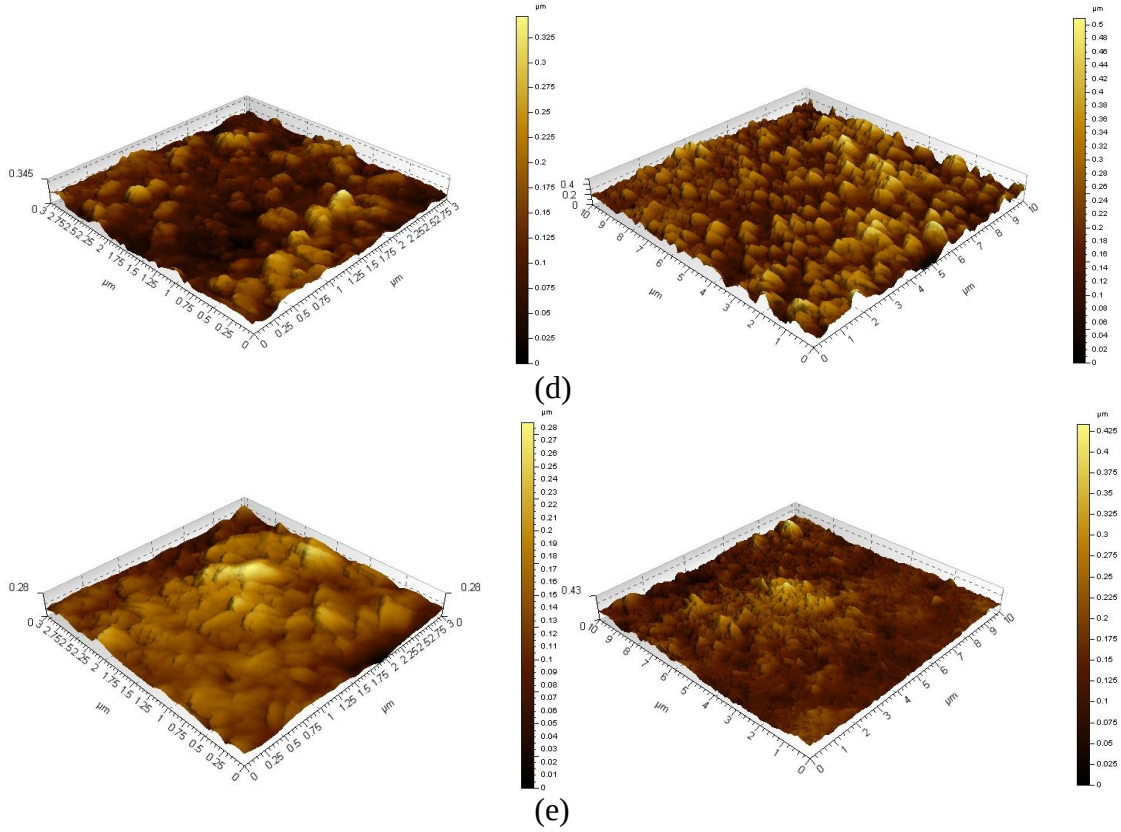

Figure 4-30 AFM images (three dimensional view) of AA7075 substrate after (a) conventional single zincating process at 1 minute and modified single zincating process at various durations, such as (b) 5, (c) 10 , (d) 15 and (e) 20 minutes

Figure 4-31 shows a surface roughness plot as a function of conventional and modified single zincating processes, which was measured at two different surface areas, 3 x 3 µm and 10 x 10 µm. The aim of this analysis is to understand the influence of various single zincating durations on the surface roughness by examining the surface characteristics of the substrates after conventional single zincating at 1 minutes and modified single zincating at 10 and 20 minutes. Both surface areas show similar trends in the variation of the surface roughness. The figure indicates a drastic increase in surface roughness of the acid cleaned sample after conventional single zincating for 1 minute. Further increasing the single zincating duration to 10 and 20 minutes, results in a gradual decrease in Ra values. The surface roughness measured on the 10 x 10 µm surface area was higher than 3 x 3 µm.

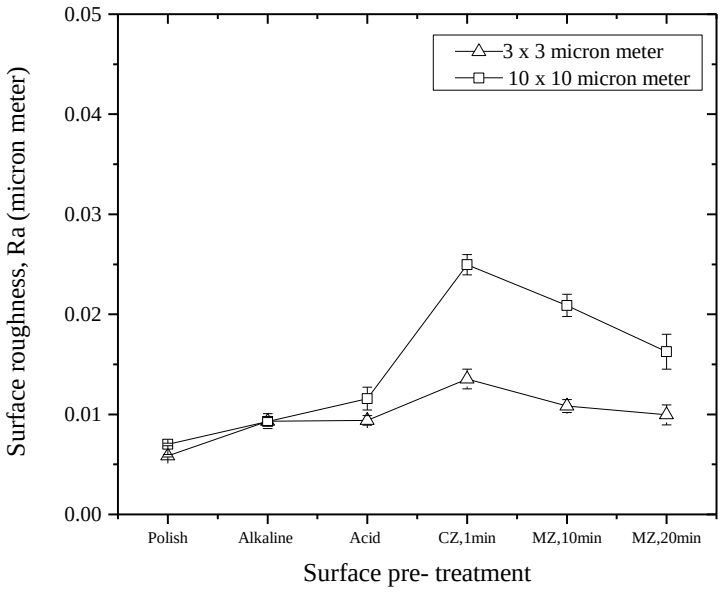

Figure 4-31 Surface roughness of substrates after conventional and modified single zincating process at various durations. CZ: conventional single zincating process, MZ: modified single zincating process.

4.4.4 Surface Topography and Roughness of AA7075 Substrate after Double Zincating Process at Various Durations

In order to investigate the zinc deposition on the AA7075 substrate during the double zincating process, AFM analysis was performed on the substrate (Figure 4-32). The first zincating process at 60 seconds produced an irregular and rough surface, with deposition of small zinc particles (Figure 4-32(a)). Then, after zinc stripping process in 50 vol.% HNO_3 solution for 20 seconds, dissolution traces and holes were observed on the surface (Figure 4-32(b)). The rough surface produced from the first zincating process was refined through this process. After second zincating process at 10 seconds (Figure 4-32(c)), the surface was covered by zinc particles again, but with a more uniform distribution and smaller particle size compared to the first zincating process. However, some unevenness of the surface was still observed from this process. As the second zincating duration was increased from 10 to 30 seconds (Figure 4-32(d)), the surface was covered by more zinc particles with a large particle size. The growth and agglomerations of the zinc particles were also observed on the surfaces. However, the

deep holes which formed during the first zincating process due to the dissolution of AA7075 substrate in high alkaline zincating process, were not fully covered during this process. After 50 seconds of second zincating process, deep holes were no longer observed on the substrates (Figure 4-32(e)). Furthermore, agglomerations of the small zinc particles deposited on the homogenous initial zinc layer were also observed.

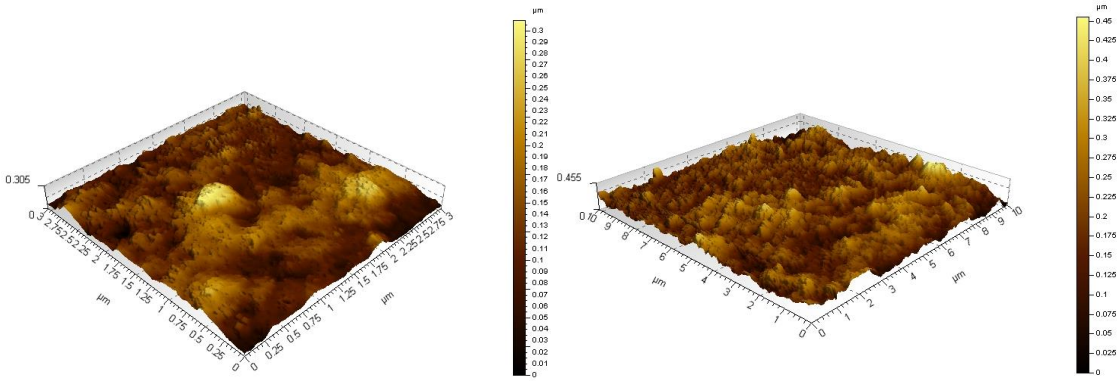

(a)

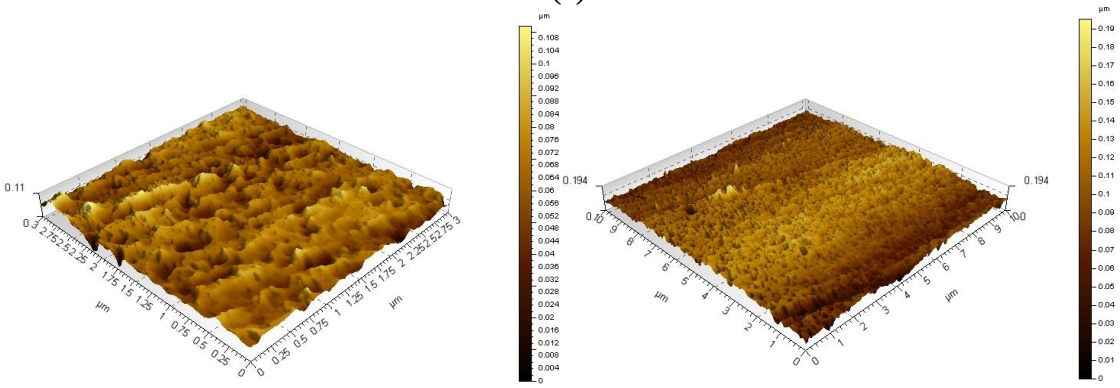

(b)

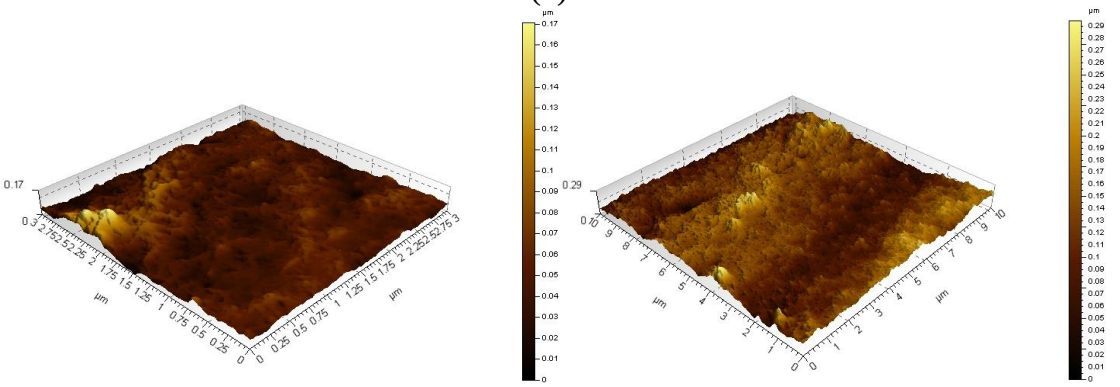

(c)

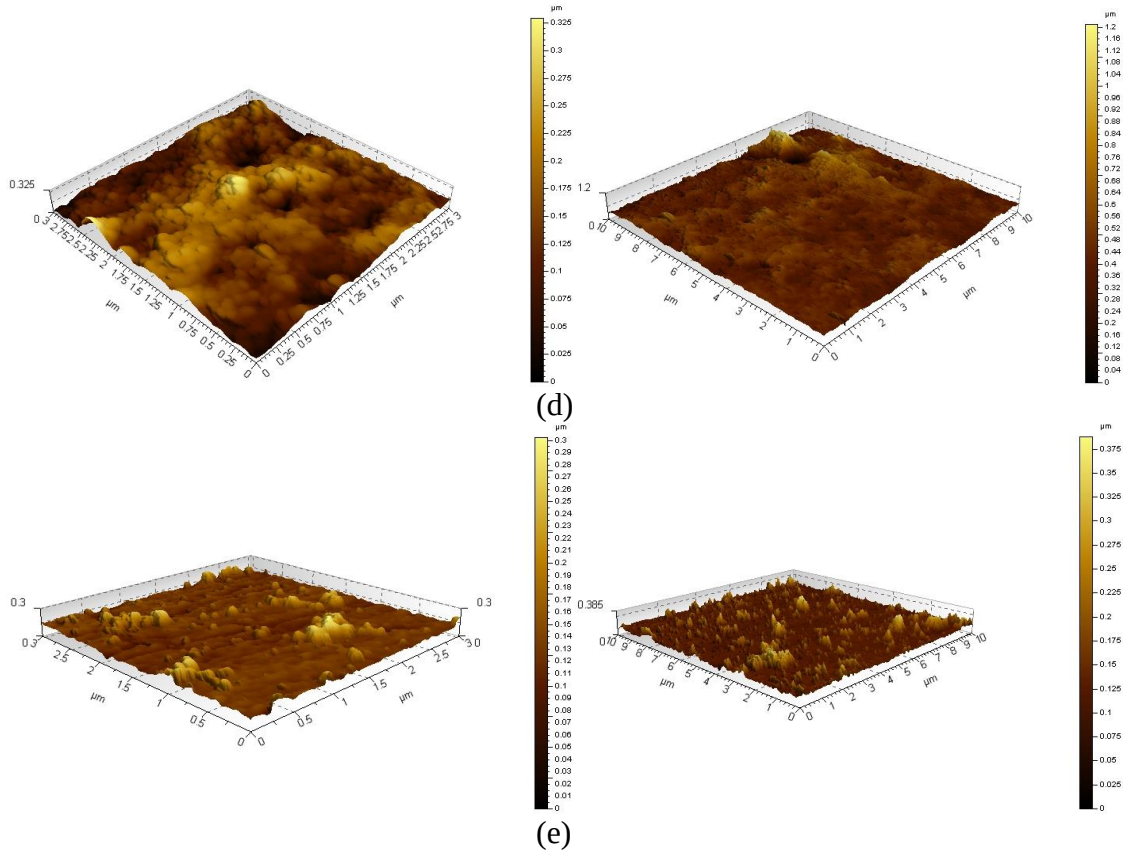

Figure 4-32 AFM images of AA7075 after double zincating process (a) first zincating at 60 seconds, (b) zinc stripping in 50 vol. % HNO_3 at room temperature for 30 minutes, (c)- (d) double zincating at 60/10, 60/30 and 60/50 seconds, respectively.

Figure 4-33 shows the average surface roughness after each treatment during the double zincating process, which was measured at two different surface areas, 3 x 3 µm and 10 x 10 µm. Both surface areas show the same pattern in the variation of the surface roughness. This figure shows a drastic decrease in the surface roughness of the first zincated substrate after the zinc stripping process, which is almost the same with the surface roughness of the polished substrate. For the 10 x 10 µm area measurement, the surface roughness gradually increased after the second zincating process at 10 seconds. Then, further increasing the second zincating duration to 50 seconds resulted in an increasing in the surface roughness. However, the surface roughness after double zincating process is lower than the first zincating process. This figure shows that the second zincating process can produce a smooth surface compared to the first zincating process.

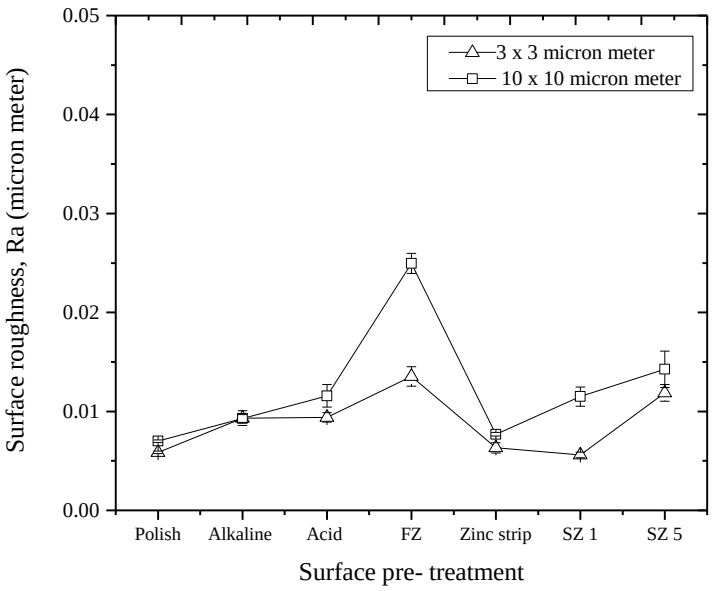

Figure 4-33 Surface roughness of double zincating process. FZ: first zincating at 60 seconds, SZ1: second zincating at 60/10 s and SZ5: second zincating at 60/50 s.

4.4.5 Surface Topography and Roughness of AA7075 Substrate after Conventional and Modified Single Zincating Process at Various Durations with Copper Activation

In order to investigate the influence of the copper activation on the surface topography and surface roughness of the conventional and modified single zincating processes, AFM observations were carried out. In this study, copper activation duration was fixed at 10 minutes due to the homogenous distribution of the copper seeds on the substrate. Figure 4-34 shows the influence of conventional single zincating process at 1 minute and modified single zincating process at various durations, such as 10 and 20 minutes, with copper activation, at different surface area, 3 x 3 µm and 10 x 10 µm. Figure 4-34 also shows a depth profile analysis in the horizontal direction. AFM measurement on 10 x 10 µm surface area clearly shows the nucleation and growth of the zinc particles on the substrate. After 1 minute of conventional single zincating process, the zinc nuclei were deposited on the surface and formed an uneven and rough surface on the substrate. (Figure 4-34(a)).

On continued zincating, the zinc particles growth and its density increased after 10 minutes in the zincating solution (Figure 4-34(b)). As the zincating duration

increased from 10 to 20 minutes, increasing in the zinc particles' size and density with some agglomeration of the zinc particles was observed on the substrate (Figure 4-34 (c)). AFM images for longer zincating durations show that the zinc particles were stacked on each other and covered the entire surface. The zinc particles were confirmed to take on a hexagonal shape, as shown in Figure 4-34(c).

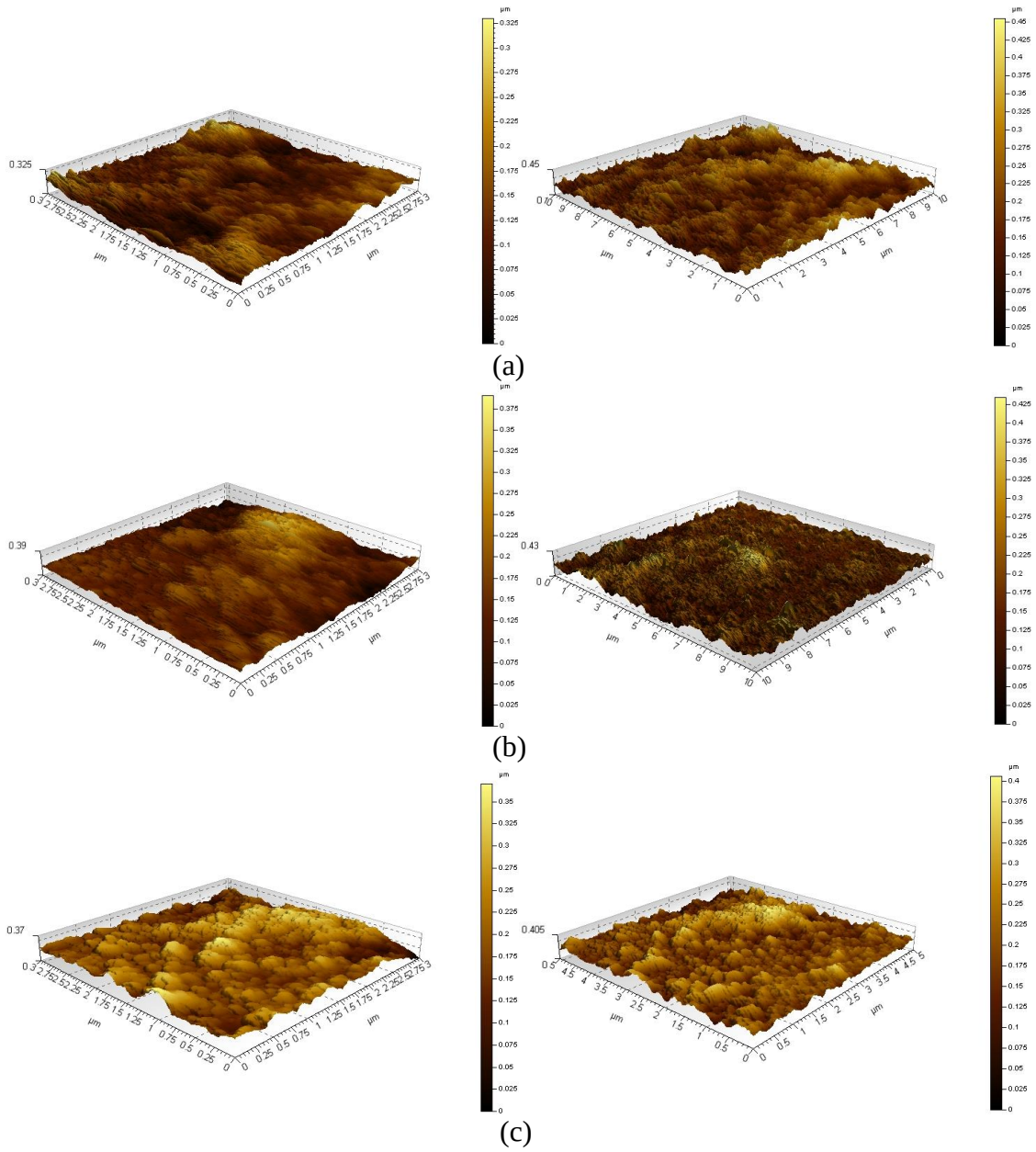

Figure 4-34 AFM images (three dimensional view) of AA7075 substrate after (a) conventional single zincating process at 1 minute and modified single zincating process at various durations, such as (b) 5, (c) 10, (d) 15 and (e) 20 minutes with copper activation

Figure 4-35 shows the measured surface roughness for various durations of single zincating process, which was measured at two different surface areas, namely 3 x 3 µm and 10 x 10 µm. This analysis was done in order to understand the influence of copper activation process on the surface roughness of conventional and modified single zincated substrates, by examining the surface characteristics of the substrates after single zincating process at 1, 10 and 20 minutes. Overall, the surface roughness of the sample after the zincating process is higher than before the zincating process. Both surface areas at 3 x 3 µm and 10 x 10 µm show an increase in the surface roughness, after zincating at 1 minute. However, an increase in the duration to 20 minutes showed a gradual decrease in the surface roughness for 10 x 10 µm area, while for 3 x 3 µm area showed inconsistent roughness. The surface roughness measurement on the 10 x 10 µm area was higher than that for 3 x 3 µm.

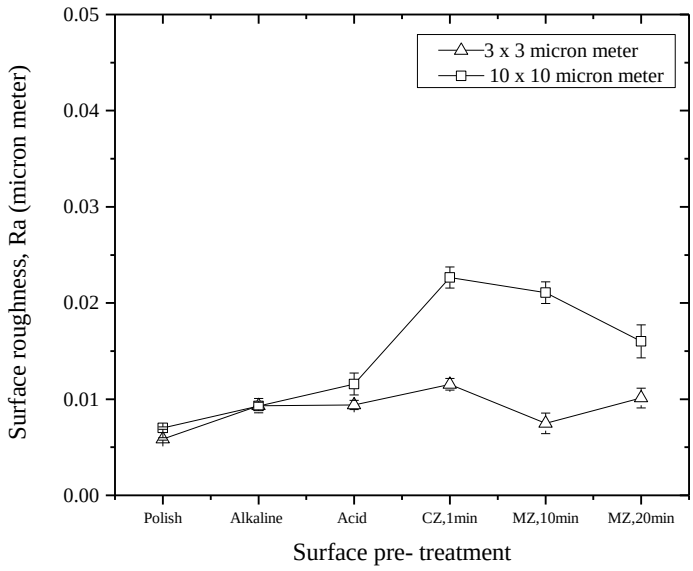

Figure 4-35 Surface roughness of modified single zincating processes with copper activation. CZ: conventional single zincating process, MZ: modified single zincating process.

4.5 Surface Morphology and Composition of Interface of Nickel Coating Electrodeposited on AA7075 Substrate through a Conventional and Modified Single Zincating Process at Various Durations

In order to investigate the effect of various zincating durations on the thickness of the zincating layer, cross-sections of the nickel coatings electrodeposited on AA7075 substrate were observed using SEM, as shown in

Figure 4-36. This study was carried out on nickel coatings electrodeposited on AA7075 substrate through a conventional and modified single zincating process only. These images show that the morphology of the coating's interface was strongly influenced by the zincating duration. For example, a non-uniform nickel deposit was observed at the interface of the coating and substrate of a sample which was produced from the conventional single zincating process at the shortest duration (1 minutes), as shown by the arrows in

Figure 4-36(a). The figure also shows a non uniform of the nickel deposit with some formation of cavities. On the other hand, a modification on the conventional single zincating duration from 1 minute to 5, 10, 15, and 20 minutes caused an improvement in the deposition of nickel particles on the substrate (

Figure 4-36(b-e)). The cross-section morphologies show a uniform interface of nickel deposits on the AA7075 substrate without any defects.

An EDX analysis using the 'point and ID' mode signal was drawn across the cross-section of the nickel coatings electrodeposited on AA7075 substrate, in order to analyse the composition at the interface of the coatings. In all samples, seven elements were detected during the analysis, namely nickel as a coating material, zinc, magnesium and copper as the alloying elements in AA7075 substrate and oxygen and carbon as impurities. Surprisingly, no significant increase in the zinc composition was observed at the interface of the nickel coatings and AA7075 substrate of all samples (

Figure 4-36(a- e)). Even though zinc was detected in this analysis, it was at very low concentrations, and was assumed to be contributed by the zinc in the AA7075 substrate

itself. Only the sample which was prepared through the conventional zincating process showed an increase in the oxygen concentrations at the interface of the coating and substrate (as shown by the arrow in

Figure 4-36(a), in the EDX analysis diagram). In all samples, results of EDX line analysis show gradual increases in the nickel signal to a steady value of the nickel layer, at the decrease of the aluminium signal.

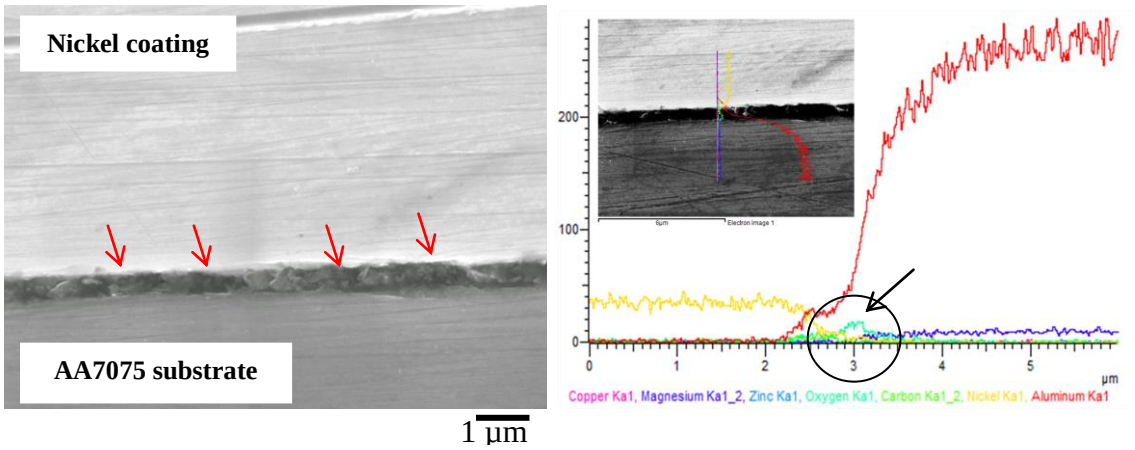

(a)

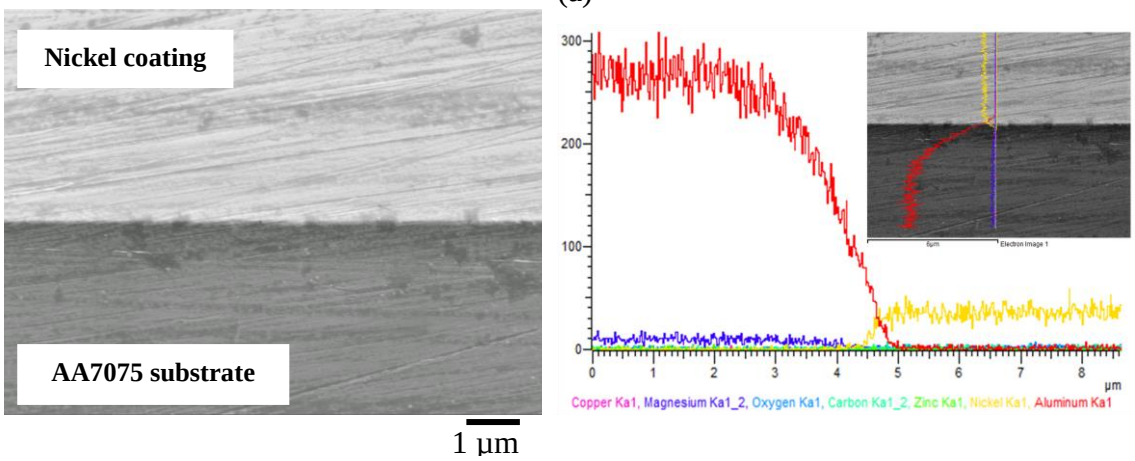

(b)

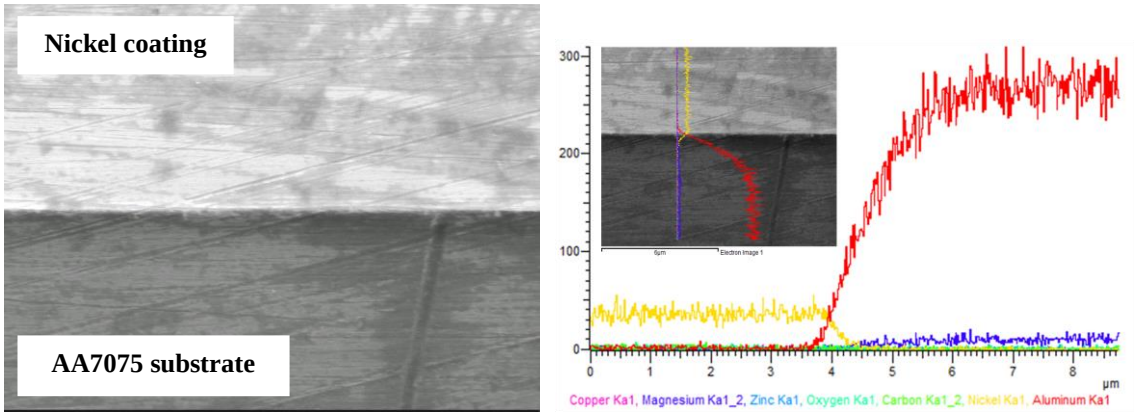

(c)

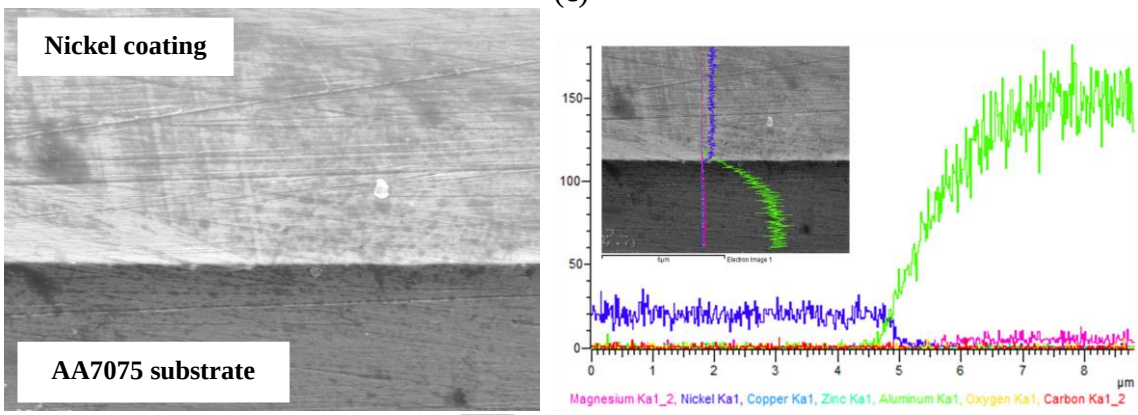

(d)

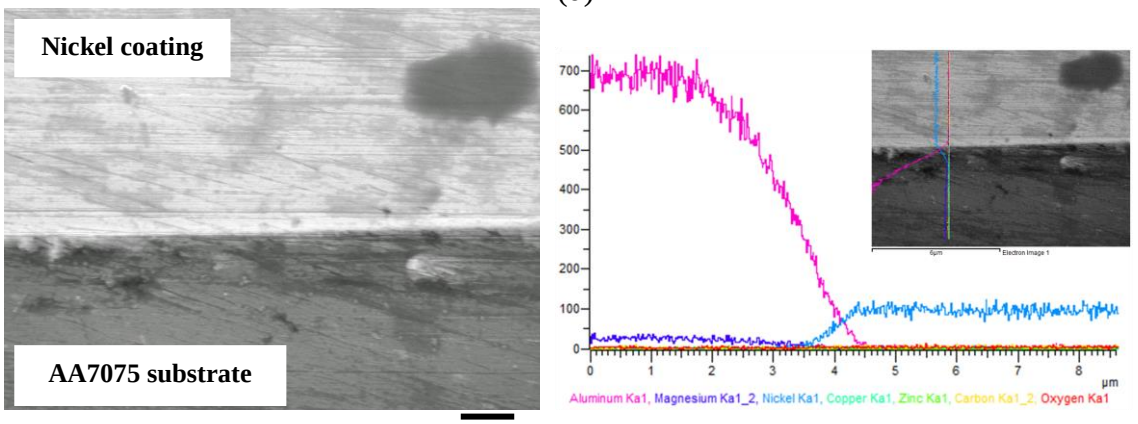

(e)

Figure 4-36 SEM morphology and EDX analysis on the cross-section of the nickel coatings electrodeposited on AA7075 substrate through (a) conventional single zincating process at 1 minute and modified single zincating process at various durations, such as (b) 5, (c) 10, (d) 15 and (e) 20 minutes

4.6 Adhesion of Nickel Coatings on AA7075 Substrate Produced from Multiple Zincating Processes

4.6.1 Effect of Conventional and Modified Single Zincating Process at various Durations on the Adhesion of the Nickel Coatings Electrodeposited on AA7075 Substrate

Acoustic emissions

Figure 4-37 compares the AE signals and friction force (F_f) curves plotted as a function of scratch distance of nickel coatings which were produced from conventional single zincating process at 1 minute and modified single zincating process at various durations, such as 5, 10, 15, and 20 minutes. The first AE signal with the highest intensity detected always represents the first critical load (L_{C1}) as the first crack occurring on the scratch track. This kind of failure event is also known as cohesive failure. The figure shows that the coating which was prepared through the conventional single zincating process at 1 minute produced the earliest AE signal with high intensity compared to the other samples.

This first AE signal or L_{C1} was detected at scratch location of 4.7 mm, which is equivalent to 53.6 N of applied load. As the single zincating duration increased to 10 minutes, the L_{C1} could only be detected at 8.40 mm of scratch location, equivalent to 87.7 N. Then, increasing in the single zincating duration up to 20 minutes quickened the occurrence of L_{C1}, which was at 60 N. Furthermore, strong evidence of adhesive failure (L_{C2}) was found on the sample which was produced from the conventional zincating process at 1 minute, due to the increasing in the AE signals (Figure 4-37(a)). In addition, all samples show increasing in the AE signals with high intensity peaks, as the progressive applied load reached the higher load at the end of the track, compared to the lower load. OM and SEM examinations were done on these samples in order to confirm the location of the coating failures (Figure 4-41 and Figure 4-42).

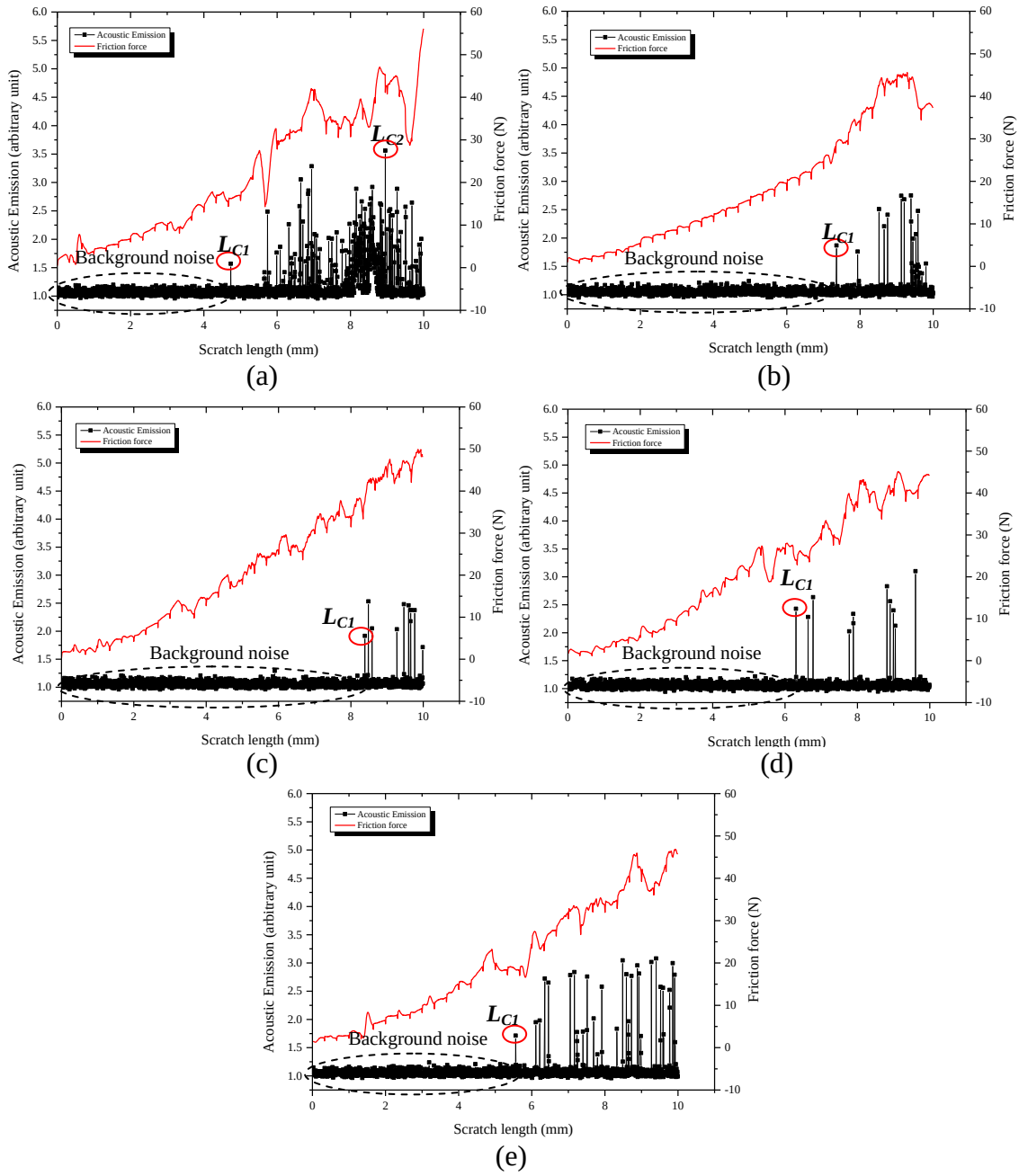

Figure 4-37 Frictional force and acoustic emission signal intensity as a function of the scratch distance for nickel coatings produced at (a) conventional single zincating process at 1 minute and modified single zincating process at various durations, (b) 5, (c) 10, (d) 15 and (e) 20 minutes

Coefficient of Friction

The instantaneous coefficient of friction (COF) was calculated by dividing the frictional force by the applied normal load. Figure 4-38 shows the COF and acoustic emission signal intensity as a function of the scratch distance for nickel coatings produced by (a) a conventional single zincating process for 1 minute, and modified single zincating process at various durations, (b) 5, (c) 10, (d) 15 and (e) 20 minutes. The results showed that for all samples which were produced by conventional and modified single zincating process, the COF increased with an increase of scratch distance. The scratch distance which was from 0 to 10 mm was equivalent to 10 to 100 N of progressive normal load applied during the test. It was also observed that there was no significant difference between the values of COF measured from samples produced at 5, 10, 15 and 20 minutes of modified single zincating process. However, the COF for the sample produced using a conventional single zincating process was greater than the COF of the sample produced using the modified single zincating process.

For all samples, the sudden simultaneous changes in both COF curve and AE signal corresponded to the failure occurring in the nickel coating, such as cohesive and adhesive failure (indicated by the red square marks in Figure 4-38). These results were verified by optical microscopy examination of the scratch tracks (Figure 4-41). The periodic bumps in the COF was due to the rapid interaction of the diamond indenter with the irregular surface of the coatings. However, the sudden bumps which appeared without a corresponding AE signal appear to be due to the interaction of the scratch track with surface voids. These can be seen clearly from samples which were single zincated at 1, 10 and 20 minutes (optical micrographs in Figure 4-41 (a, c and e) and Figure 4-38 (a, c and e), respectively).

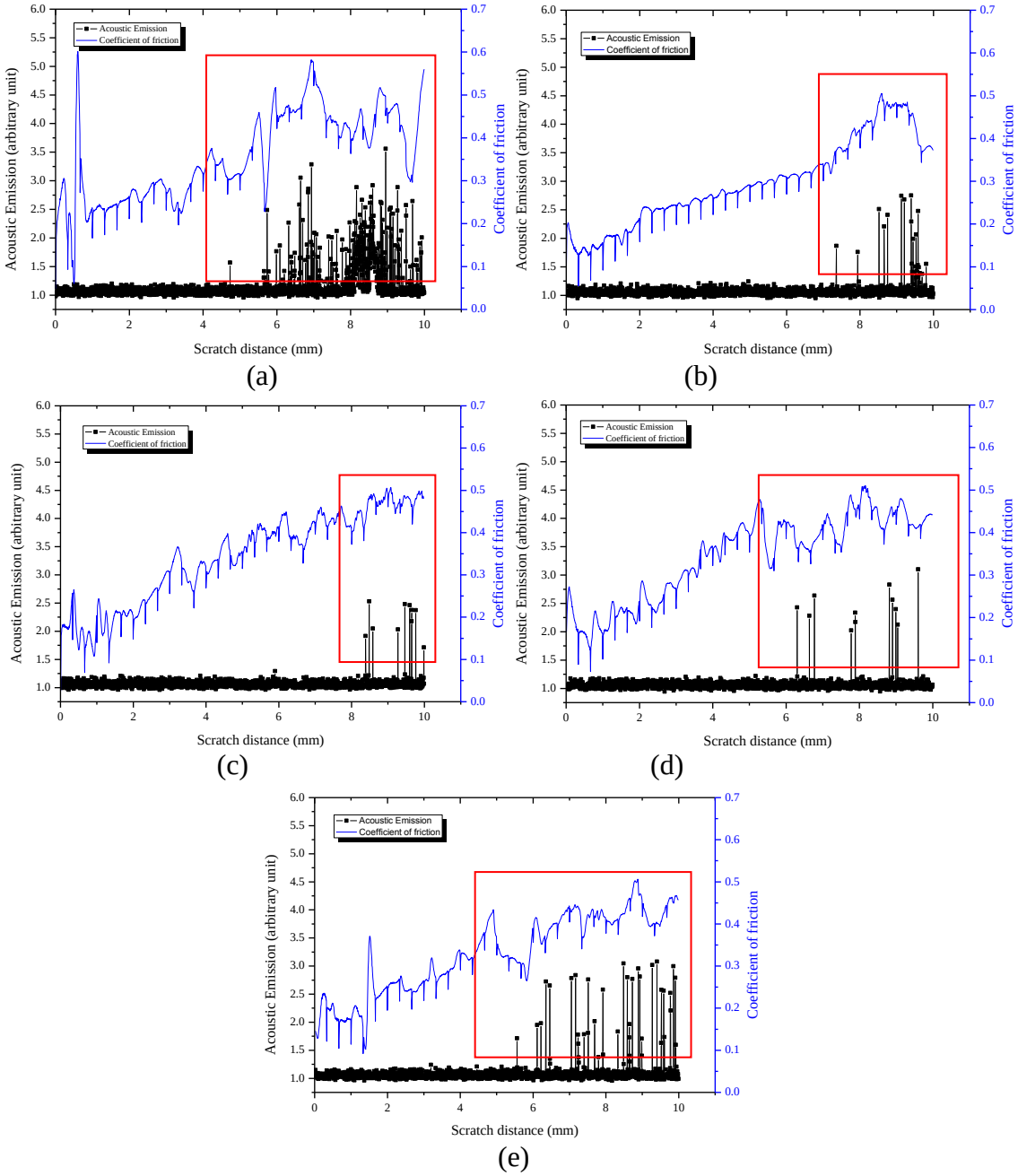

Figure 4-38 Coefficient of friction and acoustic emission signal intensity as a function of the scratch distance for nickel coatings produced using (a) conventional single zincating process at 1 minute and modified single zincating process at various durations, (b) 5, (c) 10, (d) 15 and (e) 20 minutes

Figure 4-37 only shows the AE signal and F_f versus scratch length for one selected sample from each of the single zincating durations, which is used to represent other eight scratches taken during the test. The average critical loads of L_{C1} and L_{C2} values with standard error obtained in the scratch test are presented in Figure 4-39. This

figure shows the influence of various single zincating durations on the critical loads of the nickel coatings. The conventional single zincating process at 1 minute showed the lowest L_{C1}. By applying a zincating process for 5 minutes, L_{C1} was improved up to 78.4 N. Then, L_{C1} values gradually decreased as the single zincating durations increased from 5 to 20 minutes. Furthermore, only the conventional single zincated sample showed the adhesive failure mode or L_{C2} value which at 84.5 N, as shown in Figure 4-39.

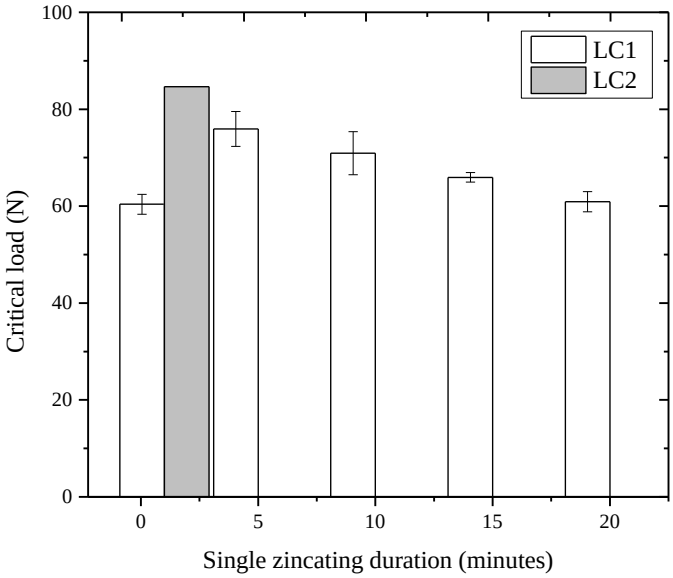

Figure 4-39 Average critical loads of nickel electrodeposited on AA7075 produced at various single zincating durations as measured by scratch testing

Figure 4-40 shows the correlation of the number of AE events (N_{AE}) with the zincating durations as extracted from the AE signal curves in Figure 4-37. The average N_{AE} was calculated from eight scratches from each sample. As shown in Figure 4-40, the nickel coating produced from the conventional single zincating at 1 minute shows the highest N_{AE} value. What is interesting in this figure is that the N_{AE} value significantly reduced from approximately 130 to 25, by increasing the zincating duration from 1 to 5 minutes. However, further increasing zincating duration to 20 minutes did not result in significant differences in the N_{AE} values.

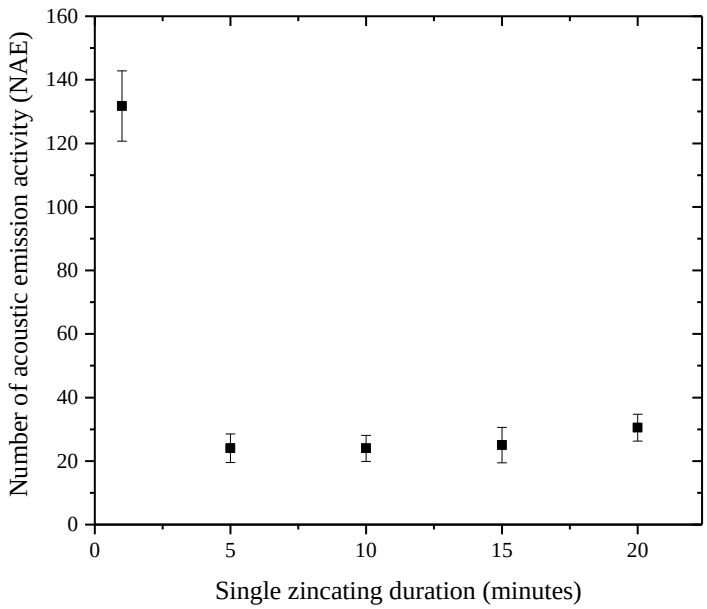

Figure 4-40 Correlation between number of acoustic emission activity (N_{AE}) and various single zincating durations

Frictional force

An alternative method to detect the occurrence of the failure event is by analysing the friction traces developed during the scratch test. Figure 4-37 also shows the variation in F_f as a function of the scratch length for nickel coatings produced at various single zincating durations. All samples in Figure 4-37(a- e) show F_f curves that are quite straight at the initial part of the curves, due to the lower loads applied to the samples at the beginning of this testing. On the other hand, at higher load, the F_f curves for all samples became fluctuate. For all samples, the values of friction force are quite similar. As shown in the figure, variation in F_f during the scratch test occurred simultaneously with the AE signal intensities. However, there was a significant difference between the samples produced at different single zincating durations. A sample which was produced from the conventional zincating process shows a change in the F_f slope which occurred at very low applied loads.

Microscopy observation

Even though an initial dramatic increase in AE signal intensities and F_f plots may represent the initiation of the first crack along the scratch track, the subsequent coating failure and its critical load could not be easily identified from the AE signals and F_f plots. Therefore, OM and SEM were utilized in this study (Figure 4-41 and Figure 4-42) to confirm or determine the actual location of the critical loads, which were initially analyzed using the AE signals and F_f curves.

In OM images of the scratch track, as shown in Figure 4-41, the progression of a scratch is shown from left to right. A microscopy examination of these scratch tracks before the L_{C1} did not show any surface damage (Figure 4-41). It is apparent from the OM images in Figure 4-41 that all samples showed a series of ductile tensile cracking at the centre of the scratch track, which is a type of through-thickness cracking under the classification of cohesive failure modes. The first cracks which occurred on the scratch tracks on all samples are labelled as L_{C1}. On all of the samples, as a scratch continued with progressive applied loads on the coatings, the stylus generated more cracks. What is interesting in this figure is that the sample produced from the conventional single zincating duration shows the coating was ruptured and separated from the substrate in the wedge spallation failure mode close to the end of the scratch track (Figure 4-41(a)). This failure is identified as an adhesion failure and was labelled as L_{C2}. This indicates that the bonding of coating to the substrate was poor.

On the other hand, the OM micrographs of other samples which were produced at 5, 10, 15 and 20 minutes only exhibited ductile tensile cracking behaviour. The scratch applied load increased with no adhesive failure observed along the scratch track (Figure 4-41(b- e)). This indicates good bonding of coating to the substrates. In addition, a further increase in the scratch applied load during the test caused an increase in size and number of cracks. Decreases in the distance from one crack to another crack were also observed on the scratch track as the scratch applied load increased.

The samples were also observed under the SEM (Figure 4-42(a-b)). More cracks were observed towards the end of the scratch track of nickel coating produced from conventional single zincating process, compared to 20 minutes of a modified single zincated sample. Rupture failure was also seen on the sample produced from the conventional single zincating process. SEM images also clearly reveal the substrate at the end of the scratch track for the conventional single zincated sample.

EDX analyses were performed at two different areas on a scratch track of nickel coating produced from the conventional single zincating process, in order to determine whether the AA7075 substrate has been revealed or not during the scratch test (Figure 4-42(a)). The EDX analyses proved that the AA7075 substrate was revealed at the end of the scratch track, which was equivalent to the highest applied load during the scratch test on coating produced from a conventional single zincating process.

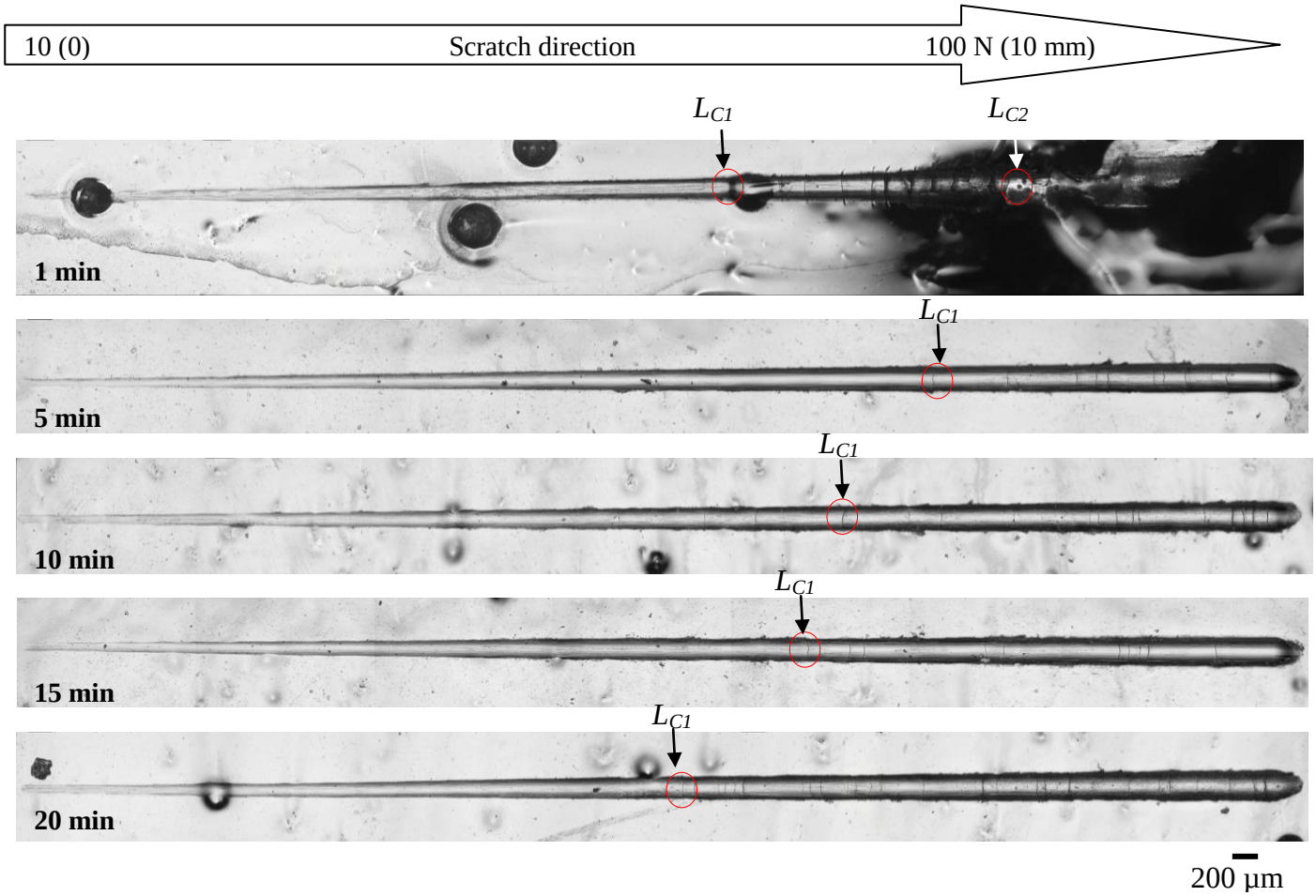

Figure 4-41 Optical micrographs of the scratch tracks of nickel electrodeposited on AA7075 substrate produced with the conventional single zincating process for 1 minute and modified single zincating process for 5, 10, 15, and 20 minutes

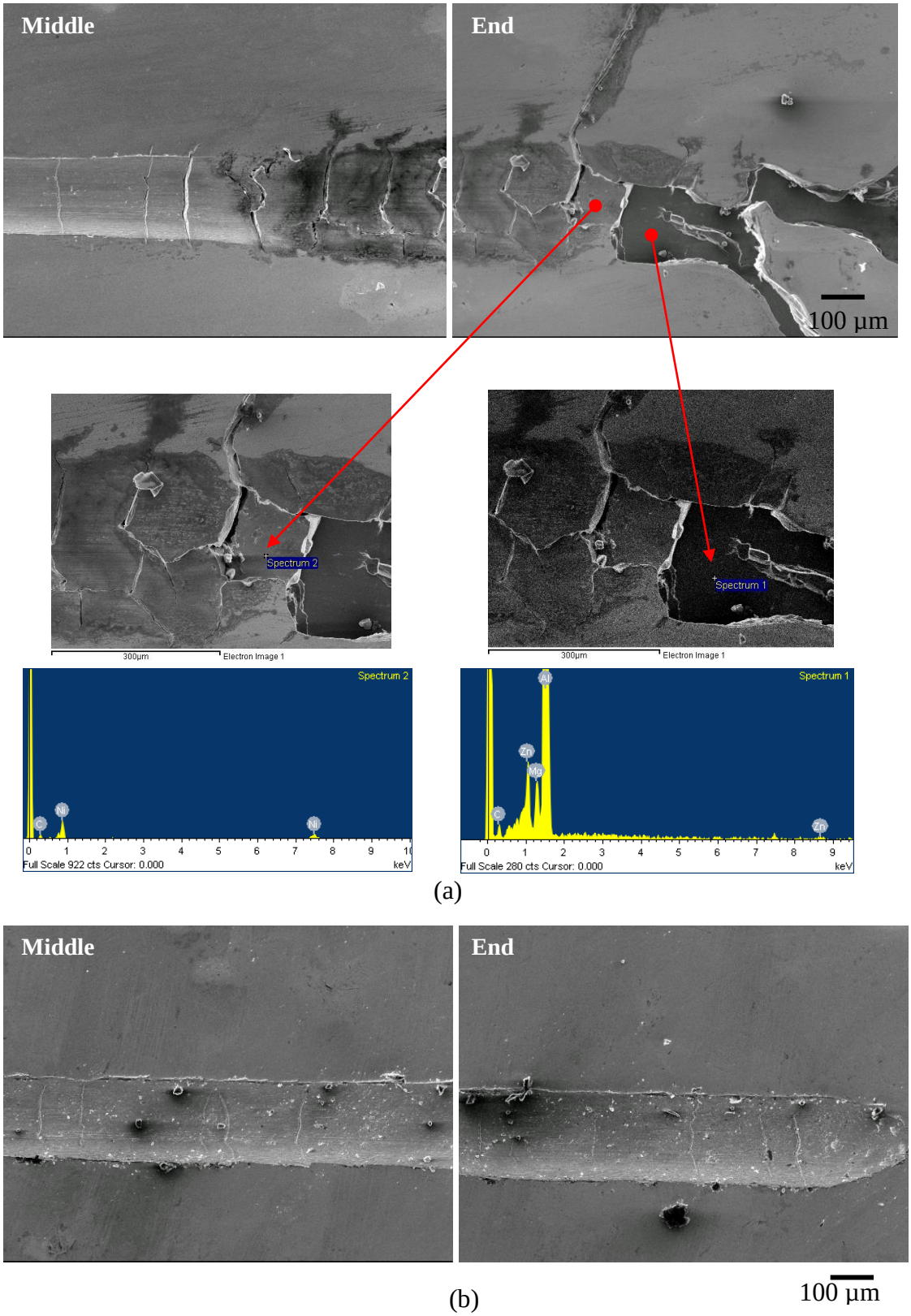

Figure 4-42 SEM images and EDX analysis showing the middle and end of the scratch tracks of nickel electrodeposited on AA7075 produced at (a) conventional single zincating process for 1 and (b) modified single zincating process for 20 minutes

4.6.2 Effect of Various Double Zincating Durations on Adhesion of the Nickel Coatings Electrodeposited on AA7075 Substrate

Acoustic emission

Figure 4-43(a- e) shows the influence of various double zincating durations on the scratch behaviour of nickel coatings on AA7075 substrates. These figures were plotted as AE signals and F_f as a function of scratch distance. In addition, on all samples, the initial dramatic increase in AE signals and F_f curves correspond directly to the initiation of the first crack during the scratch test. This was confirmed by microscopy examination of the samples (Figure 4-47 and Figure 4-48). The first crack which occurred during the scratch test is known as a first critical load (L_{C1}), or cohesive failure.

There were no significant differences in the AE signals found from the scratch test on nickel coatings produced at 60/10, 60/20, 60/30, 60/40 and 60/50 seconds of double zincating process (Figure 4-43(a- e). However, it is apparent from the AE signals that the coating which was produced through 60/20 seconds of double zincating process exhibited the lowest L_{C1} (47.3 N) which occurred at 4.09 mm of scratch length (Figure 4-43(b)). On the other hand, the highest L_{C1} (62.8 N) was obtained at 5.93 mm of scratch track from the coating produced at 60/30 seconds of double zincating process (Figure 4-43(c)).

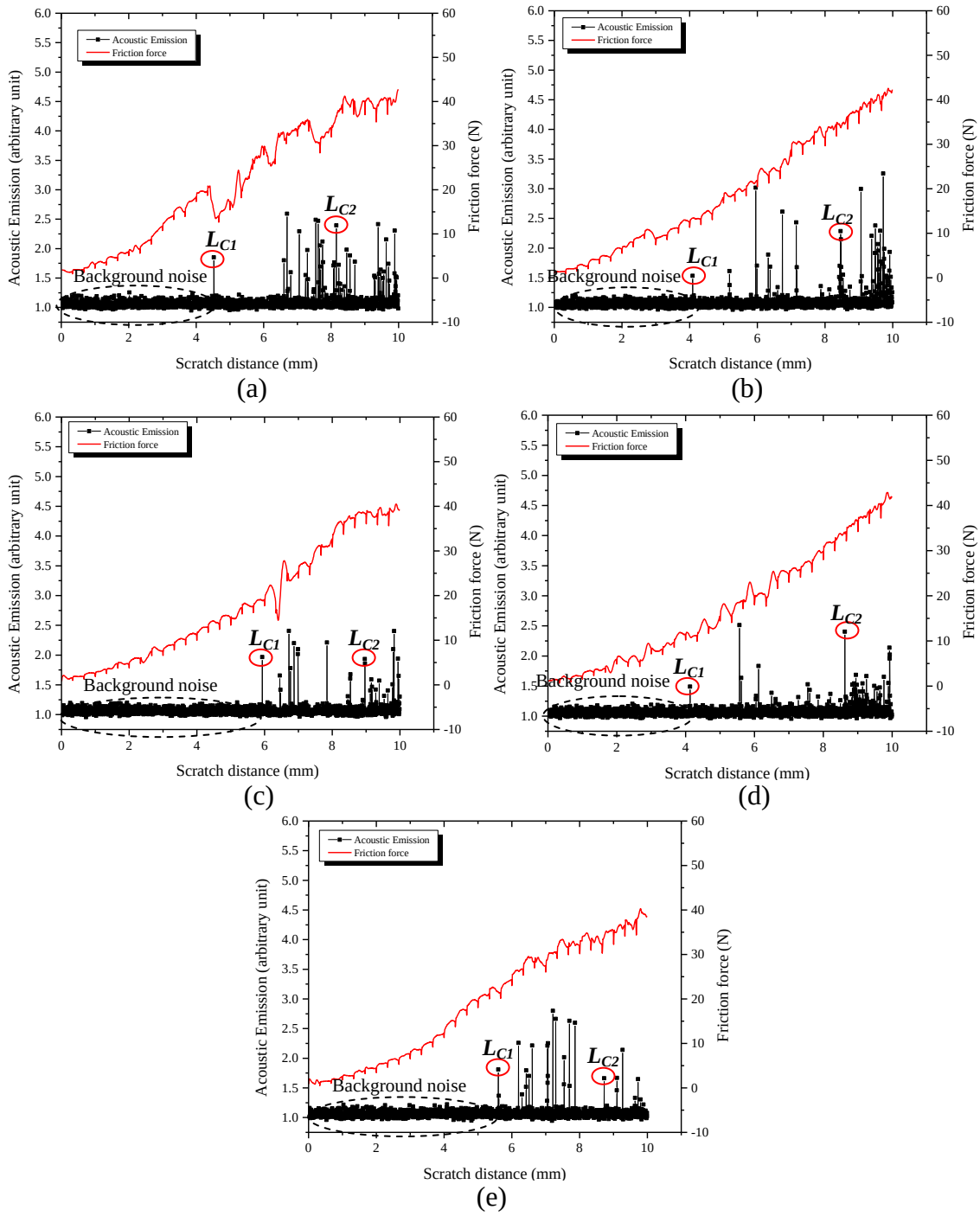

Figure 4-43 Frictional force and acoustic emission signal intensity versus scratch distance curves of nickel coatings produced at various double zincating durations (a) 60/10, (b) 60/20, (c) 60/30, (d) 60/40 and (e) 60/50 seconds.

Coefficient of Friction

Figure 4-44 presents coefficient of friction and acoustic emission signal intensity versus scratch distance curves of nickel coatings produced using various double zincating durations (a) 60/10, (b) 60/20, (c) 60/30, (d) 60/40 and (e) 60/50 seconds. The results show a clear increasing trend in the COF values with an increase of scratch distance. Scratch distance from 0 to 10 mm was equivalent to 10 to 100 N of progressive applied load during the test. A sample which was produced from the quickest second zincating process showed the quickest sudden changes in the COF values. This is most probably due to the insufficient time for zinc deposition, thus produced a non-uniform distribution zinc particles on the substrate. As the duration of the second zincating process increased from 10 to 20, 30, 40 and 50 seconds, no significant difference was observed in the trend of COF curves. Overall, the sudden simultaneous changes in both COF curve and AE signal were due to the cohesive cracks which occurred on the coatings. This was verified by the optical microscopy examination on the scratch tracks (Figure 4-47).

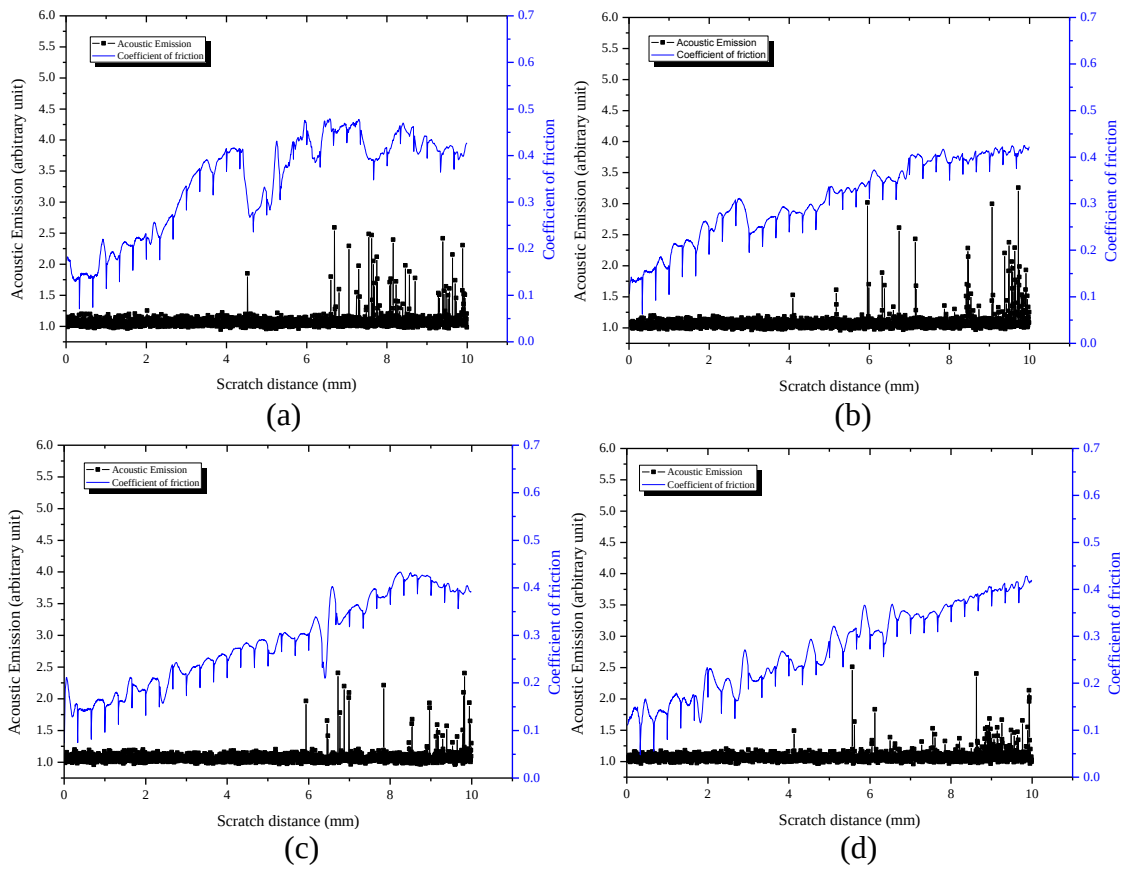

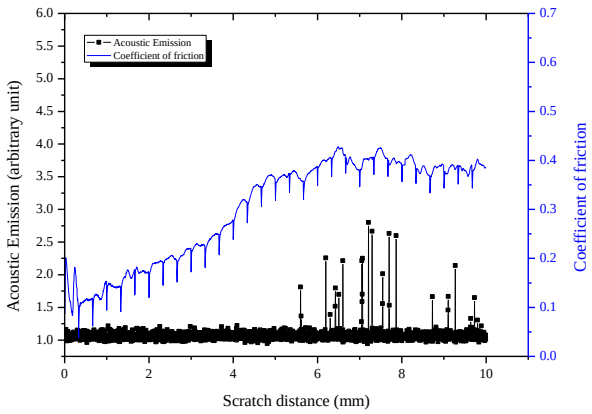

(e)

Figure 4-44 Coefficient of friction and acoustic emission signal intensity versus scratch distance curves of nickel coatings produced using various double zincating durations (a) 60/10, (b) 60/20, (c) 60/30, (d) 60/40 and (e) 60/50 seconds.

Figure 4-43 only shows AE signals and F_f curve as a function of scratch length for one selected sample from each of the double zincating durations. The average critical loads of L_{C1} and L_{C2} values with standard error calculated from two readings are shown in Figure 4-45. Overall, the L_{C1} and L_{C2} values of the nickel coatings produced at various double zincating durations do not show consistent trends. The lowest average critical loads of L_{C1} and L_{C2} values were obtained from the sample which was produced through 60/ 20 seconds of double zincating process, 45.6 N and 83 N respectively. On the other hand, the highest average critical loads of L_{C1} and L_{C2} values are from sample which was produced at 60/ 30 seconds of double zincating process, 61.3 N and 90.8 N respectively. The L_{C2} values were difficult to determine from AE signals and F_f curves as a function of scratch length; thus, a microscopy technique was used to examine the adhesive failure mode which occurred on the coatings.

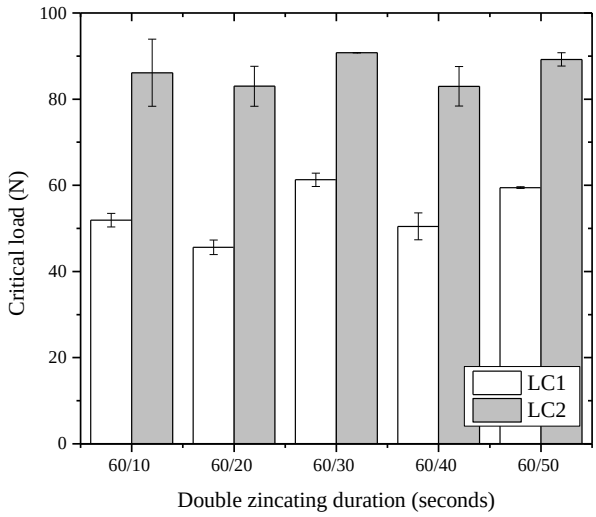

Figure 4-45 Average critical loads of nickel electrodeposited on AA7075 produced at various double zincating durations measured by scratch testing

The correlation of the number of AE events (N_{AE}) with the double zincating durations at 60/10, 60/20, 60/30, 60/40 and 60/50 seconds is shown in Figure 4-46, which was extracted from the AE signals curves as a function of the scratch distance in Figure 4-43. The average N_{AE} was calculated from eight scratches on each of the samples. As shown in Figure 4-46, no consistent trends in N_{AE} values could be determined and no significant reduction in N_{AE} occurred on increasing the zincating duration.

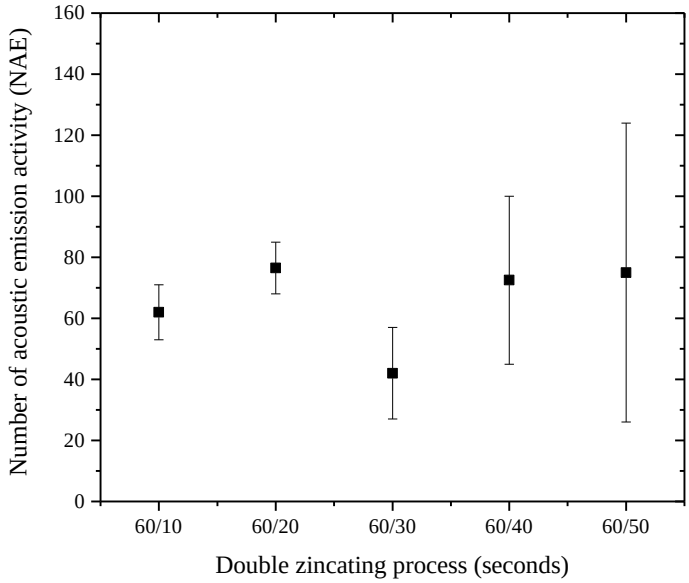

Figure 4-46 Correlation between number of acoustic emission activity (N_{AE}) and double zincating durations

Frictional force

The occurrence of the failure event developed during the scratch test can also be detected by analyzing the friction traces. Variation in F_f as a function of the scratch length for nickel coatings produced at various double zincating durations can be seen in Figure 4-43. On all samples, the F_f curves were quite straight at the beginning of the test, due to the lower loads applied in the test. As the applied load increased during the test, a sudden transition on the curves was observed. The dramatic transitions on the curves represent the critical loads at which the coating failure occurs. From Figure 4-43, we can see that sample produced from the shortest duration of double zincating process (60/10 seconds) shows significant differences to the F_f curves compared to other durations.

Microscopy observation

OM and SEM were used to examine the scratch track, and to confirm or determine the actual location of the critical loads which were initially analyzed using the AE signal intensities and F_f curves. In Figure 4-47 and Figure 4-48, the progression of the scratch is depicted from left to right. The OM images of the scratch tracks of samples produced at various double zincating durations, as shown in Figure 4-47, indicate that all samples have a series of ductile tensile cracking at the middle of the track. This failure mode is a type of through-thickness cracking, under the classification of cohesive failure.

In Figure 4-47, the first cracks on the tracks which occurred during the scratch test are labelled as L_{C1}. On all samples, further increasing the applied load during the scratch test resulted in more cracks. Under the optical microscopy observation, the raised portion of the delaminated coating towards the end of the scratch track appeared as a black region, while the scratch track and the coating surfaces are in a bright region. This is due to the various focus points at different position observed on the delaminated coating during the microscopy observation. The pile-up of the coating on these samples at the end of the scratch track is evidence that adhesive failure (L_{C2}) has occurred. The L_{C2} values were determined by drawing two straight lines on the scratch track. One line was drawn on the edge of the sample starting from the beginning of the sample, while the other line was drawn on the edge of the delamination region starting from the beginning of the black region. The intercept of these two lines is considered as a L_{C2} value. L_{C2} is considered as a starting point of the delamination which can be observed as a black region on the scratch track.

SEM images of the scratches on samples produced at 60/10 and 60/50 seconds of double zincating process are shown in Figure 4-48(a) and (b), respectively. In these figures, the failure can be seen clearly. In comparison, more cracks were observed on the scratch track of nickel coating produced at 60/10 seconds of double zincating process than the 60/50 seconds.

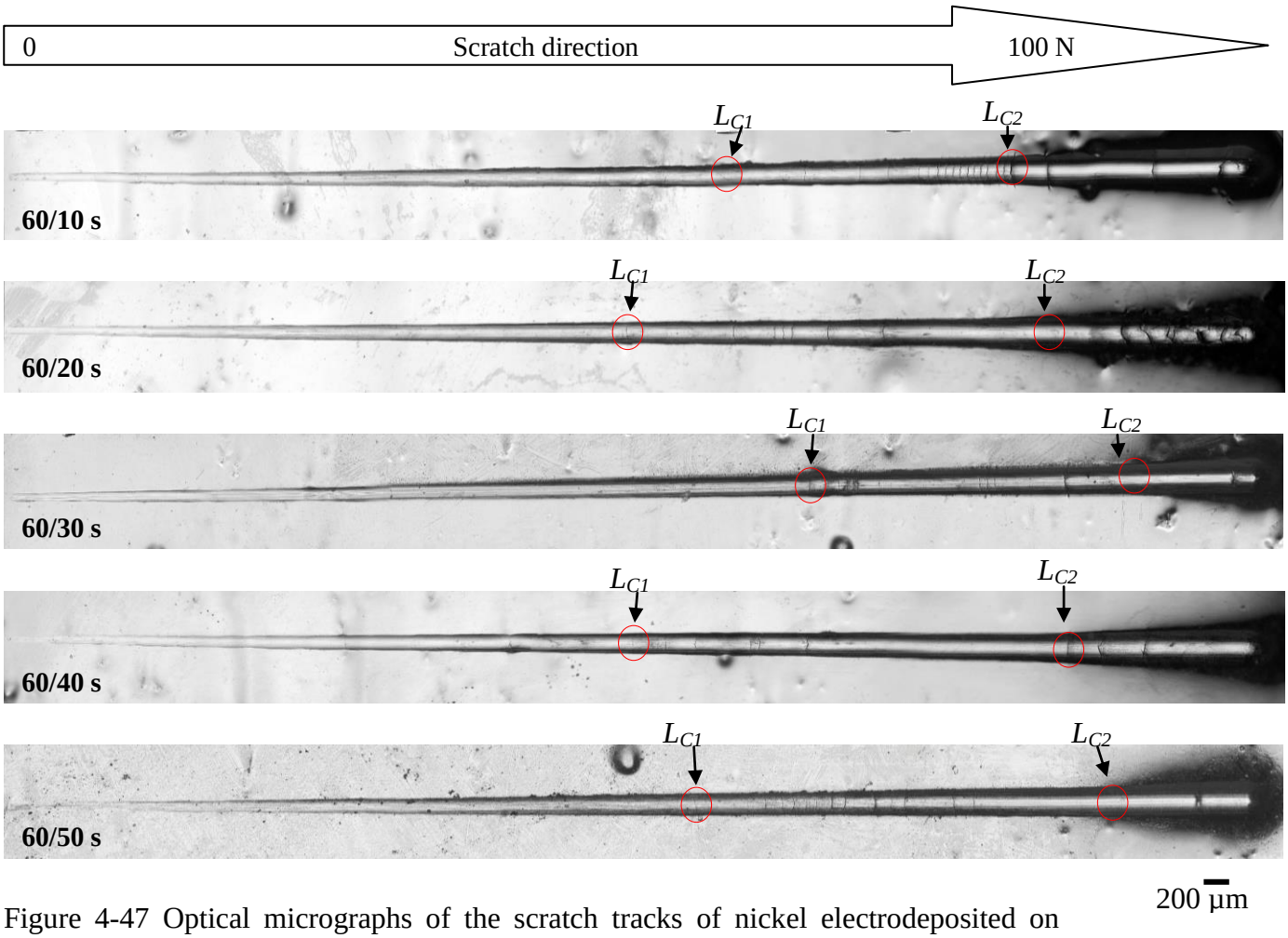

Figure 4-47 Optical micrographs of the scratch tracks of nickel electrodeposited on AA7075 produced at various double zincating durations

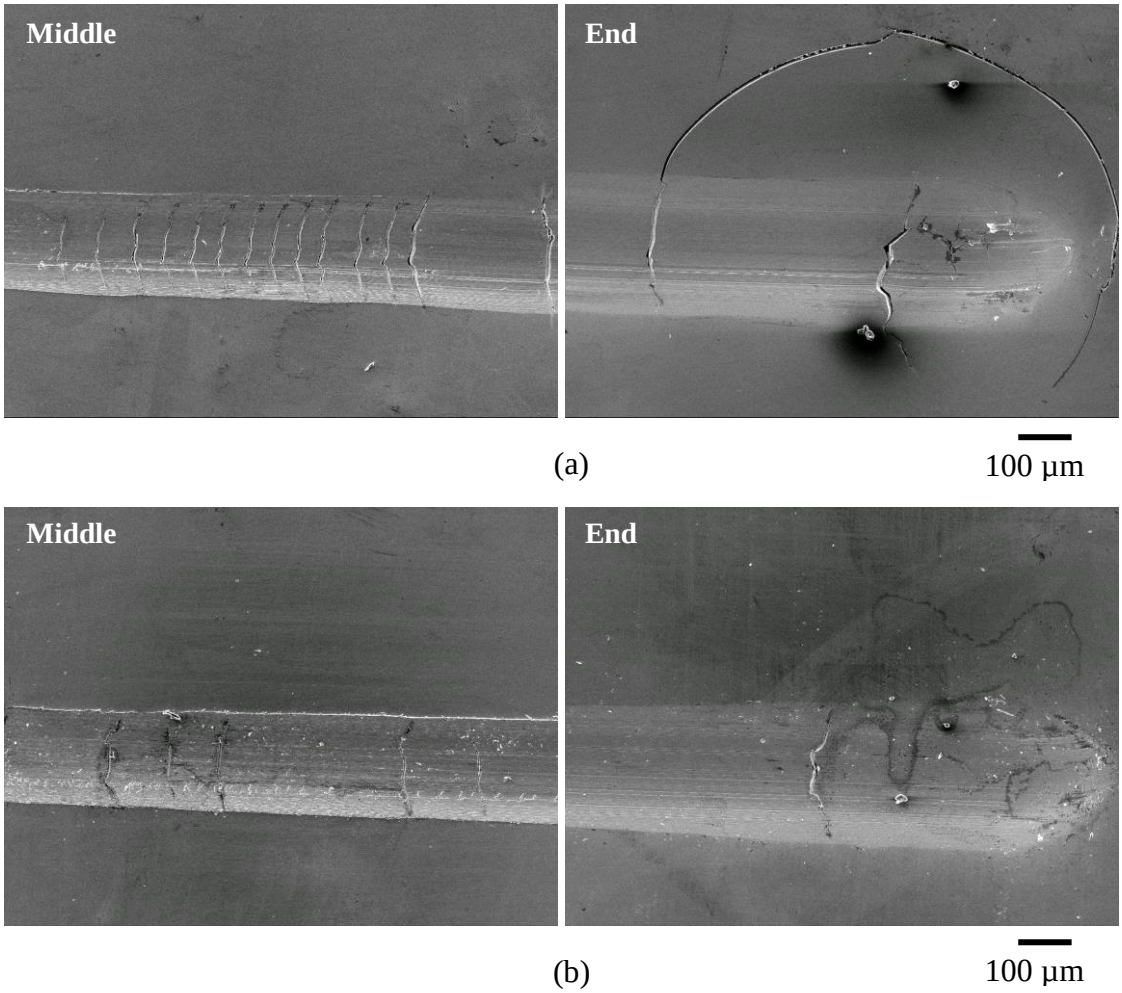

Figure 4-48 SEM images showing the middle and end of the scratch tracks of nickel electrodeposited on AA7075 produced at 60/10 and 60/50 seconds of double zincating durations.

4.6.3 Effect of Conventional and Modified Single Zincating Process at various Durations with Copper Activation on the Adhesion of the Nickel Coatings Electrodeposited on AA7075 Substrate

Acoustic emission

Figure 4-49 shows the AE signals and F_f curves as a function of scratch length for the nickel coatings produced from conventional single zincating process at 1 minute and modified single zincating process at various durations, such as 5, 10, 15, and 20 minutes with copper activation. This figure provides the first critical load (L_{C1}) and second critical load (L_{C2}), also known as cohesive and adhesive failure, respectively. As shown in the figure, coatings produced from the conventional single zincating process at 1 minute and modified single zincating at 5 and 10 minutes resulted in the low L_{C1} values. There was no significant difference in L_{C1} values among these samples. The first highest AE signal among these samples was detected at approximately at 5 mm of scratch length, which is equivalent to 57 N of applied load, from the conventional single zincated sample. As the single zincating duration increased from 10 to 15 minutes, a rise in the L_{C1} value was observed from 57 to 81 N. However, a further increase in the modified single zincating duration up to 20 minutes reduced the L_{C1} value to 66 N, which is 6 mm of scratch length. It is apparent from Figure 4-49(a) that adhesive failure (L_{C2}) occurred on the sample which was produced through the shortest duration of conventional single zincating process. This corresponds to the high scattering of AE signals with high intensity peaks, which was observed towards the end of the scratch track.

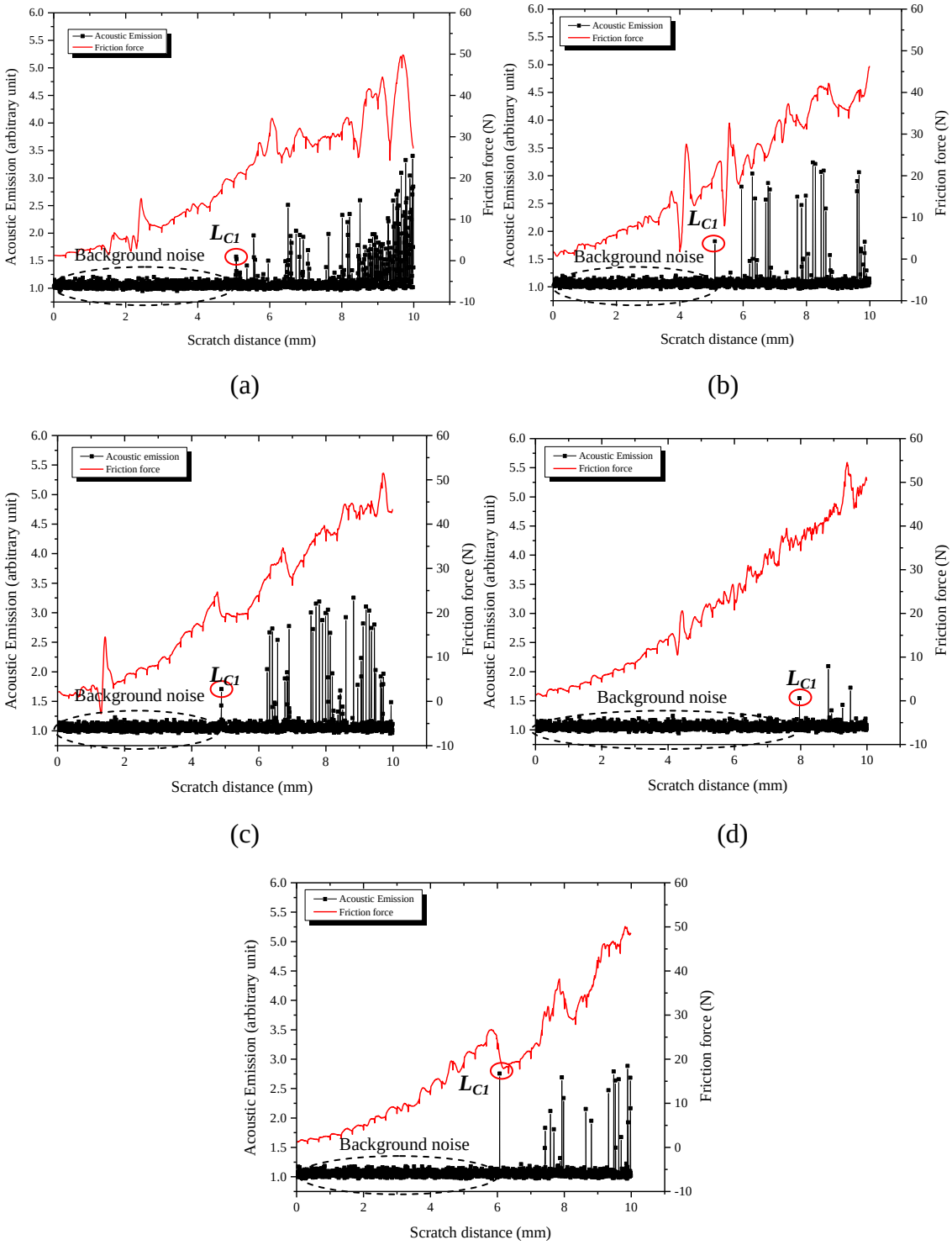

Figure 4-49 Variation of the frictional force and acoustic emission signal intensity curves as a function of the scratch distance for nickel coatings produced at (a) conventional single zincating process at 1 minute and modified single zincating process at various durations, such as (b) 5, (c) 10, (d) 15 and (e) 20 minutes with copper activation

Coefficient of Friction

In Figure 4-50, there is a clear increasing trend of the COF with an increasing scratch distance. The scratch distance which was from 0 to 10 mm was equivalent to 10 to 100 N of progressive normal load applied during the test. Overall, the sudden simultaneous changes in both COF curve and AE signal were related to the failures which occurred in the nickel coating, such as cohesive and adhesive failure. These findings were verified by the optical microscopy examination on the scratch tracks (Figure 4-54). By comparing Figure 4-50 with Figure 4-54, we can see that the periodic jumps in the COF curve corresponded to the rapid interaction of the diamond indenter with the non- uniform surface of the coatings. Figure 4-50 also shows sudden jumps in the COF values. On samples which were single zincated at 1, 5, 10 and 15 minutes, the jumps in the COF values appeared alone without AE signal. These sudden jumps were caused by the interaction of the diamond indenter with the surface voids, as shown by Figure 4-54 (a) - (d) and Figure 4-50 (a) - (d) respectively.

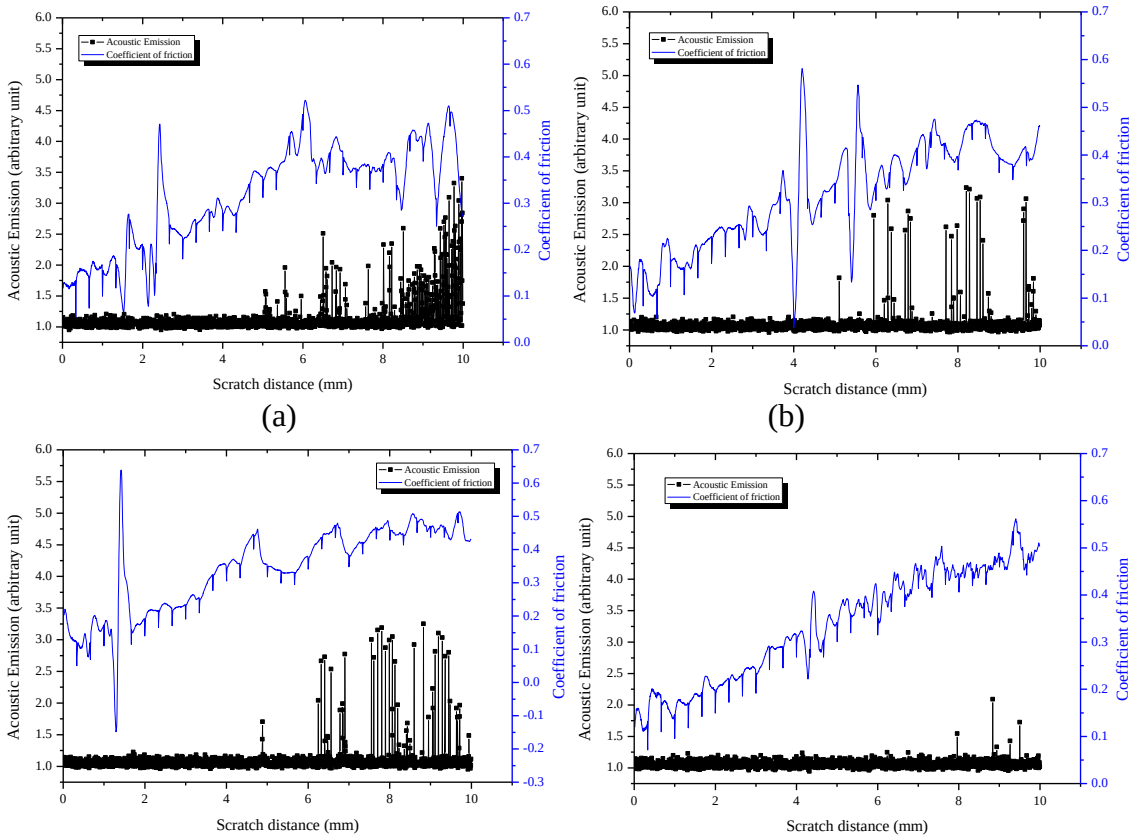

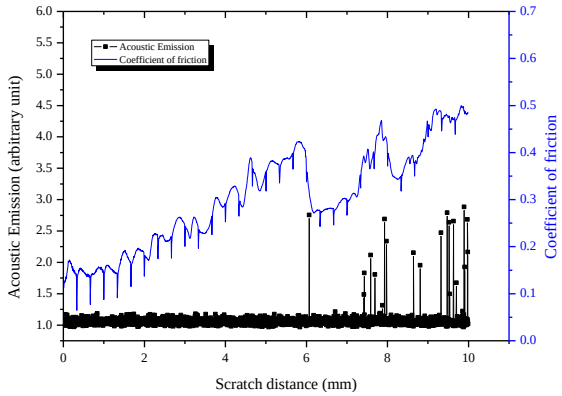

(e)

Figure 4-50 Variation of the coefficient of friction and acoustic emission signal intensity curves as a function of the scratch distance for nickel coatings produced at (a) conventional single zincating process at 1 minute and modified single zincating process at various durations, such as (b) 5, (c) 10, (d) 15 and (e) 20 minutes with copper activation

However, Figure 4-49 compares only the AE intensity signal and F_f curves as a function of scratch length for one selected sample from each of the modified zincating duration. In order to obtain a critical load (L_C) to represent the whole coating, a repeated measurement was taken eight times from the same sample.

Figure 4-51 shows the average critical loads of L_{C1} and L_{C2} values with standard error obtained from the scratch test on samples produced from the conventional and modified single zincating process at various durations with copper activation. This figure presents the influence of the single zincating process at various durations on the critical loads (L_C) of the coating under a progressive load. Overall, the durations did not have any significant influence to the L_{C1} values. The result, as shown in Figure 4-51, indicates that sample produced from the conventional single zincating process showed the lowest L_{C1} value (52.5 N). By increasing the duration to 5 minutes, the L_{C1} improved to 59 N. There was no significant difference in the L_{C1} values between the samples as the duration was increased up to 10 minutes. However, at 15 minutes, the L_{C1} of the coating rose up to the 69 N, which shows the highest L_{C1} value compared to the others. Then, a further increase in the duration to 20 minutes decreased the L_{C1} value to 60 N. Among all, only sample which was produced from the shortest zincating duration (conventional zincating process) exhibited an adhesive failure (L_{C2}) value, which was at 90 N.

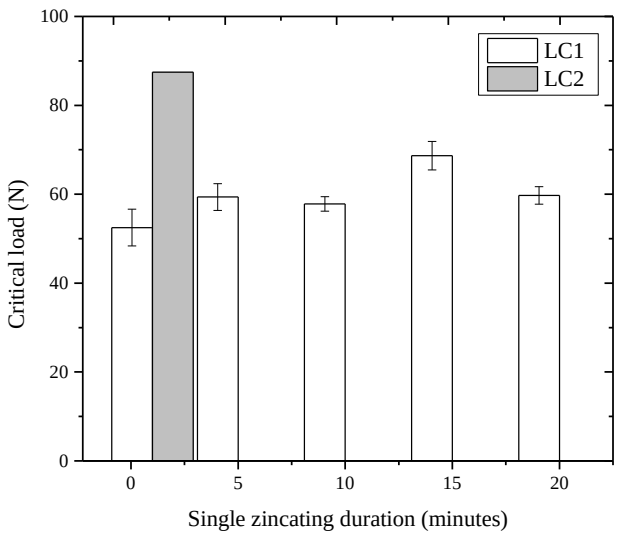

Figure 4-51 Average critical loads of nickel electrodeposited on AA7075 substrate produced from conventional and modified single zincating process at various durations with copper activation.

The correlation between the number of AE events (N_{AE}) with the zincating durations at 1 minute for the conventional single zincating process and at 5, 10, 15 and 20 minutes for modified single zincating process with copper activation is shown in Figure 4-52, which was extracted from the AE signal curves as a function of the scratch distance in Figure 4-49. Average N_{AE} was calculated from eight scratches done on each of the sample. Nickel coating produced from the conventional single duration shows the highest N_{AE} value compared to other samples. In this figure, the most striking result to emerge from the data is the significant reduction in the N_{AE} values cause by modifying the single zincating duration to 5, 10, 15 and 20 minutes. The N_{AE} value was reduced from approximately 138 to 30, with increasing in the zincating duration from 1 to 5 minutes. However, an increase in the single zincating duration to 20 minutes shows no significant differences in the N_{AE} values.

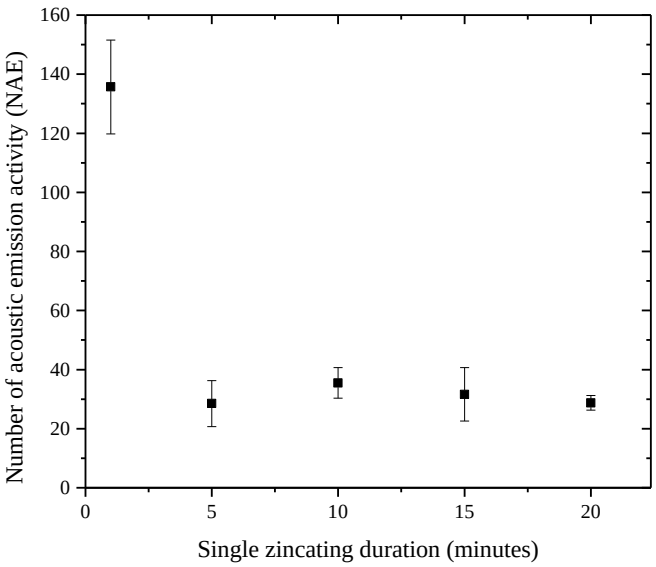

Figure 4-52 Correlation between number of acoustic emission activity (N_{AE}) and conventional and modified single zincating process at various durations with copper activation

Frictional force

Friction traces developed during the scratch test also were used to detect the failure modes occurred on the coatings. Figure 4-49 also shows variation in F_f as a function of the scratch length for samples produced from conventional and modified single zincating process with copper activation. For all samples, variation in the *Ff* curve towards the end of the scratch length is simultaneous with AE signal intensities. Figure 4-49(a- c) shows the transition in the F_f was not simultaneous with AE signal intensities at the beginning of the scratch test. As shown by the microscopy images of these samples in Figure 4-54(a- c), the interruption in the F_f curves at the beginning of the test was due to the drawing of the diamond stylus on the voids or near the voids' location. These voids are a coating defect which occurred during the electrodeposition of nickel coating on the AA7075 substrate. However, samples which were single zincated for 15 and 20 minutes showed straight curves at the beginning of the test, which is equivalent to lower loads applied in this study compared to higher loads.

Microscopic observation

SEM image of one of the voids on the coating surface produced from conventional single zincating process is shown in Figure 4-53. An EDX analysis on the void surface shows no evidence of AA7075 substrate. Thus, proves that the void was only formed on the coating surface, but not through the coating thickness. Furthermore, comparing the AE signal and F_f curves as a function of the scratch length with the OM images of the sample which was produced from conventional single zincating process with copper activation (Figure 4-49(a) and Figure 4-54(a), respectively) shows that the scratch test with a low load drawn on the voids or near the voids did not initiate any crack formation, as it could not be detected by the AE signal. However, drawing the diamond stylus on the voids or near the voids under a high progressive load initiated crack formation.

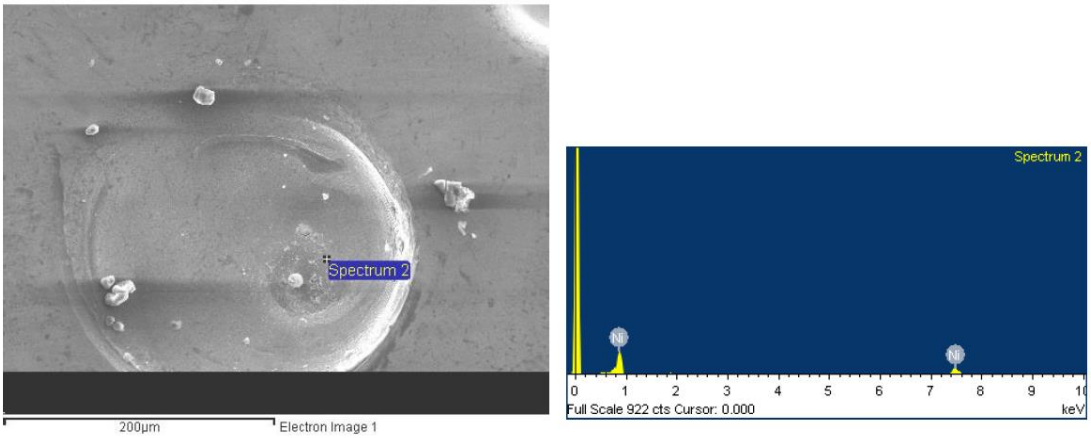

Figure 4-53 EDX analysis on a void which is formed from electrodeposition process.

From the OM images of scratch track on samples which were produced at conventional and modified single zincating process with copper activation, it is apparent that all samples show a series of ductile tensile cracking at the middle of the track (Figure 4-54). These cracks are a type of the through-thickness cracking under the classification of cohesive failure mode. On all samples, the first crack which occurred on the scratch track is labelled L_{C1}.

It can be seen from the figure that as the progressive applied loads increased during the test, more cracks were generated by the diamond stylus. The most striking result to emerge from the figure is that only sample which was produced from the conventional single zincating process show the adhesive failure. The coating was ruptured by wedge spallation at the end of the scratch track and is labelled as L_{C2} (Figure 4-54(a)).This indicates that the coating was weakly adhered to the substrate. On the other hand, samples which were produced from 5, 10, 15 and 20 minutes of modified single zincating process only exhibited cohesive failure as the progressive applied load increased, with no adhesive failure observed along the track (Figure 4-54(b-e)). This means the coatings were well adhered to the substrate.

In addition, the samples were also examined using the SEM technique to obtain a clear image of the failure (Figure 4-55). Coating rupture was observed on the sample which was produced from conventional single zincating process, while a sample which was produced at 20 minutes only exhibited a cohesive failure mode. Furthermore, a further increase in the progressive applied load resulted in an increase in the number of cracks.

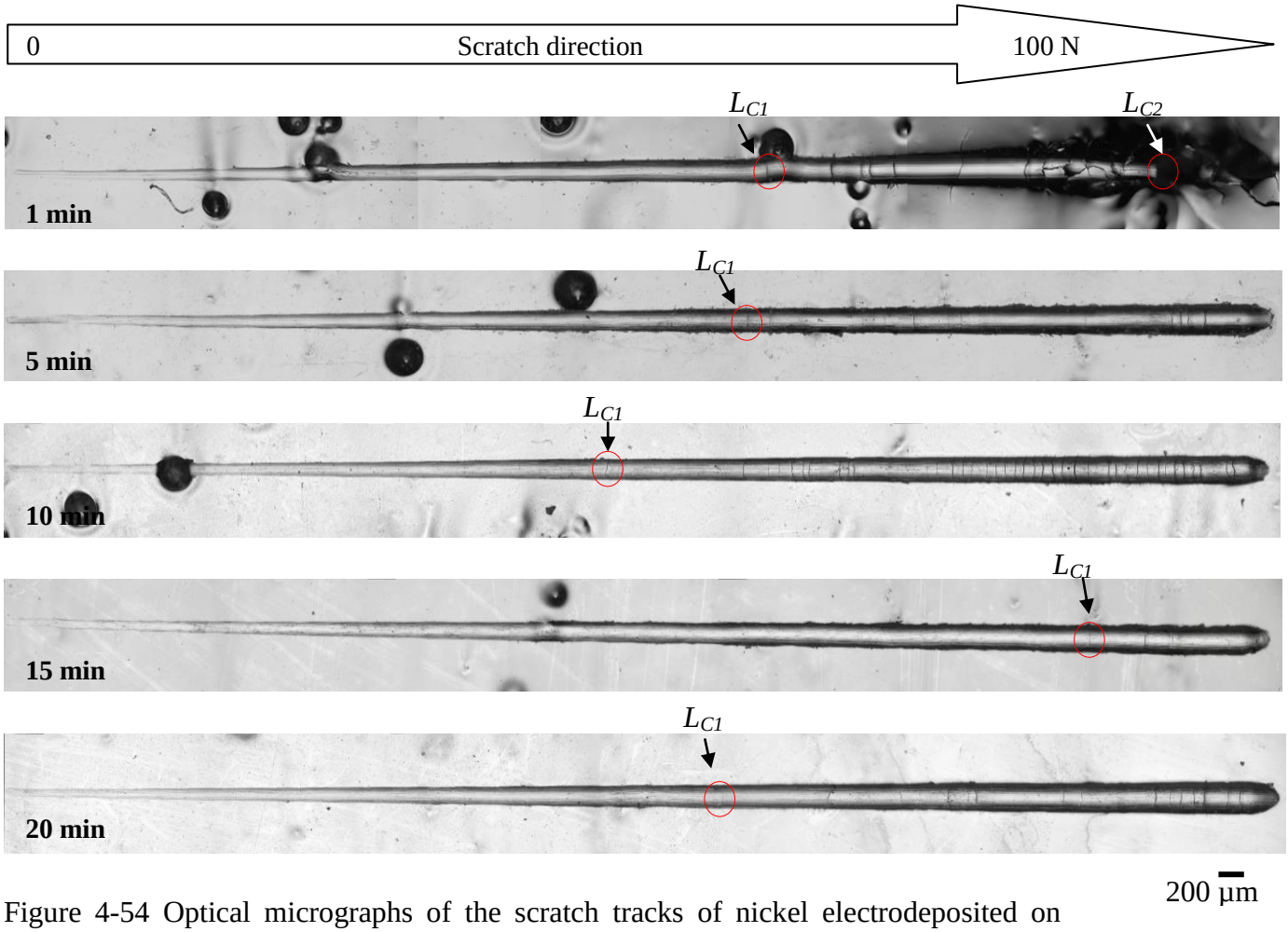

Figure 4-54 Optical micrographs of the scratch tracks of nickel electrodeposited on AA7075 produced at conventional single zincating process for 1 minute and various modified single zincating durations for 5, 10, 15 and 20 minutes with copper activation

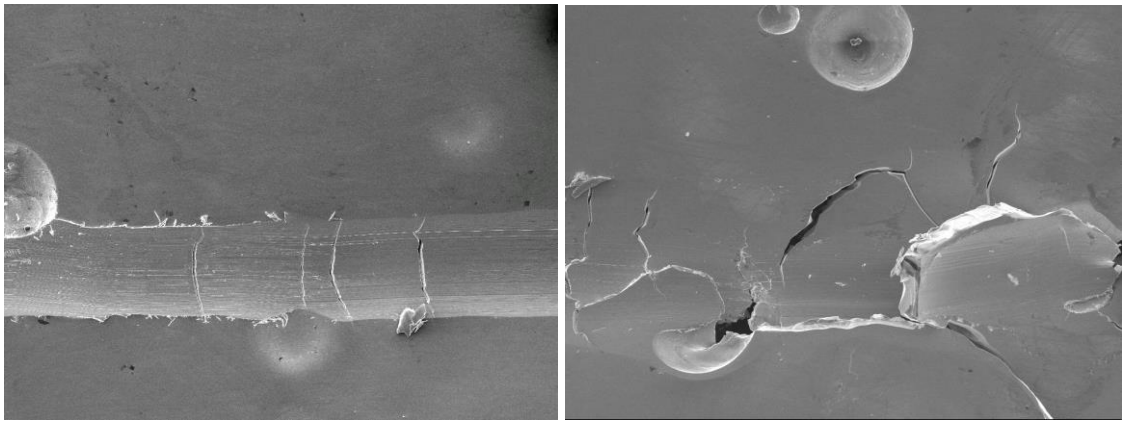

(a) 100 µm

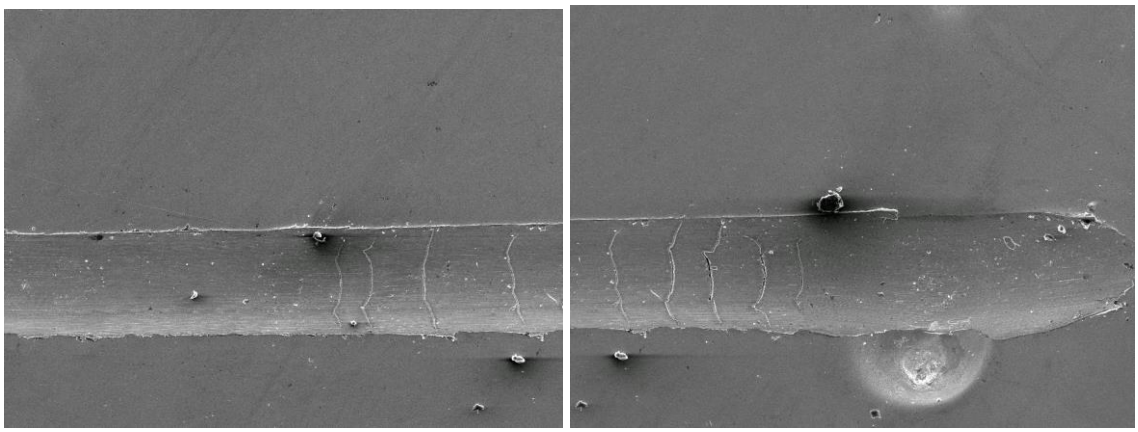

(b) 100 µm

Figure 4-55 SEM images showing the middle and end of the scratch tracks of nickel electrodeposited on AA7075 produced at (a) conventional single zincating for 1 minute and (b) modified single zincating process for 20 minutes, with copper activation

4.7 Electrochemical Corrosion Behaviour of Nickel Coatings on AA7075 Substrate Produced from Multiple Zincating Processes

4.7.1 Introduction

Potentiodynamic polarization measurements were applied in this study in order to investigate the corrosion behaviour of the nickel coatings produced using multiple zincating processes. The thickness of the nickel deposits was around 60 µm. Corrosion characteristics of the nickel coating, such as corrosion potential (E_{corr}) and corrosion current density (I_{corr}), were extracted from the electrochemistry results obtained from this study.

4.7.2 Electrochemical Corrosion Behaviour of Nickel Coatings on AA7075 Substrate Produced from Conventional and Modified Single Zincating Process at Various Durations

Figure 4-56 shows the electrochemical results of corrosion tests on nickel coatings produced from conventional single zincating process at 1 minute and modified single zincating at 10 and 20 minutes, in comparison to the as-received AA7075 substrate. The experiments were in a non-deaerated 3.5 wt. % sodium chloride (NaCl) solution. The results of the potentiodynamic corrosion tests are summarized in Table 4-3. Overall, it is clear that the corrosion potential of nickel coatings electrodeposited on AA7075 is more noble than the as-received AA7075. The corrosion current density of the nickel coatings was considerably lower than that of the as-received AA7075, except for the nickel coating produced from the conventional single zincating process at 1 minutes. The corrosion potentials shifted to the noble direction as the zincating duration increased from 1 to 10 and 20 minutes. It is apparent from the table that the corrosion resistance of the as-received AA7075 substrate was remarkably improved after electrodeposited with nickel coating through a longer zincating duration. This can be seen from the increasing corrosion potential and decreasing corrosion current density.

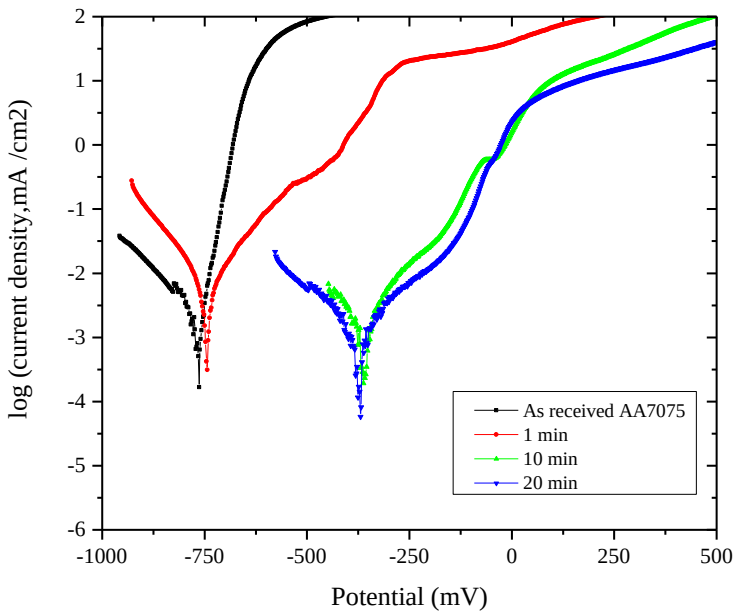

Figure 4-56 Tafel polarization curves of the as received AA7075 substrate and electrodeposited nickel coatings on AA7075 substrate produced at conventional and modified single zincating process at various durations.

Table 4-3 Tafel polarization parameters for the electrodeposited nickel on AA7075 substrate produced at conventional and modified single zincating process at various durations

Zincating duration (minutes)	Corrosion potential, E_{corr} *vs.* SCE/mV	Corrosion current density, I_{corr}/ µA cm^{-2}
As- received AA7075	-768	0.518
1	-736	0.843
10	-352	0.318
20	-384	0.195

4.7.3 Electrochemical Corrosion Behaviour of Nickel Coatings on AA7075 Substrate Produced from Double Zincating Process at Various Durations

The polarization curves of the nickel coatings produced at various double zincating durations are shown in Figure 4-57. The corrosion potential observed in Figure 4-57 and the corrosion current density calculated by the Tafel extrapolation method are summarised in Table 4-4. It was observed that the corrosion potential vs. SCE is positively increased by nickel coatings, in comparison to as-received AA7075 substrate. The nickel coating which was produced at 60/10 seconds of double zincating

process shows the lowest corrosion potential, compared to samples produced at 60/20 and 60/40 seconds. There is no significant difference in the corrosion potential for nickel coatings which were produced at 60/20 and 60/40 seconds. The corrosion current density of the nickel coatings was lower than that of the as- received AA7075 substrate, except for the nickel coating produced at 60/10 seconds of double zincating process. As the double zincating duration increased from 60/10 seconds to 60/40 seconds, the corrosion current density also decreased from 3.228 µA cm^{-2} to 0.120 µA cm^{-2}. It is apparent from this table that the double zincating process at a longer duration can markedly improve the corrosion resistance of the nickel coating in the 3.5 wt. % NaCl solution by increasing corrosion potential and decreasing corrosion current density.

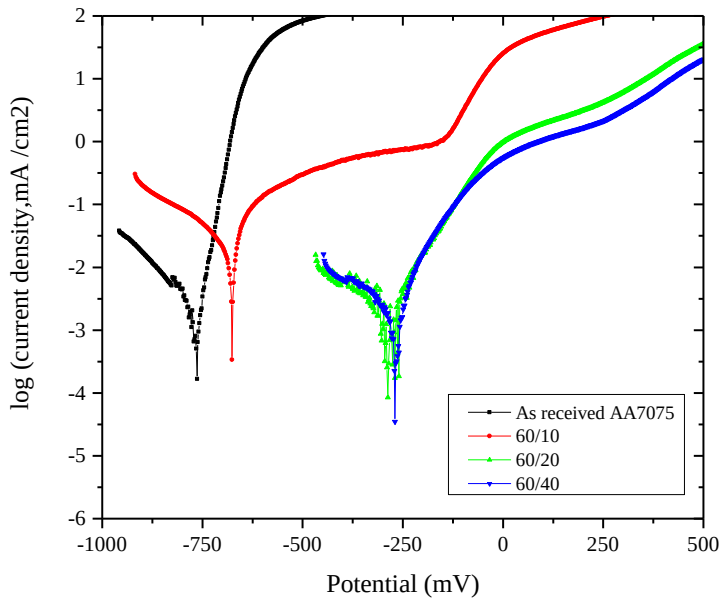

Figure 4-57 Tafel polarization curves of as- received AA7075 substrate and electrodeposited nickel coatings on AA7075 substrate produced at various double zincating durations.

Table 4-4 Tafel polarization parameters for the electrodeposited nickel coatings on AA7075 substrate produced at various double zincating durations.

Zincating duration (seconds)	Corrosion potential, E_{corr} *vs.* SCE/mV	Corrosion current density, I_{corr}/ µA cm^{-2}
As- received AA7075	-768	0.518
60/10	-672	3.228
60/20	-272	0.458
60/40	-272	0.120

4.7.4 Corrosion Behaviour of Nickel Coatings on AA7075 Substrate Produced from Conventional and Modified Single Zincating Process at Various Durations with Copper Activation

Figure 4-58 shows the electrochemical results obtained from polarization studies of nickel coatings produced using conventional and modified single zincating processes at various durations with copper activation. Table 4-5 summarizes the electrochemical corrosion parameters derived from the polarization curves. Overall, the corrosion resistance of as-received AA7075 substrate has been improved by the nickel electrodeposition process, with increases in the corrosion potential and decreases in the corrosion current density. Notably, for the nickel coated samples, samples produced from the conventional single zincating process at 1 minute showed lower corrosion potential and higher corrosion current density than the sample produced with the 10 minutes zincating process. Further increasing the zincating duration up to 20 minutes showed a further increase in corrosion potential, but no significant change in the corrosion current density. The most striking result to emerge from this result is that the nickel coating produced at a longer zincating duration can protect the as-received AA7075 substrate from attack by the chloride ions.

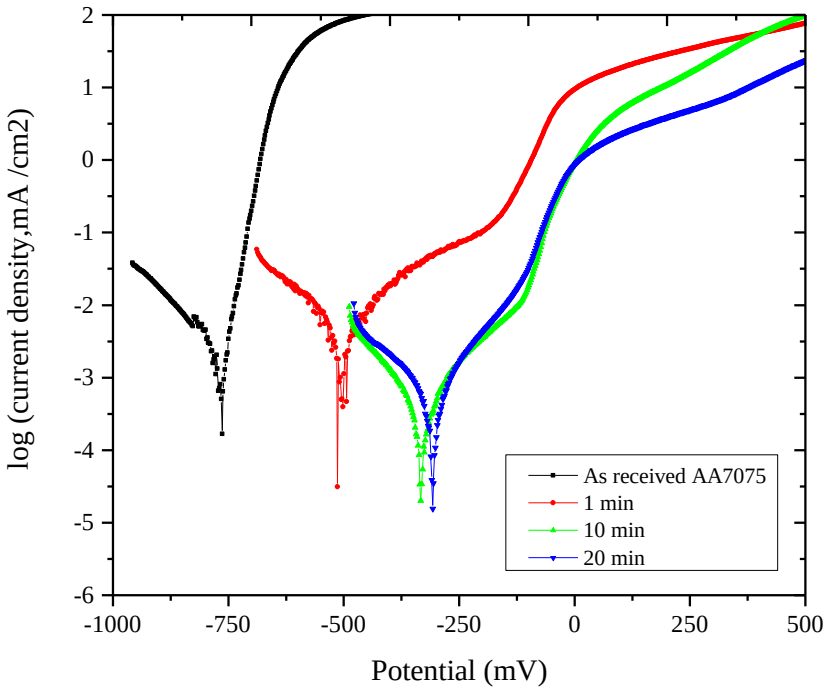

Figure 4-58 Tafel polarization curves of the as- received AA7075 substrate and electrodeposited nickel coatings on AA7075 substrate produced at conventional and various modified single zincating durations with copper activation process.

Table 4-5 Tafel polarization parameters for the electrodeposited nickel coatings on AA7075 substrate produced at conventional and various modified single zincating durations with copper activation.

Zincating duration (min)	Corrosion potential, E_{corr} *vs.* SCE/mV	Corrosion current density, I_{corr}/ µA cm^{-2}
As- received AA7075	-768	0.518
1	-512	0.661
10	-336	0.073
20	-304	0.094

5 DISCUSSIONS

5.1 Introduction

This chapter discusses the experimental results presented in Chapter 4. These results were obtained from various surface pre-treatment procedures on aluminium alloy 7075 (AA7075) substrate and mechanical testing of the nickel coating electrodeposited with various surface pre-treatment procedures prior to electrodeposition process. Discussion begins with the selection of the optimum immersion duration for the zincating process from the electrochemistry measurement, characterization of the samples prepared through a multiple zincating process at various durations using SEM, EDX and AFM, evaluation on the adhesion of the coating to the substrate and the corrosion resistance of the coating.

5.2 Electrochemical Behaviour of AA7075 Substrate during Various Surface Pre- treatment Processes

A considerable number of studies on zincating process parameters, such as type of solution, temperature, duration, agitation and so on, have been published. However, all the studies reviewed so far are lack information on electrochemical behaviour of the aluminium alloys substrate during the zincating process. Furthermore, most of the literature shows a lack of information on how the zincating immersion duration was chosen. Information from the electrochemical measurement during the zincating process, such as changes in the open circuit potential, E_{OC} of the substrate with time would help in determining the suitable and effective immersion duration for the zincating process.

In the previous chapter, the behaviour of the AA7075 substrate during the multiple zincating processes was investigated by measuring the variation of open circuit potential, E_{OC}, with immersion time. It was shown that the optimum duration for the single and double zincating processes could be determined from this experiment.

In this study, based on electrochemistry measurement (Figure 4-3), the optimum immersion duration of AA7075 substrate for the single zincating process was chosen at the beginning of the steady state potential, which was at 1200 seconds. At the same time, several durations before the steady state potential, such as 60, 300, 600 and 900 seconds were also studied, in order to observe the growth of the zinc particle on the substrate and their effect to the properties of nickel coating.

On the other hand, the duration for the first zincating process in the double zincating was also determined from this experiment. The literature revealed that most studies conducted the first zincating process at the range of 10 to 60 seconds. Therefore, in the present research, several durations, such as 10, 20, 30, 40, 50 and 60 seconds were studied in order to find the optimum duration for the first zincating process. Initially, the samples were immersed in the first zincating bath for 10 to 60 seconds before being tested using the electrochemistry measurement to study the influence of these selected first zincating durations to the second zincating process.

In this study, the specimen produced at the longest first zincating duration which shows more noble E_{OC} values during second and third stage of zincating process than other specimens was chosen as a best specimen (Figure 4.4). This more noble E_{OC} values during the second stage of zincating process indicates that the zinc deposition occurred rapidly on the surface with uniform and higher coverage of zinc particles, which was formed during the first zincating process at the longest duration (60 seconds). This result is in agreement with Hutt et al. [41], who found that the first zincating process for 60 seconds produced a more uniform zinc layer compared to 20 seconds.

In addition, the steady potential of the specimen produced from 60 seconds is consistently more noble than specimens produced at shorter first zincating treatment. This indicates a dense coverage of the zinc layer on the specimen, compared to other

specimens which were produced using a shorter first zincating treatment. Among all samples considered here, the specimen produced using a 60 seconds first zincating process shows an E_{OC} in steady state that is closest to that of a zinc plate in zincating solution (Figure 5.1). In addition, the duration for the first zincating process was also selected based on the minimum slope value of the steady state potential during the third stage of the double zincating process. The minimum slope value indicates that the electrochemical reaction between substrate and the zincating solution is in stable condition with no fluctuation of the E_{OC} values, due to the fully coverage of the zinc particles on the surface.

Therefore in this study, the first zincating process was kept constant at 60 seconds, since it posed a more noble E_{OC} curve during the deposition and steady potential stage in the second zincating process. The durations for the second zincating process were selected at 10, 20, 30, 40 and 50 seconds, as it must be shorter than the first zincating process, so that a thin and uniform zinc immersion coating layer can be produced on the substrate, as mentioned by Mallory et al. [86].

The results of this experiment are consistent with some claims in the literature. According to Robertson et al. [50], potential measurements during the zincating process often provide information on the displacement of zinc particles from zincating solution by the corrosion of aluminium [50]. This suggestion was supported by Azumi et al. [184], who reported that the transition of potential during the double zincating process was explained by the mixed potential of aluminium dissolution (anode) and zinc deposition (cathode). Furthermore, the recorded mixed potentials clearly show that the blanketing of the aluminium surface by a film of zinc metal can be achieved at high zincate concentrations, high rotation speeds and low sodium hydroxide concentrations [50].

The electrochemical curves measured during the conventional and modified single zincating with and without copper activation and double zincating processes can be divided into three different stages. The three different stages of electrochemical curves, such as dissolution of substrate, deposition of zinc particles and steady state potential found in this study are consistent with some claims made by other researchers [49, 50, 61, 185-187]. For instance, Egoshi et al. [62] reported that a decrease in E_{OC} values of

various aluminium alloys such as, Al(Cu) and Al(Si) during the first stage of zincating process is due to the simultaneous substitution reaction of aluminium dissolution and zinc deposition. According to Robertson et al. [50], the steady state potential achieved during the third stage corresponds to the deposition of zinc metal on the substrate. It also indicates the changes in anode and cathode areas during the zincating process which results in a temporary potential shift in the less-noble direction during the first stage and followed by a steady state potential near the zinc reference electrode during the third stage indicated that the substrate surface was covered with zinc particles [61].

In this study, the steady state potential of AA7075 during the single and double zincating process was approximately – 1.596 to – 1.599 V. This result is similar to the results obtained by Murakami et al. [181], who also study the electrochemistry behaviour of AA7075 in zincating solution. To compare the steady state for single and double zincating process with the pure zinc, a pure zinc plate was immersed in the same zincating solution used in this study. As shown in , the steady state potential for the pure zinc was approximately -1.59 V, which is more noble than the steady state potential for both single and double zincating process. This shows that the AA7075 substrates were not fully covered with the zinc particles even during the third stage of deposition process. According to Huang et al. [185], the substrate can not be fully covered by zinc deposits, as anodic reaction (dissolution of aluminium) occurs during the replacement reaction. Therefore, some pits or fine holes on the zincating film were generated during the corrosion of aluminium [181].

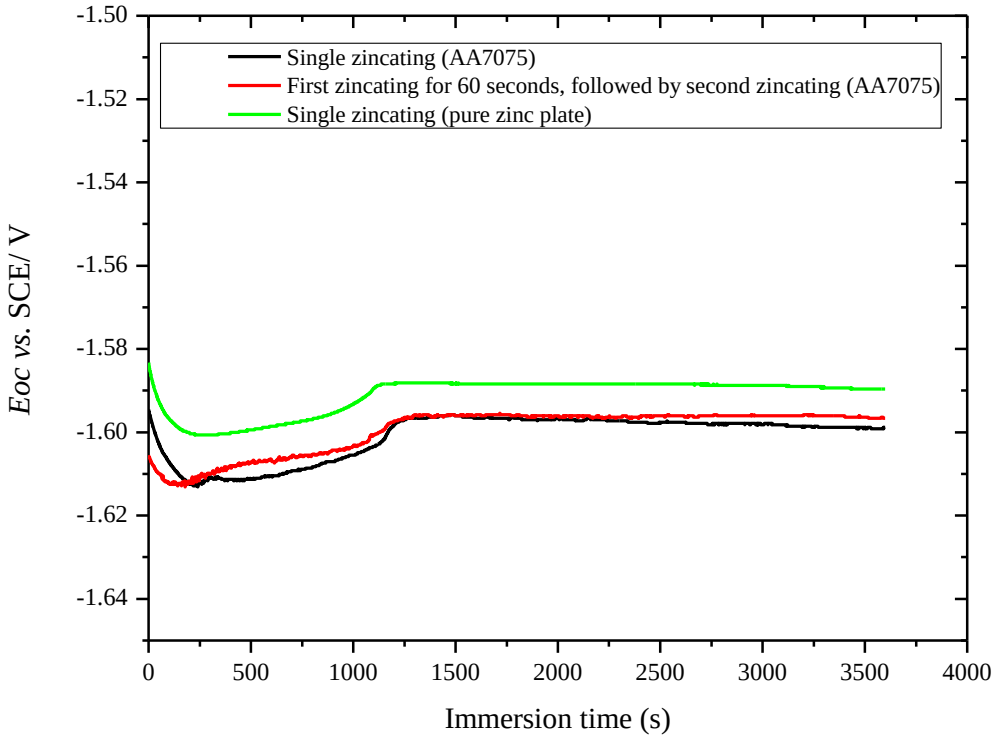

Figure 5-1 Comparison of immersion open circuit potential (E_{OC}) of AA7075 substrate during single and double zincating process with pure zinc plate during the single zincating process

Murakami et al. [186], who investigated the electrochemical behaviour of AA7075 substrate during the zincating process, reported that the E_{OC} curves for the AA7075 substrate in the zincating solution are stabilized within a few seconds of immersion for both single and double zincating processes. Lee et al. [49] reported that the optimum zincating immersion time for pure aluminium was approximately 20 seconds when the steady state potential was achieved, based on electrochemical measurement during the zincating process. Robertson et al. [50] obtained similar results, when pure aluminium was immersed in a zincating solution. However, the duration taken during the measurement of the E_{OC} value used in the literature is insufficient to determine the behaviour of the AA7075 during the zincating process. In contrast to the literature, this study indicates that the E_{OC} curves for the AA7075 substrate in the zincating solution was stabilized only after 1250 seconds of immersion. On the other

hand, a rapid reaction during the double zincating process shows that zinc deposition occurs at a high density on the surface and covers the surface almost immediately [61]. These results indicate that the substitution reaction of substrate dissolution and zinc deposition is faster on a substrate which already has zinc particles nucleated on the surface.

Beside the zincating parameters, the alloying elements in aluminium alloys also contributed to the temporary changes of E_{OC} during the zincating process. According to Murakami et al. [186], aluminium alloys which contain copper and/or zinc, such as AA2017 and AA7075 show rapid changes in E_{OC} for both single and double zincating process, whereas AA1100 and AA5052, which do not contain copper or zinc show slow changes in E_{OC} during single zincating process. This finding is in agreement with Saito et al. [187] and Egoshi et al. [63], who showed that aluminium alloys with copper as an alloying element, such as AlCu and AlSiCu, showed fast changes in E_{OC} value, indicating that copper contained in the aluminium alloy greatly increased the activity of the Al(Cu) surface for the substitution reaction during the zincating process. This is because copper is more noble than zinc and effectively mediates electron transfer from the substrate to $Zn(OH)_4^{2-}$ ions during the zincating process and accelerates the zinc deposition [63].

In addition, the effect of copper activation prior to zincating process was also investigated in this study. In this study, the duration for copper activation was chosen at 10 minutes due to the uniform surface with no cavities was observed from the SEM image of the substrate. Furthermore, the distribution of the copper seeds was also homogenous, compared to 5 and 15 minutes of copper activation. The electrochemical study shows that the copper activation process dramatically suppressed the dissolution of the AA7075 substrate in the zincating solution by rapid formation of the zincating layer. According to Azumi et al. [61], this is due to copper deposits acting as nucleation sites for zinc deposition during the zincating process. It was also found in this study that the smoothness and uniformity of the zincating layer was improved through the copper activation process. This result is consistent with the finding by Egoshi et al. [63], who studied the effect of copper activation to the zincating layer deposited on magnetron sputter-deposited Al- Si alloys films.

5.3 Surface Morphology and Elemental Composition of AA7075 Substrate after Various Surface Pre-treatment Processes

The present study was designed to investigate the effect of various zincating processes on the surface morphology and element composition of AA7075 substrate surface. Conventional single zincating was carried out at 1 minutes, while the modified single zincating process was done at various longer durations. In reviewing the literature, the conventional single zincating process was always done at only 1 minute. In this study, the single zincating process was extended to 5, 10, 15, and 20 minutes based on the electrochemistry measurement of AA7075 substrate in the zincating solution. In addition, on certain samples, a copper activation process was applied before the conventional and modified single zincating process, in order to overcome the dissolution of the substrate during the zincating process. The electrochemistry analysis of this process was reported in Section 4.2.4. In comparison, double zincating process was done at various durations. Overall, the results from this study show the importance of the zincating duration in controlling the morphology of the zinc layer deposited on the substrate, prior to the electrodeposition process.

The results indicate that the morphologies of the conventional and modified single zincating processes with increasing duration began with the nucleation of small spherical zinc particles, as illustrated in Figure 5-2. As duration increases, the zinc particles start to grow at preferred sites and change to a hexagonal shape. Further extending the duration showed stacking of the zinc particles on each other until the substrate surface becomes covered with the dispersed zinc particles. The findings are consistent with those of Lee et al. [44], Azumi et al. [43], Lee et al. [42] and Yang et al. [45]. According to Lee et al. [42], after spherical nucleation has occurred, the zinc particles continue to grow, forming the hexagonal shaped particles. Further deposition shows zinc deposits forming hexagonal platelets in a basal texture, which subsequently grow and start to stack a basal texture of the hexagonal platelets. After a longer duration, assimilation of the separate stacked hexagonal groups occurs and covers the substrate with a dispersed zinc hexagonal particles.

The size of the zinc particles from both single and double zincating process increased with the zincating duration. This finding is similar to Lin et al. [40], who

found that the zinc nuclei formation at the beginning of the reaction produces large size nodules after extending the zincating operation. This long-time deposition caused a roughened surface appearance [40].

Comparing the morphologies of conventional and modified single zincating with the double zincating process on AA7075 substrate, it may be seen that the double zincating process produced a more uniform and smooth surface. This study shows that the size of the zinc particles from double zincating process is smaller than the single zincating process even at a longer double zincating duration, as shown in Figure 4.16, Figure 4-20 and Figure 4.24 and illustrated in Figure 5-2. According to Lin et al. [40], the zinc stripping process performed after the first zincating will refine the previously deposited zinc nodules, or preferentially dissolve zinc nuclei with sizes smaller than the critical nucleation radii. Fresh zinc nuclei which form during the next zincating process result in a high density, fine and uniform deposition.

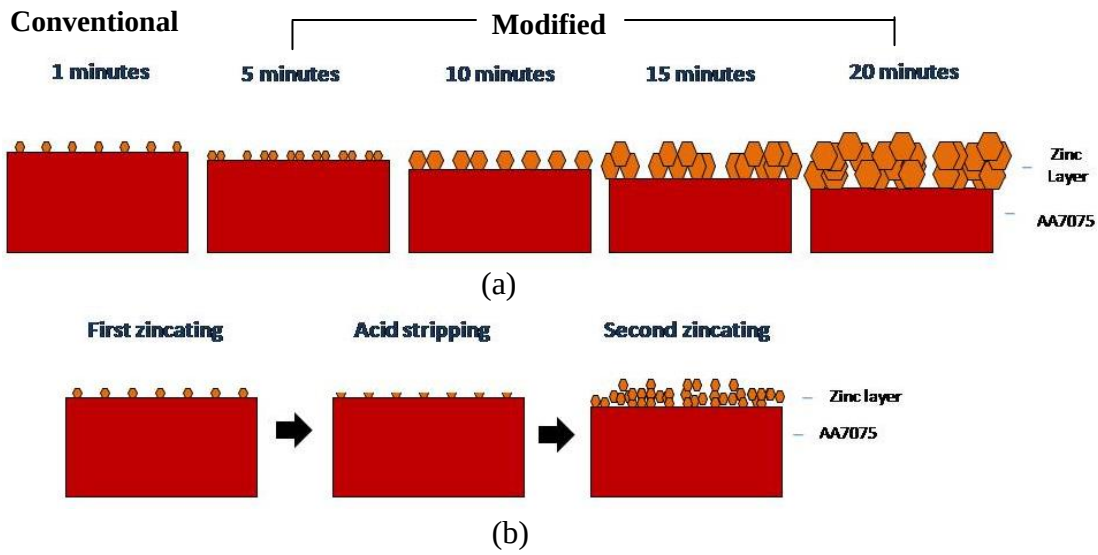

Figure 5-2 Schematic representations of the various zincating processes on AA7075. (a) conventional and modified single zincating process and (b) double zincating process.

EDX analysis on the zincated samples clearly revealed that the overall amount of zinc deposited during the double zincating process at various durations was less than the conventional and modified single zincating process. The modified single zincating

process at a longer duration (20 minutes) produced about 25 wt. % of zinc on the surface, and this value is doubled compared with the double zincating process. It may therefore be assumed that the substrate surface was fully covered by the zinc particles during the modified single zincating process. It seems possible that these results are due to longer duration of the process. However, longer immersion in the high alkaline zincating solution during single zincating will dissolve the substrate. Therefore, a longer zincating duration may be applied only to a thicker substrate, in order to prevent the dissolution of the entire substrate.

In comparison, the conventional and modified single zincating process with copper activation was shown to improve the uniformity of the zinc deposition, thus producing a compact and dense zincating layer. In addition, the copper activation reduced the size of the deposited zinc particles. The optimum duration for copper activation was chosen at 10 minutes, due to the uniform distribution of copper seeds combined with a limited agglomeration of copper seeds, as compared to the 15 minute treatment. At 5 minutes, the surface contains a lot of cavities with a lower population of copper seeds. The nucleation and growth of the zinc particles through conventional and modified single zincating with a copper activation is similar to the conventional and modified single zincating without a copper activation process. However, the zinc particles deposited on copper activated substrate are small, thus producing a smooth, compact, homogenous and dense zinc layer.

EDX analysis on the copper activated substrates at various durations shows the small increasing in the copper element, as the duration increases from 5 to 15 minutes. In order to confirm the deposition of copper particles on the substrate, the EDX analysis under the ‘point ID’ mode was done on the agglomeration of particles after the copper activation process (as shown in Figure 5-3). The figure confirms evidence of the deposition of copper particles, even though the amount of the copper particles used in this study was very low. However, this finding is contrast to Azumi et al. [61], who reported no detection of copper deposits on the copper prepared surface by EDX analysis due to the low copper concentration used in this activation process. Furthermore, copper ions were supplied under the condition of diffusion limit at a very low concentration; thus copper deposits remained very small in size and were widely

dispersed [61]. According to Tang et al. [47], although the copper deposits could not be detected by EDX analysis due to its small deposition mass, their function as an efficient catalyst for electrochemical reaction on the substrate results in a dramatic effect on surface conditioning.

This result is consistent with Azumi et al. [61] and Tang et al. [47], who suggested that a uniform and dispersed copper deposition is obtained in etching solution containing a low concentration of Cu^{2+} ions, due to substitution reaction of aluminium substrate. Thus, the copper deposits act as nucleation sites for zinc deposition in zincating process, which results in a thin, dense and fine zinc deposition layer.

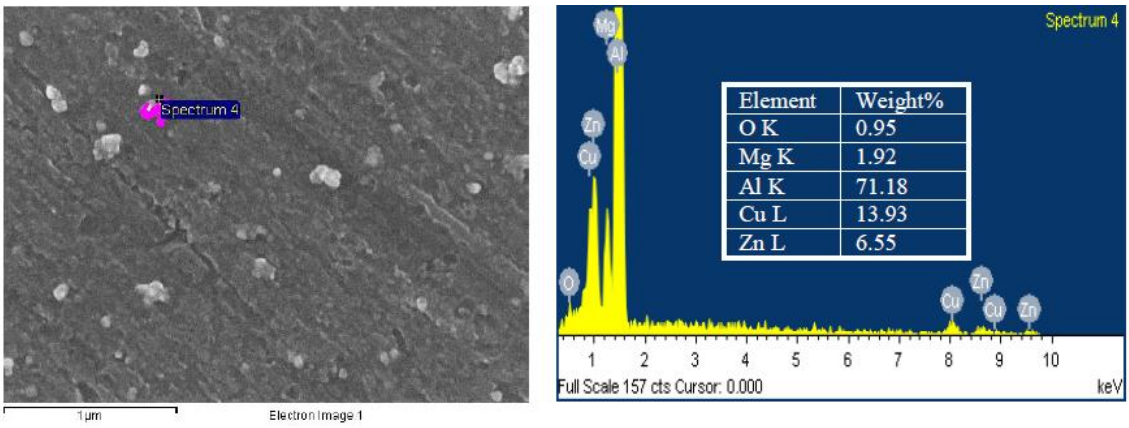

Figure 5-3 EDX analysis on copper detection of copper activated AA7075 substrates at 10 minutes

5.4 Surface Topography and Roughness of AA7075 after Various Surface Pre-treatment Processes

A part of this study was designed to investigate the effect of various zincating processes on the surface topography and surface roughness of an AA7075 substrate. During this study, conventional single zincating with and without copper activation was performed using a 1 minute zincating treatment, while modified zincating process with and without copper activation were done at various longer durations. In comparison, double zincating processes at 60/10, 60/30 and 60/50 seconds were also applied in this

study. In this study, it was found that the surface roughness of the as- received AA7075 substrate was increased after the alkaline and acid cleaning processes, due to the dissolution of the substrate in the cleaning solutions. Then, the surface roughness was steeply increased after the single zincating and the first zincating during the double zincating process. The zincating layer was then stripped away by the nitric acid during the zinc stripping process. Then, a second zincating process was applied to re-deposit zincating layer with a smooth surface roughness, due to the deposition of smaller zinc particles compared to the first zincating process.

The findings and results are consistent with some claims in the literature. According to Yang et al. [45] and Lee et al. [42], the initial surface roughness of aluminium increased a little after the alkaline cleaning due to some limited etching by the alkaline solution. Akaline and acidic solution removes the aluminium oxide and has a microetching effect to enhance the adhesion between the zinc layer and substrate [42]. The first singe zincating process results in deposition of large zinc grains, which grew to form an irregular and rough zincating layer [43, 46]. Based on Lee et al. [43], Yang et al. [46] and Arshad et al. [61], the double zincating process will smoother and reduce the surface roughness of the zincating layer.

In this study, the duration of the single zincating process with and without copper activation was extended from 1 to 20 minutes. From the results, it shows that the surface roughness of the substrate was gradually decreased with the increase of the single zincating durations. This is probably because of the sufficient duration for the zinc particles to deposit uniformly and homogenously on the substrate, thus results in complete coverage of the zinc particles on the substrate surface. However, this finding is in contrast to Arshad et al. [188] and Lin et al. [40], who found that a longer zincating duration, more than 1 minute, resulted in a thick and high density zinc layer, which caused a rough surface. In addition, Azumi et al. [44], who investigate the zinc deposition during the zincating process on a magnetron sputter- deposited aluminum film, concluded that the maximum duration for the zincating process was at 2 seconds, due to the rough surface of zincating layer.

5.5 Surface Morphology and Elemental Composition of Coating's Interface between Nickel Coatings and AA7075 Substrate through a Conventional and Modified Single Zincating Process at Various Durations

Another aim of this work was to investigate the effect of conventional and modified single zincating processes to the interface of nickel coatings electrodepositied on AA7075 substrate. The conventional single zincating process was carried out at 1 minute, while modified single zincating process was done at various longer durations. The cross-section morphology of the sample produced from the conventional single zincating process for 1 minutes (

Figure 4-36(a)) showed the non-uniform deposition of the nickel deposit on the substrate at the interface of the coating. This finding reflects the surface morphology and surface topography of the zincated sample in Figure 4-15(a) and Figure 4-30(a). The defect at the interface of this coating was contributed by the non-uniform zincating layer, which was due to the non-homogenous zinc deposition and insufficient coverage of zinc particles on the substrate. The cross-section morphology at the coating's interface indicates poor adhesion to the substrate. Improvement of the coating's interface was obtained by modifying the conventional single zincating duration to 5, 10, 15 and 20 minutes. The cross-section morphology of these samples (

Figure 4-36(b-e)) reflects to the morphology of the zincated samples shown in Figure 4-15(b-e) and Figure 4-30(b-e). The uniform deposition of the nickel coating observed on these samples indicates good adhesion to the substrate. This is due to the homogeneous distribution and good coverage of the zinc particles on the substrate during the zincating process.

It is encouraging to compare this figure with that found by Hino et al. [3], who found that zinc deposition during the zincating process at 30 seconds occurred at different sites between the anodic dissolution and the deposit by reduction. The deposition of the zinc particles on the substrate is based on the non-uniform oxide film that existed on the substrate.

In all samples, the results of EDX line analysis show no evidence of increased zinc content at the coating's interface, which is expected to occur with increasing in the zincating duration. Even though zinc was detected during the analysis, it was

contributed by the substrate itself, which contains about 5.2 wt. % of zinc. This finding suggests that the zinc layer was dissolved into the nickel plating solution during the electrodeposition process. However, the findings of the current study are in contrast to that of Tang et al. [47], who found evidence of the zincating layer at the interface of the coating to the substrate through EDX analysis.

This may be supported by the observation that during the first seconds of the voltage application in the electrodeposition process, gas could be seen bubbling from the zincated substrate's surface, which indicates a chemical reaction occurred during the process. Furthermore, more bubbles were observed on the substrate which was produced from the longest zincating process (20 minutes). The traces of the bubbles moving in the upward direction was observed on the coating's surface (Figure 5-4). This concept is in agreement with observations made by Hutt et al. [41], who studied the behaviour of the aluminium bondpads in an electroless nickel solution. They suggested that the zinc layer dissolving into the bath provided the electrons necessary to reduce the nickel ions in solution near the surface. Once a layer of nickel ions has been formed, the conventional autocatalytic electroless nickel plating process can take place, with any remaining zinc no longer dissolving due to the nickel covering.

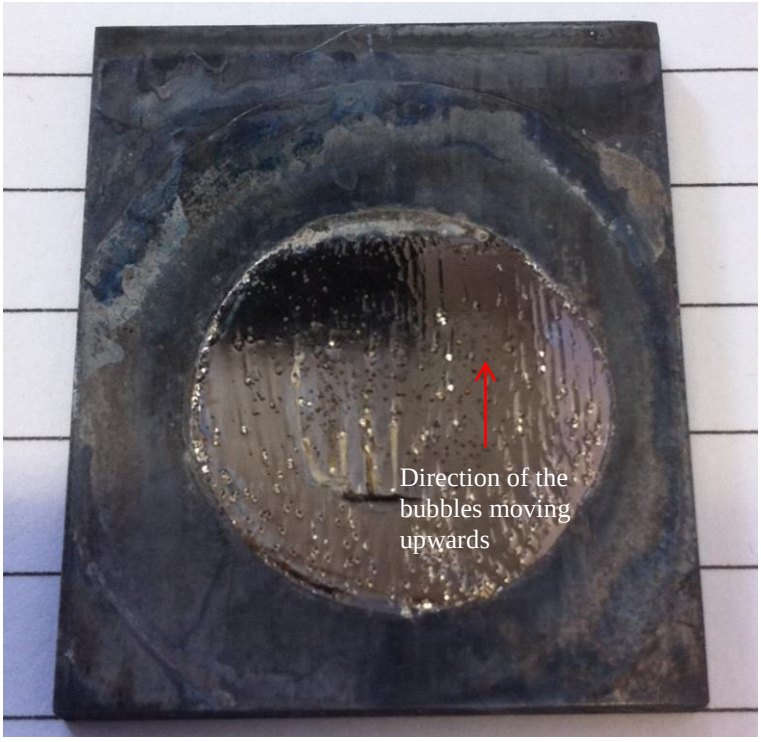

Figure 5-4 Direction of the bubbles moving upwards of the sample

An increase in the oxygen intensity at the interface of the nickel coating and substrate for a sample produced from a conventional single zincating process is due to the non-uniform deposition of the nickel on the substrate. A possible explanation for this may be that the morphology of the zincated sample produced from the conventional single zincating process shows non- homogenous and insufficient coverage of the zinc particles on the substrate, thus producing a non- homogenous nickel deposit on the zincated substrate. This structure of deposit will then lead to poor adhesion of the coating to the substrate. When adhesion is poor, there is a possibility of the aluminium substrate to be oxidised through contact with the air.

5.6 Adhesion of the Nickel Coatings Electrodeposited on AA7075 Substrate Produced from Multiple Zincating Processes

In this study, the adhesion of the coatings was assessed in terms of practical adhesion, where adhesion is measured by the critical load (L_C) for failure of the coating. However, there are several ways of determining a value for L_C. A number of published studies of practical adhesion define L_C as the minimum load at which the first failure occurs during the scratch test. On the other hand, a few studies determined L_C to be the load at which the coating is fully removed from the substrate [146, 152, 189].

A number of techniques have been utilized in order to identify the failure modes from the scratch test, such as microscopy observation, acoustic emission analysis and friction analysis. Failures from the scratch tests detected by AE signal and friction changes have a correlation with the failures observed by the microscope. Most of the studies which were using a scratch test as a tools for adhesion evaluation consider the friction force and AE signal intensity plots in order to analyze the failure modes which occurred from the scratch test [126, 127, 139, 154, 161, 171].

The present study had the aim of assessing the influence of multiple zincating processes at various durations on the adhesion behaviour of the nickel coatings under the progressive load scratch test. The multiple zincating processes include conventional

single zincating process for 1 minute and modified longer single zincating processes, with and without copper activation and double zincating process at 60/10, 60/20, 60/30, 60/40 and 60/50 seconds. In reviewing the literature, no data was found on the correlation between zincating duration and scratch behaviour.

Analysis of the scratch results in this study provided some important information. Critical loads (L_{C1} and L_{C2}) were deduced from the AE signal and F_f curves as a function of scratch length with support from the microscopy examination on the scratch scar. Furthermore, the AE data signal obtained during the test was analysed according to (1) location of data display, (2) number of AE events (N_{AE}) and (3) location of first AE signal which value is more than the average background noise value.

The results and observations of the scratch test on nickel coatings electrodeposited on AA7075 substrate in this study are consistent with some claims and observations in the literature. The results from the scratch test of nickel coatings produced from a multiple zincating processes at various durations show several L_C at different failure modes. These L_C correspond directly to the sudden changes both in the AE signal and F_f curves. In this study, the L_{C1} is indicated as a sudden increase in AE and first variation in F_f.

In the current study, the AE signal and F_f curves recorded during the scratch test were consistent with the microscopy examination on the samples. The correlation between the dramatic changes in AE and F_f curve with the initiation and propagation of crack during the scratch test were observed in Figure 4-37 and Figure 4-41 for conventional and modified single zincated samples, Figure 4-43 and Figure 4-47 for double zincated samples and Figure 4-49 and Figure 4-54 for conventional and modified single zincated samples with copper activation. Figure 4-37, Figure 4-43 and Figure 4-49 show a series of AE signals recorded towards the end of the scratch which were indicated as a series of cracks on the coatings. Furthermore, on all samples, the small transitions in the F_f curves recorded at low progressive load correspond to the occurrence of cracks or cohesive failure. On the other hand, the large transition in the F_f curves recorded at high progressive load obtained from samples which were produced from the conventional single zincating process at 1 minute with and without copper activation indicated the occurrence of coating rupture and separation from the substrate.

There are similarities between the adhesion behaviours reported in this study and those described by Bellido-Gonzalez et al. [151], Davanloo et al. [170] and Bull [139] . Those three studies concluded that the total failure of the coating or rupture occurs when the diamond stylus first contacts the substrate or the stylus touches the interface between two different types of layer, as marked by an inflection point in the measured frictional force. This is also consistent with work of Nick [136], Hintermann [135], Chouanine et al. [127] and Stallard et al. [126], who found that the failure modes are clearly associated with the drastic changes both in the AE signal and F_f curves. Furthermore, this finding is also in agreement with works by Ollendorf's et al. [161] and Chouanine's et al. [127], which showed that a series of crack nucleation and growth events during the scratch test is coincident with various AE signal intensities that occur at different applied load. In their study on Ti-N films on annealed steel 42CrMo4 substrate, Ollendorf et al. [157] suggested that the AE signals as detected were ascribed brittle micro-fractures to in the Ti-N film or the interface. According to Stallard et al. [126], AE signals observed during a scratch test corresponded to the released elastic energy generated by the propagation of cracks during scratching process.

The average critical load values (L_{C1}) of nickel coatings electrodeposited on AA7075 substrate produced from conventional and modified single zincating process at various durations, with and without copper activation, is shown in Figure 5-5. Samples which were produced from both conventional and modified single zincating process without copper activation results in higher L_{C1} values than with the copper activation, as the zincating duration increasing from 1 to 10 minutes. On the other hand, samples which were produced from modified single zincating process with copper activation show the opposite result after 10 minutes of zincating process. Figure 5-5 shows that the highest L_{C1} values for the samples produced from modified single zincating process with and without copper activation were obtained at 5 and 15 minutes of immersion, respectively. This figure also revealed the decreasing of the L_{C1} values for samples produced from modified single zincating process with and without copper activation after a long zincating immersion. A possible explanation for this may poor adhesion between the nickel coating and the AA7075 substrate. This study produced results which corroborate the findings of Yang et al. [45], who found that the coverage of the zinc is closely related with the adhesion of the coating. According to his study, part of

the substrate surface remains uncovered if the zincating duration is too short, while too much zinc is deposited on the substrate if the zincating duration is too long [45]. In comparison, samples which were produced from various double zincating durations at 60/10, 60/20, 60/30, 60/40 and 60/50 seconds show no significant difference in L_{C1} values as shown in Figure 4-45.

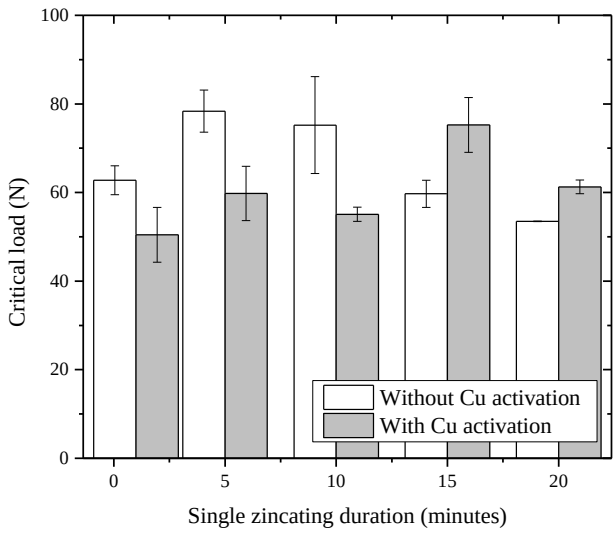

Figure 5-5 Average critical loads of nickel electrodeposited on AA7075 produced from conventional and modified single zincating process with and without copper activation

AE signal characteristics were also analysed in terms of event counts or number of acoustic emission events (N_{AE}) that correlate with the progressive applied load or scratch length. It is apparent from Figure 4-37, Figure 4-43 and Figure 4-49 that all samples show a high N_{AE} with high intensity peaks at high progressive applied load. The AE signals detected at low progressive load were due to background noise occurred during the test. It is encouraging to compare this figure with that of Stebut et al. [174], who found that the increasingly dense series of consecutive N_{AE} at high load is corresponds to numerous cracking and partial spalling event on the coating. In addition, background noise which appeared at low load was due to the vibration from the motor (vertical loading and horizontal specimen translation) as well as friction between the indenter and the specimen [174]. In addition, the main types of acoustic noise sources can be divided into friction and impact. Frictional sources are caused by the structural loading, which causes movement at movable connectors or loose bolts, while impact

sources include rain, wind-driven dust and flying objects [190]. Furthermore, the frequency of the AE signals is related to the defect density [161].

Figure 4-40, Figure 4-46 and Figure 4-52 show the correlations of N_{AE} with the zincating duration for nickel coatings produced from a multiple zincating processes at various durations. Samples which were produced from the conventional single zincating process for 1 minute, with and without copper activation, showed the highest N_{AE}. For both categories of samples, increasing in the zincating duration to 5 minutes resulted in reduction of the N_{AE}. However, further increasing in the zincating duration to 20 minutes produces no significant difference in N_{AE}. It seems possible that these results are due to the distribution of the zinc deposits during the zincating process at various durations.

Figure 4-15 (a) and Figure 4-23 (a) indicate that the conventional single zincating process for 1 minute is insufficient for the zinc deposition to cover the entire of the substrate surface, thus producing a non- homogenous of nickel deposit on the substrate. This structure of deposit leads to the bad adhesion of the coatings to the substrate. Therefore, a sufficient zincating duration is needed, in order to produce a dense population of zinc particles and increase the coverage of the zinc intermediate layer on the substrate. This study proved that a longer duration of single zincating duration is needed in order to obtain coating with a good adhesion to the substrate. The findings of the current study are consistent with those of Palaniappa et al. [54], who found that the uniform zinc layer and sufficient coverage of zinc particles on an aluminium substrate surface increased the adhesion between nickel and aluminium surface as well as the nickel and gold surface.

In the current study, comparison of the optical microscopy images of scratch track of conventional and modified single zincating process with and without copper activation showed similarities in the failure modes. On both groups, samples which were produced from a modified single zincating process at 5, 10, 15 and 20 minutes show a series of ductile tensile cracking under the increasing applied progressive load from 10 to 100 N. This crack is a type of through-thickness cracking, which is under the classification of cohesive failure mode. This failure mode shows that the coating has a good adherence to the substrate. The most interesting finding is that samples which

were conventional single zincated for 1 minute with and without copper activation were ruptured and separated from the substrate at high progressive loads. The samples experienced a wedge spallation failure, which is an adhesion failure mode. This result indicates that the coating was weakly adherent to the substrate. This corresponds to the assumption that the coating adhesion is low in samples produced using a quick zincating process. On the other hand, samples which were double zincated at various durations demonstrated a ductile tensile cracking failure mode at low progressive applied load (Figure 4-47). However, at high load or nearly the end of the track, delamination of the coatings was observed on all samples. The pile- up of the coating on these samples at the end of the scratch track is an evidence that adhesive failure (L_{C2}) was occurred on the coatings. This phenomenon can be seen from the black region which surrounded the scratch end, while the scratch track and the coating surfaces are indicated as a bright region. According to Richard et al. [171], the black region is due to the raised portion of the delaminated coating towards the end of the scratch track. This also corresponds to the different position of the focus point during microscopy observation.

The identification of the failure used in this study refers to the 'map of the main scratch test failure modes' in terms of substrate and coating hardness, which was prepared by Bull [123]. According to Bull et al. [139], the cracks which are classified as a through-thickness cracking failure mode may extend into the substrate, if it sufficiently brittle, but are usually stopped at the interface in a hard coating on a softer substrate. Coatings that are thicker than 10 µm will tend to show through-thickness fracture at stresses lower than those necessary to cause buckling and will fail by wedge spallation. A coating which fails under this failure mode can suppress the formation of a narrowly defined pile-up region and the stresses ahead of the indenter are less complex [139].

Overall results of scratch test on nickel coatings electrodeposited on AA7075 substrate produced from multiple zincating processes at various durations show a strong relationship between the zincating duration and coating adhesion behaviour. The most interesting finding can be seen in the optical micrographs of the samples produced from a modified single zincating process with and without copper activation (Figure 4-41 and Figure 4-54, respectively). For both groups, samples which were produced at a longer

duration (5, 10, 15, and 20 minutes) did not show any delamination on the coating even at high progressive load. The samples only experienced the cohesive failure mode during the scratch test under a high progressive load, which means the coatings were adhered well to the substrate. It is somewhat surprising that no delamination was observed on these samples, even though the gap between scratches is only 2 to 3 mm. Eight scratches were drawn on a coating which dimension is 20 mm in diameter. However, samples which were conventional single zincated for 1 minute with and without copper activation show ruptures at high progressive applied load due to weak adhesion between coating and the substrate. Another important finding was that all samples prepared from double zincating process, in which the immersion duration is short (60 seconds for the first zincating and followed by 10, 20, 30, 40, 50 seconds for the second zincating), indicated a delamination failure mode (adhesive failure) near the end of the track or at high progressive applied load (Figure 4-47). Only two scratches could be drawn on a coating due to the delamination failure.

However, the findings of this study do not support the findings in the literature. In the literature, most of the studies on the single zincating process were carried out at a range of 1 to 60 seconds of immersion duration [1, 2, 22, 29, 54, 104] and for the double zincating process, the second zincating duration must be shorter than the first zincating, so that a thin and uniform zinc immersion coating layer can be produced on the substrate. Most of the studies in the double zincating process were carried out for less than 60 seconds for both first and second zincating process [20, 51]. Many researchers have claimed that the single zincating process was not successful in pre-treating the substrate prior to electrodeposition process. Hino et al. [1] concluded that single zincating process results in poor adhesion to the substrate, while highest adhesion was obtained by the double zincating process. Jin et al. [22] and Lin et al. [40] reported the same observations on the morphology of the single zincated substrate. The single zincating process formed various sizes of zinc particles and left many vacant sites on the substrate [22]. The poor coverage of zinc particles during the process lead to the weak adhesion of the coating to the substrate. In addition, coarse zinc particles forming during the single zincating process is due to the spatially non-uniform anodic (dissolution of aluminium) and cathodic (precipitation of zinc) reactions [2]. Consequently, the double zincating process produces fine particles of zinc with a high population and uniform

layer, which increases the zinc coverage and decreases vacant sites on the substrate [22]. This morphology enhances the uniform growth of the subsequent coating and increases the adhesion of the coating to the substrate [22].

However in this study, the modification on the conventional single zincating duration by expanding the duration to 5, 10, 15 and 20 minutes, more than the duration mentioned by the studies stated in the literature (less than 60 seconds), proven to enhance the adhesion of the coatings to the substrates. In comparison to the double zincating process, samples which were produced at longer single zincating duration show a good adhesion to the substrate. These contradictory results may be due to the longer extension in the single zincating duration introduced in this study. A possible explanation for this may be that the morphology, zinc composition and surface roughness of the zincated substrate.

5.7 Electrochemical Corrosion Behaviour of the Nickel Coatings Electrodeposited on AA7075 Substrate Produced from Multiple Zincating Processes

Most studies in the field of corrosion behaviour of the coating have only focussed on the effects of the various types of coating materials (such as pure metal, alloys, organic and inorganic composites) [4, 97, 191-193], multilayer coating [63], heat treatment process [194] and electrodeposition mode [195]. The effect of surface pre-treatment such as the zincating process on the corrosion behaviour of the coatings is rarely reported [95]. The present study has investigated the effect of multiple zincating processes at various durations on the corrosion resistance of the nickel coatings electrodeposited on AA7075 substrate in the 3.5 wt. % NaCl solution

In this study, the corrosion results on the nickel coatings which were produced at a longer zincating duration, such as at 10 and 20 minutes for modified single zincating process with and without copper activation, indicate a higher corrosion resistance than the shortest duration of the conventional single zincating process. This is due to the increasing corrosion potential and decreasing corrosion current density. Improvement in

corrosion resistance was also found in the nickel coatings which were prepared from a longer double zincating process at 60/40 seconds.

It seems possible that these results are due to the longer zincating duration, resulting in deposition of more zinc particles that almost covered the entire surface. The homogenous coverage of the zinc particles on the substrate then leads to the formation of more uniform and compact nickel coating on the substrate.

In addition, nickel coatings produced following the double zincating process, especially at 60/20 and 60/40 seconds, show a more positive corrosion potential than the nickel coatings produced from the single zincating process with and without copper activation. The fine grain size of zinc particles observed on double zincated samples may be attributed to the increase of corrosion potential of the nickel coatings.

Another important finding was that the corrosion potential of the nickel coatings produced from conventional and modified single zincating process with copper activation was more noble than the non- copper activated samples. On the other hand, corrosion current density of nickel coatings produced from single zincating process with copper activation was lower than the non-copper activated samples, as can be seen in Table 5-1. This finding indicates that the corrosion resistance was improved for the nickel coatings produced from conventional and modified single zincating process with copper activation. A possible explanation for these results is the formation of more uniform and compact nickel coating on the substrate due to the homogenous deposition of the zinc particles on the copper activated substrate. Tang et al. also showed a formation of a dense zinc layer covering the whole surface on the substrate which underwent the copper activation process [63]. According to Tang et al. [63], copper particles deposited on the substrate during the copper activation process act as nucleation sites for the zinc deposition.

Table 5-1 Comparison table of Tafel polarization parameters for the electrodeposited nickel coatings on AA7075 substrate produced at conventional and modified single zincating process without and with copper activation.

Zincating process / Zincating duration	Without copper activation		With copper activation	
	Corrosion potential, E_{corr} *vs.* SCE/mV	Corrosion current density, I_{corr}/ μA cm^{-2}	Corrosion potential, E_{corr} *vs.* SCE/mV	Corrosion current density, I_{corr}/ μA cm^{-2}
1	-736	0.843	-512	0.661
10	-352	0.318	-336	0.073
20	-384	0.195	-304	0.094

5.8 Overall Discussion of the Results

The literature showed that there is a poor coating adhesion on aluminium by single zincating process but it can be improved by applying the double zincating process. This result has been supported by many researchers as listed in Table 5-2. This is due to the smooth surface roughness provided by the double zincating process, which is suitable for a subsequent electrodeposition process. However, the double zincating process is quite complicated in terms of the process, such as zinc stripping process and second zincating process, as compared to the single zincating process. Therefore, in this study the conventional single zincating process has been modified in terms of the immersion duration, in order to achieve a good coverage of zinc deposition on the substrate, thus improving the deposition of the nickel deposit. This leads to the achieving of good adhesion between nickel coatings and the substrate.

Although the behaviour of zinc deposits has been considered important for understanding the adhesion of the coating to the substrate, but its detailed mechanisms still remain unknown. Therefore, in this study, the surface morphology, element composition, surface topography and surface roughness of the zincated samples are believed to have influenced the coating adhesion. It is proven by this study, that the

modified single zincating process with and without copper activation at various durations did influence the surface morphology, zinc composition, surface topography and surface roughness of the AA7075 substrate.

It seems possible that these results are due to the extension in the conventional single zincating duration, which introduce a sufficient time for the zinc particles to deposit homogenously on the substrate. These sufficient times let the zinc particles to growth and finally touch to each other, which thus covered the whole surface without reveal the substrate. These results provide further support for the hypothesis that a homogenous deposition of zinc particles on a substrate during the zincating process will contributes to the uniform deposition of nickel coating, which thus contribute to the improvement in the adhesion and corrosion resistance of the coating.

In a few previous research papers on the zincating process for aluminium alloy substrates published by a group of researchers [1-3, 186, 196], the morphology of zinc particles was reported to affect adhesion of the Ni-P coating to the substrate. Monteiro and Barbosa [26] and Monteiro et al. [27] have confirmed than superior adhesion from zincating is associated with uniform, thin, fine-grained films and complete surface coverage of the zinc particles.

Table 5-2 Summary of the zincating process used by other researchers

Substrate	Coating	Zincating process				Some key observations	Ref.
		Single	Double	Triple	Quadruple		
Al-Cu	Electroless nickel	#	#			A short double zincating treatment gave the best adhesion and leads to minimal etching of the aluminium substrate.	[41]
Al	Electroless nickel	#	#			The adhesion of the electroless nickel coating is varies with the zinc morphology. A smooth zincating layer with fine grain of zinc particle formed during the double zincating process leads to a good adhesion between the coating and substrate.	[57]
AA2017	Electroless Ni-P	#	#	#		The double zincating process produced the highest adhesion strength, where a zincating	[1]

						layer with an appropriate thickness and metallurgically well-bonded structure is thought to form. A thicker zinc layer which was produced by the triple zincating showed a poor adhesive strength.	
AA1050	Electroless Ni-P	#	#	#	#	The double zincating process improved the adhesive strength due to the uniform zincating layer. Coatings with thicker zincating layer show poor adhesive strength.	[2]
AA1100 AA2017 AA5052	Electroless Ni-P	#	#			Single zincating process shows a slightly improved in the adhesive strength of all substrates, but the double zincating process shows a drastic improvement.	[3]
Al-Si	Electroless nickel	#	#			The adhesion of the nickel coating on the aluminium substrate is depends on the coverage of the zinc particles, since the electroless nickel coating and aluminium surface are connected by the zinc intermediate layer. Single zincating formed a various sizes of zinc particles and left many vacant sites, thus resulted in the poor adhesion.	[22]

6 CONCLUSION

Although double zincating process has been widely used in the industries due to the smooth and uniform zinc deposition layer which leads to a strong coating adhesion, there are some drawbacks of this process. This process is a complex zincating process which involves two additional steps compared to the conventional single zincating process, excess dissolution of aluminium substrate during the zinc stripping process in highly acidic nitric acid solution and the environmental issue of the hazardous chemical used in the zincating solution (chemical waste disposal problem). Most literature on the surface pre- treatment of aluminium alloy for electrodeposition focuses on the double zincating process, with less attention for the conventional single zincating process (Table 6.1). This is because of the formation of coarse zinc particles, non-uniform zinc layer and non- homogenous zinc deposition on the substrate during the conventional single zincating process which is not suitable for subsequent plating process. So, this project focussed on in-depth research to overcome the drawbacks of conventional single zincating process. To the best of author knowledge, the case of extending the zincating duration had previously not been given attention and this was the motivation behind the present study. In addition, there is no study conducted on the effect of copper pre-treatment on the aluminium alloy zincated substrate which exceed the immersion duration for conventional single zincating process.

Table 6-1A summary of previous research on zincating process of aluminium and its alloys

Substrate	Copper activation	Zincating process				Reference
		Single	Double	Triple	Quadruple	
Pure aluminium	x		45/ 15 s			[51]
Aluminium alloy 1050 Aluminium alloy 6061	x		90/ 30 s			[19]
Pure aluminium	x		20/ 20 s			[49]
Al- Si alloy	x	60 s	45/ 15 s			[45]
Al- Cu- Si alloy	x		1/ 10 s 5/ 10 s 10/ 10 s			[44]
Pure aluminium	x		1/ 10 s			[42]
Al-Cu alloy	x	10-60 s	20/ 20 s			[41]

			60/ 60 s			
Pure aluminium	x	45 s	45/ 15 s			[57]
Pure aluminium	x	10-40 s	10/ 10 s 20/ 20 s 30/ 30 s 40/ 40 s	10/ 10/ 10 s 20/ 20/ 20 s 30/ 30/ 30 s 40/ 40/ 40 s		[40]
Al-Cu alloy Al-Si alloy	x		30/ 30s			[62]
Al-Si alloy	✓		10/ 10s			[61]
Aluminium alloy 2017	x	30s	30/ 30s	30/ 30/ 30s		[1]
Aluminium alloy 1100 Aluminium alloy 2017 Aluminium alloy 5052	x	30s	30/ 30s			[3]
Al- Si alloy	x		5/ 5 s 10/ 10 s			[22]
Aluminium alloy 1050	x		60/ 30 s			[31]
Pure aluminium	x		2/ 2 s 8/ 8 s 32/ 32 s			[43]
Aluminium alloy 1100 Aluminium alloy 2017 Aluminium alloy 5052 Aluminium alloy 7075	x		30/ 30 s			[186]
Pure aluminium	x	30 s	30/ 30 s	30/ 30/ 30 s	30/ 30/ 30/ 30 s	[2]
Aluminium alloy 7075	✓	60 s 300 s 600 s 900 s	60/ 10 s 60/ 20 s 60/ 30 s 60/ 40 s 60/ 50 s			This research

Note: throughout this thesis, the double zincating treatments used in this study is indicated by a shortened description, e.g. 60/20 s double zincating means a double zincating treatment applying 60 s for the first zincating and followed by 20 s for the second zincating.

In this work, modification of the conventional single zincating process has been made by extending the duration in order to produce a homogenous distribution of zinc deposits which covers the whole substrate surface, thus, improving the coating adhesion. By doing this, the two additional steps of double zincating process such as second zincating process and the zinc stripping process has been eliminated, thus reducing the number and amount of chemicals involved in the zincating process.

However, the zincating duration used for the modified single zincating is longer than the conventional single zincating process. In order to prevent the dissolution of the

aluminium substrate in the zincating solution due to the long immersion time, a copper pre- treatment before the zincating process has been introduced in this research. These copper deposits act as nucleation sites for zinc deposition during the zincating process and produce a uniform and dense layer of zinc deposits which almost completely cover the substrate surface [47].

The electrochemistry measurements show that specimen produced from single zincating with copper activation dramatically suppressed the dissolution of substrate in the zincating solution, compared to single zincating without copper activation process (Figure 6.1). This is due to the rapid deposition of the zinc particles on the copper pre-treated substrate. These copper deposits act as nucleation sites for zinc deposition during the zincating process and produce a uniform and dense layer of zinc deposits which almost completely cover the substrate surface [47, 61 and 63].

As a summary of morphology changes during single zincating SEM micrographs for each of the zincating duration are shown in Figure 6.1. SEM morphologies in Figure 6.1 show that the size and density of zinc particles for both single zincating with and without copper activation increased with the increases in the zincating duration. It was also found in this study that the smoothness and uniformity of the zincating layer was improved through the copper activation process.

Overall, the results from this study show the importance of the zincating duration in controlling the morphology of the zinc layer deposited on the substrate.

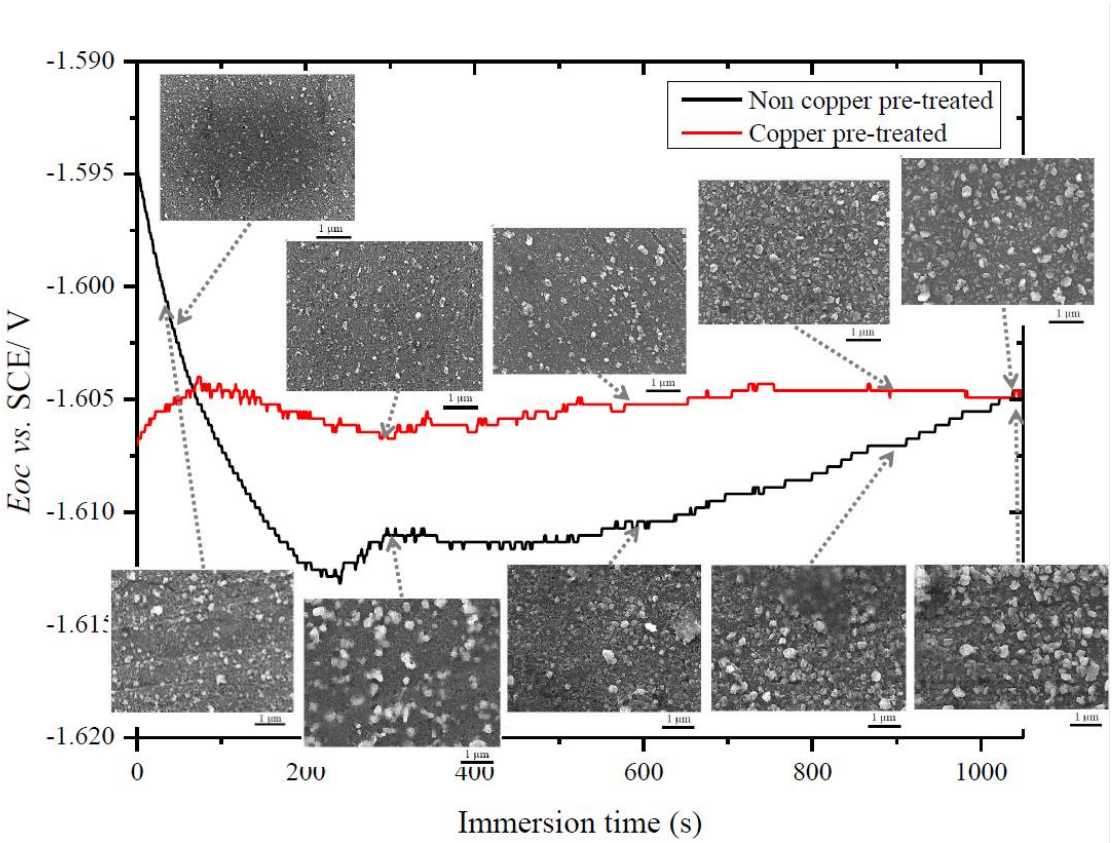

Figure 6-1Correlation between the surface morphology and the EOC curve for single zincating process with and without copper activation

The adhesion behaviour and corrosion resistance of nickel coatings electrodeposited on AA7075 substrate using this modified single zincating process at various durations have been studied and compared to the conventional single and double zincating process. The electrochemical properties of the AA7075 substrate in the zincating solution during multiple zincating processes are investigated using electrochemistry measurement, in order to find the optimum zincating duration. Therefore, the conventional single zincating, modified single zincating and double zincating processes are carried out at the following durations as shown in Table 6.2.

Table 6-2 Duration for multiple zincating process used in this research

Zincating process	Immersion duration (seconds)
Conventional single zincating process with and without copper activtaion	60 s
Modified single zincating process with and without copper activation	300 s 600 s 900 s 1200 s
Double zincating process	60/ 10 s 60/ 20 s 60/ 30 s 60/ 40 s 60/ 50 s

The effect of the multiple zincating processes with various durations on the surface morphology, surface composition, and surface roughness of the substrate were examined using SEM, EDX and AFM. The effect of multiple zincating processes at various durations on the adhesion behaviour and corrosion resistance were investigated using the scratch adhesion test and corrosion test in 3.5 wt. % NaCl solution.

The results of this study show that significant adhesion strength enhancement of nickel coatings on an aluminium alloy 7075 substrate is possible by extending the conventional single zincating duration. This modified single zincating process produced a homogenous distribution of zinc particles and increased the coverage of zinc deposit layer on the substrate. The sufficient coverage of zinc particles on the substrate increased the adhesion between nickel coating and aluminium alloy surface, since electrodeposition of nickel deposits is activated on the zinc layer.

Since adhesion is an important property for a a coating, the optimised modified single zincating process should be further investigated as a potential replacement for the complex double zincating process which is widely used in the industries. By applying this modified single zincating process in electrodeposition industries, the production line of a coating on aluminium alloy substrate will be shorter. Consequently, this will reduce the factory space, number of dipping tanks, number of chemicals, amount of chemicals, amount of chemicals waste and number of workers involved in

electrodeposition process of aluminium alloy substrate. This can contribute to solving the waste disposal problem of the chemicals used in the zincating solution.

The results of the electrochemical, surface roughness, corrosion and mechanical analysis of coatings in this research may be summarized as follows:

(1) The electrochemical measurement of the AA7075 substrates in the zincating solution during single and double zincating process showed steep drops in E_{OC} values during the first stage, followed by an increase in E_{OC} values to the noble direction and slowly approaching the steady potential of -1.596 V after 1250 seconds. However, the double zincated samples showed a rapid increase in the E_{OC} value to more noble direction at about 250 seconds, while the single zincated substrate showed a slow increase to the more noble values only after 500 seconds, indicating that the substrate was actively dissolved during the first zincating process compared to the second zincating process. This effect is considered to indicate that the substitution reaction of substrate dissolution and zinc deposition is faster on the substrate where zinc particles have already nucleated on the surface and cover the surface immediately. However, high dissolution of the substrate during the single zincating process was suppressed by applying the copper activation before the zincating process. This is due to the copper activation process, which provides nucleation sites for zinc deposition.

(2) The analysis of surface roughness is carried out to understand how the multiple zincating process influences the surface roughness of the substrate. In this study, the conventional single zincated sample has a higher surface roughness as compared to the sample after the initial surface pre-treatment, due to the deposition of zinc particles which generally do not touch each other. However, the extension in the conventional single zincating duration to 20 minutes reduced the surface roughness to less than 0.02 µm as a result of the formation of a compact and uniform zinc layer, which covers the substrate surface. For the double zincated sample, the second zincating process at 60/10 seconds showed a smoother surface than the first zincated sample. However, as the second

zincating duration increased to 50 seconds, the surface roughness was inconsistent. In this study, it is proven that reduced surface roughness of zinc layer formed during the zincating process leads to a better adhesion of nickel coating to the substrate. This is due to electrodeposition of uniform and compact nickel coating.

(4) Corrosion tests of nickel coatings electrodeposited on AA7075 substrates in 3.5 wt. % NaCl solution confirmed that the nickel coatings produced from a modified single zincating process with and without copper activation at a longer duration, such as 10 and 20 minutes and double zincating process had a better corrosion resistance than the conventional single zincating process, due to the increasing in corrosion potential and decreasing in corrosion current density of the conventional single zincated sample. The improvement in the corrosion resistance of the nickel coatings is related to formation of the dense and uniform layer of coatings on a homogenous zincating layer.

(5) The low values of first critical load (L_{C1}) of the nickel coatings electrodeposited on AA7075 substrates through a conventional single zincating with and without copper activation which were at 53.60 N and 57 N respectively, was improved to 87.60 N and 81 N respectively, by the modified single zincating process with and without copper activation at a longer duration. This is related to the homogenous and compact zincating layer with a high zinc composition obtained during the extension of zincating duration. In this study, nickel coatings produced from double zincating process showed poor coating adhesion due to the occurrence of cohesive and adhesive failure modes, while single zincated samples experienced only the cohesive failure mode.

(6) The modified single zincating process improves the coating adhesion of nickel coatings produced compared to conventional single zincating and double zincating processes. This can be seen from the correlation between number of acoustic emission activity (N_{AE}) and zincating durations. Samples from single zincating process with and without copper activation show a reduction in the N_{AE} values approximately from 130 to 20, as the zincating duration increases from 1 to 20 minutes. However, for the double zincating process, no consistent trend in

the N_{AE} values can be determined and there is no significant reduction in the N_{AE} values with the increase of the zincating duration. Overall, the N_{AE} values for the modified single zincating process is lower than the conventional single zincating and double zincating process.

7 FUTURE WORKS

This research has successfully improved the coating adhesion of nickel electrodeposited on AA7075 substrate through a modified single zincating process. The zincating duration proved to be the important parameter in zincating process, as this can strongly influence the adhesion of the coating to the substrate. However, further investigation is required on the properties of the zincating layers formed on substrate from various zincating durations, such as weight, thickness, composition, morphology and roughness, in order to understand the correlation between the zinc layers with the coating adhesion as well as a direct impact on the properties of the electrodeposited nickel coatings, such as wear and corrosion resistance. It is recommended to further the research on improving properties of coatings on light alloys through modified zincating procedures of as follows.

(1) The efficacy of modified single zincating processes should be tested for other types of aluminium alloys, such as aluminium alloy 1xxx, 2xxx, 3xxx, 4xxx, 5xxx, 6xxx and 8xxx series. An electrochemical study of these alloys in zincating solution needs to be done first in order to investigate the electrochemistry behaviour of these alloys during the zincating process. According to Murakami et al. [186], temporal changes of electrode potential during zincating and morphologies of the zincated surfaces showed that the alloying elements in the aluminium alloys 2017 (AA2017) and AA7075, such as copper and zinc, promoted uniform precipitation of zinc, resulting in rapid termination of conversion reaction.

This modified single zincating process also should be applied to magnesium alloys because these alloys are classified as light alloys same as aluminium alloys, where oxide layer can be easily formed on the surface. This oxide layer results in low adhesive strength of the electrodeposited layer to the substrate. However, based on the literature review, the zincating solution for magnesium

alloys contain different chemicals than aluminium alloys, such as zinc sulphate, potassium pyrophosphate, sodium carbonate and potassium fluoride [47, 48 and 63]. The electrochemistry measurement needs to be done first to study the electrochemical behaviour of the magnesium alloys in zincating solution. Then, from the E_{OC} curve obtained, the zincating duration on magnesium alloys can be determined and modified.

Detailed investigation of the surface morphology, surface composition, surface roughness, adhesion behaviour and corrosion behaviour of other types of aluminium alloys and magnesium alloys using the modified single zincating process should be carried out, in order to have better understanding of the modified zincating process.

(2) Measure the weight changes of the substrate during the zincating process, in order to monitor the deposition of the zinc.

(3) Focussed ion beam (FIB) investigation on the cross section of zincated sample should be carried out, in order to measure the thickness of zincating layer or the substrate after zincating pre- treatment.

(4) X-ray photoelectron spectroscopy (XPS) should be carried out on the zincated samples in order to investigate the chemical states of the zinc layer after various zincating processes and to support EDX results. This analysis will provide information whether the zinc layer has been oxidised or not.

(5) Auger electron spectroscopy (AES) should be carried out to examine the surface elemental components of interfacial region between nickel coating and AA7075 substrate, since no evidence of zinc was found using SEM and EDX in this study.

(6) Further research might investigate the effect of heat treatment process to the coating adhesion of samples produced from conventional and modified single zincating process.

(7) A future study investigating the adhesion of the coating using a scratch test on the cross section of the coating would be interesting to measure the actual interfacial strength, since the crack is generated along the coating and substrate interface.

(8) Further investigation on the electrochemistry measurement, such as cyclic voltammetry during the electrodeposition process of nickel coating on AA7075 substrate using conventional and modified single zincating process with and without copper activation is strongly recommended. This knowledge is needed in order to understand the mechanism of the modified single zincating process and copper activation in enhancing the adhesion and corrosion resistance of the coating.

(9) In this research, the SEM micrographs demonstrate preferential nucleation of zinc on surface features; hence the potential role of surface roughening on the process needs to be acknowledged. Therefore, further research should include the study of surface roughnes of the substrate after each surface pre- treatment process (e.g. alkaline cleaning, acid cleaning and multiple zincating process) using Atomic Force Microscopy (AFM) and Scanning Electron Microscopy (SEM). This knowledge is needed in order to have better understanding on the nucleation and growth of zinc particles during the zincating process. According to Lee et al. [42], zinc particles preferentially form clusters on convex areas, such as peaks or edges of aluminium alloy surfaces during the zincating process. In addition, it is also very important to know the roughening effect of the substrate during the immersion in the alkaline and acid cleaning prior to zincating process.

References

1. Hino, M., K. Murakami, M. Hiramatsu, K. Chen, A. Saijo, and T. Kanadani, *Effect of zincate treatment on adhesion of electroless Ni-P plated film for 2017 aluminum alloy.* Materials Transactions, 2005. **46**(10): p. 2169-2175.
2. Murakami, K., M. Hino, M. Hiramatsu, K. Osamura, and T. Kanadani, *Effect of zincate treatment on adhesion of electroless nickel-phosphorus coating for commercial pure aluminum.* Materials Transactions, 2006. **47**(10): p. 2518-2523.
3. Hino, M., K. Murakami, Y. Mitooka, K. Muraoka, R. Furukawa, and T. Kanadani, *Effects of zincate treatment on adhesion of electroless Ni-P coating onto various aluminum alloys.* Transactions of Nonferrous Metals Society of China, 2009. **19**(4): p. 814-818.
4. Aal, A.A., *Hard and corrosion resistant nanocomposite coating for Al alloy.* Materials Science and Engineering a-Structural Materials Properties Microstructure and Processing, 2008. **474**(1-2): p. 181-187.
5. Wernick, S., R. Pinner, and P.G. Sheasby, *The surface treatment and finishing of aluminium and its alloys*. 5th. ed. 1987, Metals Park, Ohio: ASM International.
6. Gregg, B.R., R.D. William, E.N. John, and R.K. Richard, *Modern materials and manufacturing processes*. Third edition ed. 2004: Pearson, Prentice Hall.
7. Hatch, J.E., *Aluminium : properties and physical metallurgy*. 1984, Metals Park, Ohio: American Society for Metals.
8. Smith, C.J.E., M.S. Higgs, and K.R. Baldwin, *Advances in protective coatings and their application to ageing aircraft*, in *New metallic materials for the structure of ageing aircraft*. 1999, RTO-AVT: Corfu, Greece. p. 15-1, 15-8.
9. Vinod, S.A. and W.B. Dieter, *Electrochemical impedance spectroscopy of trivalent chromium pre- treated aluminium alloys*. 1993, Naval air warfare centre. p. 1- 14.
10. Puchi-Cabrera, E.S., C. Villalobos- Gutierrez, I. Irausquin, J. La Barbara- Sosa, and G. Mesmacque, *Fatigue behavior of a 7075-T6 aluminum alloy coated with an electroless Ni-P deposit.* International Journal of Fatigue, 2006. **28**(12): p. 1854-1866.
11. Oleynik, S.V., Y.A. Kuzenkov, S.A. Karimova, and T.I. Tararaeva, *Non-Chromate Conversion Coatings on A7075 Aluminum Alloy after Various Thermal Treatment.* Protection of Metals and Physical Chemistry of Surfaces, 2011. **47**(7): p. 889-894.
12. Bocking, C. and A. Reynolds, *Mechanism of adhesion failure of anodised coatings on 7075 aluminium alloy.* Transactions of the Institute of Metal Finishing, 2011. **89**(6): p. 298-302.
13. Visser, P., *Novel totally chrome free corrosion inhibiting coating technology for protection of aluminium alloys.* Transactions of the Institute of Metal Finishing, 2011. **89**(6): p. 291-294.
14. Bielewski, M., *Replacing cadmium and chromium- progress in developing eletrodeposition for substitute hard chromium, New Technology and New Process,* Institute for Aero Research, 2009
15. Heather, F., *Technical alternatives to cadmium electroplating*. 1994, National defense center for environmental excellence (NDCEE): Pennsylvania. p. 1-46.

16. Frank, A., *Guide to cleaner technologies: Alternative metal finishes*. 1994, United States Environmental Protection Agency: Ohio. p. 1-60.
17. Wang, L.P., Y. Gao, T. Xu, and Q. Xue, *Corrosion resistance and lubricated sliding wear behaviour of novel Ni-P graded alloys as an alternative to hard Cr deposits.* Applied Surface Science, 2006. **252**(20): p. 7361-7372.

18. Ul-Hamid, A., Abdul Quddus, F.K. Al- Yousef, A.I. Mohammed, H. Saricimen, and L.M. Al- Hadhrami, *Microstructure and surface mechanical properties of electrodeposited Ni coating on Al 2014 alloy.* Surface & Coatings Technology, 2010. **205**(7): p. 2023-2030.
19. Khan, E., C.F. Oduoza, and T. Pearson, *Surface characterization of zincated aluminium and selected alloys at the early stage of the autocatalytic electroless nickel immersion process.* Journal of Applied Electrochemistry, 2007. **37**(11): p. 1375-1381.

20. Molina, J.M., R.A. Saravanan, J. Narciso, and E. Louis, *Surface modification of 2014 aluminium alloy - Al2O3 particles composites by nickel electrochemical deposition.* Materials Science and Engineering a-Structural Materials Properties Microstructure and Processing, 2004. **383**(2): p. 299-306.
21. Monteiro, F.J., M.A. Barbosa, D.R. Gabe, and D.H.Ross, *Surface pre-treatments of aluminium for electroplating.* Surface & Coatings Technology, 1988.

22. Jin, J.G., S.K. Lee, and Y.H. Kim, *Adhesion improvement of electroless plated Ni layer by ultrasonic agitation during zincating process.* Thin Solid Films, 2004. **466**(1-2): p. 272-278.
23. Gawne, D.T. and U. Ma, *Friction and Wear of Chromium and Nickel Coatings.* Wear, 1989. **129**(1): p. 123-142.
24. Correia, A.N. and S.A.S. Machado, *Electrodeposition and characterisation of thin layers of Ni-Co alloys obtained from dilute chloride baths.* Electrochimica Acta, 2000. **45**(11): p. 1733-1740.
25. Golodnitsky, D., Y. Rosenberg, and A. Ulus, *The role of anion additives in the electrodeposition of nickel-cobalt alloys from sulfamate electrolyte.* Electrochimica Acta, 2002. **47**(17): p. 2707-2714.
26. Sriraman, K.R., S.G.S. Raman, and S.K. Seshadri, *Synthesis and evaluation of hardness and sliding wear resistance of electrodeposited nanocrystalline Ni-W alloys.* Materials Science and Engineering a-Structural Materials Properties Microstructure and Processing, 2006. **418**(1-2): p. 303-311.
27. Capel, H., P.H. Shipway, and S.J. Harris, *Sliding wear behaviour of electrodeposited cobalt-tungsten and cobalt-tungsten-iron alloys.* Wear, 2003. **255**: p. 917-923.
28. Azumi, K., T. Yugiri, T. Kurihara, M. Seo, H. Habazaki, and S. Fujimoto, *Direct plating of electroless Ni-P layers on sputter-deposited Al-Ni alloy films.* Journal of the Electrochemical Society, 2003. **150**(7): p. C461-C464.
29. Sudagar, J., K. Venkateswarlu, and J.S. Lian, *Dry Sliding Wear Properties of a 7075-T6 Aluminum Alloy Coated with Ni-P (h) in Different Pretreatment Conditions.* Journal of Materials Engineering and Performance, 2010. **19**(6): p. 810-818.

30. Delaunois, F. and P. Lienard, *Heat treatments for electroless nickel-boron plating on aluminium alloys.* Surface & Coatings Technology, 2002. **160**(2-3): p. 239-248.

31. Delaunois, F., J.P. Petitjean, P. Lienard and M. Jacob- Duliere, *Autocatalytic electroless nickel-boron plating on light alloys.* Surface & Coatings Technology, 2000. **124**(2-3): p. 201-209.
32. Vitry, V., F. Delaunois, and C. Dumortier, *Mechanical properties and scratch test resistance of nickel-boron coated aluminium alloy after heat treatments.* Surface & Coatings Technology, 2008. **202**(14): p. 3316-3324.
33. Pavlatou, E.A., M. Raptakis, and N. Spyrellis, *Synergistic effect of 2-butyne-1,4-diol and pulse plating on the structure and properties of nickel nanocrystalline deposits.* Surface & Coatings Technology, 2007. **201**(8): p. 4571-4577.
34. Elsherik, A.M. and U. Erb, *Synthesis of Bulk Nanocrystalline Nickel by Pulsed Electrodeposition.* Journal of Materials Science, 1995. **30**(22): p. 5743-5749.
35. Gawne, D.T. and U. Ma, *Wear Mechanisms in Electroless Nickel Coatings.* Wear, 1987. **120**(2): p. 125-149.
36. Apachitei, I. and J. Duszczyk, *Hydrogen evolution, incorporation and removal in electroless nickel composite coatings on aluminium.* Journal of Applied Electrochemistry, 1999. **29**(7): p. 837-843.
37. Walsh, F.C., C. Ponce de Leon, C. Kerr, S. Court, and B.D. Barker, *Electrochemical characterisation of the porosity and corrosion resistance of electrochemically deposited metal coatings.* Surface & Coatings Technology, 2008. **202**(21): p. 5092-5102.
38. Rajendran, R., W. Sha, and R. Elansezhian, *Abrasive wear resistance of electroless Ni-P coated aluminium after post treatment.* Surface & Coatings Technology, 2010. **205**(3): p. 766-772.
39. Apachitei, I. and J. Duszczyk, *Autocatalytic nickel coatings on aluminium with improved abrasive wear resistance.* Surface & Coatings Technology, 2000. **132**(1): p. 89-98.
40. Lin, K.L. and S.Y. Chang, *The morphologies and the chemical states of the multiple zincating deposits on Al pads of Si chips.* Thin Solid Films, 1996. **288**(1-2): p. 36-40.
41. Hutt, D.A., C. Liu, P.P. Conway, D.C Whalley and S.H. Mannan, *Electroless nickel bumping of aluminum bondpads - Part I: Surface pretreatment and activation.* Ieee Transactions on Components and Packaging Technologies, 2002. **25**(1): p. 87-97.
42. Lee, S.K., J.H. Lee, and Y.H. Kim, *Nucleation and growth of zinc particles on an aluminum substrate in a zincate process.* Journal of Electronic Materials, 2007. **36**(11): p. 1442-1447.
43. Azumi, K., T. Yugiri, M. Seo and S. Fujimoto, *Double zincate pretreatment of sputter-deposited Al films.* Journal of the Electrochemical Society, 2001. **148**(6): p. C433-C438.
44. Lee, S.K., J.G. Jin, Y.H. Kim and J.H Lee, *A study on the nucleation behavior of zinc particles on aluminum substrate.* Advances in Electronic Materials and Packaging 2001: p. 73-78.

45. Yang, Y., J. Cai, S. Wang and S. Jia, *The impact of zincation on the electroless nickel UBM for low cost flip technology.* 6th International Conference on Electronic Packaging Technology, 2005.
46. Keller, W.G.Z., *Conditioning aluminium alloys for electroplating.* Electrochemistry Society, 1949.
47. Tang, J.W. and K. Azumi, *Effect of Copper Pretreatment on the Zincate Process and Subsequent Copper Electrodeposition of AZ31 Magnesium Alloy.* Journal of the Electrochemical Society, 2011. **158**(9): p. D535-D540.
48. Tang, J.W. and K. Azumi, *Influence of zincate pretreatment on adhesion strength of a copper electroplating layer on AZ91 D magnesium alloy.* Surface & Coatings Technology, 2011. **205**(8-9): p. 3050-3057.
49. Lee, J.H., I.G. Lee, T. Kang, N.S. Kim and S.Y. Oh, *The effects of bath composition on the morphologies of electroless nickel under-bump metallurgy on Al input/output pad.* Journal of Electronic Materials, 2005. **34**(1): p. 12-18.
50. Robertson, S.G., I.M. Ritchie, and D.M. Druskovich, *A Kinetic and Electrochemical Study of the Zincate Immersion Process for Aluminum.* Journal of Applied Electrochemistry, 1995. **25**(7): p. 659-666.
51. Qi, G., X. Chen, and Z. Shao, *Influence of bath chemistry on zincate morphology on aluminum bond pad.* Thin Solid Films, 2002. **406**(1-2): p. 204-209.
52. Panagopoulos, C.N. and E.P. Georgiou, *Surface mechanical behaviour of composite Ni-P-fly ash/zincate coated aluminium alloy.* Applied Surface Science, 2009. **255**(13-14): p. 6499-6503.
53. Materials, A.S., *Surface engineering of aluminium and aluminium alloys*. 1994.
54. Palaniappa, M., M. Jayalakshmi, and K. Balasubramanian, *Effect of Zincation/Sonication on Electroplated Gold Deposited on Aluminum Substrate.* Journal of Materials Engineering and Performance, 2011. **20**(6): p. 1028-1035.
55. Robertson, S.G. and I.M. Ritchie, *The role of iron(III) and tartrate in the zincate immersion process for plating aluminium.* Journal of Applied Electrochemistry, 1997. **27**(7): p. 799-804.
56. Stoyanova, E. and D. Stoychev, *Electrochemical aspects of the immersion treatment of aluminium.* Journal of Applied Electrochemistry, 1997. **27**(6): p. 685-690.
57. Qi, G.J., L.G.J. Fokkink, and K.H. Chew, *Zincating morphology of aluminum bond pad: its influence on quality of electroless nickel bumping.* Thin Solid Films, 2002. **406**(1-2): p. 219-223.
58. Ng, W.-C., T.-M. Ko, W. Chen, and G.J. Qi, *The effects of immersion zincation to the electroless nickel under-bump materials in microelectronics packaging.* 2nd Electronics Packaging Technology Conference, Proceedings, 1998: p. 89-94.
59. Han, J.I. and S.J. Hong, *Ni electroless plating process for solder bump chip on glass technology.* Japanese Journal of Applied Physics Part 1-Regular Papers Short Notes & Review Papers, 1997. **36**(4A): p. 2091-2095.
60. Arshad, M.K.M., I. Ahmad, A. Jalar, and G. Omar, *The surface characteristics of under bump metallurgy (UBM) in electroless nickel immersion gold (ENIG) deposition.* Microelectronics Reliability, 2006. **46**(2-4): p. 367-379.

61. Azumi, K., S. Egoshi, S. Kawashima, and Y. Koyama, *Effect of copper pretreatment on the double zincate process of aluminum alloy films.* Journal of the Electrochemical Society, 2007. **154**(4): p. D220-D226.
62. Egoshi, S., K. Azumi, H. Konno, K. Ebihara, and Y. Taguchi, *Effects of minor elements in Al alloy on zincate pretreatment.* Applied Surface Science, 2012. **261**: p. 567-573.
63. Tang, J.W., and K. Azumi, *Effect of copper pretreatment on the zincate process and subsequent electroplating of a protective copper/nickel deposit on the AZ91D magnesium alloy.* Electrochimica Acta, 2011. **56**(24): p. 8776-8782.
64. Bach, F.W., A. Laarman, and T. Wenz, *Modern surface technology*. 2006, Weinheim: Wiley-VCH ; Chichester : John Wiley [distributor]. p. 325
65. *Surface Treatment to Reduce Wear, Friction and Corrosion: The Poeton Guide to Surface Engineering*. [cited 2010 9th December].
66. Kanani, N., *Electroplating : basic principles, processes and practice*. 2004, Oxford: Elsevier Advanced Technology.
67. Mellor, B.G., *Surface coatings for protection against wear*. 2006, Cambridge: Woodhead ; Boca Raton, : CRC Press.
68. Dini, J.W., *Electrodeposition : the materials science of coatings and substrates*. 1993, Park Ridge, N.J.: Noyes Publications.
69. Lowenheim, F.A., *Modern Electroplating*. 3rd. edition. ed. 1974, [S.l.]: J. Wiley.
70. Paunovic, M. and M. Schlesinger, *Fundamentals of electrochemical deposition*. 1998, New York ; Chichester: John Wiley.
71. Ebrahimi, F., G.R. Bourne, M.S. Kelly, and T.E. Matthews, *Mechanical properties of nanocrystalline nickel produced by electrodeposition.* Nanostructured Materials, 1999. **11**(3): p. 343-350.
72. Rasmussen, A.A., P. Moller, and M.A.J. Somers, *Microstructure and thermal stability of nickel layers electrodeposited from an additive-free sulphamate-based electrolyte.* Surface & Coatings Technology, 2006. **200**(20-21): p. 6037-6046.
73. Legrand, L., M. Heintz, A. Tranchant, and R. Messina, *Sulfone-Based Electrolytes for Aluminum Electrodeposition*. Electrochimica Acta, 1995. **40**(11): p. 1711-1716.
74. Pavlatou, E.A. and N. Spyrellis, *Influence of pulse plating conditions on the structure and properties of pure and composite nickel nanocrystalline coatings.* Russian Journal of Electrochemistry, 2008. **44**(6): p. 745-754.
75. Gyftou, P., E.A. Pavlatou, and N. Spyrellis, *Effect of pulse electrodeposition parameters on the properties of Ni/nano-SiC composites.* Applied Surface Science, 2008. **254**(18): p. 5910-5916.
76. Li, Y.D., H. Jiang, L.J. Pang, B. Wang, and X.H. Liang, *Novel application of nanocrystalline nickel electrodeposit: Making good diamond tools easily, efficiently and economically.* Surface & Coatings Technology, 2007. **201**(12): p. 5925-5930.
77. Landolt, D. and A. Marlot, *Microstructure and composition of pulse-plated metals and alloys.* Surface & Coatings Technology, 2003. **169**: p. 8-13.
78. Li, Y.D., H. Jiang, W.H. Huang, and H. Tian, *Effects of peak current density on the mechanical properties of nanocrystalline Ni-Co alloys produced by pulse electrodeposition.* Applied Surface Science, 2008. **254**(21): p. 6865-6869.

79. Qu, N.S., D. Zhu, K.C. Chan, and W.N. Lei, *Pulse electrodeposition of nanocrystalline nickel using ultra narrow pulse width and high peak current density.* Surface & Coatings Technology, 2003. **168**(2-3): p. 123-128.
80. Chandrasekar, M.S. and M. Pushpavanam, *Pulse and pulse reverse plating - Conceptual, advantages and applications.* Electrochimica Acta, 2008. **53**(8): p. 3313-3322.
81. Youssef, K.M.S., C.C. Koch, and P.S. Fedkiw, *Influence of additives and pulse electrodeposition parameters on production of nanocrystalline zinc from zinc chloride electrolytes.* Journal of the Electrochemical Society, 2004. **151**(2): p. C103-C111.
82. Liu, Y.C., L. Lei, J. Li, B. Shen, and W.B. Hu, *Effect of 2-butyne-1,4-diol on the microstructure and internal stress of electrodeposited Fe-36 wt.%Ni alloy films.* Journal of Alloys and Compounds, 2009. **478**(1-2): p. 750-753.
83. Oliveira, E.M., G.A. Finazzi, and I.A. Carlos, *Influence of glycerol, mannitol and sorbitol on electrodeposition of nickel from a Watts bath and on the nickel film morphology.* Surface & Coatings Technology, 2006. **200**(20-21): p. 5978-5985.
84. Moti, E., M.H. Shariat, and M.E. Bahrololoom, *Electrodeposition of nanocrystalline nickel by using rotating cylindrical electrodes.* Materials Chemistry and Physics, 2008. **111**(2-3): p. 469-474.
85. Apachitei, I., J. Duszczyk, L. Katgerman, and P.J.B. Overkamp, *Particles co-deposition by electroless nickel.* Scripta Materialia, 1998. **38**(9): p. 1383-1389.
86. Mallory, G.O. and J.B. Hajdu, *Electroless plating : fundamentals and applications*. 1990, Orlando, Fla.: The Society.
87. Parthasaradhy, N.V., *Practical electroplating handbook*. 1989: Prentice Hall.
88. Schlesinger, M. and M. Paunovic, *Modern electroplating*. 4th ed. ed. 2000, New York ; Chichester: John Wiley.
89. ElSherik, A.M., U. Erb, and J. Page, *Microstructural evolution in pulse plated nickel electrodeposits.* Surface & Coatings Technology, 1997. **88**(1-3): p. 70-78.
90. Chang, L.M., D. Chen, J.H. Liu, and R.J. Zhang, *Effects of different plating modes on microstructure and corrosion resistance of Zn-Ni alloy coatings.* Journal of Alloys and Compounds, 2009. **479**(1-2): p. 489-493.
91. Marlot, A., P. Kern, and D. Landolt, *Pulse plating of Ni-Mo alloys from Ni-rich electrolytes.* Electrochimica Acta, 2002. **48**(1): p. 29-36.
92. Baer, D.R., P.E. Burrows, and A.A. El-Azab, *Enhancing coating functionality using nanoscience and nanotechnology.* Progress in Organic Coatings, 2003. **47**(3-4): p. 342-356.
93. Callister, W.D., *Materials science and engineering : an introduction*. 5th ed. ed. 2000, New York ; Chichester: Wiley.
94. Perez, N., *Electrochemistry and corrosion science*. 2004, Boston ; London: Kluwer Academic.
95. Tang, J.W. and K. Azumi, *Improvement of Al coating adhesive strength on the AZ91D magnesium alloy electrodeposited from ionic liquid.* Surface & Coatings Technology, 2012. **208**: p. 1-6.
96. Gleiter, H., *Nanostructured materials: Basic concepts and microstructure.* Acta Materialia, 2000. **48**(1): p. 1-29.

97. Bekish, Y.N., S.K. Poznyak, L.S. Tsybulskaya, and T.V. Gaevskaya, *Electrodeposited Ni-B alloy coatings: Structure, corrosion resistance and mechanical properties.* Electrochimica Acta, 2010. **55**(7): p. 2223-2231.
98. Wu, Y.Y., D.Y. Chang, D.S. Kim, and S.C. Kwon, *Influence of boric acid on the electrodepositing process and structures of Ni-W alloy coating.* Surface & Coatings Technology, 2003. **173**(2-3): p. 259-264.
99. International, A., *Nickel plating*, in *Surface engineering*. 1994.
100. Wernick, S. and R. Piner, *The surface treatment and finishing of aluminium and its alloys*. 5 ed. Vol. 1. 1987, Ohio, USA: Finishing Publications Ltd. 661.
101. Kalpakjian, S. and S.R. Schmid, *Manufacturing engineering and technology*. 4th ed. ed. 2001, Upper Saddle River, NJ: Prentice Hall.
102. Sun, Y., *Tribological rutile-TiO2 coating on aluminium alloy.* Applied Surface Science, 2004. **233**(1-4): p. 328-335.
103. Hutt, D.A., C. Liu, P.P. Conway, D.C. Whalley, and S.H. Mannan, *Electroless nickel bumping of aluminum bondpads - Part II: Electroless nickel plating.* Ieee Transactions on Components and Packaging Technologies, 2002. **25**(1): p. 98-105.
104. Takacs, D., L. Sziraki, T.I. Torok, J. Solyom, Z. Gacsi, and K. Gal- Solymos, *Effects of pre-treatments on the corrosion properties of electroless Ni-P layers deposited on AlMg2 alloy.* Surface & Coatings Technology, 2007. **201**(8): p. 4526-4535.
105. Wu, L.P., J.J. Zhao, Y.P. Xie, and Z.D. Yang, *Progress of electroplating and electroless plating on magnesium alloy.* Transactions of Nonferrous Metals Society of China, 2010. **20**: p. S630-S637.
106. Arshad, M.K.M., A. Jalar, and I. Ahmad, *Characterization of parasitic residual deposition on passivation layer in electroless nickel immersion gold process.* Microelectronics Reliability, 2007. **47**(7): p. 1120-1126.
107. Lai\ner, V.I. and T. Pelz, *Modern electroplating*. 1970, Jerusalem: Israel Program for Scientific Translations.
108. International, A., ASM Handbook, *Surface engineering of aluminium and aluminium alloys.* . 1994. p. 784-804.
109. International, A., *Standard guide for cleaning metals prior to electroplating*, in *Nonferrous metal products*. 2004: United States. p. 9.
110. Apachitei, I., J. Duszczyk, L. Katgerman, and P.J.B. Overkamp, *Electroless Ni-P composite coatings: The effect of heat treatment on the microhardness of substrate and coating.* Scripta Materialia, 1998. **38**(9): p. 1347-1353.
111. Howard, A.M., *Method for zincating aluminium articles*, U.S. Patent, Editor. 1976, Eltra Corporation, Toledo, Ohio: United States of America.
112. Einerhand, R.E.F., W.H.M. Visscher, and E. Barendrecht, *Hydrogen-Production during Zinc Deposition from Alkaline Zincate Solutions.* Journal of Applied Electrochemistry, 1988. **18**(6): p. 799-806.
113. Peter, V., *Zincate treatment of aluminium*, in *Technical Letter 15*. 2004, SurTec.
114. Morin, L.C., and A.K. Molnar, *Electroplated aluminium parts and process for production*, U.S. Patent, Editor. 2004, The Westaim Corporation, Fort Saskatchewan (CA): United States of America.
115. *Regulation (EC) No 1272/ 2008 of The European Parliament and of The Council.* Official Journal of The European Union, 2008: p. 35.

116. Aldrich, S., *Safety data sheet*, in *Sodium Hydroxide*. 2013. p. 7.
117. Aldrich, S., *Safety data sheet*, in *Zinc oxide*. 2012. p. 7.
118. Aldrich, S., *Safety data sheet*, in *Iron (III) chloride*. 2014. p. 8.
119. ASTM Standard D907, 12a, "Standard Terminology of Adhesives", ASTM International, West Conshohocken, PA, 2012, DOI: 10.1520/ D0907-12 A, www. astm.org
120. Durney, L.J., *Electroplating engineering handbook*. 4th ed. / edited by Lawrence J. Durney. ed: London : Chapman & Hall, 1984 (1996 [printing]).
121. Mittal, K.L., *Adhesion measurement of films and coatings*. 1995, Utrecht: VSP.
122. Mittal, K.L., *Adhesion measurement of films and coatings: a commentary*, in *Adhesion measurement of films and coatings*, K.L. Mittal, Editor. 1995, VSP BV: The Netherlands. p. 1-13.
123. Bull, S.J., *Failure mode maps in the thin film scratch adhesion test.* Tribology International, 1997. **30**(7): p. 491-498.
124. Heinke, W., A. Leyland, A. Matthews, G. Berg, C. Friedrich, and E. Broszeit, *Evaluation of PVD nitride coatings, using impact, scratch and Rockwell-C adhesion tests.* Thin Solid Films, 1995. **270**(1-2): p. 431-438.
125. Gonczy, S.T. and N. Randall, *An ASTM standard for quantitative scratch adhesion testing of thin, hard ceramic coatings.* International Journal of Applied Ceramic Technology, 2005. **2**(5): p. 422-428.
126. Stallard, J., S. Poulat, and D.G. Teer, *The study of the adhesion of a TiN coating on steel and titanium alloy substrates using a multi-mode scratch tester.* Tribology International, 2006. **39**(2): p. 159-166.
127. Chouanine, L., M. Takano, F. Ashihara, and O. Kamiya, *Surface failure mode evaluation of pure AlN and AlN with Al2O3(0.1 µm) oxide layer by microscratch testing.* Journal of Materials Science, 2005. **40**(21): p. 5703-5710.
128. Totik, Y., *Investigation of the adhesion of NbN coatings deposited by pulsed dc reactive magnetron sputtering using scratch tests.* Journal of Coatings Technology and Research, 2010. **7**(4): p. 485-492.
129. Czyzniewski, A., *Preparation and characterisation of a-C and a-C:H coatings deposited by pulsed magnetron sputtering.* Surface & Coatings Technology, 2009. **203**(8): p. 1027-1033.
130. Sander, T., S. Tremmel, and S. Wartzack, *A modified scratch test for the mechanical characterization of scratch resistance and adhesion of thin hard coatings on soft substrates.* Surface & Coatings Technology, 2011. **206**(7): p. 1873-1878.
131. Randall, N.X., G. Favaro, and C.H. Frankel, *The effect of intrinsic parameters on the critical load as measured with the scratch test method.* Surface & Coatings Technology, 2001. **137**(2-3): p. 146-151.
132. Jacobs, R., J. Meneve, G. Dyson, D.G. Teer, N.M. Jennett, and P. Harris, *A certified reference material for the scratch test.* Surface & Coatings Technology, 2003. **174**: p. 1008-1013.
133. Aldrich-Smith, G., N. Jennett, and J. Housden, *Adhesion of thin coatings - the VAMAS (TWA 22-2) interlaboratory exercise.* Surface & Coatings Technology, 2005. **197**(2-3): p. 336-344.
134. Shum, P.W., Z.F. Zhou, and K.Y. Li, *Enhancement of adhesion strength and tribological performance of pure carbon coatings on Ti-6Al-4V biomaterials*

with ion implantation pre-treatments. Tribology International, 2007. **40**(2): p. 313-318.
135. Hintermann, H.E., *Characterization of Surface-Coatings by the Scratch Adhesion Test and by Indentation Measurements.* Fresenius Journal of Analytical Chemistry, 1993. **346**(1-3): p. 45-52.
136. Nick, R., *Modified Pin-on-Disc Tribometer for controlled lubricant studies*, in *Application Bulletin*. 1997, CSM Instrument: Peseux, Switzerland.
137. Aldrich-Smith, G., and N.M. Jennet, *A Round Robin to Measure the Adhesion of Thin Coatings*, in *NPL Report DEPC- MPE 001*. 2004, National Physical Laboratory: Cambridge, United Kingdom.
138. Park, H.S. and D. Kwon, *An energy approach to quantification of adhesion strength from critical loads in scratch tests.* Thin Solid Films, 1997. **307**(1-2): p. 156-162.
139. Bull, S.J. and E.G. Berasetegui, *An overview of the potential of quantitative coating adhesion measurement by scratch.* Tribology International, 2006. **39**(2): p. 99-114.
140. Xie, Y. and H.M. Hawthorne, *A controlled scratch test for measuring the elastic property, yield stress and contact stress-strain relationship of a surface.* Surface & Coatings Technology, 2000. **127**(2-3): p. 130-137.
141. Xie, Y. and H.M. Hawthorne, *Effect of contact geometry on the failure modes of thin coatings in the scratch adhesion test.* Surface & Coatings Technology, 2002. **155**(2-3): p. 121-129.
142. Xie, Y. and H.M. Hawthorne, *A model for compressive coating stresses in the scratch adhesion test.* Surface & Coatings Technology, 2001. **141**(1): p. 15-25.
143. Vasinonta, A. and J.L. Beuth, *Measurement of interfacial toughness in thermal barrier coating systems by indentation.* Engineering Fracture Mechanics, 2001. **68**(7): p. 843-860.
144. Benjamin, P., and C. Weaver, *Measurement of Adhesion of Thin Films.* Proceedings of the Royal Society of London, 1960. **254**(A): p. 163-176.
145. Blees, M.H., G.B. Winkelman, A.R. Balkenede, and J.M.J. den Toonder, *The effect of friction on scratch adhesion testing: application to a sol-gel coating on polypropylene.* Thin Solid Films, 2000. **359**(1): p. 1-13.
146. Berg, G., C. Friedrich, E. Broszeit, and C. Berger, *Scratch test measurement of tribological hard coatings in practice.* Fresenius Journal of Analytical Chemistry, 1997. **358**(1-2): p. 281-285.
147. Katia, M.D., *Adhesion characterization of hard ceramic coatings by the scratch test*, in *Department of Physics*. 1999, Queen's University at Kingston: Ontario, Canada.
148. Takadoum, J., *Materials and surface engineering in tribology*. 2008, London: ISTE.
149. Kamminga, J.-D., P.V. Essen, R. Hoy and G.C.A.M. Janssen, *Substrate dependence of the scratch resistance of CrNx coatings on steel.* Tribology Letters, 2005. **19**(2): p. 65-72.
150. Subramanian, C., G. Cavallaro, and G. Winkelman, *Wear maps for titanium nitride coatings deposited on copper and brass with electroless nickel interlayers.* Wear, 2000. **241**(2): p. 228-233.

151. Bellido-Gonzailez, V., N. Stefanopoulos, and F. Deguilhen, *Friction monitored scratch adhesion testing.* Surface & Coatings Technology, 1995. **74-75**(1-3): p. 884-889.
152. Wang, C.T., N. Gao, M.G. Gee, R.J. Wood, and T.G. Langdon, *Processing of an ultrafine-grained titanium by high-pressure torsion: An evaluation of the wear properties with and without a TiN coating.* Journal of the Mechanical Behavior of Biomedical Materials, 2013. **17**: p. 166-175.
153. Hoy, R., V.G.M. Sivel, J.-D. Kamminga and G.C.A.M. Janssen, *Failure during scratch testing of thick and thin CrN coatings examined using focused ion beam.* Surface & Coatings Technology, 2005. **200**(1-4): p. 149-152.
154. Vencl, A., N. Manic, V. Popovic, and M. Mrdak, *Possibility of the Abrasive Wear Resistance Determination with Scratch Tester.* Tribology Letters, 2010. **37**(3): p. 591-604.
155. Bull, S.J., R.I. Davidson, K. Harvathova, D. Mitchell, and J.R. White, *Preliminary investigation into the application of scratch testing to marine coatings.* Journal of Materials Science, 2002. **37**(22): p. 4937-4943.
156. Bemporad, E., M. Sebastiani, C. Pecchio, and S.D. Rossi, *High thickness Ti/TiN multilayer thin coatings for wear resistant applications.* Surface & Coatings Technology, 2006. **201**(6): p. 2155-2165.
157. Paschke, H., M. Weber, P. Kaestner, and G. Braeuer, *Influence of different plasma nitriding treatments on the wear and crack behavior of forging tools evaluated by Rockwell indentation and scratch tests.* Surface & Coatings Technology, 2010. **205**(5): p. 1465-1469.
158. Subramanian, C. and E. Pallotta, *Two-body abrasive wear of electroless nickel composite coatings.* Tribology Letters, 1996. **2**(2): p. 133-150.
159. Pan, Z.Y., Y. Wang, X.W. Li, C.H. Wang and Z.W. Zou, *Effect of Submicron and Nano SiC Particles on Erosion Wear and Scratch Behavior of Plasma-Sprayed Al2O3/8YSZ Coatings.* Journal of Thermal Spray Technology, 2012. **21**(5): p. 995-1010.
160. Bolelli, G., E. Gualtieri, L. Lusvarghi, F.P. Mantini, F. Pitacco, S. Valeri, and H. Volz, *Thermally Sprayed Coatings as Interlayers for DLC-Based Thin Films.* Journal of Thermal Spray Technology, 2009. **18**(2): p. 231-242.
161. Ollendorf, H. and D. Schneider, *A comparative study of adhesion-test methods for hard coatings.* Surface & Coatings Technology, 1999. **113**(1-2): p. 86-102.
162. Ramos, F. and M.T., Vierra, *Adhesion improvement of RF-sputtered alumina coatings as determined by the scratch test*, in *Adhesion measurement of films and coatings*, K.L. Mittal, Editor. 1995, VSP BV: The Netherlands. p. 115-126.
163. Shum, P.W., Z. F. Zhou, K.Y. Li, and C.Y. Chan, *Mechanical and tribological properties of amorphous carbon films deposited on implanted steel substrates.* Thin Solid Films, 2004. **458**(1-2): p. 203-211.
164. Shum, P.W., W.C. Tam, K.Y. Li, Z.F. Zhou, Y.G. Shen, *Mechanical and tribological properties of titanium-aluminium-nitride films deposited by reactive close-field unbalanced magnetron sputtering.* Wear, 2004. **257**(9-10): p. 1030-1040.
165. Shum, P.W., Z.F. Zhou, and K.Y. Li, *Tribological performance of amorphous carbon films prepared on steel substrates with carbon implantation pre-treatment.* Wear, 2004. **256**(3-4): p. 362-373.

166. Bull, S.J., *Can the scratch adhesion test ever be quantitative?*, in *Adhesion measurement of films and coatings*, K.L. Mittal, Editor. 2001, VSP BV: The Netherlands. p. 107-130.
167. International, A., *Standard test method for adhesion strength and mechanical failure modes of ceramic coatings by quantitative single point scratch testing*. 2010: United States. p. 27.
168. Ollivier, B., *Adhesion of diamond-like carbon films on polymer: an assessment of the validity of the scratch test technique applied to flexible substrates*, in *Adhesion measurement of films and coatings*, K.L. Mittal, Editor. 1995, VSP BV: The Netherlands. p. 103-114.
169. Kattamis, T.Z., *On the evaluation of adhesion of coatings by automatic scratch testing*, in *Adhesion measurements of films and coatings*, K.L. Mittal, Editor. 1995, VSP BV: The Netherlands. p. 143-160.
170. Davanloo, F., C.B. Collins and K.J. Koivusaari, *Scratch adhesion testing of nanophase diamond coatings on industrial substrates*, in *Adhesion measurement of films and coatings*, Vol. 2. K.L. Mittal, Editor. 2001, VSP BV: The Netherlands. p. 141-157.
171. Richard, P., J. Thomas, D. Landolt, and G. Gremaud, *Combination of scratch-test and acoustic microscopy imaging for the study of coating adhesion.* Surface & Coatings Technology, 1997. **91**(1-2): p. 83-90.
172. Jennett, N.M., R. Jacobs, and J. Meneve, *Advances in adhesion measurement good practice: Use of a certified reference material for evaluating the performance of scratch test instrumentation*, in *Adhesion aspects of thin films*, K.L. Mittal, Editor. 2005, VSP BV: The Netherlands. p. 179-193.
173. Meneve, J., *Scratch adhesion testing of coated surfaces- Challenges and new directions*, in *Adhesion measurement of films and coatings*, K.L. Mittal, Editor. 2001, VSP BV: The Netherlands. p. 79-106.
174. Stebut, J.V., F. Lapostolle, M. Bucsa, and H. Vallen, *Acoustic emission monitoring of single cracking events and associated damage mechanism analysis in indentation and scratch testing.* Surface & Coatings Technology, 1999. **116**: p. 160-171.
175. Piotrkowski, R., A. Gallego, E. Castro, M.T. Garcia- Hernandez, and J.E. Ruzzante, *Ti and Cr nitride coating/steel adherence assessed by acoustic emission wavelet analysis.* Ndt & E International, 2005. **38**(4): p. 260-267.
176. International, A., *Guide for preparation of aluminium alloys for electroplating*, in *Nonferrous metal products*. 2005.
177. Callister, W.D. and D.G. Rethwisch, *Fundamentals of materials science and engineering : an integrated approach*. 3rd ed., International student / William D. Callister, Jr., David G. Rethwisch. ed. 2008, [Hoboken, N.J.?]: Wiley ; [Chichester : John Wiley [distributor].
178. Wikipedia (10 October 2013) *Energy- dispersive X-ray spectroscopy*.
179. Blanchard, C.R., *Atomic Force Microscopy.* The Chemical Educator, 1996. **1**(5): p. 8.
180. Technologies, A., *User's Guide*, in *5500 Scanning Probe Microscope*. 2008: California, USA. p. 232.
181. Xie, Y. and H.M. Hawthorne, *On the possibility of evaluating the resistance of materials to wear by ploughing using a scratch method.* Wear, 2000. **240**(1-2): p. 65-71.

182. Duncan, B.C., and L.E. Crocker, *Review of tests for adhesion strength*, in *Interfacial adhesion strength*. NPL Reporrt MATC)A)67, 2001. National Physical Laboratory: London. p. 35.
183. Chao, M., *Electodeposited Nanocrystalline Ni-Co and Co- Ni- P Coatings for Hard Chromium Replacement*, in *Faculty of Engineering and the Environment and national Centre for Advanced Tribology of Southampton (nCATS)*. June 2013, University of Southampton, United Kingdom: Southampton. p. 204.
184. Azumi K., M. Seo, and L. Nanis, *Changes in Potential and Weight of Aluminum Alloy during Double Zincate Process* Journal of Surface Finishing Society Japan, 1996. **47**: p. 529-535
185. Huang, X.M., L. Ning, Li, and D.Y. Jiang, *Zincate mechanism on cast Al-Si alloy in non-cyanide multi-metal zincate solutions.* Transactions of Nonferrous Metals Society of China, 2006. **16**(2): p. 414-420.
186. Murakami, K., M. Hino, R. Furukawa, and T. Kanadani, *Effects of Alloying Elements in Aluminum Alloys and Activations on Zincate Treatment and Electroless Nickel-Phosphorus Plating.* Materials Transactions, 2010. **51**(1): p. 78-84.
187. Saito, M., T. Maegawa, and T. Homma, *Electrochemical analysis of zincate treatments for Al and Al alloy films.* Electrochimica Acta, 2005. **51**(5): p. 1017-1020.
188. Arshad, M.K.M., A. Jalar, I. Ahmad, and G. Omar, *The characterization of aluminium bondpad surface treatment in electroless nickel immersion gold (ENIG) deposition.* American Journal of Applied Science, 2007. **4**(3): p. 133-141.
189. Perry, A.J., *Scratch Adhesion Testing of Hard Coatings.* Thin Solid Films, 1983. **107**(2): p. 167-180.
190. Hellier, C., *Handbook of nondestructive evaluation*. 2001, New York ; London: McGraw-Hill.
191. Liu, Y., D. Sun, H. You, and J.S. Chung, *Corrosion resistance properties of organic-inorganic hybrid coatings on 2024 aluminum alloy.* Applied Surface Science, 2005. **246**(1-3): p. 82-89.
192. Zhao, M.J., C. Cai, L. Wang, Z. Zhang, and J.Q. Zhang, *Effect of zinc immersion pretreatment on the electro-deposition of Ni onto AZ91D magnesium alloy.* Surface & Coatings Technology, 2010. **205**(7): p. 2160-2166.
193. Hamid, Z.A., M.T. Abou El-khair, and H.B. Hassan, *Synthesis and protection of AM50 magnesium alloy and its composites using environmentally pretreatment electrolyte.* Surface & Coatings Technology, 2011. **206**(6): p. 1041-1050.
194. Vitry, V., A. Sens, A.-F. Kanta, and F. Delaunois, *Wear and corrosion resistance of heat treated and as-plated Duplex NiP/NiB coatings on 2024 aluminum alloys.* Surface & Coatings Technology, 2012. **206**(16): p. 3421-3427.
195. Mishra, R. and R. Balasubramaniam, *Effect of nanocrystalline grain size on the electrochemical and corrosion behavior of nickel.* Corrosion Science, 2004. **46**(12): p. 3019-3029.
196. Murakami, K., M. Hino, M. Hiramatsu, K. Osamura, and T. Kanadani, *Influence of zincate treatment on adhesion strength of electroless nickel-phosphorus plated film for commercial pure aluminum.* Aluminium Alloys 2006, Pts 1 and 2, 2006. **519-521**: p. 759-764.

197. Schwankl, M., R. Kellner, R.F. Singer, and C. Korner, *The influence of sandblasting on the morphology of electroless deposited zinclayers on aluminium sheets.* Applied Surface Science, 2013. **283**: p. 202-208.

198. Rhonda, R.W., C. Lei, and R.J. Mark, *Bimetallic zincating processing for enhanced adhesion of aluminium on aluminium alloys.* 2014. WO 2014150482A1, PCT/ US PATENT 2014/ 023369.

199. Pedraza, A.J., *Effects of surface treatments on the adhesion of metallic films to ceramic substrates.* Adhesion Aspects of Thin Films, 2001. **Vol. 1**: p. 67- 77.

200. Kumar, A., and B. Bhushan, *Nanomechanical, nanotribological and macrotriboloogical characterization of hard coatings and surface treatment of H-13 steel.* Tribology International, 2015. **81**: p. 149- 158.

201. Takaqoum, J., and B. Cretin, *Study of adhesion and tribological properties of some ceramic films*. Adhesion Aspects of Thin Films, 2001. **Vol. 1**: p. 195- 205.

202. Staia, M.H., E.S. Puchi Cabrera, A. Lost, A. Zairi, S. Belayer and A. Van Gorp, *Tribological response of AA 2024- T3 aluminium alloy coated with a DLC duplex coating.* Tribology International, 2015. **85**: p. 74- 87.

203. Farokhzadeh, K., A. Edrisy, G. Pigott and P. Lidster, *Scratch resistance analysis of plasma- nitrided Ti- 6Al- 4V alloy*. Wear, 2013. **302**: p. 845- 853.

204. Zaidi, H., A. Djamai, K.J. Chin and T. Mathia, *Characterisation of DLC coating adherence by scratch testing.* Tribology International, 2006. **39**: p. 124- 128.